Dedicated to my parents

&

dearest wife

ACKNOWLEDGEMENT

In the name of Allah, Most Gracious, Most Merciful

First and foremost, all praise to Allah, *subhanahu-wa-ta'ala*, the almighty, Who gave me an opportunity, courage and patience to carry out this work, I feel privilege to glorify His name in the sincerest way through this small accomplishment. I seek his mercy, favor and forgiveness. And I ask Him to accept my little effort. May He, *subhanahu-wa-ta'ala,* guide us and the whole humanity to the right path (Ameen).

Acknowledgement is due to the King Fahd University of Petroleum and Minerals for providing the research facilities and research assistantship.

I wish to submit my sincere gratitude to my thesis advisor, Dr. Habib D. Zughbi for his invaluable support, guidance, continuous encouragement and every possible cooperation through out the period of my research and in the preparation of this manuscript. His priceless suggestion made this work interesting and learning for me. He was always kind, understanding and sympathetic to me.

I am also indebted to my thesis committee members Dr. M. A. Al-Shalabi, Dr H.H. Al-Ali, Dr. U.A. Al-Mubaiyadh, Dr. R. Alnaizy; completion of this work would not have been possible without their sincere help, constructive suggestion and cooperation.

I would like to thank Dr. M. B. Amin, chairman, Chemical Engineering Department, King Fahd University of Petroleum and Minerals for providing me all the available facilities. I am also grateful to all the faculty members and staffs of the Chemical Engineering Department who have in one way or other enriched my academic and research experience at KFUPM.

I gratefully acknowledge the support of my fellow graduate students and to the members of the Bangladeshi community at KFUPM.

My best wishes are also due to my friends who took care for me and were the source of gratification during all period of stay in KFUPM.

Last but not least, I would like to appreciate my family members for their prayers, encouragement and support that permitted me to indulge my passion for the long task to completing this work.

Table of Contents

List of Tables

List of Figures

THESIS ABSTRACT

FULL NAME OF THE STUDENT: SHAIKH ABDUR RAZZAK

TITLE: NUMERICAL INVESTIGATIONS OF FLOW IN A PARTIALLY PACKED VESSEL

MAJOR FIELD: CHEMICAL ENGINEERING

DATE OF DEGREE: APRIL 2004.

Three dimensional CFD models are developed to investigate the flow distribution, heat transfer and chemical reactions in a partially packed vessel. The vessel of interest is similar to a catalytic sulfur converter used for sweetening sour gas. The vessel considered is a large horizontal cylinder and contains a catalyst bed. The height of the bed is about one fourth of the vessel diameter and placed almost in the central region of the vessel. A gas stream enters the vessel, reacts over the catalyst before leaving it. The main reaction is that of H_2S with SO_2 to produce sulfur gas and water vapor. Flow in a three dimensional model of the unpacked vessel is simulated. The effects of flow rates and number of outlets were investigated and found to have a limited effect on the flow distribution.

Flow in a partially packed vessel is also simulated without chemical reactions. Results show that packed beds act as a good flow distributor, however, there is still significant differences in the values of velocity across the various regions of the packed bed. The flow in a partially packed column with chemical reaction is also simulated. Limited kinetics information is available in the literature. A finite rate model is used to simulate the chemical reactions and the results show reasonable agreement with the available industrial data.

ARABIC ABSTRACT
خلاصة البحث

الإســم : شيخ عبدالرزاق

العنـوان : بحوث عددية للسريان في وعاء يحتوي على مواد محفزة

الـدرجة : الماجستير

التخصص: هندسة كيميائية

التاريـخ : ربيع الآخر 1425هـ

هذا البحث يشتمل على نمذجة ثلاثية الأبعاد لسريان غاز داخل وعاء يحتوي على مواد محفزة وتشمل النمذجة على سريان غاز وانتقال حرارة وتفاعل كيميائي.

إن الوعاء المستخدم في هذه الدراسة مشابه للمفاعل المحفز المستخدم لتنقية الكبريت من الغازات في الصناعة، إن شكل الوعاء اسطواني ويحتوي على مواد محفزة وتبلغ نسبة طول الوعاء إلى قطره 4 إلى 1 ، هذا الوعاء يمر به غاز يتفاعل مع المواد المحفزة قبل خروجه وينتج من هذا التفاعل الذي يحدث بين كبريتات الهيدروجين و ثاني أكسيد الكبريت غاز الكبريت وبخار الماء.

هذه الدراسة تشتمل على نمذجة سريان الغاز في ثلاثة أبعاد مع الأخذ في الاعتبار تأثير معدل السريان وعدد المخارج التي وجد أن تأثيرها محدود على شكل السريان، أيضاً أجريت نمذجة سريان الغاز حينما لا يوجد تفاعل، ولقد ثبت من النتائج أن الوعاء المشتمل على مواد محفزة هو عبارة عن موزع جيد، من جهة أخرى وجد فرق لنتائج السرعة خلال الإناء، وقد شملت الدراسة أيضاً على نمذجة وعاء جزئي يحتوي على مواد محفزة.

إن المعلومات عن حركة التفاعل لهذه الدراسة محدودة جداً في الدوريات العلمية. وقد استخدم قانوناً من الدوريات العلمية لنمذجة هذا التفاعل وقد قورنت النتائج من هذا البحث مع نتائج من الصناعة وقد كانت موفقة إلى حد بعيد.

درجة الماجستير في العلوم

جامعة الملك فهد للبترول والمعادن

ربيع الآخر 1425هـ

Chapter 1
Introduction and Objective of Works

1.1 Introduction

A detailed description of flow distribution in packed and unpacked vessels is often necessary for efficient operations in the process industries. Computational fluid Dynamics (CFD) is increasingly used to investigate the flow and energy distribution and chemical reactions in many applications of the chemical and petrochemical industries. Most emission of sulfur into the atmosphere is in the form of sulfur dioxide resulting from the combustion of fossil fuel for heating and energy production. Various industrial activities such as petroleum processing, smelter operations and wood-pulping, also produce significant emissions of sulfur dioxide and sulfur compounds. The World Health Organization (WHO) estimated that the quantity above which the effect of sulfur dioxide is harmful for public health is 50 micro grams per m^3. The increasingly stringent standards for sulfur emissions that are being imposed upon the petroleum and natural gas processing industries around the world are putting unprecedented pressure on those industries.

One process that is commonly used to reduce the emission of sulfur compounds into the atmosphere is the Claus process. This process recovers elemental sulfur from hydrogen sulfide. The Claus process is shown schematically in Figure 1.1. It consists of a high-temperature front-end reaction furnace followed by catalytic reaction converters. Each of these converters contain a catalyst bed provides residence time and surface area for further conversion of hydrogen sulfide and sulfur dioxide to sulfur. The heated gases flow downward through the catalyst bed. The exothermic reaction causes the temperature of the gas to

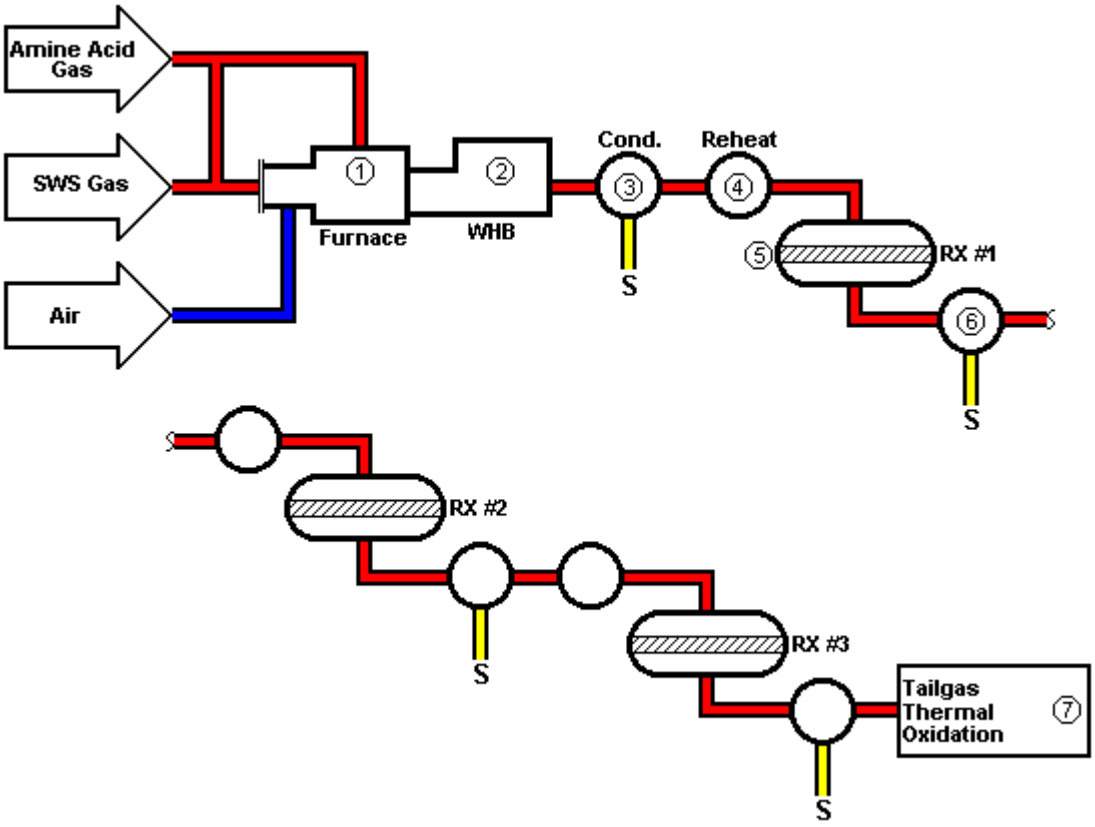

Figure 1.1: A schematic diagram of the Claus Process (Internet)

increase as it passes through the bed. This study is concerned with flow and reactions in the Claus process catalytic converter. In the reaction furnace, roughly one-third of the H_2S in the acid gas feed is oxidized with combustion of air to form SO_2:

$$H_2S + \frac{3}{2}O_2 \longrightarrow SO_2 + H_2O$$

The SO_2 thus formed reacts with the remaining H_2S (the Claus reaction) to yield elemental sulfur:

$$2H_2S + SO_2 \rightleftharpoons \frac{3}{n}S_n + 2H_2O$$

The S_n can be S_2, S_6 or S_8 depending on the temperature of the vessel. Thus the Claus process converts the hydrogen sulfide contained in sour oil and natural gas to elemental sulfur.

The conversion in the furnace is limited by thermodynamics to about 70% and three to four catalytic steps are usually needed to obtain 98% conversion. With the current environmental laws, a conversion higher than 98% is required, and further downstream operations, such as tail gas treatment, are used to achieve that.

A typical catalytic converter consists of a large horizontal vessel, containing in its middle zone a packed bed of catalyst. A schematic diagram of a converter is shown in Figure 1.2. About two thirds of the H_2S reacts with SO_2 in the furnace reaction. The furnace is maintained high temperature and most of the H_2S and SO_2 converted here. Then remaining one third H_2S then carrying to the converter to be converted to elemental sulfur in the converter. For this purpose three catalytic converters are used one after another. These entire three converters maintain different temperature inlet to get high conversion of H_2S and SO_2.

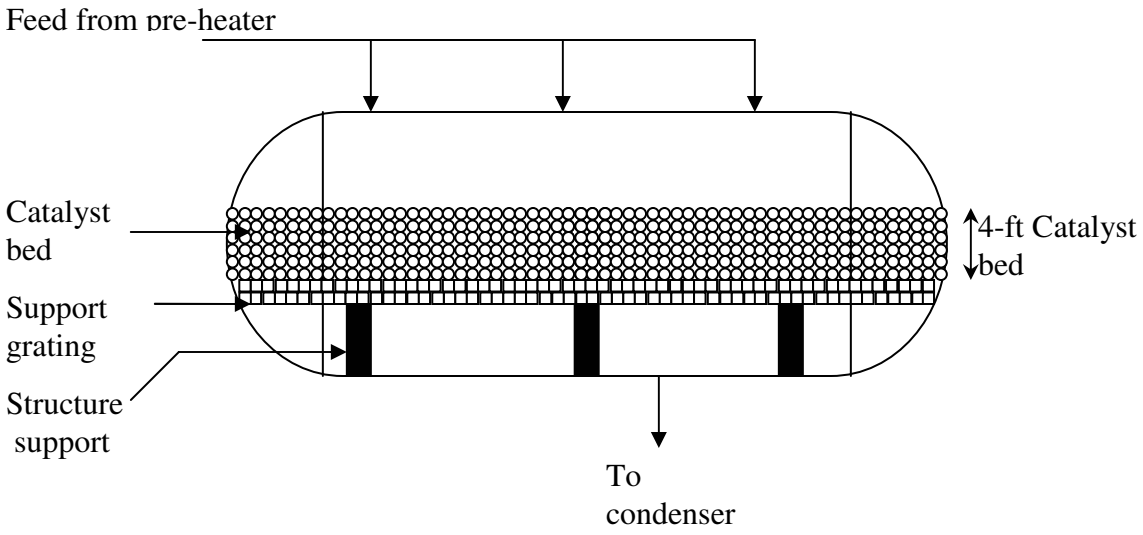

Figure 1.2: The layout of a Claus catalytic converter

A typical inlet gas feed to the converter has the following mole fraction composition:

Table 1.1: A Typical Feed Composition to the First Converter

Name of Component	**Feed composition (mass fraction)**	**Feed composition (mole fraction)**
Hydrogen	0.00018	0.003357
Argon	0.003043	0.002863
Nitrogen	0.1784	0.2394
Methane	0.0005165	0.00121
Carbon Monoxide	0.001193	0.001263
Carbon Dioxide	0.6453	0.5497
Ethane	0.000062	0.0001476
Hydrogen Sulfide	**0.06377**	**0.07063**
Water	0.04443	0.0927
Sulfur Dioxide	**0.06075**	**0.03564**
Carbon Disulfide	0.001141	0.0005636

The feed gas density is 1.261 kg/m^3 and the viscosity is 0.02475 centipoise. Usually the inlet temperature and pressure are known. Most of the contaminants in the feed gas such as hydrocarbons and ammonia are combusted in the furnace to produce CO_2 and H_2O from hydrocarbons and N_2 and H_2O from ammonia. A detailed discussion of the Claus process is presented in the next chapter. However, since the packed bed in the catalytic converter plays

a crucial role, a discussion of the significance of packed beds is presented in the following paragraphs.

In the chemical and petrochemical industry, packed beds can be found in diverse applications, and are used as reaction, separation or purification units. Fluid flow plays a significant role in these operations. Successful reaction engineering crucially depends on the ability to understand and control the fluid dynamics and mixing occurring in the industrial reactor. Therefore a good understanding of flow behavior and flow distribution is often crucial for proper design and operation of the equipment such as packed and unpacked reactors. However, detailed knowledge of the flow is rather limited mainly because most vessels are operated at high temperature and pressure, which makes measurements of velocities a difficult task.

Abbott and Basco [1989] investigated unsteady and three-dimensional flows that involve fluids that are to some degree compressible. In order to model the main flow features, many simplifying assumptions are usually made, such as assuming steady and incompressible flow. Complete understanding of the gas flow distribution in packed beds is of considerable practical importance due to its significant effect on transport and reaction rates. In this study, the flow in a Claus process catalytic converter is examined using Computational Fluid Dynamics (CFD).

CFD offers the possibility of predicting the detailed flow distribution in the reactor under different geometrical and operating conditions. It also allows the inclusion of different types of reaction models. Over the last three decades, CFD has undergone a rapid transformation and is nowadays an integral part of research related to fluid flow, chemical reactions, and heat and mass transfer. CFD is now well established for single-phase flow

problems and problems involving chemical reactions and is gaining a widespread recognition for solving multiphase flow problems. CFD can model chemical reactions including a) gas phase reactions b) surface reactions in which the reaction occurred at the solid boundary (wall) and c) surface reactions in which the reaction occurs at a surface of a discrete-phase particle.

1.2 Objectives of the work

The objectives of the present work may be summarized as follows:

1. Develop three-dimensional numerical models that predict flow in a partially packed vessel. The dimensions and the geometry of the vessel correspond to those of an industrial sulfur converter.
2. Validate qualitatively the model against some published data of flow in packed beds.
3. Include heat transfer calculations into flow model.
4. Include chemical reactions into the flow model.

Chapter 2

Literature Review

2.1 Introduction

This study is concerned with the flow distribution in a catalytic converter, which is used in the Claus process. This converter is a partially packed vessel. Therefore the literature will be surveyed for the flow in unpacked vessels, flow in packed beds and chemical reactions involved in the catalytic converter. Gas flow through packed beds is commonly encountered in industrial applications involving mass or/and momentum transfer both with and without chemical reaction. A complete understanding of the gas flow distribution in packed beds is of considerable practical importance due to its significant effect on transport and reaction rates. This flow is simulated using Computational Fluid dynamics (CFD). CFD can be applied with confidence to solve a variety of single-phase flow problems. CFD encompasses the numerical solution of the equations of mass, momentum, and energy conservation in a flow-geometry of interest. Equations accounting for turbulence quantities, chemical species present in the flow and the dynamics of the flow in porous media (packed bed) are also solved.

In recent years, CFD started to deal with reaction kinetics in both single and multiphase flow species. These calculations help to identify possible problems occurring in existing systems and provide useful insights in the operation of industrial processes. Furthermore, once they are accepted as a reasonably accurate description of the process in a reactor, CFD models can be used for scale up, re-design and troubleshooting.

There has been an extensive research in the area of single-phase flow applications in stirred tanks, packed bed reactors, polymeric flows and chemically reactive flows. The

following sections discuss the highlights of investigations in single-phase flow modeling and reaction kinetics modeling using CFD for a partially packed Claus sulfur converter.

2.2 Single-Phase Flow

The single-phase flow is by far the most common phenomena in day-to-day life, from the simple flow of water through a tap to many complex industrial operations. For single-phase isothermal systems involving laminar flows the conservation equations (Continuity and Navier-Stokes) are firmly established by Bird *et al.* [1960]. For the closure of the continuity and the Navier-Stokes equations, an equation for the density is required. For non-isothermal systems, the transport equations have to be supplemented with a thermal energy equation whereas for systems involving chemical conversion, species conservation equations (reaction rates) have to be added.

The present study involves the simulation of a single-phase highly turbulent flow with chemical reactions, in a partially packed vessel. The papers reviewed in this sections are somewhat related to the type of flow of interest or to some concepts that are of interest in this study such as operations of industrial vessels.

Single-phase flow modeling using CFD has been extensively applied to systems involving 1) laminar flow in complex geometry, 2) turbulent flows, 3) flow with complex rheology, and 4) fast chemical reactions [Kuipers and Swaaij, 1997]. CFD simulations of flow in baffled stirred tank reactors (BSTRs) are described because they provide a supplement to the poorly established scale-up criteria that are traditionally used to design reactors in conjunction with the results of laboratory or pilot scale tests. The first two-dimensional CFD simulation in BSTRs was carried out by Harvey and Greaves [1982]. The overall flow patterns obtained in these simulations were in encouragingly good agreement

with experiments and paved the way for further developments of BSTR modeling using CFD.

Harris *et al.* [1996] reported results of single-phase CFD simulations of industrial scale BSTRs. They carried out three-dimensional simulation of stirred tanks and found good agreement with experimental work. They concluded that simulation predictions for mean velocities and turbulence quantities are still not entirely satisfactory, even for single-phase non reacting flows.

Harris *et al.* [1996] also carried out single-phase CFD simulation for non-Newtonian, non-isothermal flow (polymeric flow) in an extruder. CFD modeling was successful in optimizing the extrusion process by improving the residence time distribution of the fluid so as to avoid hot spots, which caused polymer degradation. Mier *et al.* [1999] presented numerical results for single and multiphase flows using staggered and collocated grids in the finite volume methods for developing turbulent single-phase flow at the entrance of a tube and considered as a incompressible flow. They analyzed the converged rate, the stability of the pressure-velocity coupling, and the dependence of the solution on the grid size and the capability to reproduce the experimental data and/or analytical solutions. The numerical results were in a good agreement with experimental data.

Another critical issue in single-phase flow modeling is the behavior of the jets. Lane [1981] presented a detailed account of the jet behavior in tanks. A jet is either laminar or turbulent depending on the jet Reynolds number. Lane [1981] gave the ranges of the jet Reynolds number for characterizing whether a jet is laminar or turbulent. In this investigation, since the inlet velocity is very high (57 m/s), the jets are turbulent. The jet expansion plays a crucial role in the flow distribution pattern. Turbulent jets have a lower

expansion angle than laminar jets. The cone angel of the jet gives an indication of the jet expansion. The cone angles for the turbulent jets that have been reported in literature vary between 8 and 20^0. If the angle of spread or expansion were more, it would be beneficial as it can reduce the size of low velocity zones between adjacent jets.

In summary, single-phase turbulent flow has been widely studied using CFD. Simulation results have been validated for many complex flows and geometries including multiphase flows and flow of non-Newtonian fluids. Therefore the simulation of the flow in the unpacked part of the vessel in the present study is expected to match the actual flow with a high degree of confidence.

2.3 Flow through Packed Beds

Fluid flow through packed beds is commonly encountered in industrial applications involving mass and heat transfer both with and without chemical reactions. In chemical engineering processes, packed beds are frequently used as catalytic reactors, filters or separation processes like absorption, adsorption and distillation. Packed beds are extensively used in petroleum, petrochemical and biochemical applications. In the design of these devices, fluid dynamics plays an important role, since the transport of the chemical species, mixing or contacting catalytic surfaces, is entirely described by the conservation laws. Complete understanding of the fluid flow distribution in packed bed is of considerable practical importance due to its significant effect on transport and reaction rates.

Flow modeling in packed beds is a challenging task because of the difficulty of incorporating the complex geometry (e.g., tortuous interstices) into the flow equations and the difficulty in accounting for the interactions in the presence of complex contacted between the fluid-particle contacting [Jiang *et al.* 2000].

CFD can be used to model a wide variety of flows through porous media, including flow through packed beds, perforated plates, flow distributors and tube banks. In one type of modeling, a zone is defined in which the porous media model is applied and the pressure loss in the flow is determined via user-defined inputs. Heat transfer through the medium can also be represented; subject to the assumption of thermal equilibrium between the mediums. Typically a porous media model incorporates an empirically determined flow resistance in a region of the model defined as porous. A porous media model is nothing more than an added momentum sink to the governing momentum equations.

Quantitative understanding of flow nonuniformities in packed beds is of considerable practical importance in chemical reaction engineering. Szekely and Poveromo [1975] investigated the flow mal-distribution which may occur due to spatially variable resistance to flow, as brought about by variable porosity or particle diameter. Non-uniformities of flow will also occur when the fluid passing through the system is introduced in non-uniform manner. The significance of Szekely's work is to provide direct experimental verification for the differential, vectorial form of the Ergun equation which should provide a sound starting point for representing more complex problems where flow mal-distribution may be accompanied by heat and mass transfer.

In industrial packed beds, some non-uniformities either due to presence of internal structures [Berninger and Vortemeyer, 1987] or due to irregular gas inlet design [Szekely and Poveromo, 1975] could cause the flow not to be one dimensional and gas velocity vary in both radial and axial direction. Jiang *et al.* [2002] simulated single-phase flow in a bed scale. The Ergun equation to describe the pressure drop velocity relation at the cell level was

successfully used to describing flows in packed beds for a wide range of Reynolds numbers, fluid densities and velocities.

Delmas and Froment. [1988] and Daszkowski and Eigenberger [1992] showed that reaction and radial heat transfer can only be modeled correctly if the non uniformities of the bed structure are properly accounted for. A number of studies investigated the radial variation of the axial gas velocity in packed beds. Lerou and Froment [1977], McGreavy *et al.* [1996] and Bey and Eigenberger [1997] included axial velocity measurements at various radial positions, and measurement of radial porosity profiles. Ziolkowska and Ziolkowski [1993], Johnson and Kapner [1990] included the modeling of the radial variation of axial velocity. Berninger and Vortemeyer [1987] noted that in industrial packed beds, some nonuniformity due to the presence of internal structures or due to irregular gas inlet design. In general, three types of mathematical models have been developed for the treatment of non-parallel gas flow in packed beds. They are:

1) The vectorized Ergun equation model

2) The equations of motion model

3) The discrete cell model (DCM)

The Vectorized Ergun equation model is based on the assumption that a packed bed can be treated as a continuum. The model utilizes the empirical Ergun equation, which holds well for overall pressure drop in the macroscopic beds with unidirectional flow, for an infinitesimal length of the bed and applied in the direction of the flow. Berninger and Vortemeyer [1987], Szekely and Poveromo [1975], Stanek and Szekely [1974] utilized this method to model two- and three-dimensional flow in packed beds. Factors determining the energy loss in the packed beds due to large pressure drops and some of them are not

susceptible to complete and exact mathematical solutions. Ergun [1952] established that the total energy losses in the fixed bed are the sum of viscous and kinetic energy losses.

The statement of the Ergun equation in a vectorial form is presented by Stanek and Szekely [1974] for three-dimensional flow of fluids through packed beds having a spatially variable resistance to flow. They calculated flow mal-distribution in packed beds, and that was thought to be a necessary first step in the representation of hot spot formation and flow non-uniformities in packed bed reactors.

In many practical applications, the unsteady state and convection terms in the momentum equation may be neglected. In this case the reduced momentum equation and therefore, it may be considered as a generalized form of Darcy's law. Since the effective permeability is a function of the microscopic Reynolds number, this generalized form of Darcy's law describes both Stokes flow and non-Stokes flow in porous media [Teng and Zhao 2000].

The equations of motion model, solves the mass and momentum conservation equations for the flowing phase provided the solid boundaries are precisely specified. Such a direct numerical simulation (DNS), however, is beyond reach at present for large industrial-scale packed beds. By employing the effective-viscosity as an adjusting factor, Ziolkowska and Ziolkowski [1993] and Bey and Eigenberger [1997] developed a mathematical model for interstitial velocity distribution.

Another possibility of modeling packed bed reactors involves the use of the Discrete Cell Model (DCM). Jiang *et al.* [2000] approach which is based on the concept that the packed bed may be represented by a number of inter-connected discrete cells with the bed porosity allowed to vary in two-directions from cell to cell. The fluid flow is assumed to be

governed by the minimum rate of total energy dissipation in the packed bed (i.e. flow follows the path of least resistance). It is assumed that the Ergun equation is applicable at the cell scale. Therefore, the solution for velocity at each cell interface can be achieved by solving the non-linear multivariable minimization problem.

Fluid flow between particles in packed beds is characterized by a random packing geometry, high turbulence and strong velocity fluctuations. Any realistic flow model must therefore be based on some averaging assumptions. One generally accepted procedure by Bey and Eigenberger [1997] is to assume angular symmetry (in case of cylindrical coordinate system) of the flow profile and to consider a continuous distribution of the void fraction in the packing. Then any fluid flow will create continuously distributed interstitial velocity. The flow can be described by the Navier-Stokes equations if additional terms of fluid particle interactions are incorporated. Vortmeyer and Schuster [1983] proposed the application of the extended Brinkman equation where the fluid-particle interactions are described by a two-dimensional Ergun pressure correlation and the fluid wall friction is separately taken into account. This allows the application of a no-slip boundary condition at the wall where the void fraction approaches unity. The conceptual difficulty is that the fluid-wall friction affects the flow profile only in the immediate vicinity of the wall, whereas inside the packing, the Ergun pressure drop, describing fluid-particle interaction, is far dominating.

Vortmeyer and Schuster [1983] have used this variation approach to evaluate the steady two-dimensional velocity profiles for isothermal incompressible flow in rectangular and cylindrical packed beds. They used the continuity equations, Brinkman's equation and a semi empirical expression for the radial porosity profile in the packed bed to compute these profiles. Their results showed that significant preferential wall flow occurs in cases where the

ratio of channel diameter and particle diameter becomes significantly small. Although their study was done for an idealized solution, it laid the foundation for more detailed studies. The momentum equations for interstitial velocity were used assuming laminar viscosity. Bey and Eigenberger [1997] used the increased "turbulent viscosity" which accounts for highly turbulent interstitial flow. They took measurements outside the fixed bed behind a monolith of the fluid shifts from the region near the wall to the center. When the comparison was carried out between measured velocity profiles outside the bed with simulations, they concluded that these changes have to be taken into account. These researchers used a two-dimensional model containing the continuity equation and the momentum balance equations in the radial and axial directions. The momentum balances are composed of Ergun equation and of shear stress and inertia effects.

In this investigation the approach of Bey and Eigenberger [1997] has been used, but model equations are for a cartesian coordinate system instead of the cylindrical system used by them. The pressure drop in packing has been evaluated by the well-established correlation of Ergun [1952] wherein factors determining the (energy loss) pressure drop in packed beds should be considered. These factors are: 1) the rate of fluid flow, 2) the viscosity and density of the fluid, 3) the closeness and orientation of the packing, and 4) the size, shape, and surface of the particles. The first two variables concern the fluid while the last two the solids. In this investigation, the first two variables have been considered for modeling the pressure drop through the packed bed while the values of the other two factors are assumed to remain constant.

Zughbi and Sheikh [2002] developed a two-dimensional model of flow in a packed vessel. Their finding shed some light on flow distribution in such vessel. However, due to a

number of severe simplifications that were used in it, the simplified model is unable to predict flow in a three-dimensional vessel.

2.4 Reactions in Packed-bed Reactor (Claus Converter)

The increasingly stringent standards for sulfur emissions that are being imposed upon the petroleum and natural gas processing industries around the world are putting unprecedented pressure on those industries. Complying with those sulfur standards is expected to require a significant amount of capital spending. On the positive side, a variety of more efficient methods, based on the conventional Claus process, are now available to the industry. These methods overcome thermodynamic equilibrium limitations of the Claus reactions, thereby enhancing sulfur recovery, and they can be incorporated into a conventional Claus plant.

The modified Claus process is used to recover elemental sulfur from hydrogen sulfide present in gases from refineries, and natural gases. A wide range of catalysts dedicated to sulfur recovery and based on the Claus process are available. According to Larraz [1999] the most widely used Claus catalyst in sulfur recovery units is spherical activated alumina. Properties associated with optimum non-promoted activated Claus catalyst include high surface area, appropriate pore size distribution and enhanced physical properties. These catalysts provide the necessary sites to catalyze the conversion of H_2S and SO_2 to elemental sulfur.

The Claus recovery unit generally consists of two distinct sections: the thermal (front-end) section, from the inlet up to the waste heat boiler and condenser, and the catalytic (back end) sections, downstream of the condenser as shown in Figure 1.1. According to Chen *et al.* [2002], the characteristics of the acid-gas feed, such as H_2S concentration, mainly determine

the configuration of the thermal section, while the desired sulfur recovery efficiency generally dictates the selection of the processes used in the back-end section, which also include tailgas treatment. About 60% of the hydrogen sulfide gets converted in the thermal section and the balance in the catalytic stage.

Monnery *et al.* [2000] modeled the reaction kinetics in the furnace by carrying out an experimental study and also a study of a sulfur plant Claus furnace to obtain kinetic data and model it using a simple reaction kinetic rate expression. They developed accurate kinetic data and a subsequent rate expression for the Claus reaction in the furnace and also validated their data against the work of Howboldt *et al*. [2002].

The reaction of H_2S and SO_2 is endothermic under the conditions of the Claus furnace and exothermic under the conditions of the catalytic converters. Temperature is a critical parameter of these exothermic processes in which conversion increases as temperature decreases, but obviously the temperature cannot be lowered below the sulfur dew point, since that it would plug the pores and, presumably, deactivate the catalyst

If the reaction temperature is lower than the sulfur melting point ($<119^0$C) high conversions of SO2 should be achieved and the reaction could be useful for the elimination of SO_2 from the gas effluent. However sulfur deposited on the solid phase will, probably, deactivate the catalyst suddenly and may cause diffusion problems. Some of these problems have been predicted theoretically by Razzaghi *et el.* [1978] through simple models based on kinetic and deactivation equations, though these equations have not been tested experimentally.

Chen *et al.* [2002] proposed two common ways to increase sulfur recovery beyond the standard 98%. These are achieved by adding on a tailgas-treatment unit, or by enhancing

the performance of the catalytic sections. The first approach generally involves the addition of a hydrogenation section, followed by a selective amine treatment, down-stream from the Claus unit. The catalytic section enhancement improves recovery by employing special oxidation and reduction catalyst, or operating the Claus converters under sub-dew point conditions.

Jaree *et al.* [2001] showed that when a packed-bed reactor is perturbed by an external input such as the inlet temperature or concentration, there is a decoupling of heat and mass waves as result of a difference in propagation velocities of heat and mass waves as result of differential flow instability. They also referred to this decoupling as differential flow instability in unsteady-state operations.

In the past several decades, approaches based on residence-time distribution (RTD), together with macro-mixing and micro-mixing models have been a primary tool in reactor modeling used to characterize the nonideal flow pattern and mixing in reactors without solving the complete velocity field [Levenspiel, 1972]. The disadvantages of such approaches are that they cannot be adopted well to serve as a diagnostic tool for operating units. Trambouze [1993], Kuipers and Swaaij [1998] proposed that to improve these reactor models, one has to solve the complete multidimensional flow equations coupled with chemical species transport, reaction kinetics, and kinetics of phase change. Fortunately Computational Fluid Dynamics (CFD) has made great progress during the last few years, and can now be applied to chemical processes.

The literature survey for the present investigation can be summarized in the following tables.

Table 2.1: Single-Phase Flow

Investigators	Year	Technique Used
Abid *et al.*	1992	Experimental and CFD
Wang and Andrews	1995	CFD
Harris *et al.*	1996	CFD
Mier *et al.*	1999	Experimental & CFD

Table 2.2: Flow through Packed Beds

Investigators	Year	Technique Used
Ergun	1952	Experimental
Stanek and Szekely	1974	Theoretical & Simulation
Szekely and Poveromo	1975	Experimental & Simulation
Lerou and Froment	1977	Experimental
Vortmeyer and Schuster	1983	Simulation
McGreave *et al.*	1983	Experimental
Delmas and Froment	1988	Experimental & Simulation
Daszkowski and Eigenberger	1992	Theoretical & Simulation
Bey and Eigenberger	1997	Experimental & Simulation
Jiang *et al.*	2000	CFD and DCM

Teng and Zhao	2000	Experimental
Zughbi and Sheikh	2002	CFD
Jiang *et al.*	2002	CFD & DCM

Table 2.3: Reaction in Packed Beds Reactor (Claus Converter)

Investigators	Year	Technique Used
Razzaghi *et al.*	1978	Theoretical
Alaverz *et al.*	1996	Catalyst property & Experimental
Larraz	1999	Theoretical & Experimental
Monnery *et al.*	2000	Reaction Kinetics
Jaree *et al.*	2001	Experimental
Chen *et al.*	2002	Theoretical
Jiang *et al.*	2002	Experimental & Simulation

From the above extensive literature review, it can be concluded that the importance of the uniform flow distribution had been recognized for a long time, but all the investigations were attempted for lab scale models and there is a scarcity of data for large industrial scale vessel such as the one considered in this investigation. The $\kappa - \varepsilon$ turbulence model is the most widely used for turbulence modeling and it is used in this investigation. Lastly the modified Ergun equation is the most popular equation for analyzing flow through packed beds and the same is used in simulating flow through packed beds.

2.5 Proposed Work

The proposed work is prepared in view of a need by the local industry to address problems faced while operating sulfur converters. At the end of a run, a part of the catalyst in the bed is deactivated while a significant part is underused and is not adequately utilized. This is a problem that has serious economical implications.

The full extent of the problem is rather complex and includes flow in a partially packed vessel, heat transfer, and chemical reactions. Sheikh and Zughbi [2002] worked to investigate the flow in both cases of unpacked and packed vessels. However, due to a number of simplifications that were used in it, the simplified model is unable to predict flow in a three-dimensional vessel. The most limiting of the simplification of their study is the two-dimensionality of the model, as the flow inside the actual vessel is not axi-symmetric and cannot be approximated by a two-dimensional model. Their model did not account for chemical reactions.

For a partially packed vessel, a rigorous model of the flow needs to be developed to better understand the problem. The bed is expected to act as a distributor for the flow. The question remains as to how a good distributor the packed (catalyst) bed will be. That is why a detailed flow model using Computational Fluid Dynamics (CFD) is needed. In this study a general purpose three dimensional CFD package, FLUENT, is used to carry out the simulations and the effects of chemical reactions and heat transfer are also simulated.

Chapter 3
Mathematical Formulation

3.1 Introduction

Numerical simulation of flow in a vessel, involves formulation of governing transport equation, and the necessary constitutive and closure equations and formulation of appropriate boundary conditions. It also involves the selection of a suitable computer code to solve the governing equations. Validation of simulation results is highly desirable. These aspects are discussed in the following sections.

3.2 Mathematical Formulation of Single-Phase Flow

The vessel of interest is cylindrical in shape, however, the CFD package used, allows the usage of Cartesian coordinates to represent such geometry. Therefore the equations will be presented in Cartesian coordinates. The problem investigated is three-dimensional. The flow is considered to be incompressible in this study. The simulations are carried out under steady state conditions; therefore the time dependent terms are not included in the governing equations.

The single-phase flow is governed by the conservation laws of mass, momentum and energy which can be expressed as:

The mass conservation (continuity equation):

$$\nabla . \underset{\sim}{v} = 0 \tag{3-1}$$

The momentum conservation equation (Navier-Stokes equation):

$$\rho(\underset{\sim}{v} . \nabla \underset{\sim}{v}) = -\nabla p + \mu \nabla^2 \underset{\sim}{v} + \rho \underset{\sim}{g} \tag{3-2}$$

The energy conservation equation:

$$\rho \hat{C}_p \left(\vec{v} . \nabla \vec{T} \right) = k \nabla^2 \vec{T} + \mu \phi_v \tag{3-3}$$

where

$$\phi_v = 2\left(\nabla^2 \vec{v}\right) + \left(\frac{\vec{\tau}}{\mu} \right)^2 - \frac{2}{3} \left(\nabla . \vec{v} \right)^2 \tag{3-4}$$

all the terms in the above equations are considered. The energy equation is only solved for cases where the chemical reactions are also considered.

3.3 Boundary Conditions

In setting up a flow-simulation it is crucial to correctly specify the proper boundary conditions. In particular, it involves the specification of convective and diffusive fluxes at the flow domain. In this study the inlet condition corresponds to the flow conditions. In FLUENT, defining an inlet condition means specifying the cells through which the fluid is introduced, the velocities (x-, y-, and z-direction), and the pressure (mass flux-specification). This means that the velocity normal to the face of each inlet is set equal to a constant value specified by the gas feed rate.

An outlet condition refers to the physical conditions at the flow exit. The specification involves the location of cells, which are desirable to keep open, and the exit pressure. Mathematically this is represented by setting the pressure gradient over the last two rows of cells across the outlet face to zero.

Wall conditions are also required to be specified for a complete description of the boundary conditions. For this study, a general no-slip condition is imposed on all solid walls. These are the boundary conditions required to solve the case of isothermal flow.

3.4 Mathematical Formulation for Packed Bed Flow

The steady state continuity equation for an incompressible fluid in packed beds region is:

$$0 = \nabla.(\theta \vec{v}) \tag{3-5}$$

where the void fraction θ and the velocity v are assumed to be continuously varying functions.

In Cartesian coordinates, v_x, v_y and v_z are the dependent variables, the steady state continuity equations can be written as:

$$0 = \frac{\partial(\theta v_x)}{\partial x} + \frac{\partial(\theta v_y)}{\partial y} + \frac{\partial(\theta v_z)}{\partial z} \tag{3-6}$$

The stationary momentum balances are formulated according to Bey and Eigenberger [1997] as:

$$0 = -\rho[\nabla \theta . \vec{v}\vec{v}] - \nabla \theta p + [\nabla \theta \vec{\tau}] - \theta \rho \vec{g} + \vec{F} \tag{3-7}$$

where $\vec{F}$ is the pressure drop and it is model dependent source terms for porous media.

In Cartesian coordinate system the definition of the ∇ operator is:

$$\nabla = \hat{i}\frac{\partial}{\partial x} + \hat{j}\frac{\partial}{\partial y} + \hat{k}\frac{\partial}{\partial z} \tag{3-8}$$

$$\vec{v}.\vec{v} = \left(v_x \hat{i} + v_y \hat{j} + v_z \hat{k}\right).\left(v_x \hat{i} + v_y \hat{j} + v_z \hat{k}\right) \tag{3-9}$$

which can be expanded to:

$$\vec{v}.\vec{v} = \left(v_x^2 \hat{i}\hat{i} + v_x v_y \hat{i}\hat{j} + v_x v_z \hat{i}\hat{k}\right) + \left(v_y v_x \hat{j}\hat{i} + v_y^2 \hat{j}\hat{j} + v_y v_z \hat{j}\hat{k}\right) + \left(v_z v_x \hat{k}\hat{i} + v_z v_y \hat{k}\hat{j} + v_z^2 \hat{k}\hat{k}\right) \tag{3-10}$$

Thus $\nabla.(\theta \vec{v}.\vec{v})$ can be written as:

$$\nabla.(\theta\rho\vec{v}\vec{v}) = \frac{\partial\left(\theta v_x^2\hat{i} + \theta v_x v_y\hat{j} + \theta v_x v_z\hat{k}\right)}{\partial x} + \frac{\partial\left(\theta v_y v_x\hat{i} + \theta v_y^2\hat{j} + \theta v_y v_z\hat{k}\right)}{\partial y}$$

$$+ \frac{\partial\left(\theta v_z v_x\hat{i} + \theta v_z v_y\hat{j} + \theta v_z^2\hat{k}\right)}{\partial z} \tag{3-11}$$

Also: $$\nabla\vec{p} = \frac{\partial p}{\partial x}\hat{i} + \frac{\partial p}{\partial y}\hat{j} + \frac{\partial p}{\partial z}\hat{k} \tag{3-12}$$

$$\nabla.\theta\vec{\tau} = \theta\left(\tau_{xx}\hat{i}\hat{i} + \tau_{xy}\hat{i}.\hat{j} + \tau_{xz}\hat{i}.\hat{k} + \tau_{yx}\hat{j}.\hat{i} + \tau_{yy}\hat{j}.\hat{j} + \tau_{yz}\hat{j}.\hat{k} + \tau_{zx}\hat{k}.\hat{i} + \tau_{zy}\hat{k}.\tilde{j} + \tau_{zz}\hat{k}.\hat{k}\right) \tag{3-13}$$

The various shear stresses in terms of the velocity gradients and the fluid properties for Newtonian fluids are given by Bird *et al.* [2002]:

$$\tau_{xx} = -\mu\left[2\frac{\partial v_x}{\partial x}\right] \tag{3-14}$$

$$\tau_{xy} = \tau_{yx} = -\mu\left[\frac{\partial v_x}{\partial y} + \frac{\partial v_y}{\partial x}\right] \tag{3-15}$$

$$\tau_{yy} = -\mu\left[2\frac{\partial v_y}{\partial y}\right] \tag{3-16}$$

$$\tau_{yz} = \tau_{zy} = -\mu\left[\frac{\partial v_y}{\partial z} + \frac{\partial v_z}{\partial y}\right] \tag{3-17}$$

$$\tau_{zz} = -\mu\left[\frac{\partial v_z}{\partial z}\right] \tag{3-18}$$

$$\tau_{zx} = \tau_{xz} = -\mu\left[\frac{\partial v_x}{\partial z} + \frac{\partial v_z}{\partial x}\right] \tag{3-19}$$

3.5 Pressure Drop Correlations for Packed Bed

Flow in porous media are modeled by the addition of a momentum source term to the standard fluid flow equations. The source term is composed of two parts, a viscous loss term

(the first term on the right-hand side of Equation (3-23), and an inertial loss term (the second term on the right-hand side of Equation (3-23). This source term can be written as:

$$\vec{F} = \sum_{j=1}^{3} D_{ij}\mu v_j + \sum_{j=1}^{3} C_{ij}\frac{1}{2}\rho|v_j|v_j \tag{3-20}$$

where $\vec{F}$ is the source term for the (*x*-, *y*-, or *z*-) momentum equation, and *D* and *C* are prescribed matrices. This momentum sink contributes to the pressure gradient in the porous cell, creating a pressure drop that is proportional to the fluid velocity (or velocity squared) in the cell.

To recover the case of simple homogeneous porous media, $\vec{F}$ can be written as (FLUENT manuals):

$$\vec{F} = -\left(\frac{\mu}{\alpha}v_i + C_2\frac{1}{2}\rho|v_i|v_i\right) \tag{3-21}$$

where α is the permeability and C_2 is the inertial resistance factor, *D* and *C* are specified as diagonal matrices with $\frac{1}{\alpha}$ and C_2, respectively, on the diagonals (and zero for the other elements).

Laminar flow in porous media can be successfully modeled by Darcy's law, which can be mathematically stated as

$$\Delta P = \frac{-\mu}{\alpha}\vec{v} \tag{3-22}$$

where α is the permeability and $\vec{v}$ is the superficial velocity. If the flow is such that the inertial loss term cannot be neglected, then the source terms must be calculated using the modified Ergun equations as explained in this section.

The flow in the bed of the partially packed vessel considered in this study may or may not be in the laminar regime. The Reynolds number for a packed bed is defined as:

$$\mathrm{Re} = \frac{D_p v_y \rho}{(1-\theta)\mu} \tag{3-23}$$

where D_p the particle diameter, θ is porosity, and v_y is the velocity.

Ergun [1952] found that the pressure drop through the granular bed is proportional to the fluid velocity at low flow rates, and approximately to the square of the velocity at high flow rates. Ergun also found that for pressure drops in fixed bed, the total energy losses can be treated as the sum of viscous and kinetic energy losses. In turbulent flows, packed beds are modeled using both permeability and an inertial loss coefficient. The Ergun equation, a semi-empirical correlation applicable over a wide range of Reynolds numbers and for many types of packing can be written as:

$$\frac{|\Delta P|}{L} = \frac{150\mu}{D_p^2}\frac{(1-\theta)^2}{\theta^3}\vec{v} + \frac{1.75\rho}{D_p}\frac{(1-\theta)}{\theta^3}|\vec{v}|\vec{v} \tag{3-24}$$

when modeling laminar flow through a packed bed, the second term in the above equation may be dropped. In this equation, μ is the viscosity, L is the bed depth, D_p is the mean diameter of the catalyst, and θ is the porosity. The permeability α (viscous resistance) and inertial loss coefficient C_2 (inertia resistance) in each component direction may be identified as follows:

$$\alpha = \frac{D_p^2}{150} \frac{\theta^3}{(1-\theta)^2} \tag{3-25}$$

and

$$C_2 = \frac{3.5}{D_p} \frac{(1-\theta)}{\theta^3} \tag{3-26}$$

These values of α and C_2 are used in Equation (3-24) to obtain the value of $\vec{F}$ which in turn is used in the momentum equations as the additional sink term to account for the additional pressure drop in a packed bed.

3.6 Boundary Conditions for the Partially Packed Vessel

The same boundary conditions specified in section 3.3 for the unpacked vessel are also used for the packed vessel.

Additional boundary conditions are needed at the bottom and the top faces of the packed bed. The velocity at every cell of the bottom face of the packed bed is taken from the adjacent unpacked cell. A similar condition is applied at the top face where the velocity calculated for the top packed cell is used as a boundary value for the adjacent unpacked cell.

Bed characteristics such as the size of the catalyst particles and the void fraction are used in this study.

3.7 Modeling of Turbulence

The Navier-Stokes equations describe flow under laminar and turbulent regimes. However, because of the existence of an extremely wide range of length and time scales in turbulent flows, the computational resources required for the exact numerical simulation of turbulent flows is prohibitively high. For most engineering applications, it is still necessary to use turbulence models along with time-averaged Navier-Stokes equations. The cautious

application and interpretation of turbulence models have proved to be a valuable tool in engineering research and design, despite their physical deficiencies.

No single turbulence model is universally accepted as being superior for all classes of problems. The choice of a turbulence model depends on considerations such as the physics encompassed in the flow, the level of accuracy required and availability of computational resources. To make the most appropriate choice of a model for an application, one needs to understand the capabilities and limitations of the various options.

The computational effort and cost in terms of CPU time and memory for each turbulence model is discussed. While it is impossible to state categorically which model is best for specific application, general guidelines are available in the literature to help one chooses the appropriate turbulence model for the flow you want to model. The turbulence models most commonly used can be summarized in the following subsections:

3.7.1 The zero Equation Models

These include constant eddy viscosity and constant Prandtl mixing length models. These are early models and they are not available any more in most CFD packages.

3.7.2 The One- Equation Models

There is a one-equation model known as Spalart-Allmaras model, available in FLUENT. But it is not suitable for the present applications and consequently will not be discussed in details.

3.7.3 The Two-Equation Turbulence Models

The two equation turbulence models include the standard $\kappa-\varepsilon$ model, the Renormalization Group (RNG) $\kappa-\varepsilon$ model and the Realizable $\kappa-\varepsilon$ model, the $\kappa-\omega$

model and the Reynolds Stress model (RSM). Although, the Reynolds-averaged Navier-Stokes (RANS) equations represent transport equations for the mean flow quantities only with all the scales of the turbulence being modeled. The approach of permitting a solution for the mean flow variables greatly reduces the computational effort. If the mean flow is steady, the governing equations will not contain time derivatives and a steady-state solution can be obtained economically. The Reynolds-averaged approach is generally adopted for practical engineering calculations.

3.7.3.1 The Standard $\kappa-\varepsilon$ Turbulence Model

The most common approach to determine the kinetic energy of turbulence κ and its dissipation rate ε is to solve transport equations for these quantities in parallel with the solution of the mean momentum equations. In symbolic forms the equations may be written as:

$$\frac{D\kappa}{Dt} = d_\kappa + P_\kappa + G_\kappa - \varepsilon \tag{3-27}$$

$$\frac{D\varepsilon}{Dt} = d_e + c_{\varepsilon 1} + \frac{\varepsilon}{\kappa}\left(P_\kappa + G_\kappa\right) - c_{\varepsilon 2}\frac{\varepsilon^2}{\kappa} + S_e \tag{3-28}$$

where d_κ, P_κ, and G_κ denote the rate of gain of κ at a point by diffusion and generation by mean strain and body forces. $c_{\varepsilon 1}$, $c_{\varepsilon 2}$ are the coefficients and have standard values (primary source/sink terms). In most cases, the secondary source/sink term S_e has been taken as zero. Habitually, the simple gradient form represents diffusive transport:

$$d_\varphi = \frac{\partial}{\partial x_j}\left(\frac{v_t}{\sigma_\varphi}\frac{\partial \varphi}{\partial x_j}\right) \tag{3-29}$$

where φ stands for κ or ε and the σ_φ are constants of order unity. While the κ equation may be regarded as exact, the ε transport equation rests on a dimensional analogy (with the κ equation). Standard values for the coefficients of the primary source and sink terms are $c_{\varepsilon 1} = 1.44$ and $c_{\varepsilon 2} = 1.92$.

The effects of turbulence on mean flow behavior is solved. The model relates the turbulent stresses $\overline{v_i v_j}$ and the average velocity gradient du / dx by a simple relationship:

$$\overline{v_i v_j} = \varepsilon \frac{\partial v_i}{\partial x_i} + \frac{\partial v_j}{\partial c_j} - \frac{2}{3} \kappa \delta_{ij} \tag{3-30}$$

where δ_{ij} is the Kroncker delta and κ is the turbulent kinetic energy.

By assuming isotropic turbulence, two dependent variables can be defined. The first is turbulent kinetic energy κ:

$$k = \frac{1}{2} \overline{v_i v_j} \tag{3-31}$$

and the second is the viscous rate of turbulent energy, ε:

$$\varepsilon = v \overline{v_{ij} v_{ij}} \tag{3-32}$$

The transport equations of these two variables follow the same form as other dependent variables as explained above. The turbulent viscosity μ_t is written as:

$$\mu_t = \rho C_\mu \frac{\kappa^2}{\varepsilon} \tag{3-33}$$

where C_μ is the parameter of the $\kappa - \varepsilon$ model.

3.7.3.2 Other $\kappa-\varepsilon$ Models

The RNG $\kappa-\varepsilon$ model was derived using a rigorous statistical technique (called renormalization group theory). It is similar in form to the standard $\kappa-\varepsilon$ model, but includes the following refinements:

The RNG model has an additional term in its ε equation that significantly improves the accuracy for rapidly strained flows. The effect of swirl on turbulence is included in the RNG model, enhancing accuracy for swirling flows.

- The RNG theory provides an analytical formula for turbulent Prandtl numbers, while the standard $\kappa-\varepsilon$ model uses user-specified, constant values.
- While the standard $\kappa-\varepsilon$ model is a high-Reynolds-number model, the RNG theory provides an analytically derived differential formula for effective viscosity that accounts for low-Reynolds-number effects. Effective use of this feature does, however, depend on an appropriate treatment of the near-wall region.

The realizable $\kappa-\varepsilon$ model is a relatively recent development and differs from the standard $\kappa-\varepsilon$ model in two important ways:

- The realizable $\kappa-\varepsilon$ model contains a new formulation for the turbulent viscosity.
- A new transport equation for the dissipation rate ε has been derived from an exact equation for the transport of the mean-square vorticity fluctuation.

The term ``realizable'' means that the model satisfies certain mathematical constraints on the Reynolds stresses, consistent with the physics of turbulent flows. Neither the standard $\kappa-\varepsilon$ model nor the RNG $\kappa-\varepsilon$ model is realizable.

3.7.3.3 The RSM Model

The Reynolds stress model (RSM) is the most elaborate turbulence model that **FLUENT** provides. Abandoning the isotropic eddy-viscosity hypothesis, the RSM closes the Reynolds-averaged Navier-Stokes equations by solving transport equations for the Reynolds stresses, together with an equation for the dissipation rate. This means that four additional transport equations are required in 2D flows and seven additional transport equations must be solved in 3D. The fidelity of RSM predictions is still limited by the closure assumptions employed to model various terms in the exact transport equations for the Reynolds stresses. The RSM might not always yield results that are clearly superior to the simpler models in all classes of flows to warrant the additional computational expense. However, use of the RSM is a must when the flow features of interest are the result of anisotropy in the Reynolds stresses. Among the examples are cyclone flows, highly swirling flows in combustors, rotating flow passages, and the stress-induced secondary flows in ducts.

3.7.4 The Large Eddy Simulation (LES) Model

LES provides an alternative approach in which the large eddies are computed in a time-dependent simulation that uses a set of ``filtered" equations. Filtering is essentially a manipulation of the exact Navier-Stokes equations to remove only eddies that are smaller than the size of the filter, which is usually taken as the mesh size. Like Reynolds averaging, the filtering process creates additional unknown terms that must be modeled in order to achieve closure. Statistics of the mean flow quantities, which are generally of most engineering interest, are gathered during the time-dependent simulation. The attraction of LES is that, by modeling less of the turbulence (and solving more), the error induced by the turbulence model will be reduced. One might also argue that it ought to be easier to find a

``universal" model for the small scales, which tend to be more isotropic and less affected by the macroscopic flow features than the large eddies.

3.7.5 The Direct Numerical Simulation

This solves directly all scales of turbulence. It requires extremely large computational power.

Based on the discussion in the previous sections, it can be seen that the simplest ``complete model" of turbulence is the two-equation models in which the solutions of two separate transport equations allow the turbulent velocity and length scales to be independently determined. The standard $\kappa-\varepsilon$ model in **FLUENT** falls within this class of turbulence model and has become the workhorse of practical engineering flow calculations in the time. Robustness, economy, and reasonable accuracy for a wide range of turbulent flows explain its popularity in industrial flow and heat transfer simulations. It is a semi-empirical model, and the derivation of the model equations relies on phenomenological considerations and empiricism.

Based on the above discussion, the governing equations in this investigation are formulated using the standard $\kappa-\varepsilon$ model.

3.8 Reaction Kinetics Modeling

In chemical engineering processes, packed beds are frequently used as catalytic reactors, filters or in separation processes like absorption, adsorption and distillation. Packed beds are extensively used in petroleum, petrochemical and biochemical applications. One process that uses a packed bed is the modified Claus process.

The modified Claus process is used to recover elemental sulfur from hydrogen sulfide present in gases from refineries, and natural gases. A wide range of catalysts

dedicated to sulfur recovery and based on the Claus process are available. Catalysts provide the necessary sites to catalyze the conversion of H_2S and SO_2 to elemental sulfur. The Claus reaction is:

$$2H_2S + SO_2 \rightleftharpoons \frac{3}{n}S_n + 2H_2O$$

The modified Claus process is the most common method for the conversion to sulfur of the hydrogen sulfide contained in sour oil and natural gas. As mentioned earlier, The Claus process consists of a furnace followed by three catalytic converters. The Kinetics of the reactions in the furnace are well studied. An important part of the Claus process is the kinetics of the reactions, that occurred in different units. Monnery *et al.* [2000] investigated the Claus furnace reaction rate expression by performing experiment on a laboratory scale set- up. The reaction rate expression is as follows:

$$r = A_f \exp^{E_{af}/RT} P_{H_2S} P_{SO_2}^{0.5} - A_r \exp^{E_{ar}/RT} P_{H_2O} P_{S_2}^{0.75} \qquad (3\text{-}34)$$

where

A_f = 15,762 mol.cm^{-3} s^{-1} atm$^{-1.5}$

E_{af} = 49.9 kcal mol^{-1}

A_r = 506 mol.cm^{-3} s^{-1} atm$^{-1.75}$

E_{ar} = 44.9 kcal mol^{-1}

P = the partial pressure.

The kinetics of the Claus reaction in the catalytic converter is not well studied. Professor Peter Clark has recently started investigating the kinetics of the Claus reaction in a catalytic converter.[a]

a. Professor Peter Clark, University of Alberta, Private communication, 2003

The only kinetic model found for the manufacturing of elemental sulfur that is used in this present studies that was developed by Abaskuliev *et al* [1990].

$$R(C,T) = 7.3919 * 10^4 \exp\left(\frac{-30594}{8.314T}\right) \frac{T^{1.5} C_{H_2S} C_{SO_2}^{0.5}}{\left(1 + 46.56 T C_{H_2O}\right)^2} \tag{3-35}$$

To apply this kinetic model for the laminar finite rate chemistry in FLUENT it needs further simplification. This simplification does not effect on the model. Since water concentration is very high, the 1 in the denominator can be neglected. After ignoring it, the model becomes simple and can be applied in FLUENT.

Following the simplification the model becomes:

$$R(C,T) = 34.0981 \exp\left(\frac{-30594}{8.3145T}\right) T^{-0.5} C_{H_2S} C_{SO_2}^{0.5} C_{H_2O}^{-2} \tag{3-36}$$

The Claus reaction is exothermic at converter temperatures, and the reaction is favored by lower temperatures. Process calculations for a Claus sulfur recovery unit are complicated by the existence of various species of gaseous sulfur (S_2, S_6 and S_8) whose equilibrium concentrations in reaction to each other are often not precisely known, and by a number of side reactions involving other feed gas components such as CO_2, hydrocarbons, ammonia, COS, CS_2 etc., which take place simultaneously. However, the concentrations of all these other components are low compared to those SO_2 and H_2S.

For calculating the equilibrium composition, the three reactions are simultaneously considered for the production of S_2, S_6 and S_8 respectively. At the low temperature Claus converter, most of the production is S_8 and S_6 with a trace of S_2. For this case the temperature exponent has a significant effect on getting the exact solution of the simulation result. Based

on experimental data it is found that for the production of S_2, S_6 and S_8, the suitable temperature exponents that match the experimental data are -0.7, -0.5 and -0.4 respectively.

$$R(C,T) = 34.0981 \exp\left(\frac{-30594}{8.3145}\right) T^{-0.7} C_{H_2S} C_{SO_2}^{0.7} C_{H_2O}^{-2} C_{S_2}^{0} \tag{3-37}$$

$$R(C,T) = 34.0981 \exp\left(\frac{-30594}{8.3145}\right) T^{-0.5} C_{H_2S} C_{SO_2}^{0.7} C_{H_2O}^{-2} C_{S_6}^{0} \tag{3-38}$$

$$R(C,T) = 34.0981 \exp\left(\frac{-30594}{8.3145}\right) T^{-0.4} C_{H_2S} C_{SO_2}^{0.7} C_{H_2O}^{-2} C_{S_8}^{0} \tag{3-39}$$

Kinetics of the side reactions such as hydrolysis of COS, CS_2 etc are not available in the literature.

Chapter 4
The Numerical Scheme

A control-volume based technique is used to convert the governing equations to algebraic equations that can be solved numerically. This control volume technique consists of integrating the governing equations about each control volume, yielding discrete equations that conserve each quantity on a control-volume basis.

4.1 The Grid System

FLUENT can use grids that comprise of triangular or quadrilateral cells (or a combination of the two) in 2D, and tetrahedral, hexahedral, pyramid, or wedge cells (or a combination of these) in 3D. The choice of the mesh type depends on the application. When choosing the mesh type, one should consider the following issues: the set-up time, the computational expenses and the numerical diffusion.

For the discretization scheme in CFD, a staggered grid system is generally used. It is generally accepted that a staggered grid results in a more stable solution. In this system, the scalar quantities are computed at the center of the grid, while the vector quantities are computed at the center of the faces. A recent study Mier *et al*. [1999] indicated that staggered grid based methods are the same for all types of grids. A computational domain accurately representing the domain of the vessel is needed. The co-ordinate system and the meshing technique is chosen depending on the complexity of the geometry.

In the present work, the three dimensional Claus converter's geometry was constructed and meshed with a tetrahedral grid. Since it is a complex geometry and many

sharp edges and faces created, it needs a complex grid that can finely mesh the whole geometry so that the simulator can compute the variables in every cell.

4.2 Solver Types

A segregated solver is used to solve the governing equations. This model is used to solve the governing equations for the conservation of mass and momentum and (when appropriate) for energy and other scalars such as turbulence and chemical species. A control-volume based technique is used. This consists of:

(i) division of the computational domain into discrete control volumes.

(ii) integration of the governing equations around the individual control volumes to construct algebraic equations for the discrete dependent variables ("unknowns") such as velocities, pressure, temperature, and conserved scalars.

(iii) linearization of the discretized equations and solution of the resultant linear equations system to yield updated values of the dependent variables.

4.2.1 The Segregated Solution Method

Using this approach, the governing equations are solved sequentially (i.e. segregated from one another). Because the governing equations are non-linear (and coupled), several iterations of the solution loops must be performed before a converged solution is obtained. Each iterations consists of the steps illustrated in Figure 4.1 and outlined below:

1. Fluid properties are updated, based on the current solution. (If the calculation has just begun, the fluid properties will be updated based on the initialized solution.)

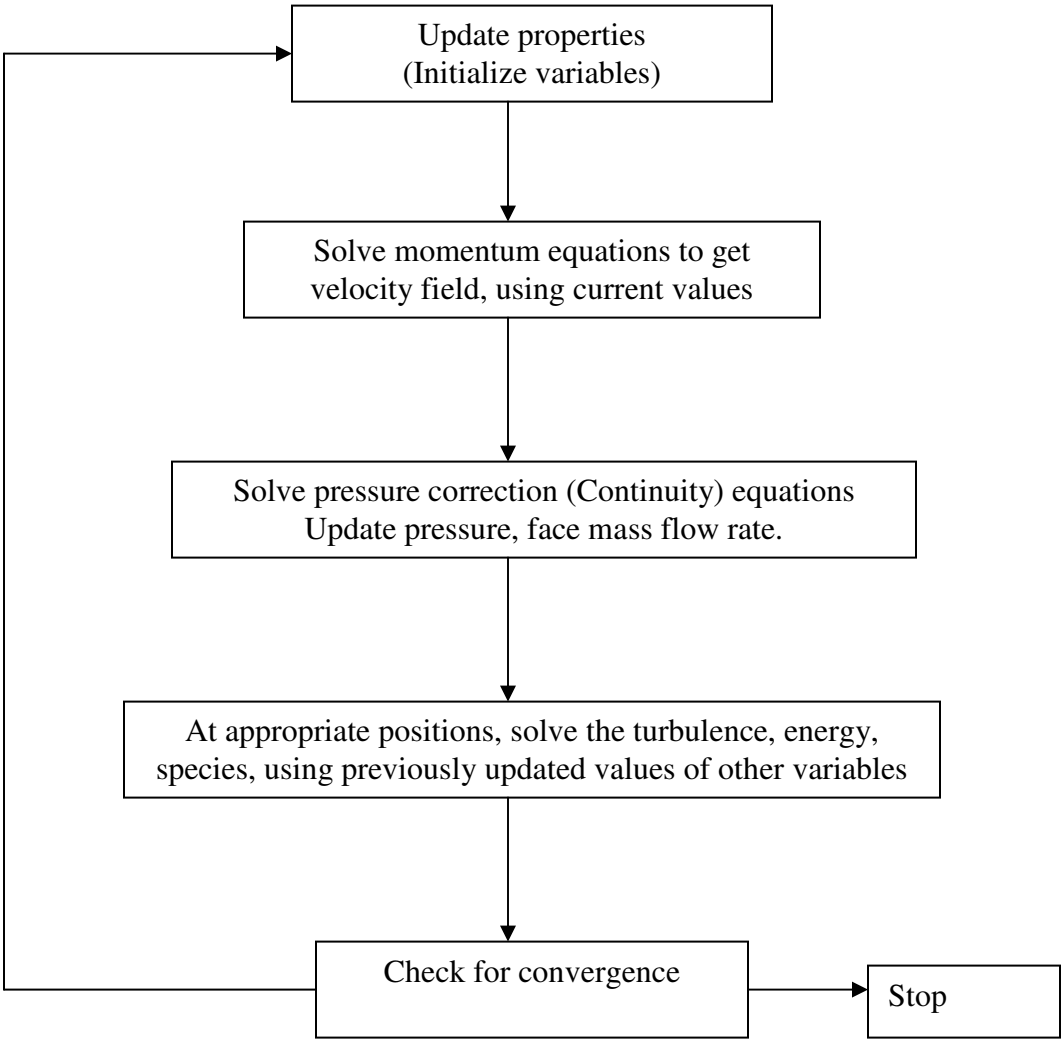

Figure 4.1: An overview of the segregated solution method

2. The x-, y-, and z- momentum equations are each solved using current values for pressure and face mass fluxes, in order to update the velocity field.

3. Since the velocities obtained in step 2 may not satisfy the continuity equation locally, a “Poisson-type” equation for the pressure correction is derived from the continuity equation and linearized momentum equations. This pressure correction equation is then solved to obtain the necessary corrections to the pressure and velocity and the face mass fluxes such that continuity is satisfied.

4. Where appropriate, the equations for scalars such as turbulence, energy, species, and radiation are solved using the previously updated values of the other variables.

5. A check for convergence of the equations set is made.

Steps 1 to 5 are repeated until the pre-set convergence criteria are met. The convergence means that the difference in the solution between two successive iterations is less than a pre-set value.

4.3 The Solution Procedure

After determining the important feature of the problem, the following procedure is followed to solve the problem.

1. Create the model geometry and grid-using the package pre-processor
2. Start the appropriate solver (FLUENT 6.1).
3. Import the grid to the solver.
4. Check the grid and scale to the desired units e.g. m, cm, mm etc.
5. Select the solver formulation, e.g. single precision, algorithm, segregated etc.
6. Choose the basic equations to be solved: turbulence, chemical species or reaction, and heat transfer models.
7. Specify the material properties (fluid or solid)
8. Specify the boundary conditions: inlets, outlet and walls.
9. Adjust the solution control parameters. i.e. the under-relaxation parameters.
10. Initialize the flow field.
11. Calculate a solution (iterate to convergence).
12. Examine the results.
13. Save the results (case and data files).

14. If necessary, refine the grid or consider revision to the numerical or physical model.

Results include plots of the total temperature and velocity fields that show clearly the effects of the parameters under investigation including geometry, boundary conditions, physical properties and flow rates.

Chapter 5
Results of Single Phase Flow in An Unpacked Vessel

5.1 Introduction

The vessel of interest in this work is an industrial sulfur converter. This converter consists of a horizontal cylinder 18.2 m long and 4.9 m in diameter. The feed gas comes in through 3 inlets and leaves through one outlet. The converter has an 1.2 m high packed catalyst bed installed around its middle zone.

The ultimate objective of this study is to simulate the flow in this partially packed vessel including the effects of heat transfer and chemical reactions in the packed bed. However, as a first stage, the flow in the converter without the packed bed and consequently without the heat transfer and chemical reactions, is examined. The actual converter configuration shows that the gas is fed from the top and exits from the bottom. This is the geometry used in chapters 8 and 9. The geometry considered in this chapter has the same dimensions as those of sulfur converter except the flow direction is reversed. The gas is fed from the bottom and leaves from the top of the converter. There is no strong reason for this choice and since the feed is gas, the body forces are not likely to drastically change the flow distribution if the flow direction is reversed.

5.2 The Vessel Geometry and Operating Conditions

A vessel similar to the sulfur converter except for the direction of flow is shown schematically in Figure 5.1. A gas stream is injected into the bottom of the vessel through

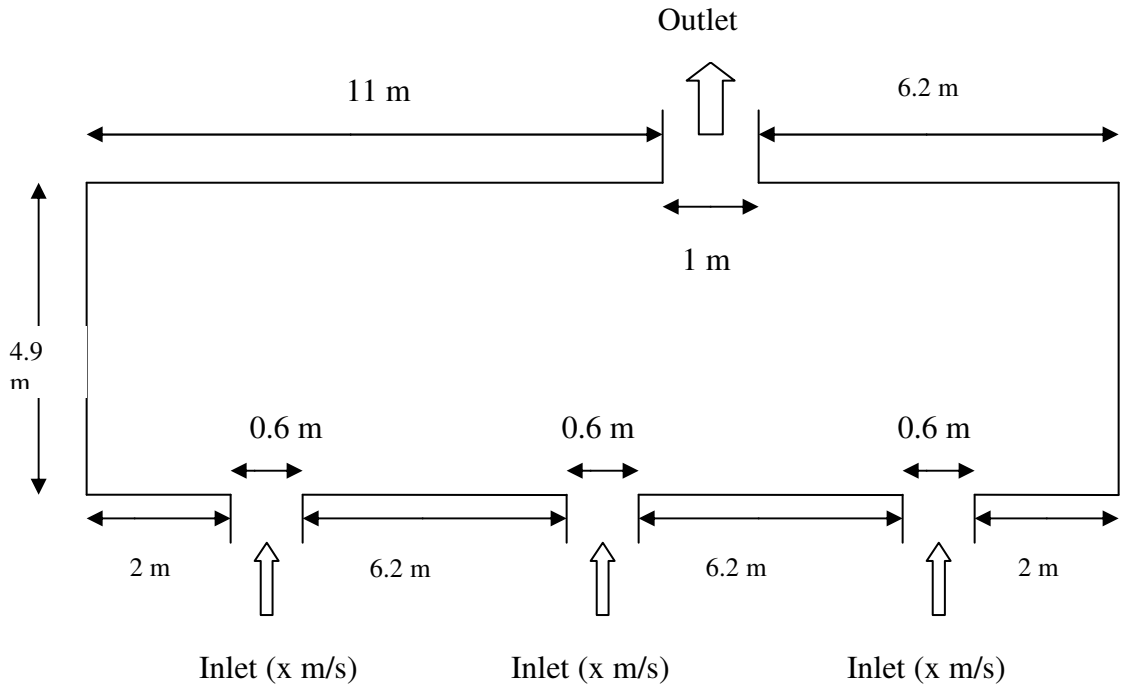

Figure 5.1: A schematic diagram of the vessel geometry used in this chapters with the feed inlets through the bottom.

three inlets each of 0.6 m diameter. The vessel has a single 1m diameter outlet. The geometry of the actual sulfur converter without the packed bed is shown schematically in Figure 5.2.

The feed gas is a mixture consisting mainly of CO_2, H_2S, SO_2, and H_2O with trace concentrations of other components such as methane and hydrogen. The density of the inlet gas is 1.36 kg/m^3 and the kinematic viscosity is 2.18×10^{-5} m^2/s or a dynamic viscosity of 2.96×10^{-5} Pa.s.

A number of feed gas velocities are investigated. The effect of the chemical reactions and heat transfer are not included and only the flow fields are resolved using a single-phase flow.

5.3 Simulation Results of Single Phase Flow

A three dimensional numerical model of the geometry shown in Figure 5.1 was constructed. The effects of the mesh size, the feed flow rate, the turbulence model and different outlet arrangements were investigated.

Turbulence was modeled using the standard $\kappa-\varepsilon$ model. The model was run until a final converged solution was obtained. A convergence criterion is pre-set for each of the solved for variables including the x-, y-, z-velocities, the kinetic energy of turbulences κ and its dissipation rate, ε. The numerical results in two-dimensional plots for the velocity vectors, velocity contours, turbulence characteristics and the pressure drop in the vessel are presented in this chapter.

5.3.1 Effects of Mesh Size on a Typical Solution

Figure 5.3 shows the flow field in a vertical plane (y-z plane) passing through the inlets and the outlet of the vessel. The flow field shows that the incoming jet hit the opposite

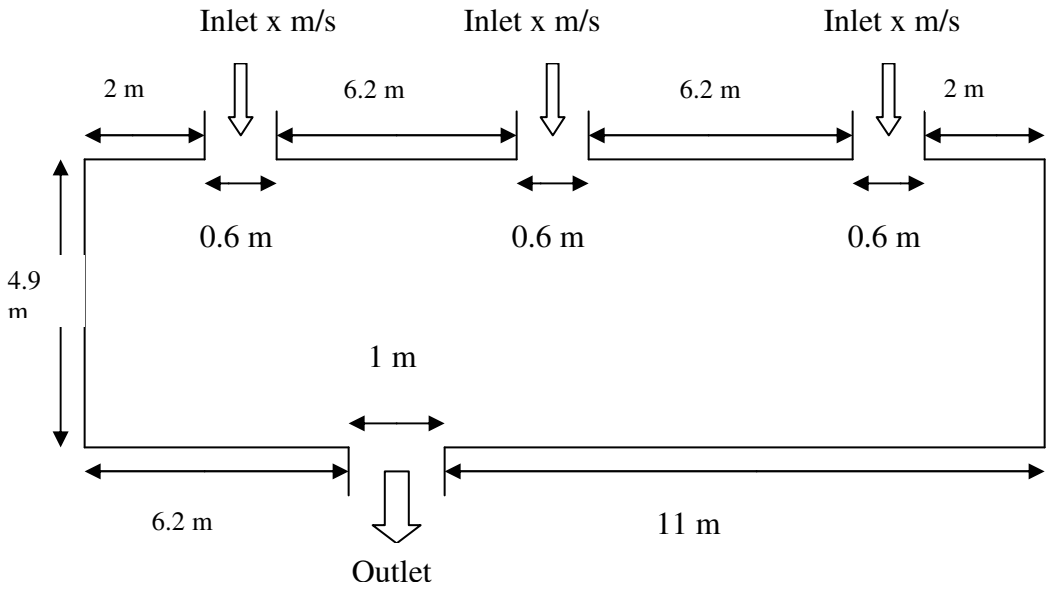

Figure 5.2: A schematic diagram of the actual vessel with geometry which is used in chapters 8 and 9.

wall of the converter with a high velocity and subsequently moves towards the outlet. Despite a high injection of 57 m/s, there are many zones inside the converter where the velocities are very small. These zones are referred to as zones of low velocities and sometimes as 'dead' zones. These zones are more pronounced in the regions between any two adjacent jets and are more prominent in the lower half of the vessel and near the vessel center. In the upper half, there is a good flow distribution, which is due to the jets impingement on the upper walls and their heading towards the outlet. The ultimate objective is to reduce the size of the low velocity zones. In a packed bed, is likely to result in under-utilization of the catalyst.

In order to test the independence of the numerical solution any significant variation in velocity values of the mesh size on the solution, four different mesh sizes, 28, 27, 26 and 25 mm were used. The number of computational cells in each case was 101030, 109457, 119751 and 157922 cells respectively.

Figures 5.3, 5.4 and 5.5 illustrate the effects of mesh size on the results. Figure 5.3 shows that the flow distribution is rather similar for all four mesh sizes used. Figure 5.4 shows the plots of the velocity magnitude versus location along a center line coinciding with the axis of the vessel (horizontal cylinder). This figure shows that the velocity plots are rather similar for all four mesh sizes. Minor differences are observed especially in the height of the peaks. Results for mesh size 25 and 26 mm are almost identical. Therefore a mesh size of 25 mm was used although a mesh size of 26 mm could have been used. This choice was re-enforced by Figure 5.5 which shows that the velocity magnitude along a line shown in Figure 5.5(a) is almost identical for mesh sizes of 25 and 26 mm.

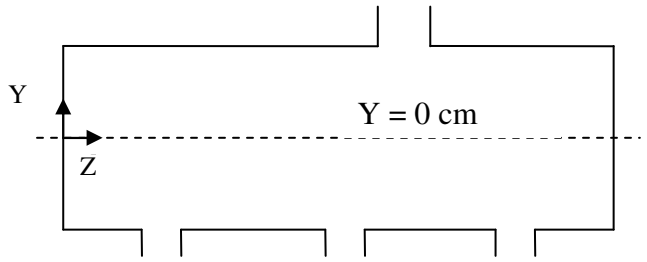

(a)

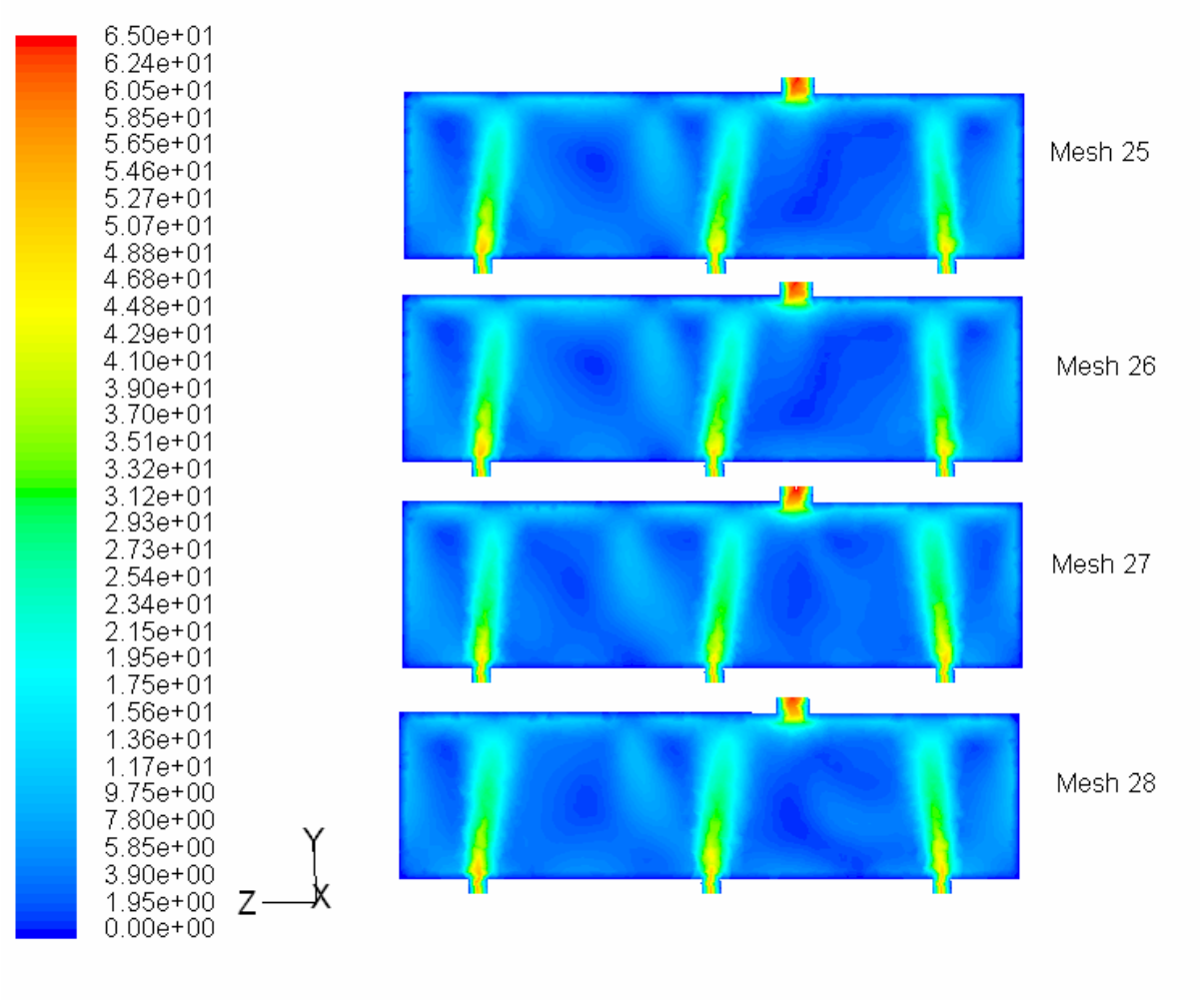

Figure 5.3: Plots of the velocity vectors in vertical centered planes (y-z planes) passing through the inlets and the outlet for an inlet velocity of 57 m/s and for a number of mesh sizes.

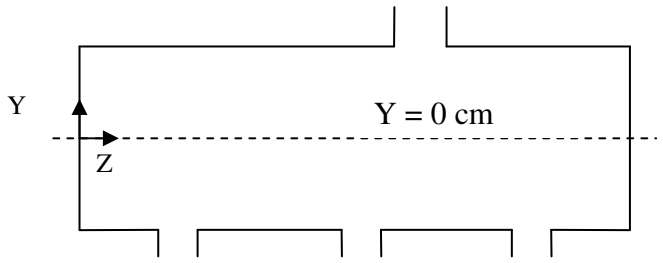

(a)

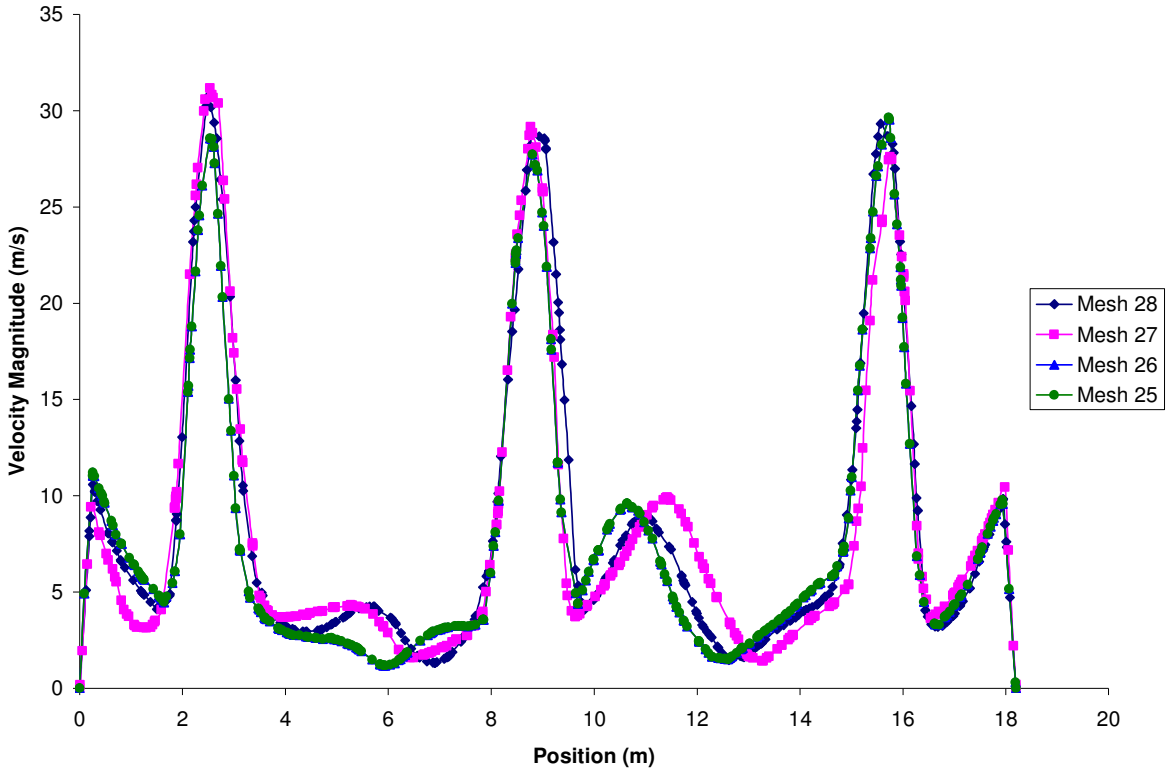

(b)

Figure 5.4: Plots of velocity magnitudes versus locations along the centerline, as shown in figure (a) above, for four different mesh sizes and an inlet velocity of 57 m/s.

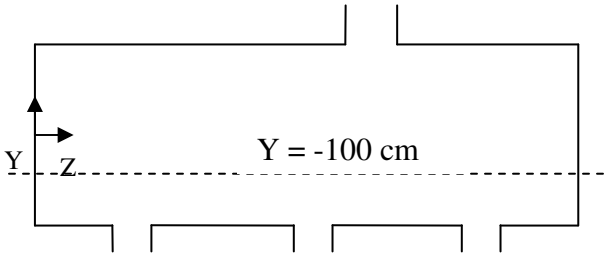

(a)

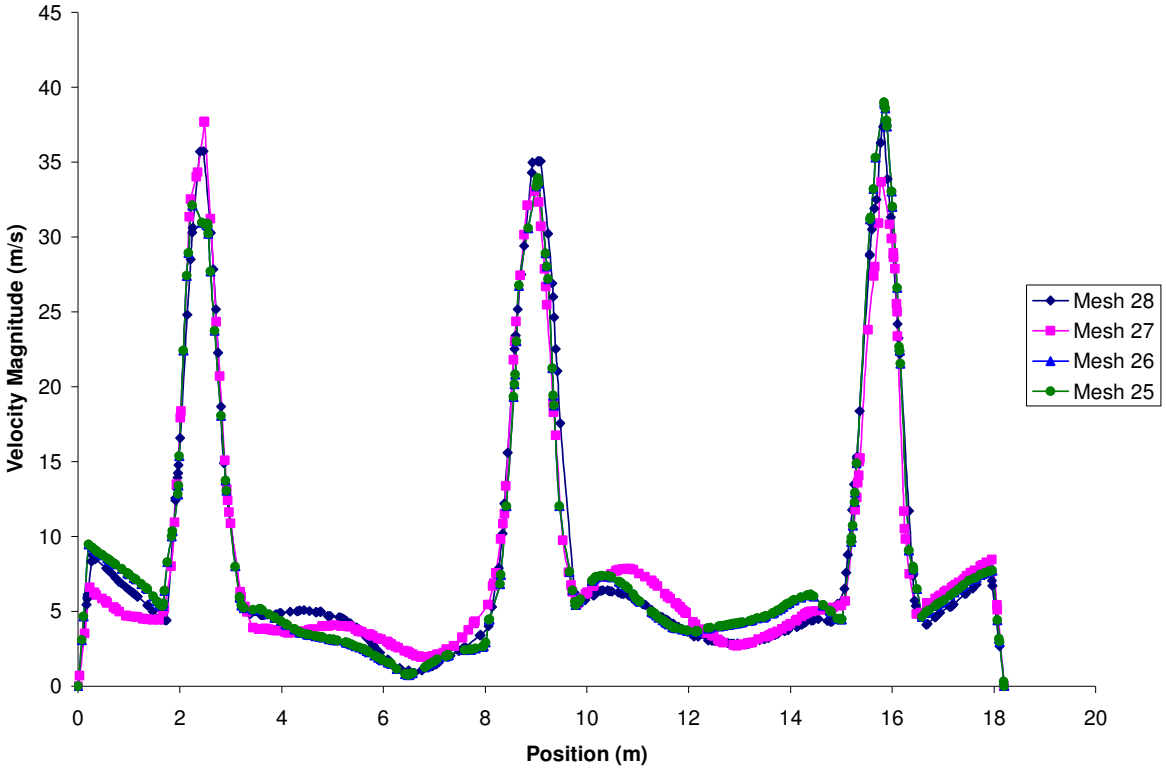

(b)

Figure 5.5: Plots of velocity magnitudes versus locations along the centerline, as shown in figure (a) above, for four different mesh sizes and an inlet velocity of 57 m/s.

5.3.2 Effects of the Feed Gas Flow Rate

Increasing the flow rate may be useful in increasing the circulation and in reducing the sizes of the dead zones. It is expected that increasing the velocity should lead to variations in the flow profile inside the vessel. This increase is not always practically possible due to the limit on compressors or other equipment. However, it may useful to investigate the effects of varying the injection velocity.

Figure 5.6 illustrates a comparison of the flow fields for the cases with an injection velocity of 45, 57 and 70 m/s respectively. The injection velocity was increased keeping the inlet area constant. Results show no appreciable improvement in the flow distribution as the injection velocity is increased by 55.6%, i.e. from 45 m/s to 70 m/s. Figures 5.7 and 5.8 show a comparison of the velocity line plot. These line plots allow a closer inspection of the variations in the velocity values. Once again no significant increase in the values of the velocity magnitudes in the low velocities zones was observed. The increase in the jet velocities (the peaks) is expected due to the increase in the inlet velocity magnitudes.

5.3.3 Effects of Different Arrangements of Inlets and Outlets

An intuitive approach to improve the flow distribution in a vessel points to the necessity of a better design and arrangement of the inlets and outlets. In this section, the effects of increasing the number of outlets on the flow distribution within the vessel are investigated. Figure 5.9 shows a comparison of the flow field for the three selected arrangements keeping the same inlets and varying the number of outlets. The arrangements compared are one with a single outlet, one with two outlets and one with multiple outlets.

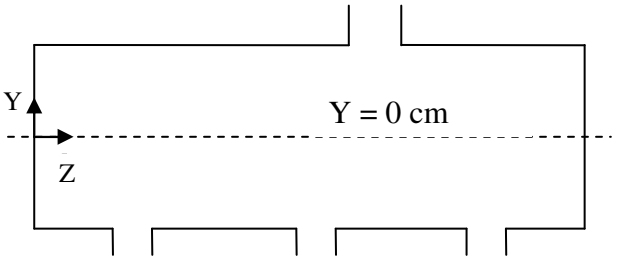

(a)

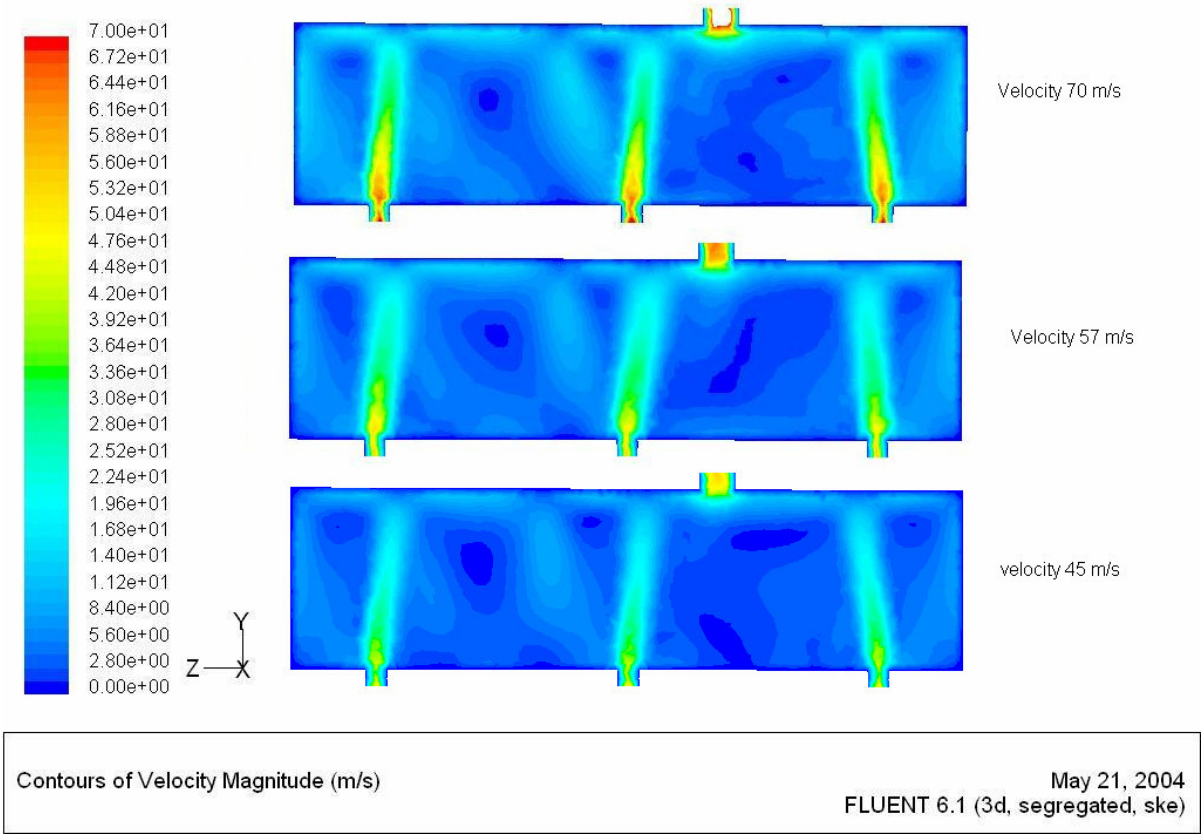

Figure 5.6: Contours plots of the velocity magnitude in centered y-z vertical planes passing through the inlets and the outlet, for three different inlet velocities.

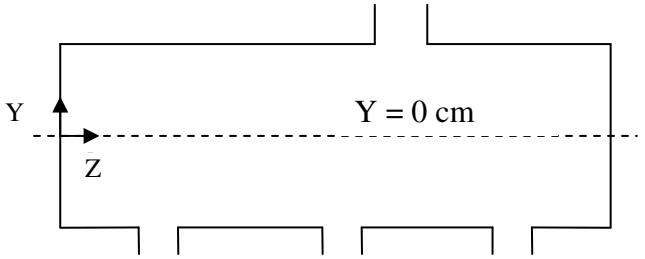

(a)

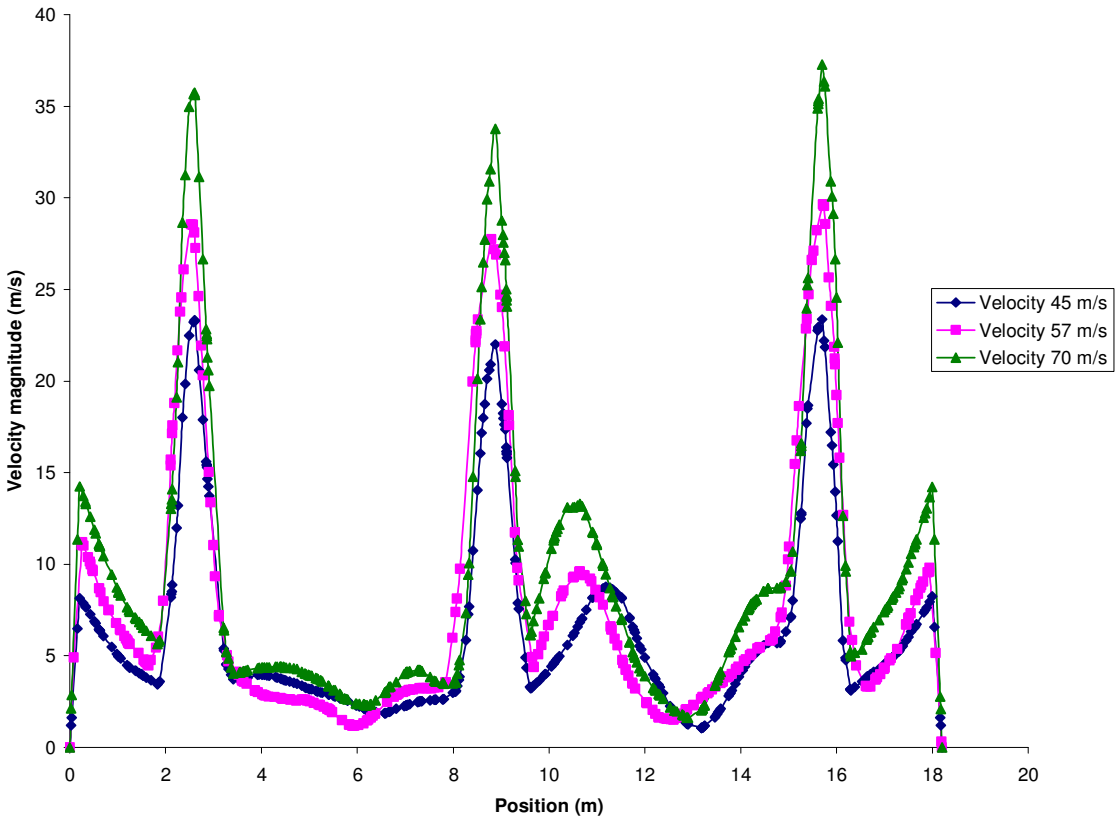

(b)

Figure 5.7: Plots of velocity magnitudes versus locations along the centerline, as shown in figure (a) above, for three different inlet velocities.

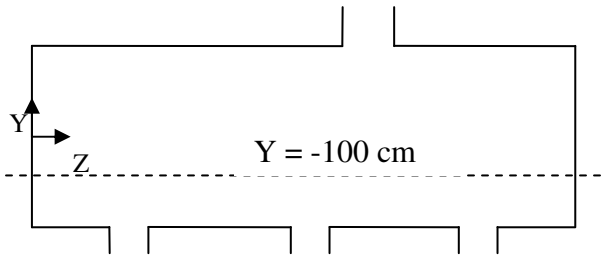

(a)

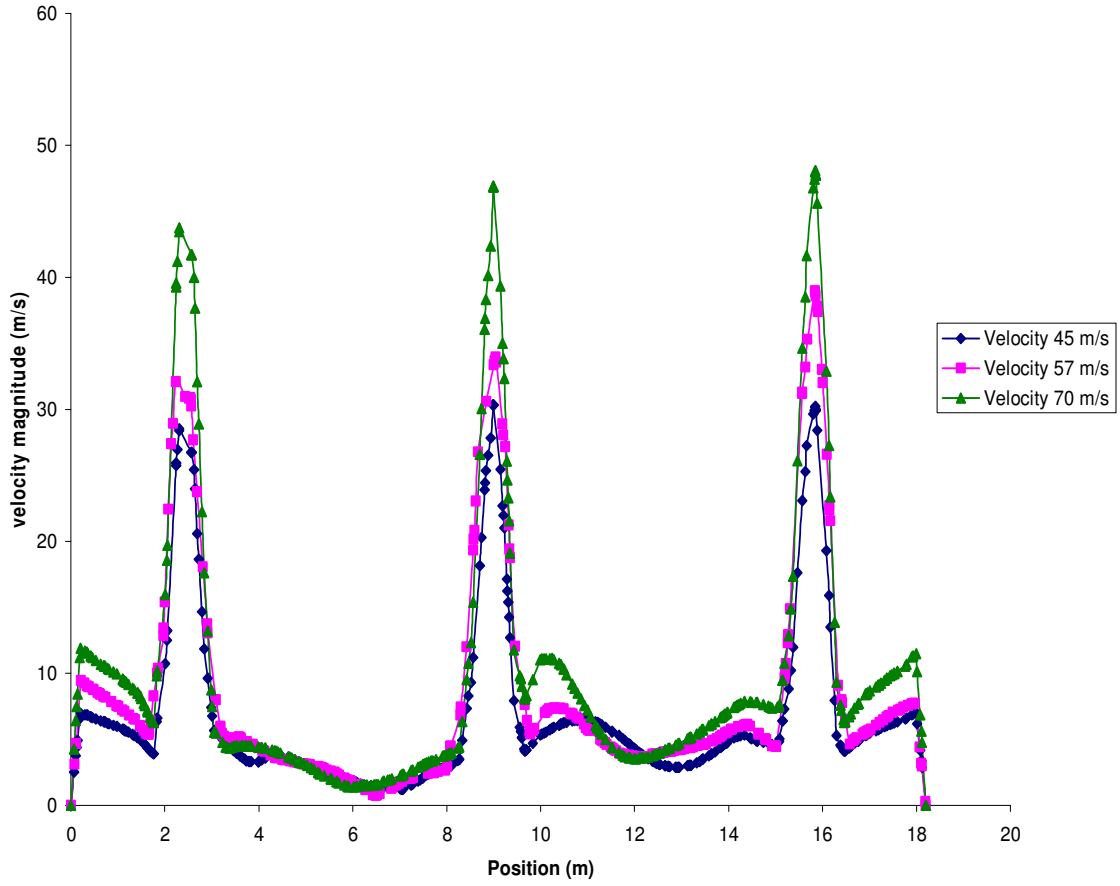

(b)

Figure 5.8: Plots of velocity magnitudes versus locations along the centerline, as shown in figure (a) above, for three different inlet velocities.

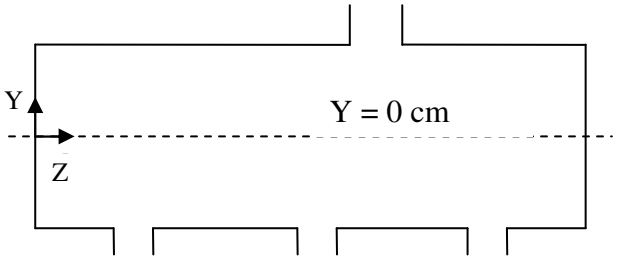

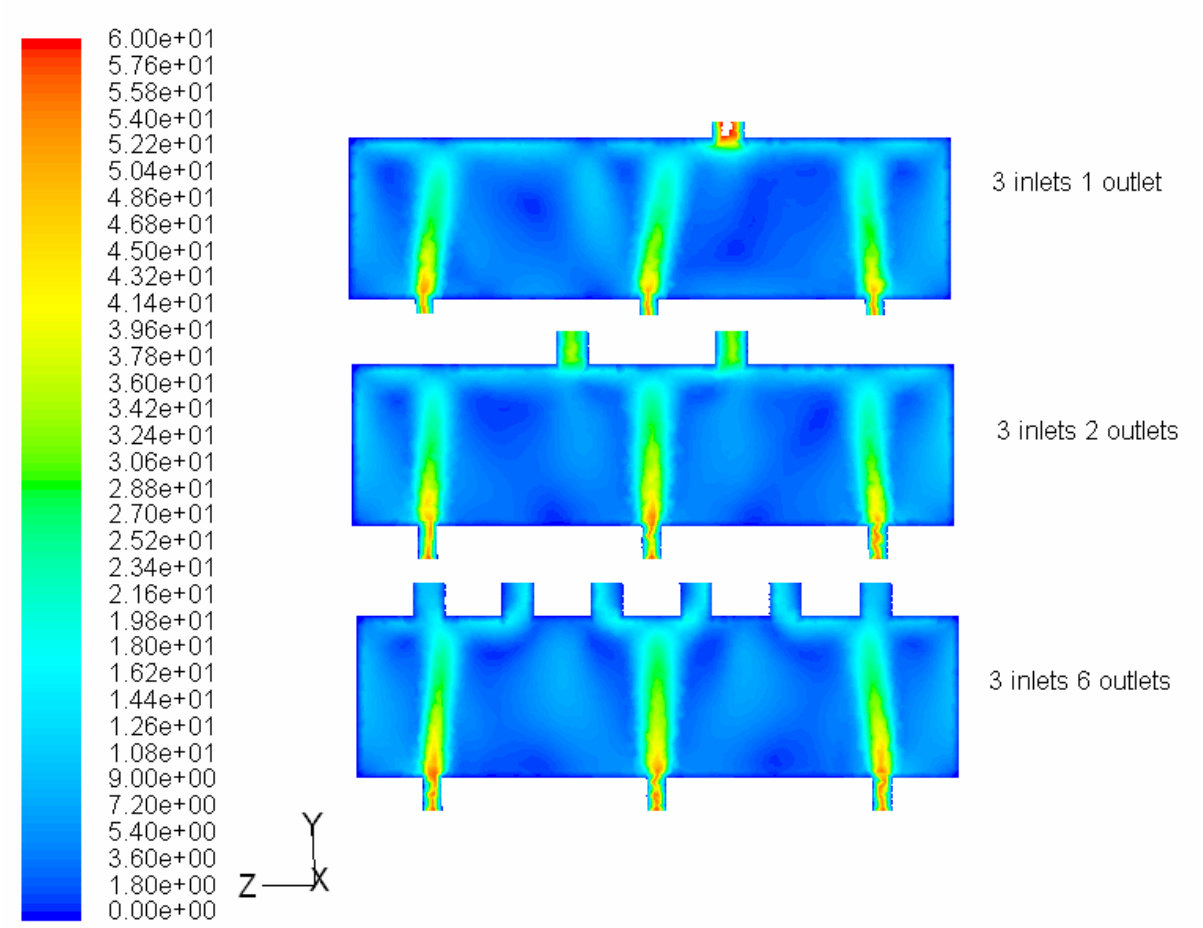

Figure 5.9: Velocity contours for different inlet and outlet positions of the velocity field for an injection velocity 57 m/s.

For all three cases, the inlets are 2 m, 8.8 m, and 15.6 m respectively from the right side of the vessel. For the case of a single outlet, it positioned 6.2 m away from the right end of the vessel. For the case of two outlets, those are 6.2 m and 11 m away from right end of the vessel respectively. Finally for the case of 6 outlets, those outlets are 2 m, 4.9 m, 7.6 m, 10.3 m, 13 m, and 15.7 m away from the right side of the vessel respectively. Figure 5.9 shows the velocity vectors flow fields for different outlet positions. It illustrates that the size of the zones with low velocity is smaller in the case of two-outlets compared with the case of a single outlet. It can also be seen that these low velocity zones are smallest for the case with multiple outlets. However, many low velocity zones can still be seen and consequently the improvement of the flow distribution due to additional outlets is rather limited. An increase in the number of inlets or adding orifice plates above the jet inlets inside the vessel to split the jets have been attempted by Sheikh [2002]. It was found that for an unpacked vessel, those measures significantly improved the flow distribution.

Chapter 6
Experimental Validation

The quantitative understanding of flow nonuniformities in packed beds is of considerable practical importance in chemical reaction engineering. Flow mal-distribution may occur due to spatially variable resistance to flow. Szekely and Poveromo [1975] experimentally investigated flow mal-distribution in packed beds. They carried out experiments in a packed column with a gas stream flowing upwards. The actual experimental technique restricted the determination of the velocity field of the gas stream exiting the column through the use of a hot wire anemometer. They compared their experimental measurements with predictions based on a numerical solution using the Ergun equation. The numerical solution was restricted to 2D geometry. Figure 6.1 shows the experimental setup that was used to predict the velocity profile by Szekely and Poveromo [1975]. The column is 15.2 cm in diameter and the height of the packed column is 60 cm.

The actual experimental measurement of the gas velocities for nonuniform flows in packed beds has been confined to study the wall effect in uniformly packed beds in parallel flow. Figure 6.2 explained the comparison of the experimental outlet velocity profile with the predicted velocity. This figure shows a good qualitative agreement between the experimental and simulation values. An increase in the velocity next to the wall is observed. This mainly occurs due to a higher void fraction in the near wall zone.

In this work, a simple geometry was created to qualitatively validate the velocity profile predicted by the CFD package FLUENT for the flow in a packed bed. The

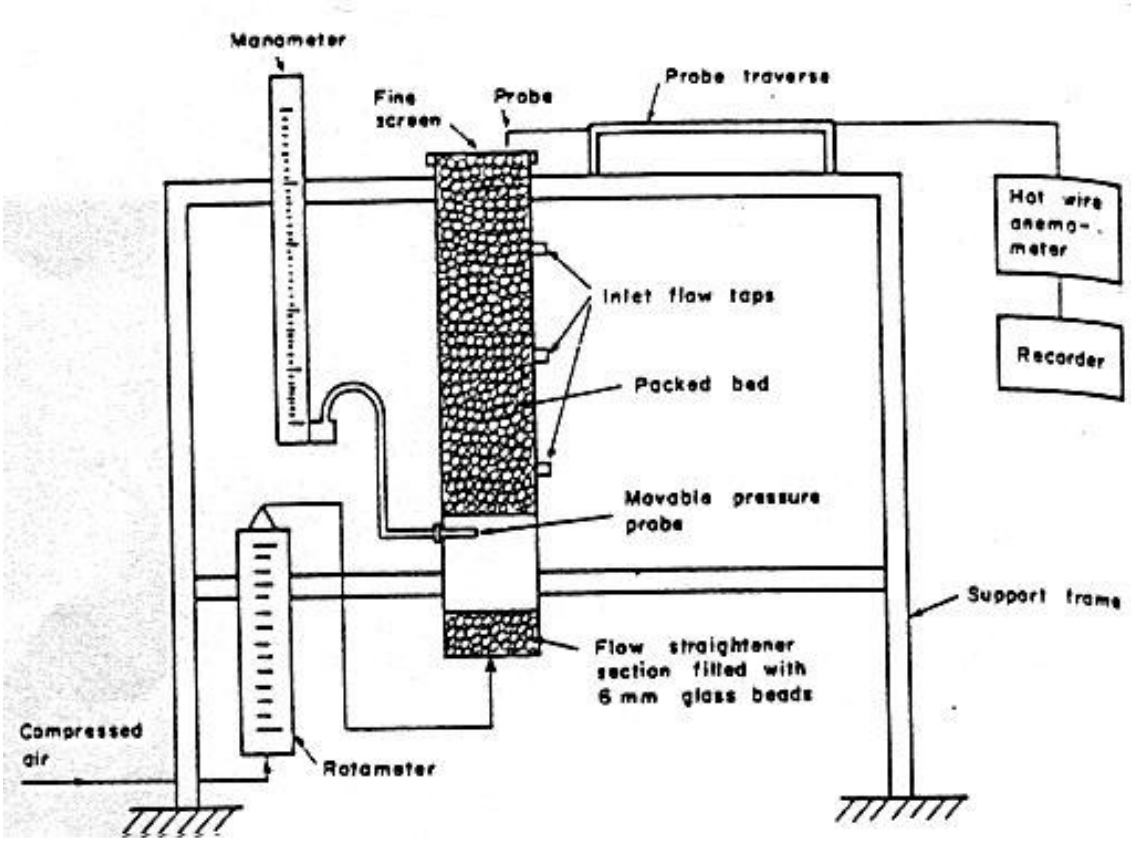

Figure 6.1: The experimental setup for the measurement of nonuniform flow in the packed bed used by Szekely and Poveromo [1975].

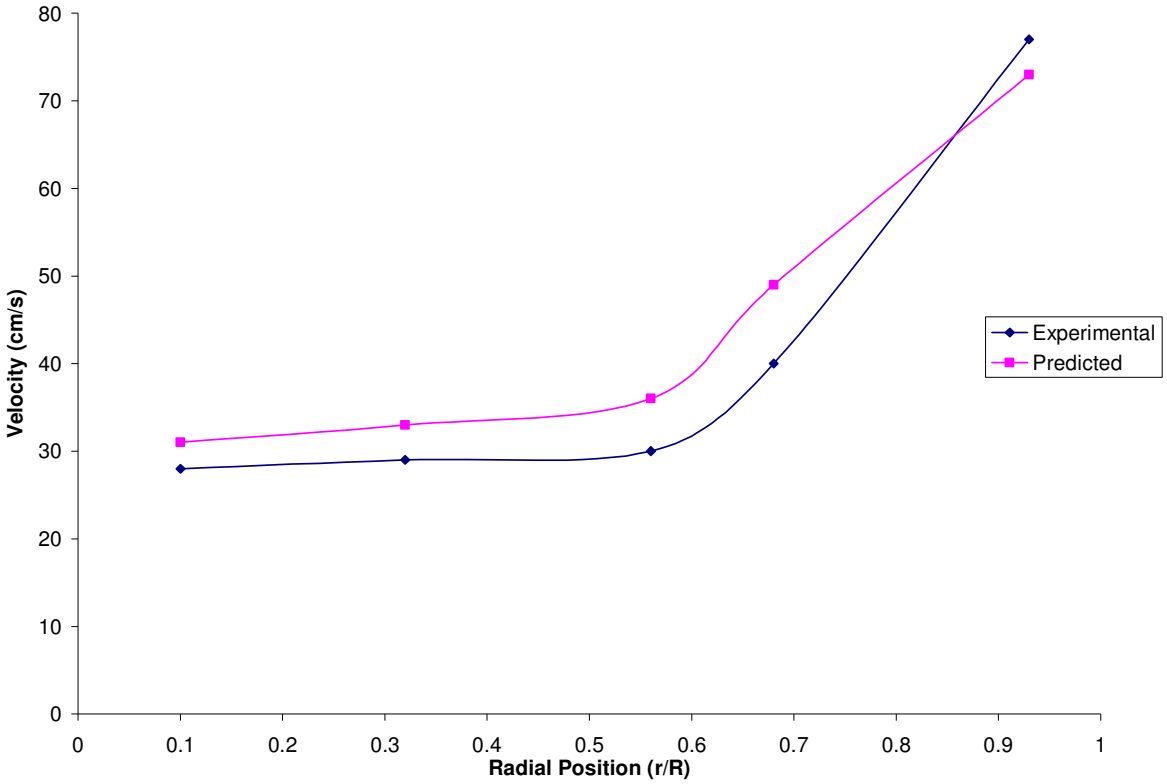

Figure 6.2: A comparison of the predicted and experimental outlet velocity profiles for parallel flow through a bed with 0.6cm diameter particles, (from Szekely and Poveromo [1975]).

geometry created is a three-dimensional rectangular columns, 4 cm wide, 2.1 cm deep and 2.6 cm high was placed halfway through the column. The bed was pre-packed with uniform spherical particles of 0.5 cm in diameter.

Figure 6.3 depicts the column with the packing. An inlet cylindrical nozzle, 1 cm in diameter is positioned centrally as shown in Figure 6.3. Air with an inlet velocity of 2 m/s is used as the fluid. A mesh size of 0.25 mm is used. The computational domain needed a total of 53127 cells.

Figure 6.4 depicts the contours of the velocity profile at a cross section of x-y plane, passing through the center of the column. Contours show that the air jet has spread well before it reached the packed bed and the velocity profile at the bed entrance is almost flat with the highest value in the middle of the column. Through the bed, the flow is distributed and the highest value is observed close to the wall. Figure 6.5 shows more clearly those local maxima in the velocity profile in the vicinity of the wall. This finding is consistent with that of the predicted and the experimental value reported by Szekely and Poveromo [1975].

Figures 6.6 and 6.7 show the line plots if the values of the velocity along the center of the bed extending to the wall. A comparison of the at the top of the bed and at the outlet positions within the bed shows clearly the change in the velocity profile. The profiles show qualitative agreement with those reported by Szekely and Poveromo [1975]. The dimensions of the bed in this study are different from those used by Szekely and Poveromo and hence the difference in the profiles. It should be also mentioned that such a velocity profile can be predicted only if a fine enough numerical mesh is used. This means that there must be enough mesh cells in that near wall region in order to predict an accurate velocity profile. This near wall effect may not be always important. In a case such as the Claus converter

considered in this study, the packed bed is 18.2 m wide, 4.9 m deep and 1.2 m high. The large dimensions of this packed bed make the effects of the wall region much less significant compared to those in a smaller bed.

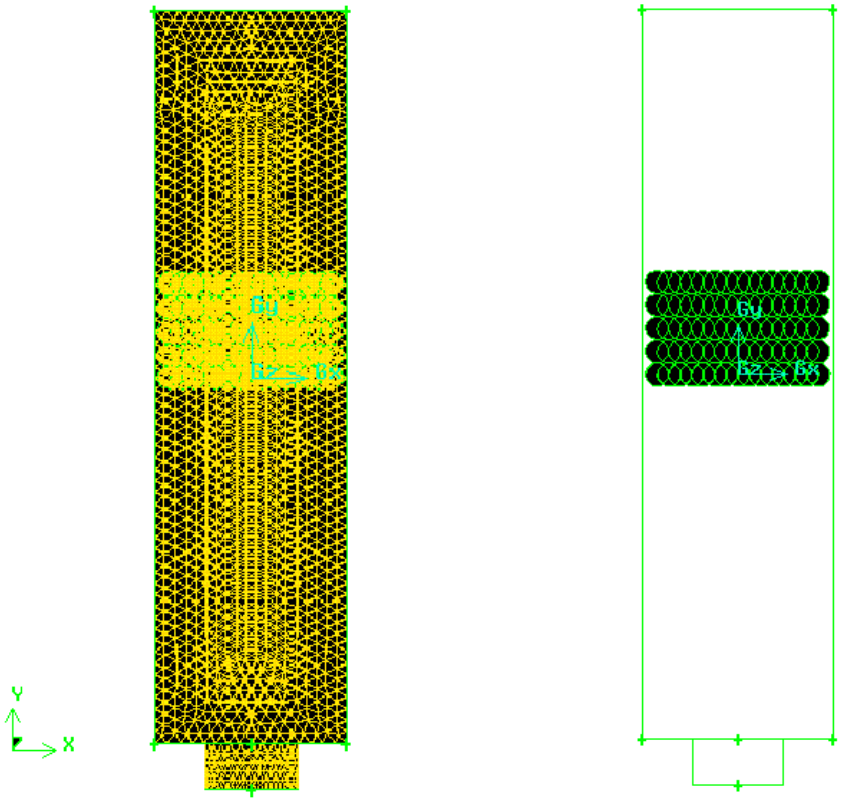

Figure 6.3: A schematic diagram of the partially packed column used in this study.

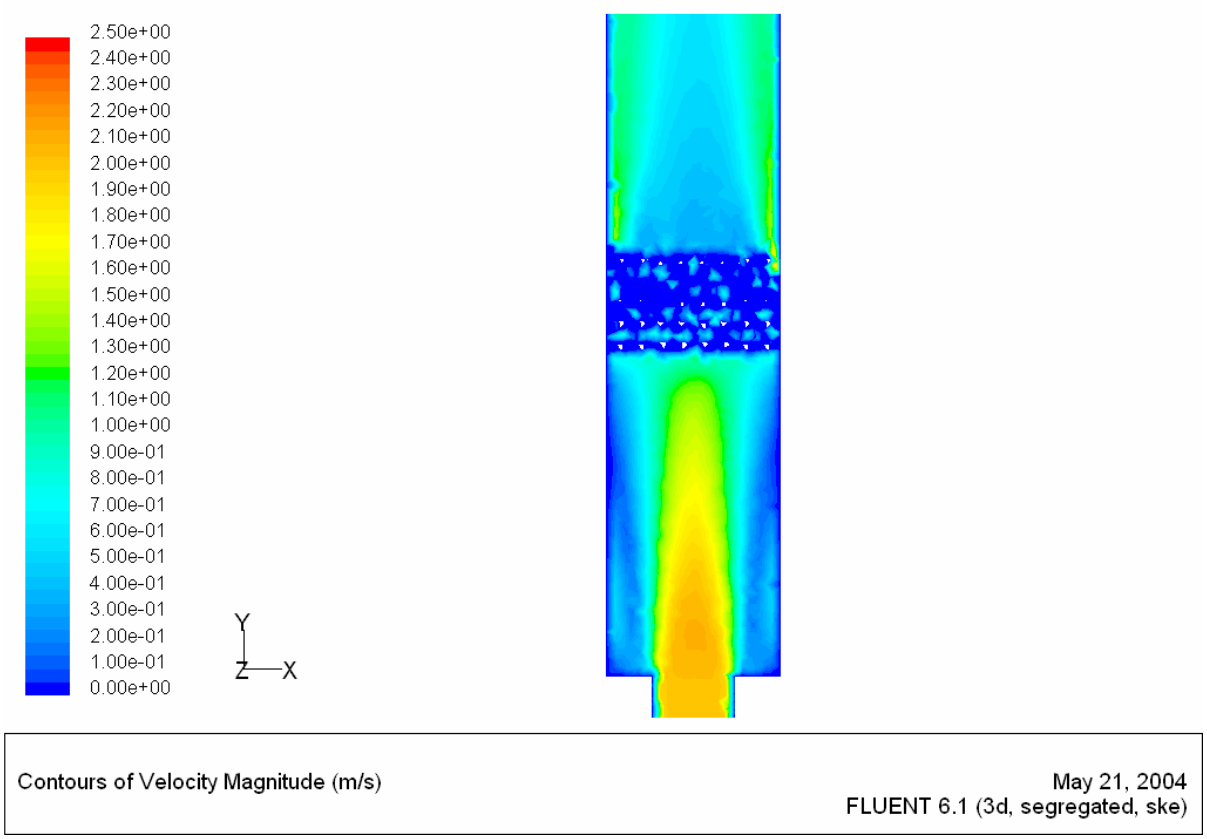

Figure 6.4: Contours of the velocity magnitude for parallel flow through a bed packed with 0.5 diameter particles.

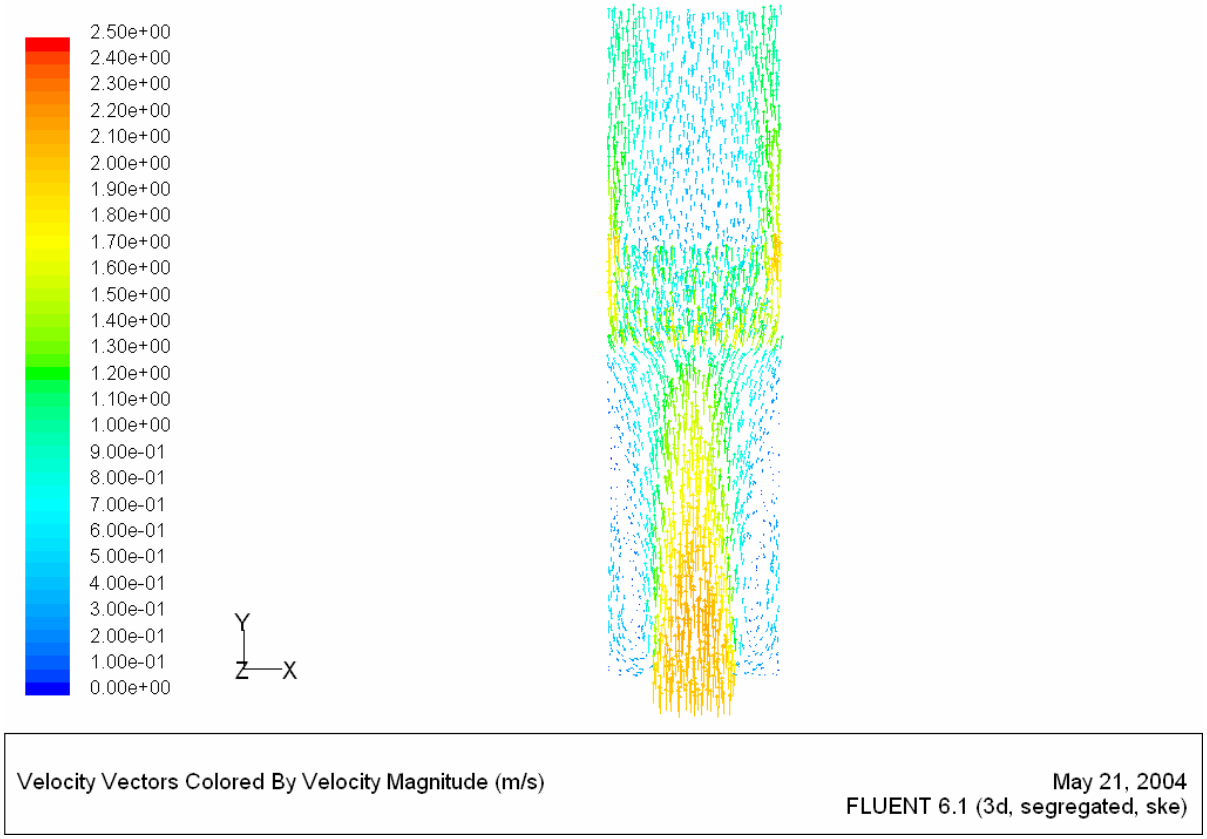

Figure 6.5: Velocity for flow in the region between the packed bed and outlet region.

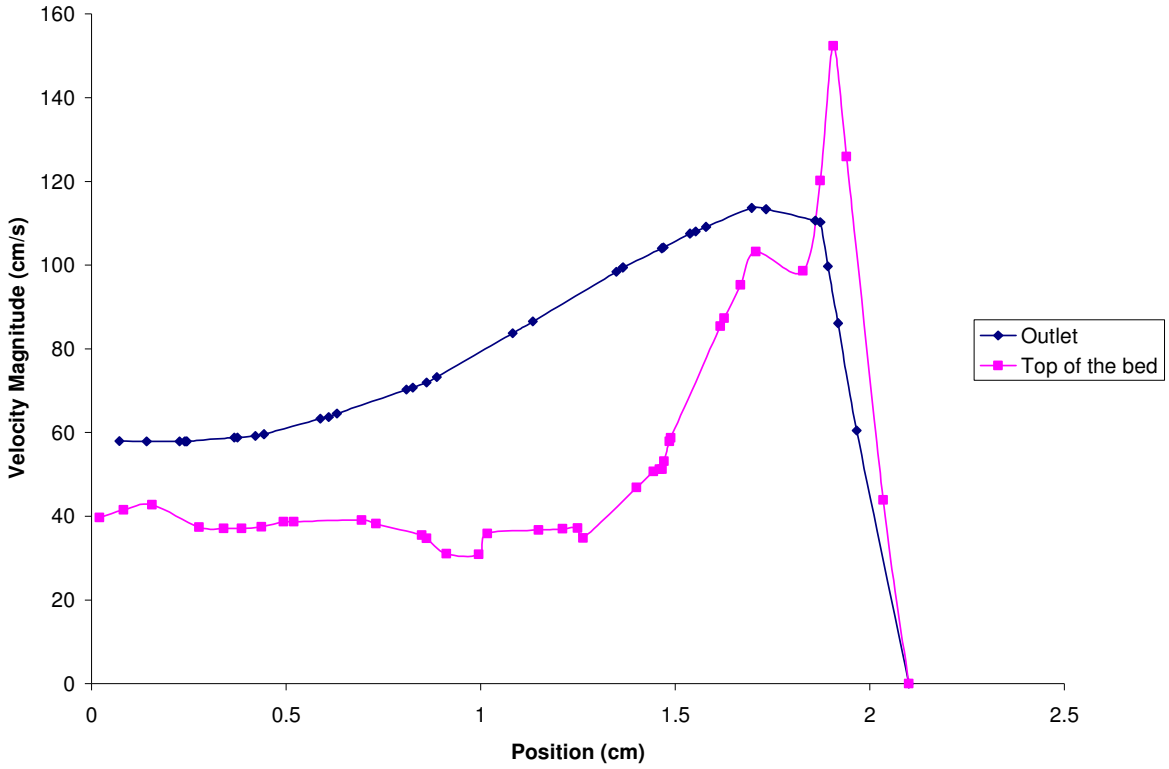

Figure 6.6: Line plots of the velocity values in packed bed for parallel flow through the packed bed with 0.5 cm diameter particles from center of the column to the wall.

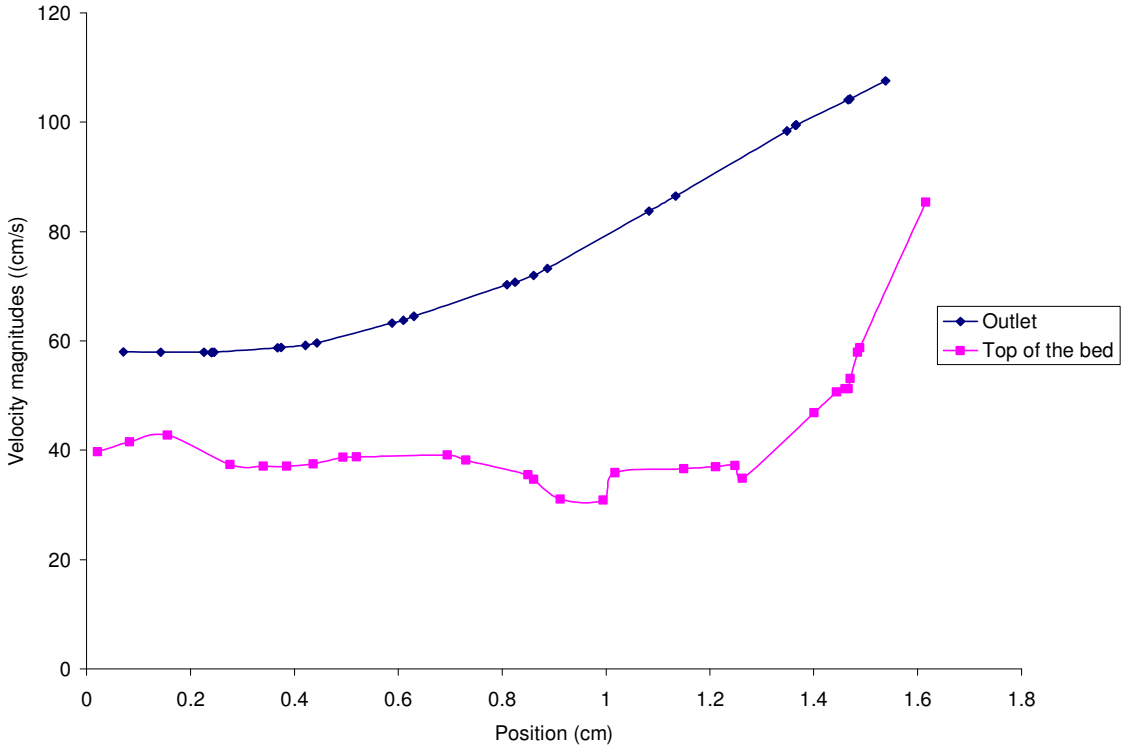

Figure 6.7: Line plots of the velocity profiles for parallel flow through the packed bed with 0.5 cm diameter particles from center of the column to close to the wall.

Chapter 7
Simulation Results of Flow in a Partially-Packed Vessel

7.1 Introduction

A detailed understanding of the fluid flow within catalytic packed beds is of fundamental importance in many industrial processes and especially in reaction engineering. Until now, most experimental and theoretical studies of fluid flow through packed beds have been restricted to the description of the beds in terms of macroscopic properties such as pressure drop, permeability and dispersion. These properties are usually averaged over the bed. Nowadays a number of visualization techniques are applied to study transport of fluid through packed beds including conductance, capacitance, optical and X-ray topography, and magnetic resonance imaging (MRI) techniques.

As far as predicting the flow distribution in a packed bed using CFD is concerned, very few results are available and most of those available are for lab-scale size geometries.

In this investigation, flow simulations were carried out in a partially packed vessel of industrial dimensions. The investigations were carried out in the same geometry as that used in the previous chapter. In addition, a packed bed 1.2 m high is inserted 1.4 m above the vessel bottom as shown in Figure 7.1.

An unstructured tetrahedral mesh is used. The mesh size is 25 mm, as explained in section 5.3.1. This means a total of 157922 cells are used in the simulations reported in this chapter.

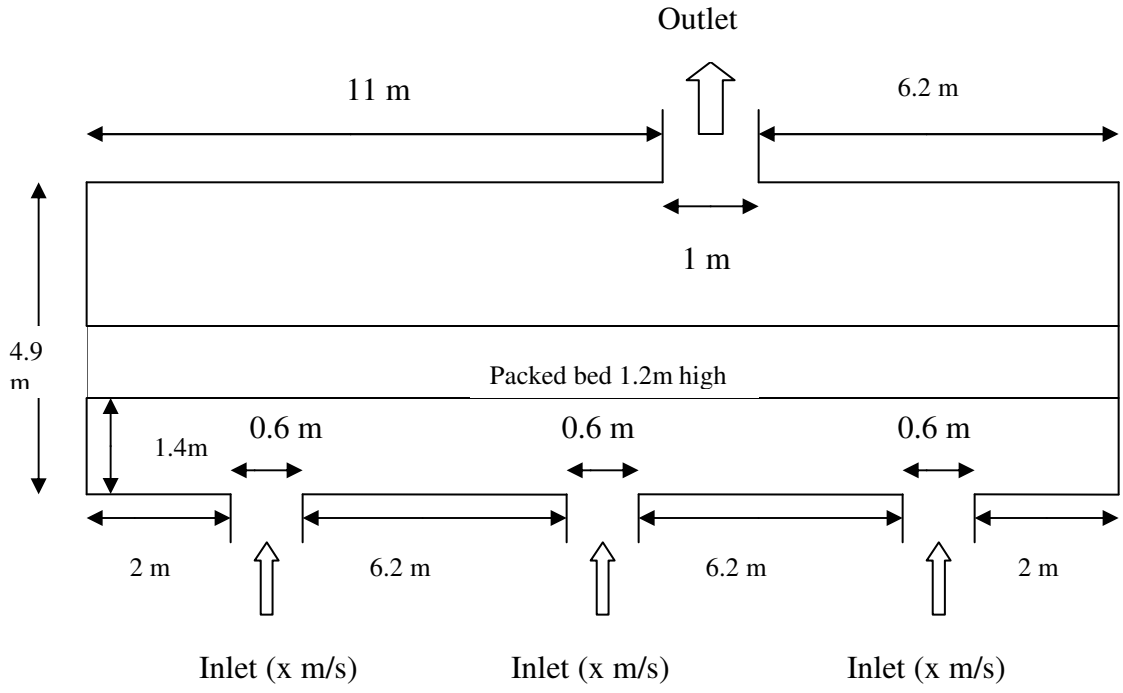

Figure 7.1: A schematic diagram of the partially packed vessel used in the this chapter.

7.2 Simulation Results with Modified Ergun Equation

The Ergun equation was used to derive porous media inputs required for modeling flow in a packed bed using FLUENT. In turbulent flows, packed beds are modeled using both permeability and an inertial loss coefficient. Permeability is a function of the bed characteristics and is defined as:

$$\alpha = \frac{D_p^2}{150} \frac{\theta^3}{(1-\theta)^2} \tag{7-1}$$

and the inertial loss coefficients is defined as:

$$C_2 = \frac{3.5}{D_p} \frac{(1-\theta)}{\theta^3} \tag{7-2}$$

$\vec{F}$ is used in the momentum equations as the additional sink term to account for the additional pressure drop in a packed bed.

$$\vec{F} = -\left(\frac{\mu}{\alpha} v_i + C_2 \frac{1}{2} \rho |v_i| v_i \right) \tag{7-3}$$

where α is the permeability and C_2 is the inertial resistance factor.

7.2.1 Treatment of Turbulence in Porous Media

FLUENT will, by default, solve the standard conservation equations for turbulence quantities in the porous medium as though the solid medium has no effect on the turbulence generation or dissipation rates. This assumption may be reasonable if the medium's permeability is quite large and the geometric scale of the medium does not interact with the scale of the turbulent eddies.

In the case of using the $\kappa - \varepsilon$ model, one can suppress the effect of the turbulence in a porous region by setting the turbulent contribution to the viscosity, μ_t equal to zero. When one chooses this option, FLUENT will transport the inlet turbulence quantities through the medium, but their effect on the fluid mixing and momentum will be ignored.

7.2.2 User Input for the Porous Media

For the modeling of the porous region, the only additional inputs for the problem setup are as follows.

1. Define the coordinates of the porous zone.
2. Identify the fluid flowing through the porous medium.
3. Set the viscous resistance coefficients $\left(1/\alpha_{ij}\right)$ and the inertial resistance coefficients $C_{2_{ij}}$ and define the direction vectors for which they apply.
4. Define the materials contained in the porous medium and its porosity.

7.2.3 Simulation Results of the Partially Packed Bed Using a Catalyst of Diameter 0.3175 cm

In the present case, flow distribution is observed in the bed which consists of particles with a size of 0.3175 cm in diameter. The porosity of the bed is chosen as a fixed value of 0.5. The porosity of catalytic beds such as those used in Claus converters ranges between 0.4 and 0.6. Figures 7.2 to 7.4 show plots of velocity contours for different inlet velocity. The present work is three dimensional so the actual flow distribution in the bed from all three directions can be observed.

In order to investigate the flow distribution inside the packed bed, contour plots of the velocity are presented in horizontal x-z planes across the bed. Three planes are selected. The first one, as shown in Figure 7.2, is located at y = -100 cm, which means near the inlet to the bed. The second plane, as shown in Figure 7.3, is located at y = -50 cm, which means near the center of the bed, and the third plane shown in Figure 7.4, at y = 10 cm which means near the outlet of the bed. the contours in these planes provide a plane view of the velocity distribution which helps in obtaining a clear understanding of how the flow changes across the whole bed.

It should also be mentioned that the near wall velocity profile discussed in chapter 6 and reported by many researchers in the literature including Szekely and Poveromo [1975] will not be noticed in the current simulations. This is due to the mesh size. The size of each mesh cell is 25 mm while the catalyst particles are 0.3175 cm in diameter. This means that every mesh cell covers a large number of particles. The numerical solution gives one average value of each variable including velocity over each cell, hence, the inability of the simulations in this chapter to re-produce an accurate account of the near wall velocity distribution. It should also be mentioned that given the large dimensions of the packed bed, 18.2 m wide, 4.9 m deep and 1.2 m high, the influence of the near wall region on the total operation within the bed can be neglected.

By closely inspecting the velocity contours in the three chosen horizontal planes one could obtain a clear picture of the flow distribution which may have a direct impact on the degree of conversion of the Claus reactions and consequently on the degree of the catalyst utilization.

Figure 7.2 shows velocity contours in a horizontal (x-z) plane at y = -100 cm, which means near the bottom end of the packed bed. Velocity contours for the three different inlet velocities (45, 57 and 70 m/s) are compared. The contours plots show that the maximum velocity at that position of the bed is 22 m/s. although the initial 10 cm of the bed helped to better distribute the velocity, zones of high velocities are observed above the locations of the impingement of the jets. Varying the inlet velocity from 45 m/s to 70 m/s did not have a significant impact on the flow distribution inside the bed. The distribution was similar for all three inlet velocities; however, the values of the velocities were higher for a higher inlet velocity.

Figure 7.3 shows the plots of velocity contours for different values of the inlet velocity in a horizontal plane near the center of the bed. A sharp fall is observed in the maximum value of the velocity in these planes compared to the velocities in Figure 7.2. Based on these contour plots, one could not conclude that it is advantageous to change the operational inlet velocity of 57 m/s to 45 m/s or 70 m/s. The velocity magnitudes lies between 0.1 and 5 m/s compared to the range of 0.1 to 22 m/s in Figure 7.2

Figure 7.4 depicts the contours at a horizontal (x-z) plane located y = 10 cm, that is near the top of the catalyst bed. The velocity magnitudes decrease further compared to the previous figure. The velocity magnitudes lie in between 0.1 to 2 m/s in this case.

A better flow distribution with less low velocity zones is observed for inlet velocities of 57 and 70 m/s. The flow distribution for an inlet velocity of 45 m/s was relatively poorer. Line plots give a clearer and a more quantitative picture of how the flow distribution changes in the bed. Three line plots are created at three different depths (x-z) of the bed. All three lines are taken at the center position of horizontal x-z surfaces. In all cases the x position is taken

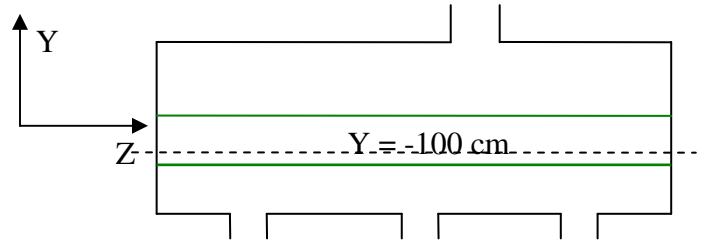

(a)

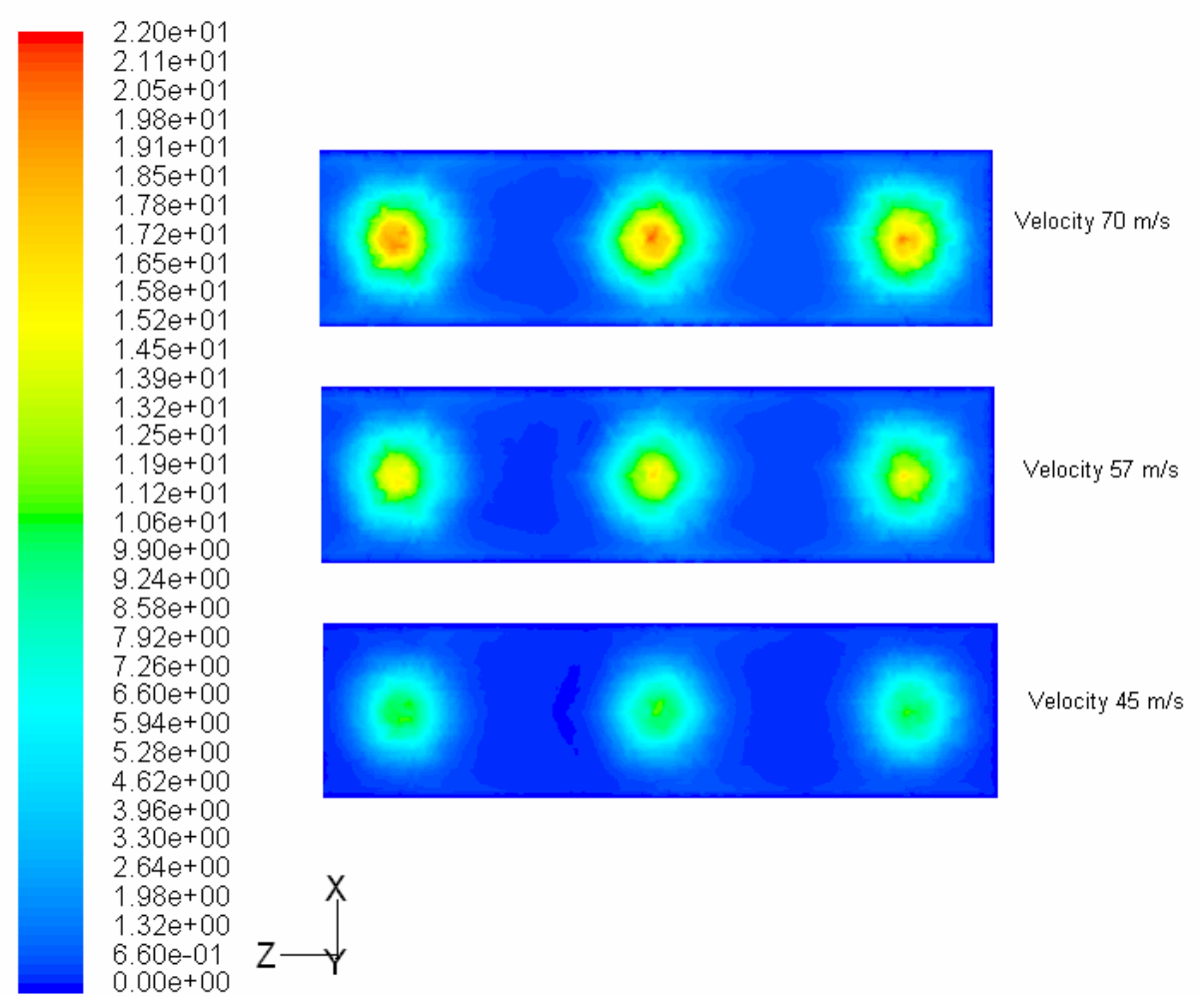

(b)

Figure 7.2: Plots of velocity contours for different values of inlet velocity, the contours are shown in a horizontal plane located, near the inlet of the bed, at y = -100 cm and for a catalyst size of 0.3175 cm.

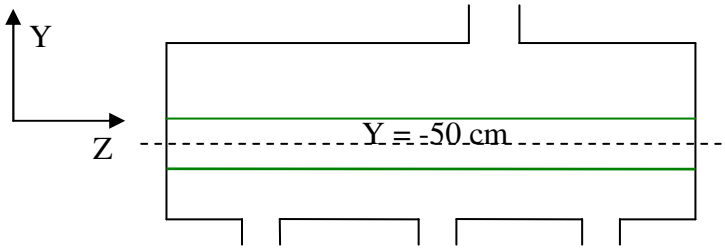

(a)

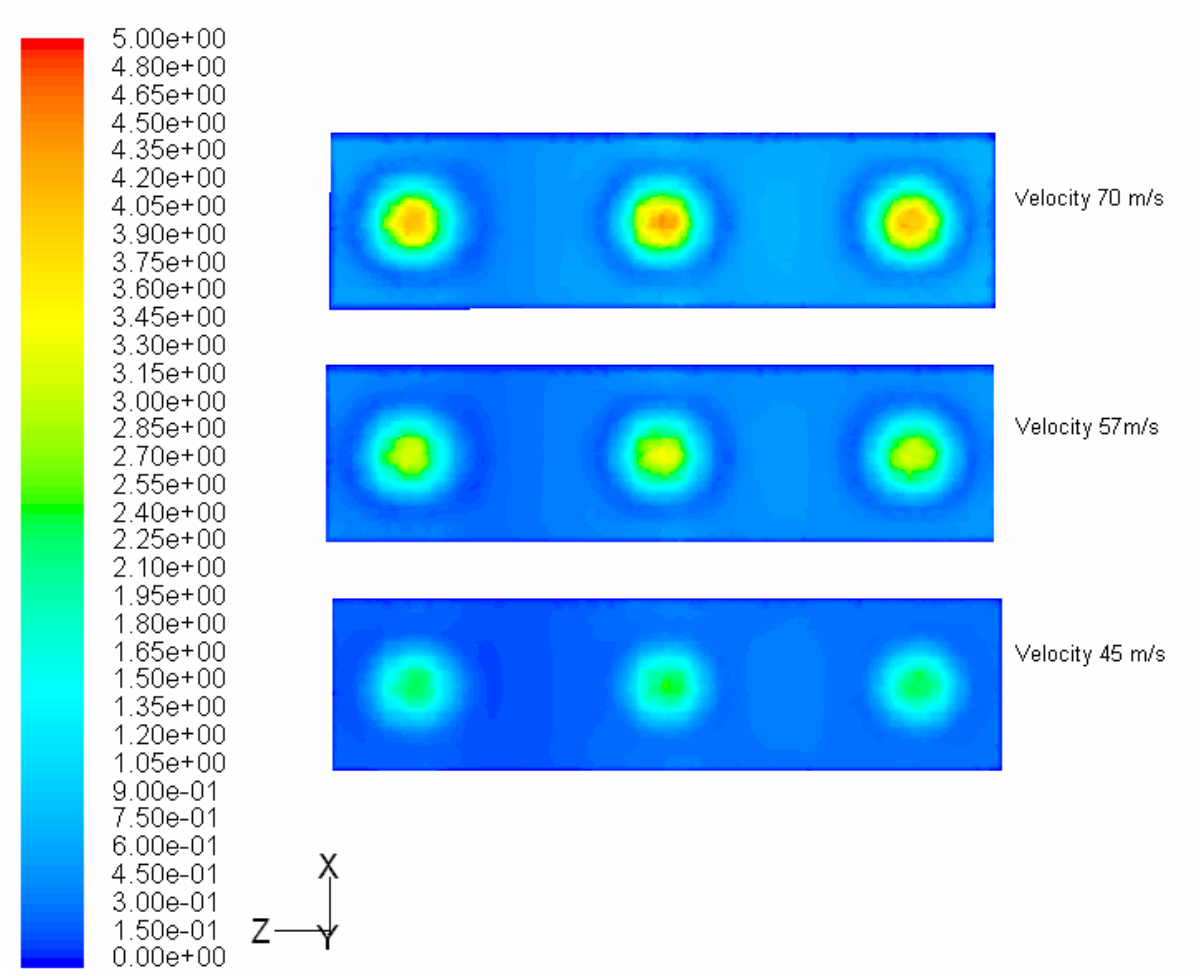

(b)

Figure 7.3: Plots of velocity contours for different values of inlet velocity, the contours are shown in a horizontal plane located at y = -50 cm and for a catalyst size of 0.3175 cm.

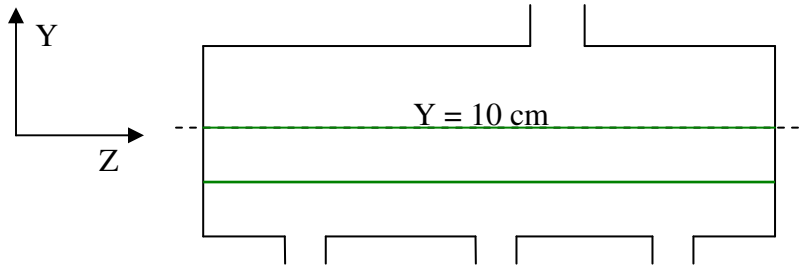

(a)

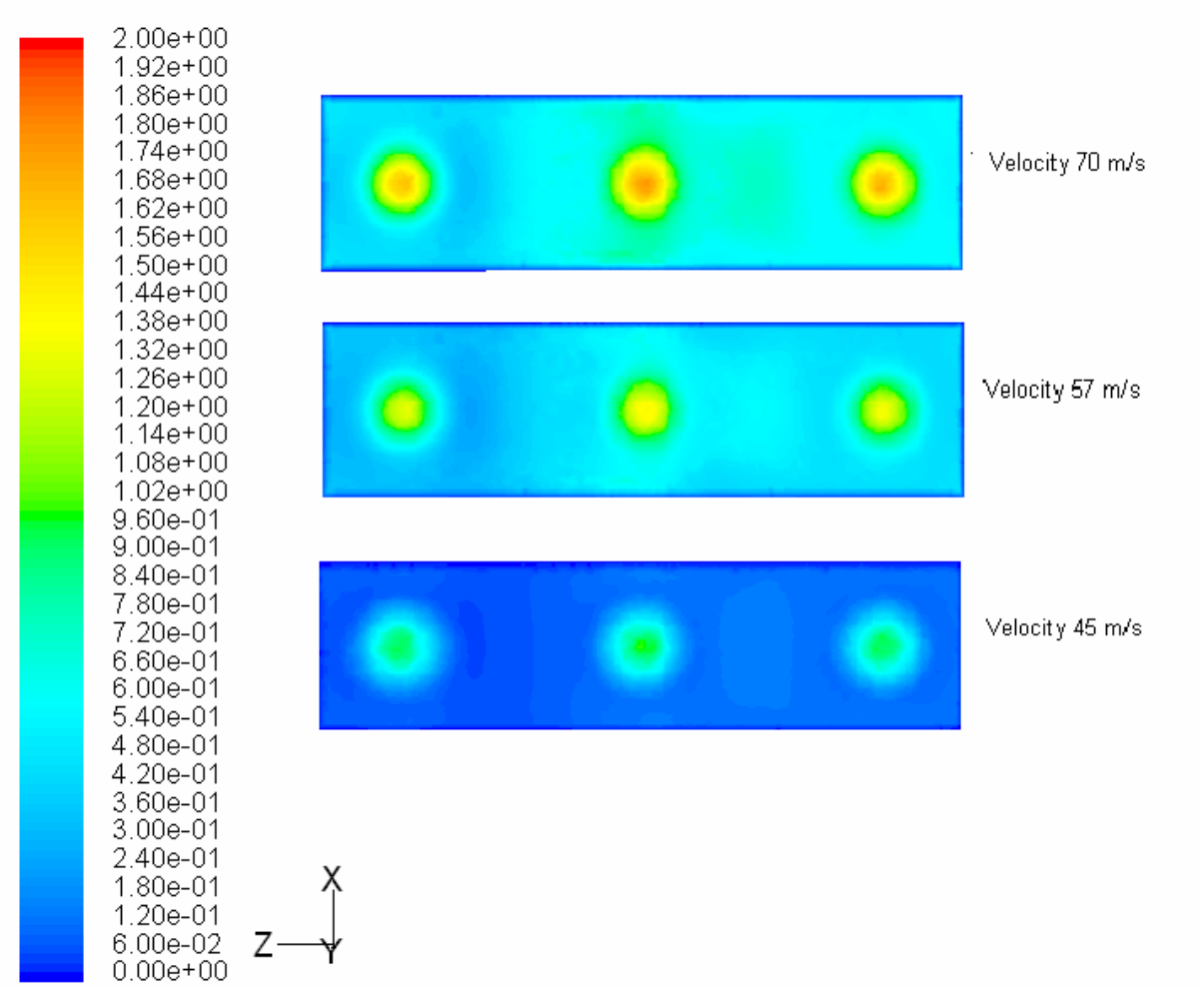

(b)

Figure 7.4: Plots of velocity contours for different values of inlet velocity, the contours are shown in a horizontal plane located at y = 10 cm and for a catalyst size of 0.3175 cm.

as zero and the variation along the length of the bed is observed. Positions are selected at three depths of the bed, i.e. in the y direction. The positions of the bed are taken as the same as those for the contours plots described earlier, i.e. y = -100 cm, y = -50 cm and y = 10 cm.

Figure 7.5 shows the line plots of velocity magnitudes versus position for three different values of the inlet velocity. These plots present the variation of the velocity magnitude along the length of the reactor i.e. the z axis. The lines are drawn at the position of y = -100 cm, that is near the inlet of the bed. This central line shown in this plot is created in between (0, -100, 0) and (0, -100, 1820). These plots show the variation in the velocity clearer than the contours plots. The velocity variations in the three areas of the jet impingements are much higher compared to those in other areas. The velocities lie between 0.2 and 2 m/s. The flow distribution is similar except for the peak values which increase as the inlet velocity increases. There are three noticeable peaks in the velocity plots and they correspond to the incoming jets or to their areas of impingement. These three regions are large and extend almost 4 m in width. The right jet impingement zone is slightly smaller in magnitude than the other two adjacent jets. The middle jet shows the highest velocity magnitudes. However the velocity in the zones between any two adjacent jets is very low.

Figure 7.6 depicts the line plots of the velocity along a line at y = -50 cm. The velocity magnitudes are found much lower than those of the previous figure. These fall between 0.1 to 5 m/s. The middle jet zone shows the highest peak compared to the other two jet impingement zones.

Figure 7.7 shows the line plots of the velocity along a line located at y = 10 and x = 0 cm. Velocity values ranges from 0.1 to 2.5 m/s. The interesting phenomenon found in the

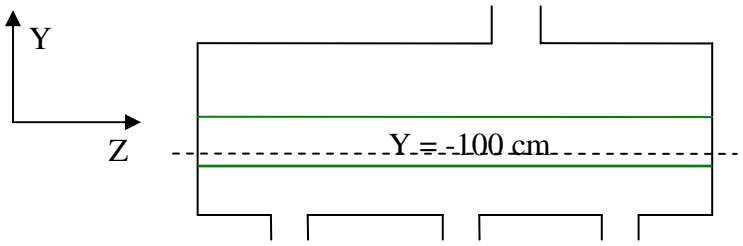

(a)

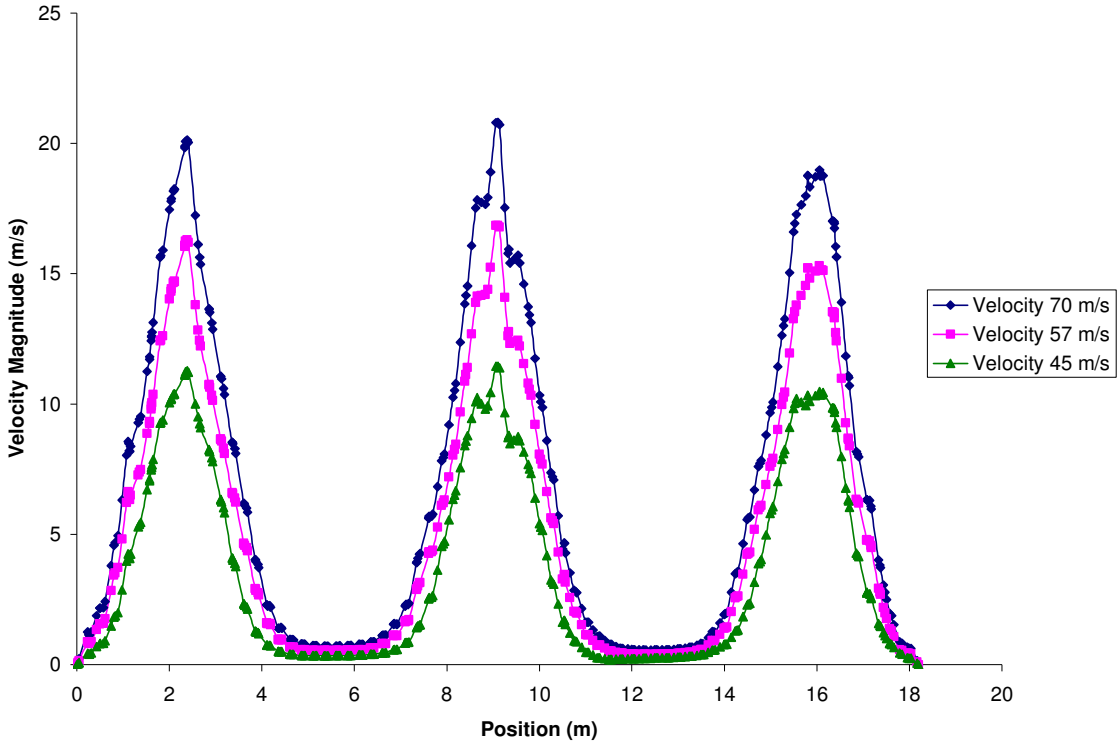

(b)

Figure 7.5: Line plots for different values of the inlet velocity, these plots present the variations of the velocity magnitude along the z- axis at y = -100 cm and for a catalyst size of 0.3175 cm.

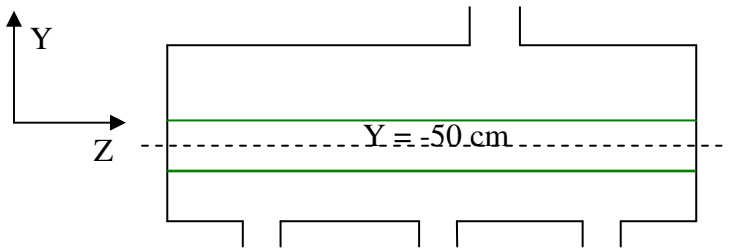

(a)

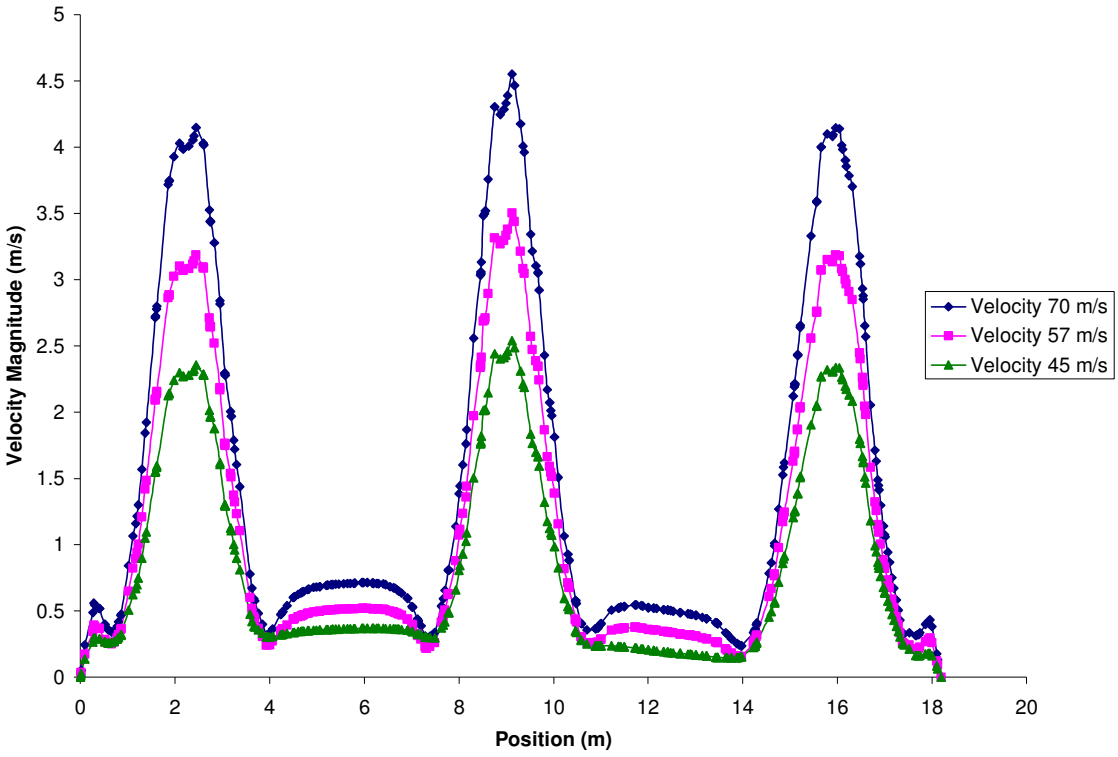

(b)

Figure 7.6: Line plots for different values of the inlet velocity, these plots present the variations of the velocity magnitude along the z- axis at y = -50 cm and for a catalyst size of 0.3175 cm.

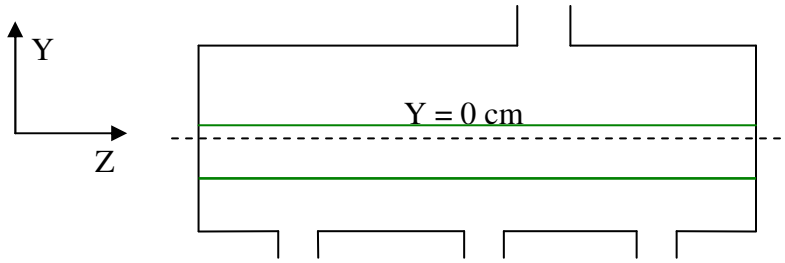

(a)

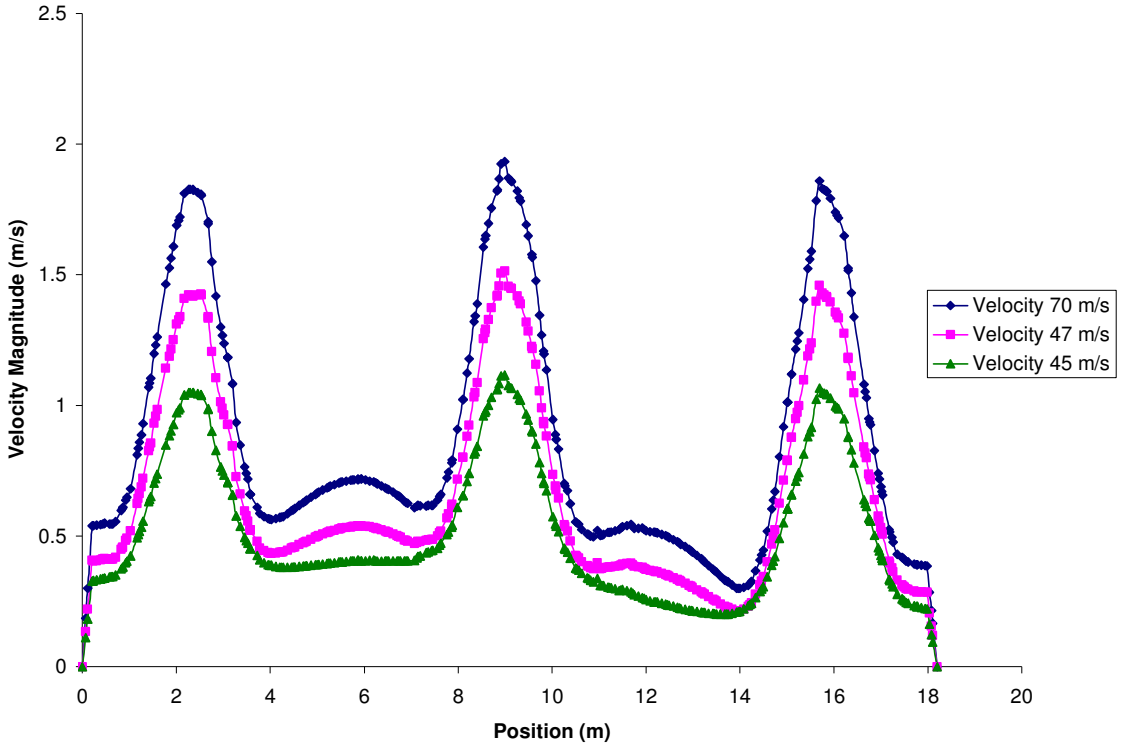

(b)

Figure 7.7: Line plots for different values of the theinlet velocity, these plots present the variations of the velocity magnitude along the z- axis at the centerline at y = 0 cm and for a catalyst size of 0.3175 cm.

bed that the velocity distributed evenly in low velocity areas. The velocity magnitude in the jet impingements is much closer to the adjacent low velocity areas. This means that the packed bed acts as a good distributor however, significant differences in the values of the velocity are still observed at the outlet of the bed.

In the last three line plots, the velocity fluctuations through the centerline of the bed i.e. the x = 0 were discussed. But it is also required to observe the velocity fluctuations in the horizontal directions i.e. y-z plane of the bed. In Figures 7.8 to 7.10, the fluctuations in the bed along different x positions in a y-z plane are discussed. For this purpose three x-positions are considered. These are one line at x = -50 cm, one at x = -100 cm and one closer to the wall at x = -200 cm position. All three positions are taken just before the outlet of the bed and it is at y = 0 cm.

Figure 7.8 shows the line plots at x = -50 cm. The line is slightly away from the center line. This line lies between (-50, 0, 0) and (-50, 0, 1820). The velocity magnitudes are slightly lower than that of the x = 0 cm and lie in between 0.1 and 1.6 m/s. The difference of velocity magnitudes among the impingement position and its adjacent low velocity zones becomes lower and it seems that the bed performs as a good flow distributor.

Figure 7.9 shows the velocity fluctuations in the bed at the point x = -100 cm. This line is taken at a position between the wall and the center of the bed. The line lies between (-100, 0, 0) and (-100, 0, -1820). In this case, a reasonably even distribution of the velocity is observed along the length of the converter and the difference between the maximum and minimum values of the velocities is rather small. The size of the low velocity zones is significantly reduced.

Figure 7.10 depicts velocity magnitudes along a line very close to the wall, i.e. at x= -200 cm. The line lies between (-200, 0, 0) and (-200, 0, 1820). Velocity magnitudes are much lower and lie in between 0.1 and 0.8 m/s. There are no impingement effect have found. It can be concluded after observing three different positions of the y-z plane that the outlet of the bed perfectly works as a good flow distributor and flow becomes evenly distributed near much more at the outlet of the bed.

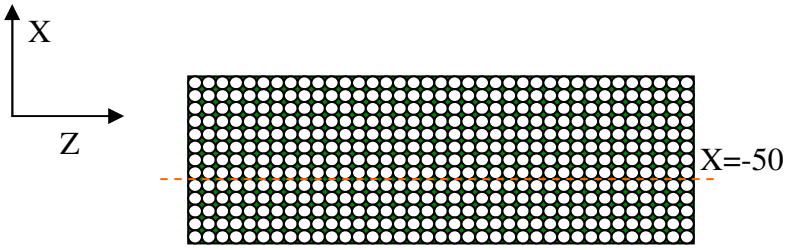

(a)

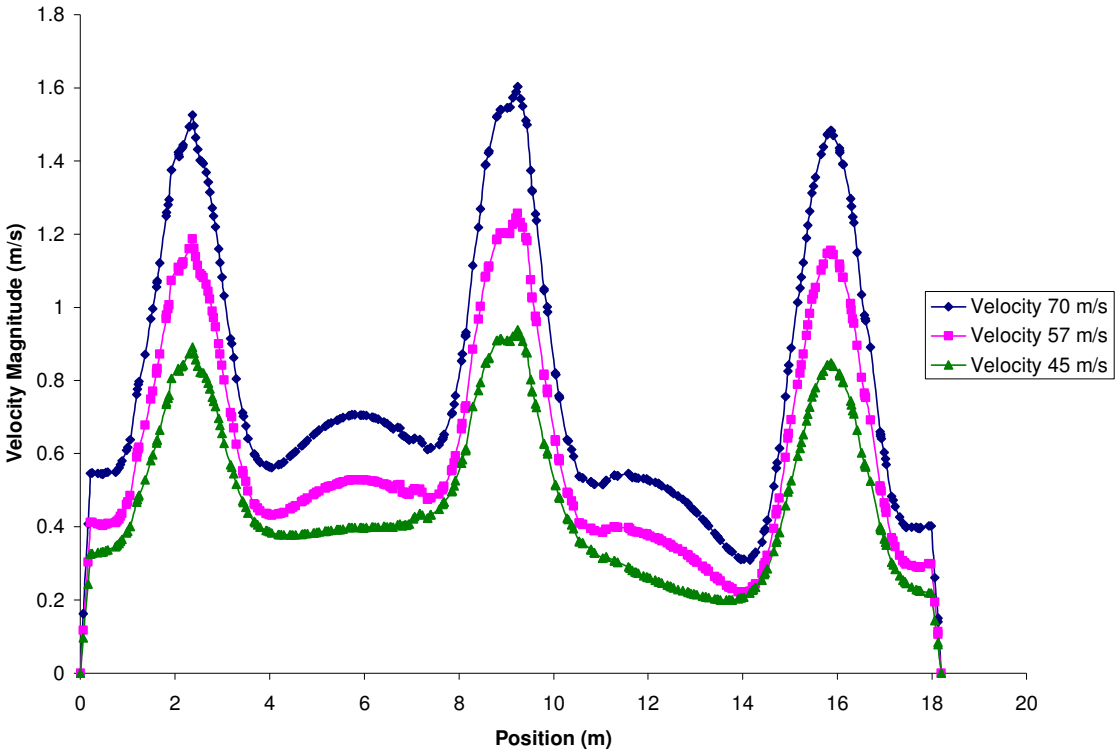

(b)

Figure 7.8: Line plots for different values of the inlet velocity, these plots present the variations of the velocity magnitude along the z- axis at x = -50 cm and for a catalyst size of 0.3175 cm.

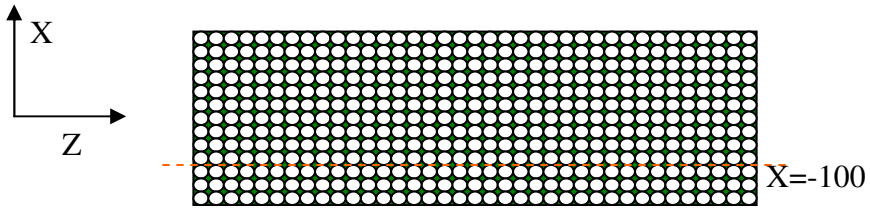

(a)

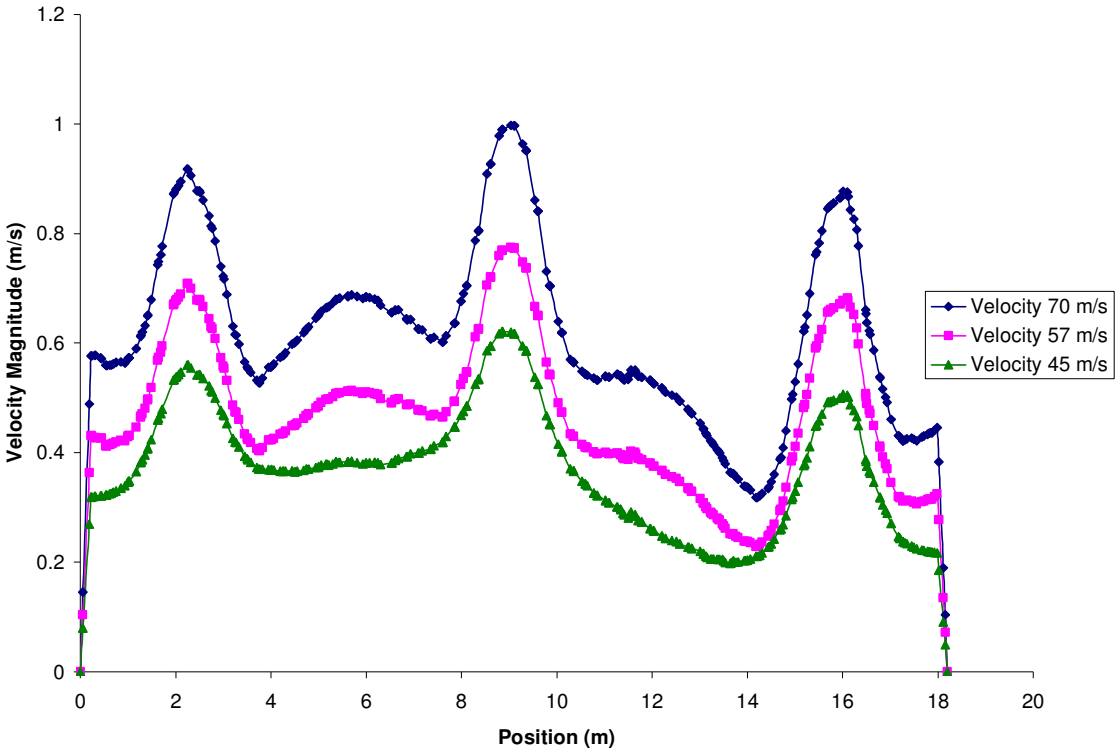

(b)

Figure 7.9: Line plots for different values of the inlet velocity, these plots present the variations of the velocity magnitude along the z- axis at x = -100 cm and for a catalyst size of 0.3175 cm.

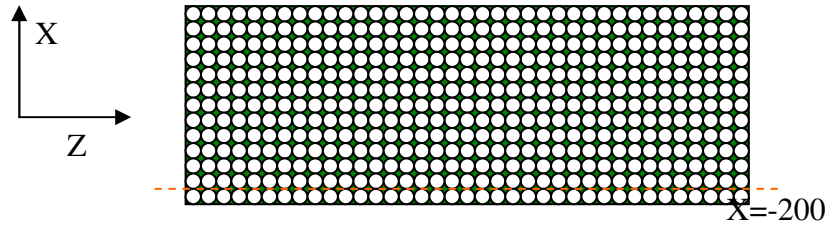

(a)

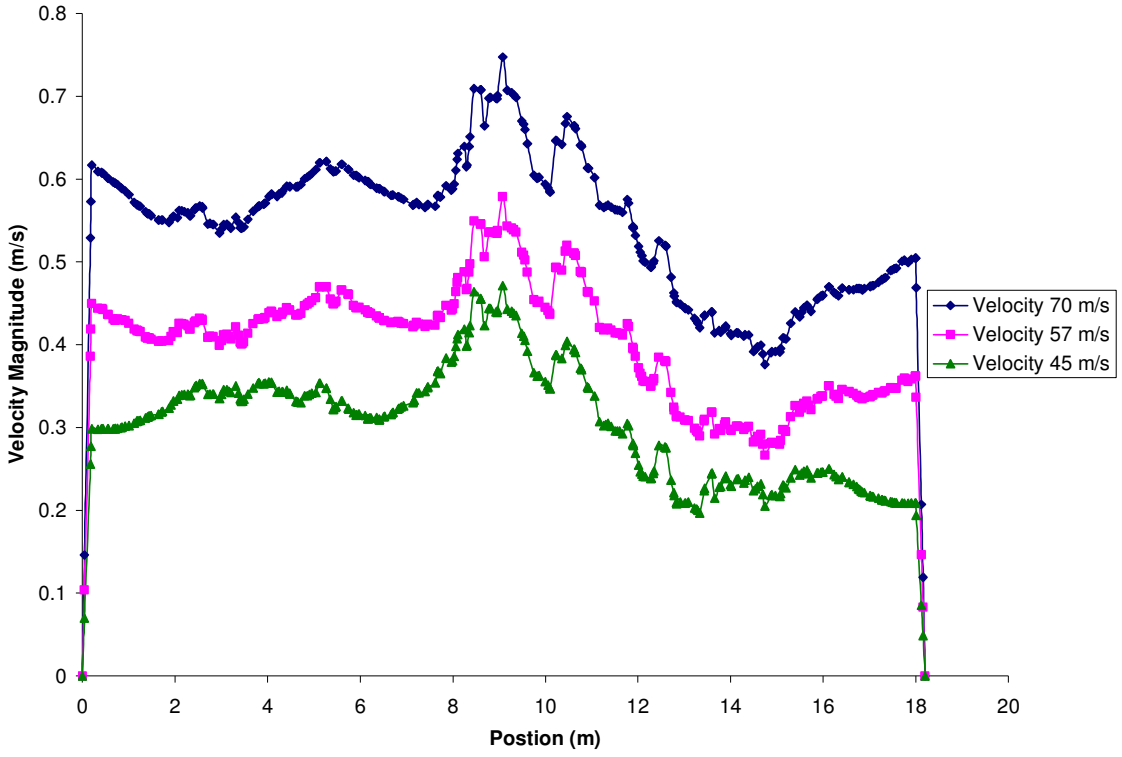

(b)

Figure 7.10: Line plots for different values of the inlet velocity, these plots present the variations of the velocity magnitude along the z- axis at x = -200 cm and for a catalyst size of 0.3175 cm.

Chapter 8
Simulation Results of Flows in an Industrial Partially Packed Vessel

8.1 Introduction

Fluid flow through packed beds is commonly encountered in industrial applications involving mass and heat transfer both with and without chemical reactions. In chemical engineering processes, packed beds are frequently used as catalytic reactors or filters and in separation processes like absorption, adsorption and distillation. Packed beds are extensively used in petroleum, petrochemical and biochemical applications. In the design of these devices, fluid dynamics plays an important role, since the transport of the chemical species, mixing or contacting catalytic surfaces, is entirely described by the conservation laws. A complete understanding of the fluid flow distribution in packed bed is of considerable practical importance due to its significant effect on the species transport and reaction rates.

CFD can be used to model a wide variety of flows through porous media, including flow through packed beds, perforated plates, flow distributors and tube banks. In one type of modeling, a zone is defined in which the porous media model is applied and the pressure loss in the flow is determined via user-defined inputs. Heat transfer through the medium can also be represented, subject to the assumption of thermal equilibrium between the mediums. Typically a porous media model incorporates an empirically determined flow resistance in a region of the model defined as porous. A porous media model is nothing more than an added momentum sink to the governing momentum equations.

Quantitative understanding of flow nonuniformities in packed beds is of considerable practical importance in chemical reaction engineering. Non-uniformities of flow will also occur when the fluid passing through the system is introduced in non-uniform manner. The present work is specially focused on the particle diameter and changing the velocities to investigate the flow distribution. A porosity of 0.5 was used in the previous chapter and is in the range of the porosities of industrial packed beds. Consequently this value of 0.5 is used in the current simulations. The effects of varying the particle size and the inlet velocity on the flow patterns are investigated. Two sizes, commonly used in industries, namely 0.3175 cm (1/8 inches) and 0.254 cm (1/10 inches) are used in the current simulations.

In this study, the flow simulation was carried out in a partially packed vessel of industrial dimensions, the feed gas in this chapter is injected through the top of the converter and the gas products leave through the bottom. This direction is the reverse of that used in the previous chapter. There is no main reason why the flow in the previous chapter was chosen to be upwards. However, as will be explained later, the flow pattern inside the vessel was not greatly influenced by changing the inlets from the top of the vessel to its bottom. The investigations were carried out in a geometry similar to that of an industrial Claus converter. The dimensions are the same as in the previous chapter that is a horizontal cylinder 18.2 m long and 4.8 m in diameter. In addition, a packed bed of 1.2 m height is inserted 1.4 m above the vessel bottom as shown in Figure 8.1. The feed gas is introduced through three inlets located at the top of the vessel, and the outlet product is located at the bottom of the vessel. The first and the third inlets are 2 m apart from the end of the reactor. The middle inlet is placed symmetrically between the other two inlets, i.e. 6.2 m away from each of the other

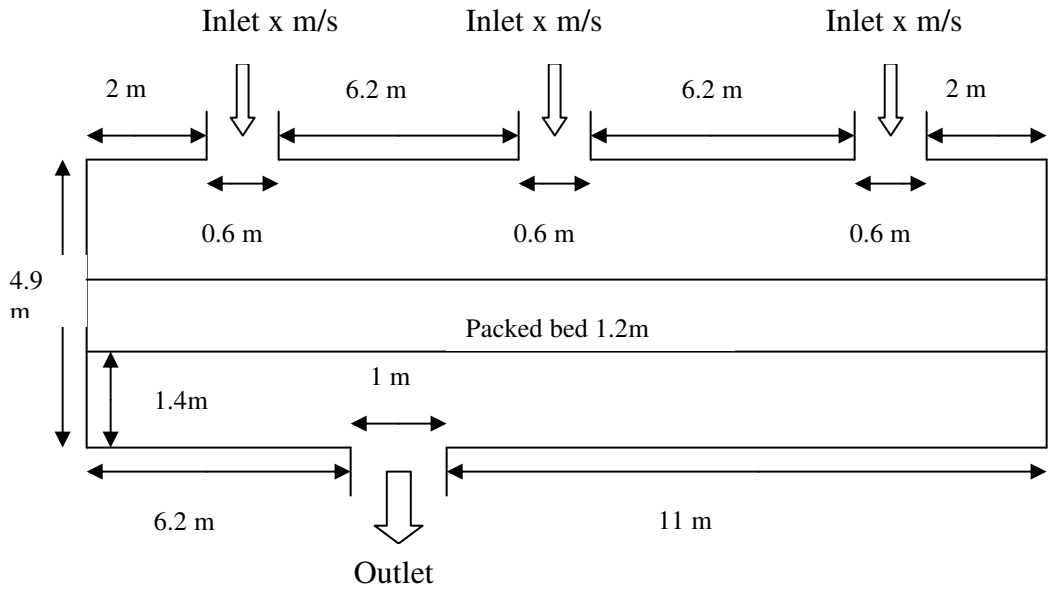

Figure 8.1: A schematic diagram of the partially packed vessel used in the present chapter.

two inlets. Each inlet is 0.6 m in diameter and the only outlet is 1 m. The outlet is placed 6.2 m away from the left end and 11 m from the right end of the vessel.

8.2 Simulation Results of the Partially Packed Vessel Using a Catalyst of Diameter 0.3175 cm

Results of the simulation of the partially packed vessel are presented in this section. An alumina based spherical catalyst of 0.3175 cm diameter is used in the packed bed. The porosity of the bed is taken as 0.5. Figures 8.2 to 8.4 show plots of velocity contours for different values of the inlet velocity. The present work is three dimensional so the flow distribution in the bed from all three directions can be examined. The velocity contours are plotted in three horizontal (x-z) planes, one is near the top of the bed, one near the middle of the bed and a third plane near the bottom of the bed. Through this top view of the velocity contours one can get a clear understanding of how the flow changes across the bed.

The x-z planes used in Figures 8.2 to 8.4 are positioned along the depth of the bed, namely at y = 10 cm, y = -50 cm and y = -100 cm, the origin being at the center of the converter. The total bed depth is 120 cm. The origin of the coordinate system is located 10 cm below the top of the bed. So the plane at y = 10 cm means it is at the top or the inlet of the bed where the three jets are impinging. The y = -50 cm position represents the middle of the bed. The y = -100 cm position represents the bottom or the outlet position of the packed bed. Through these three top views one could closely examine the flow distribution in the bed. Three different inlet velocities (70 m/s, 57 m/s and 45 m/s) were used in order to investigate the effects of varying the inlet velocity on the flow distribution.

Figure 8.2 shows the velocity contours in a horizontal plane near the top or the inlet position of the bed. Due to the high bed resistance to flow, the velocity suddenly drops when

it hits the bed. The contour plots in Figure 8.2 show a maximum velocity of 20 m/s The velocity magnitudes are much higher in the jet impingement zone. Varying the inlet velocity from the 45 m/s to 70 m/s did not have a significant impact on the flow distribution inside the bed. The flow distribution was similar for all the three inlet velocities, however, the values of the velocities were higher for a higher inlet velocity. Significantly lower velocities are observed in the regions located between two adjacent jets.

Figure 8.3 shows the plots of the velocity contours for three different values of the inlet velocity. The contours are shown in a horizontal plane at y = -50 cm, i.e. at the middle of the bed. The velocity magnitudes in this location are much lower than those near the inlet of the bed. The velocity magnitudes lie between 0.2 and 5 m/s compared to values between 0.2 and 20 m/s in Figure 8.2. The velocity distribution observed in each of the three cases showed a similar trend. Based on these contour plots, no clear advantage could be seen in changing the operational inlet velocity from 57 m/s to 45 m/s or 70 m/s.

Figure 8.4 shows the velocity contours in a horizontal (x-z) pane at y = -100 cm, this means the plane is near the bottom or the outlet of the catalyst bed. The velocity magnitudes decreased slightly compared to those in the middle position of the bed. In this figure the velocities are between 0.2 to 3 m/s. In these low velocity zones the cases with an inlet velocity of 70 and 57 m/s gave a velocity distribution better than that of the 45 m/s.

Line plots give a clearer and a more quantitative picture of how the flow distribution changes in the bed. The three central line plots are presented at three different depths of the bed. All three lines are taken at the center position of horizontal x-z surfaces. In all cases the x position is taken as zero and the variation along the length of the bed was observed. Positions are selected at three depths of the bed i.e. in the y-direction. The positions of the

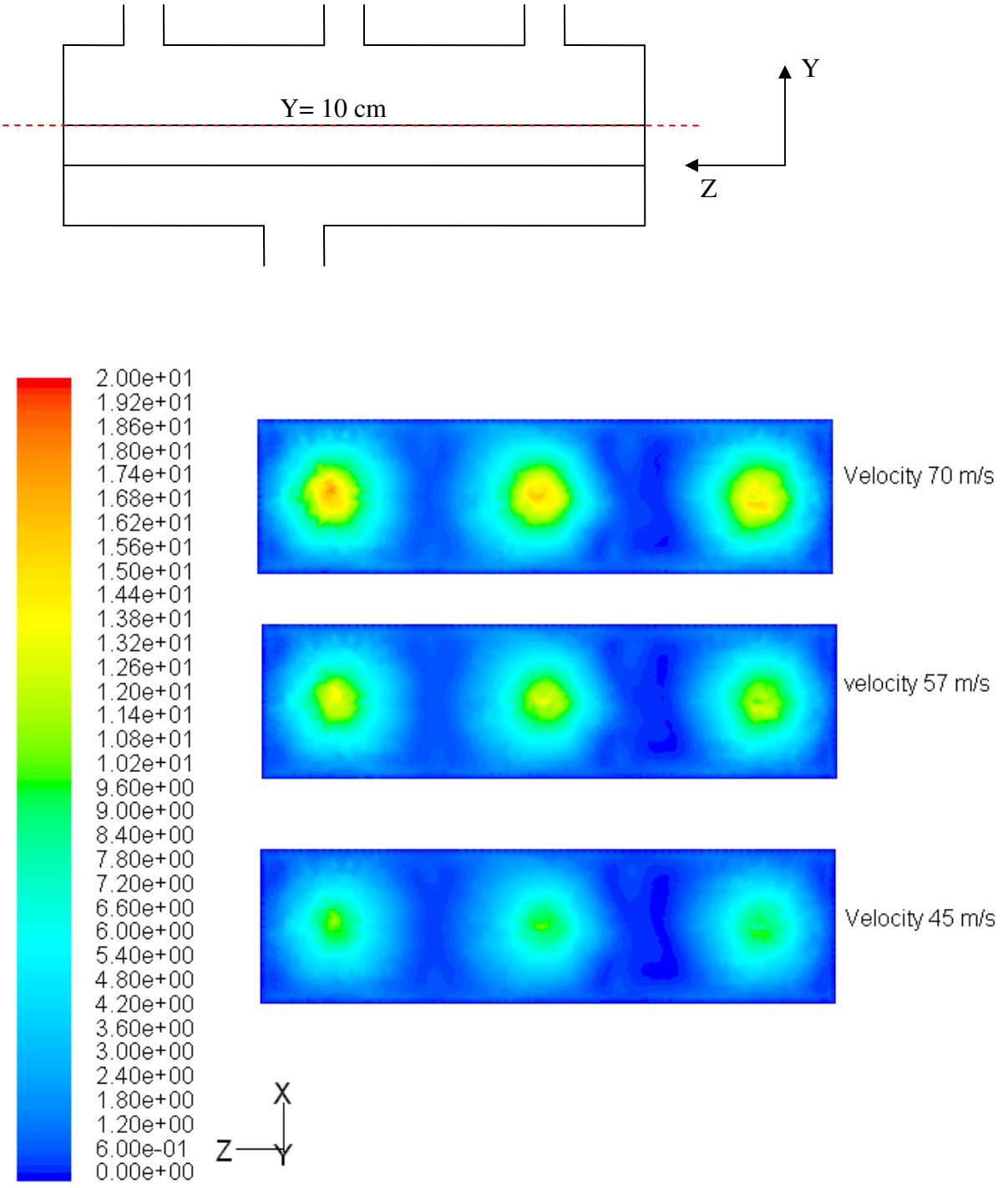

Figure 8.2: Plots of the velocity contours for different values of the inlet velocity, the contours are shown in a horizontal plane located at y = 10 cm and for a catalyst size of 0.3175 cm.

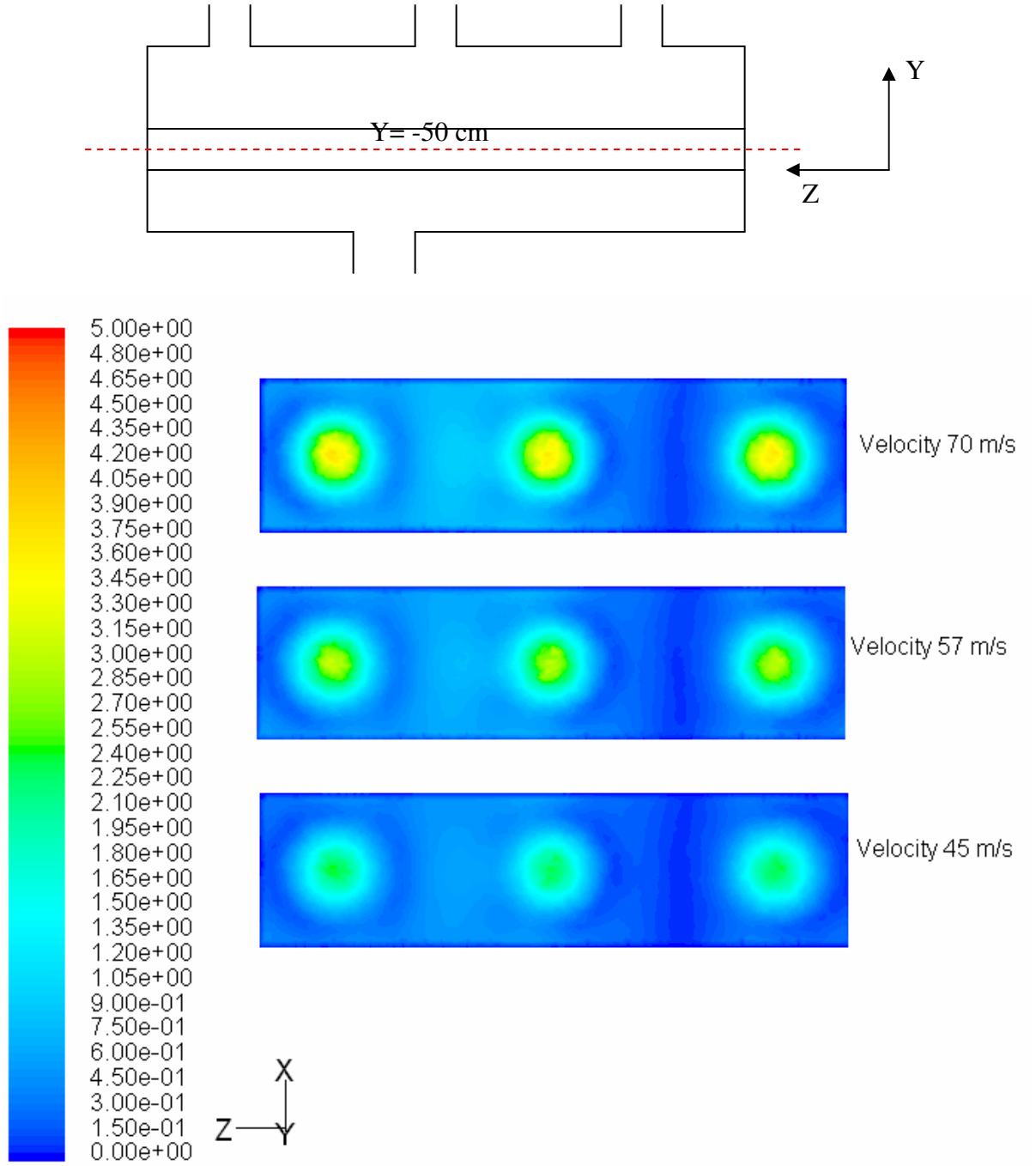

Figure 8.3: Plots of the velocity contours for different values of the inlet velocity, the contours are shown in a horizontal plane located at y = -50 cm and for a catalyst size of 0.3175 cm.

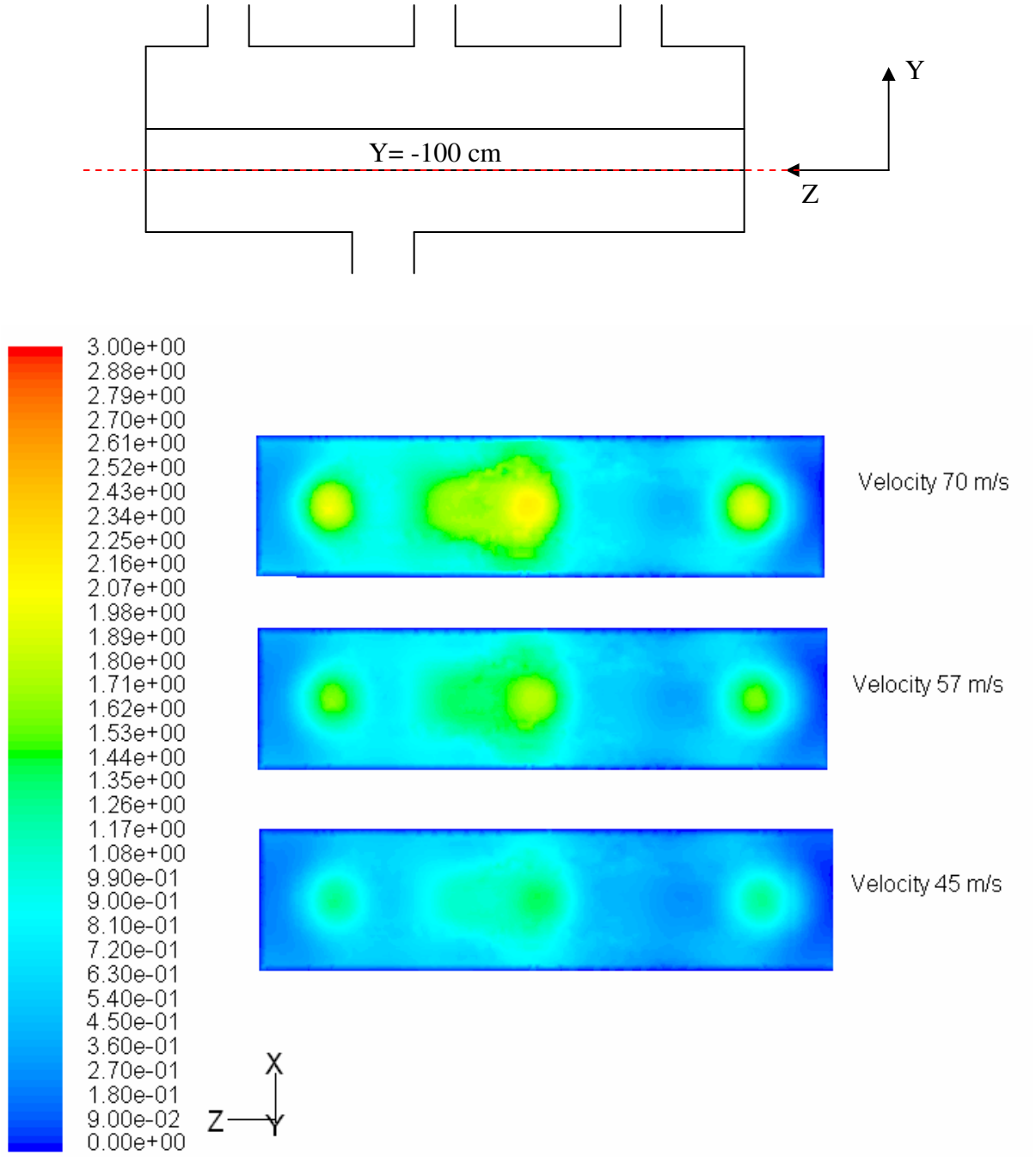

Figure 8.4: Plots of the velocity contours for different values of the inlet velocity, the contours are shown in a horizontal plane located at y = -100 cm and for a catalyst size of 0.3175 cm.

bed are the same as for the contours plots described earlier, i.e. y = 0 cm, y = -50 cm and y = -100 cm.

Figure 8.5 shows the line plots for the three different values of the inlet velocity. These plots present the variation of the velocity magnitudes along the length of the vessel i.e. the z axis. The lines are drawn at y = 10 cm, that is at the inlet or top of the bed. This central is drawn between (0, 10, 0) and (0, 10, 1820). The plots show that the variations in the velocity distribution clearer than in the contours plots. These plots show the variations in the three areas of the jet impingement are much higher than those velocities in other areas. The velocities lie between 0.2 and 18 m/s. The flow distribution is similar except for the peak values which increase as the inlet velocity increases. There are three noticeable peaks in the velocity plots and they correspond to the incoming jets or to their areas of impingement. These three areas are large and extend almost 4 m in width. The first jet impingement area in the bed is slightly smaller in magnitude than the other two impingements areas. The middle jet shows the highest magnitude. However, the magnitude of the velocity in the areas between adjacent jets is very low.

Figure 8.6 depicts the line plots at a position of the bed at y = -50 cm. This is a central line between (0, -50, 0) and (0, -50, 1820). The velocity magnitudes are found to be much lower than those in the plane near the bed inlet. Velocities in Figure 8.6 lie between 0.1 to 4 m/s. The highest velocity is observed in the area of impingement of the middle jet. This observation is also applicable to Figure 8.5. The velocity magnitude in the zone between the middle and the right peaks has significantly increased compared to the same zone in Figure 8.5. This is due to the role of the catalyst bed as a flow distributor.

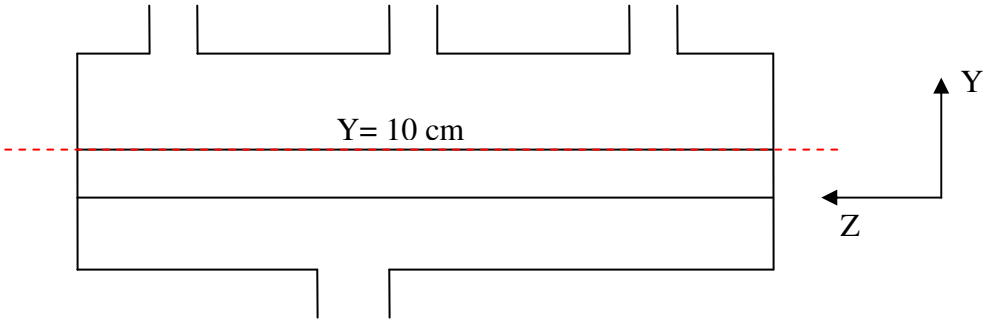

(a)

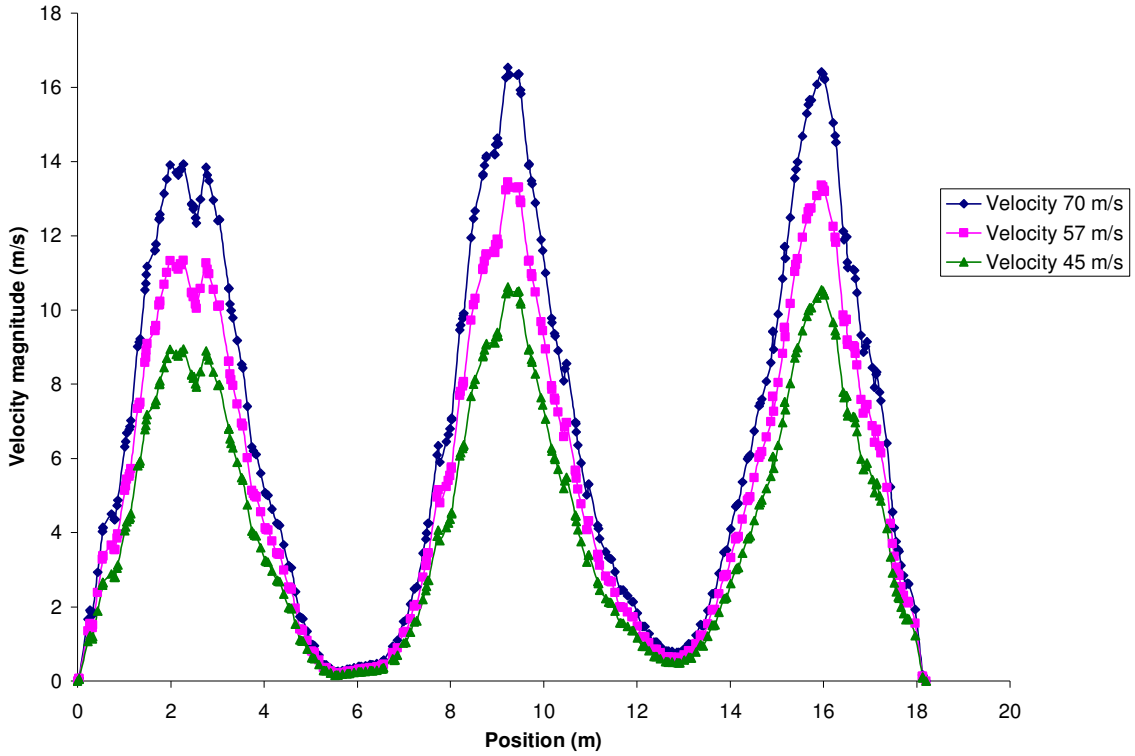

(b)

Figure 8.5: Line plots for three different values of the inlet velocity, these plots show the variation of the velocity magnitude along the z-axis at y = 10 cm and for a catalyst size of 0.3175 cm.

Figure 8.7 shows the velocity values along a central line in a horizontal plane at y = -100 cm. The line is between (0, -100, 0) and (0, -100, 1820) and is located near the outlet of the bed. The velocity magnitude is between 0.4 m/s and 1.7 m/s for the case of 57 m/s inlet velocity. For an inlet velocity of 70 m/s, the velocity range is 0.5 to 2.2 m/s. This range is 0.2 m/s to 1.4 m/s for an inlet velocity of 45 m/s. the velocity distribution in the lower part of the bed is significantly more even than in the upper part of the bed.

The previous three figures showed the velocity distribution along central lines at various depth of the bed. It is also worthwhile investigating the flow distribution in the same horizontal plane. Figures 8.8 to 8.11 show the velocity fluctuations along lines in the same horizontal plane. Four such lines are chosen in an x-z plane at y = 0 cm. These are located at x = 0 cm, x = -50 cm, x = -100 cm and x= -200 cm. x = 0 cm is a central line and the radius of the vessel is 245 cm. This means that x = -200 cm is close to the wall of the vessel.

Figure 8.8 depicts the velocity values along a central line at x = 0 cm. This plot presents the variation of velocity magnitude along the z- axis. This line lies between (0, 0, 0) and (0, 0, 1820). The velocity magnitudes vary from 0.2 to 14 m/s. The flow distribution is similar except for the peak values which increase as the inlet velocity increases. There are three noticeable peaks in the velocity plots and they correspond to the incoming jets or to their areas of impingement. These three areas of impingement are large and extend almost 4 m in width. The left velocity peak is slightly smaller in magnitude than the other two adjacent jets. The velocity between any two adjacent jets is very low.

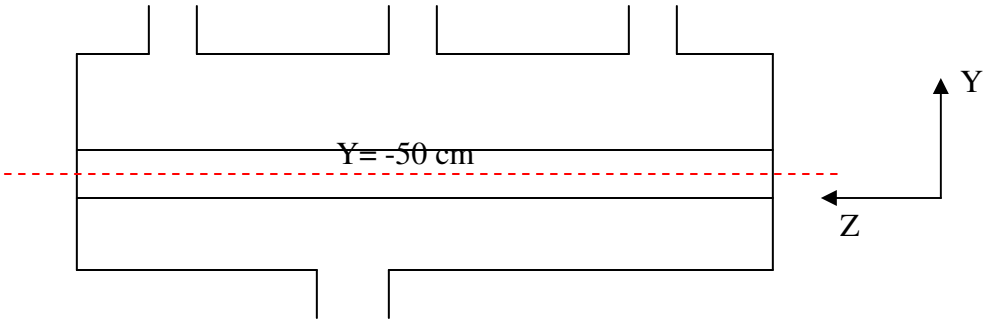

(a)

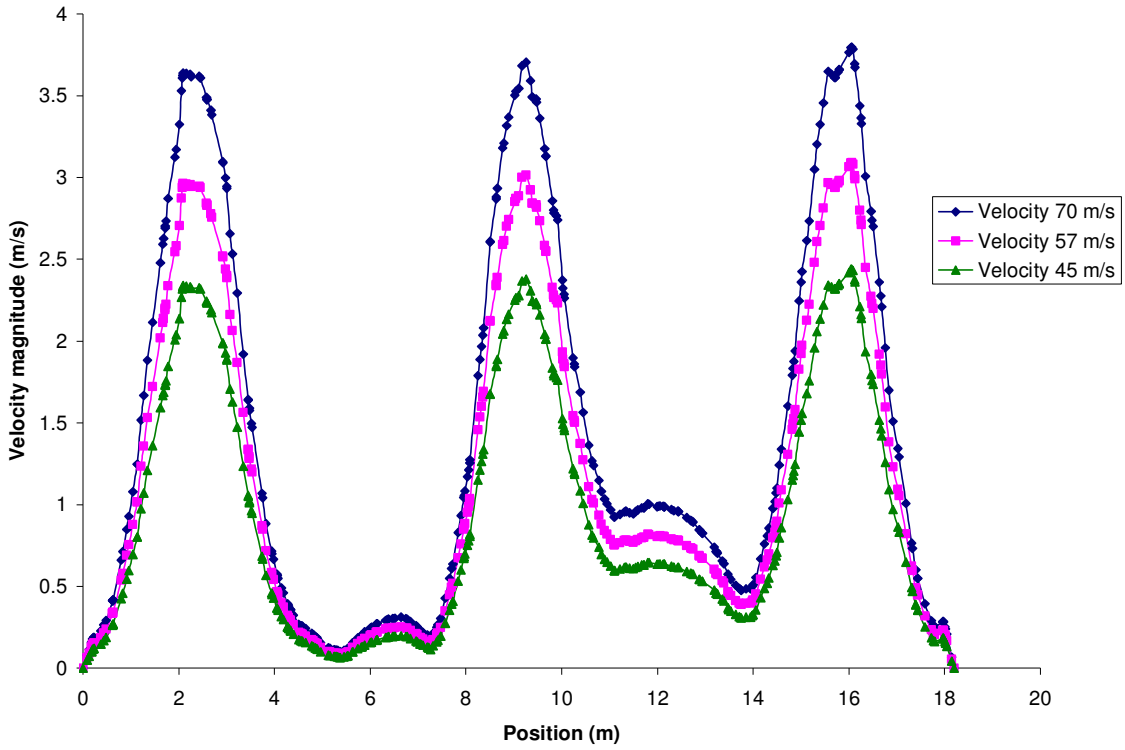

(b)

Figure 8.6: Line plots for three different values of the inlet velocity, these plots show the variations of the velocity magnitude along the z-axis at y = -50 cm and for a catalyst size of 0.3175 cm.

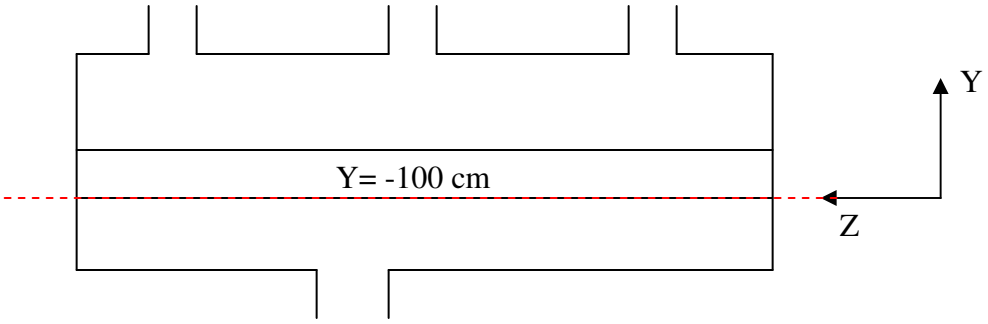

(a)

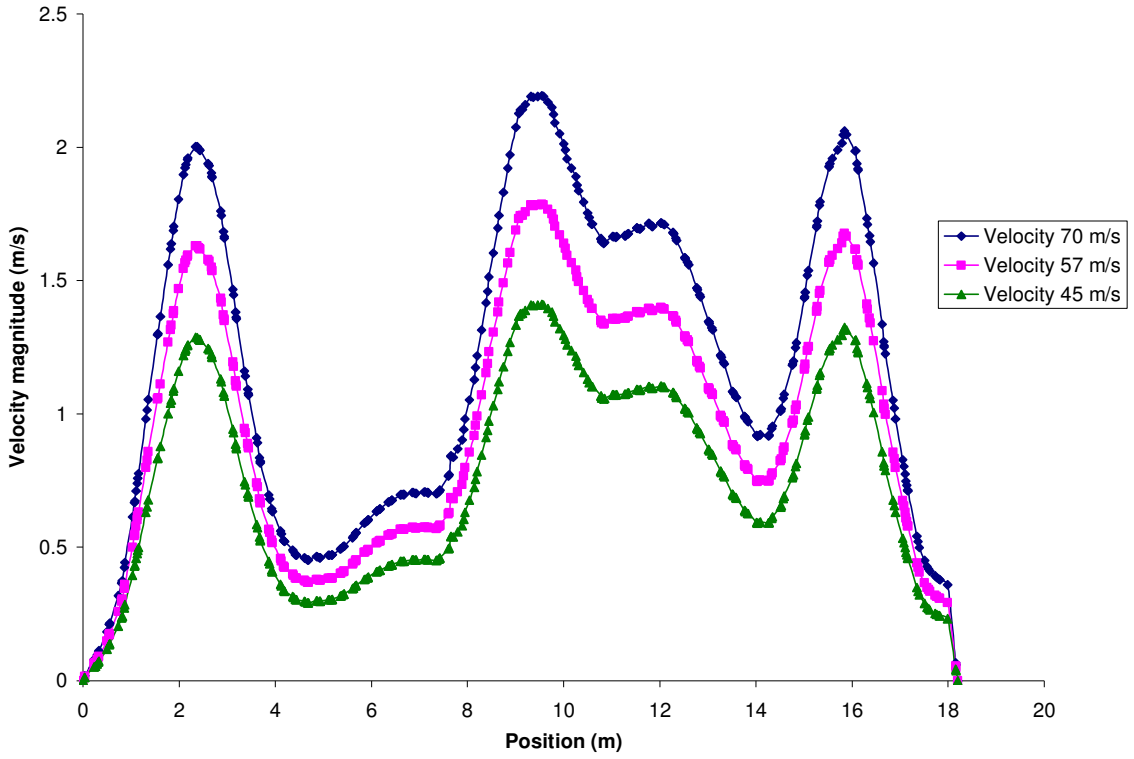

(b)

Figure 8.7: Line plots for three different values of the inlet velocity, these plots show the variations of the velocity magnitude along the z-axis at y = -100 cm and for a catalyst size of 0.3175 cm.

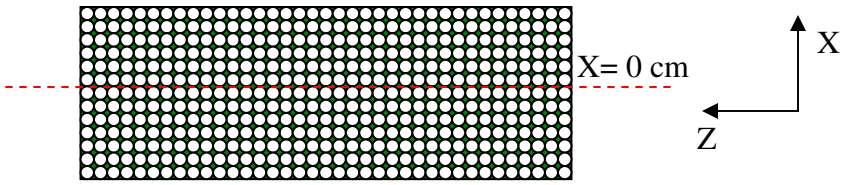

(a)

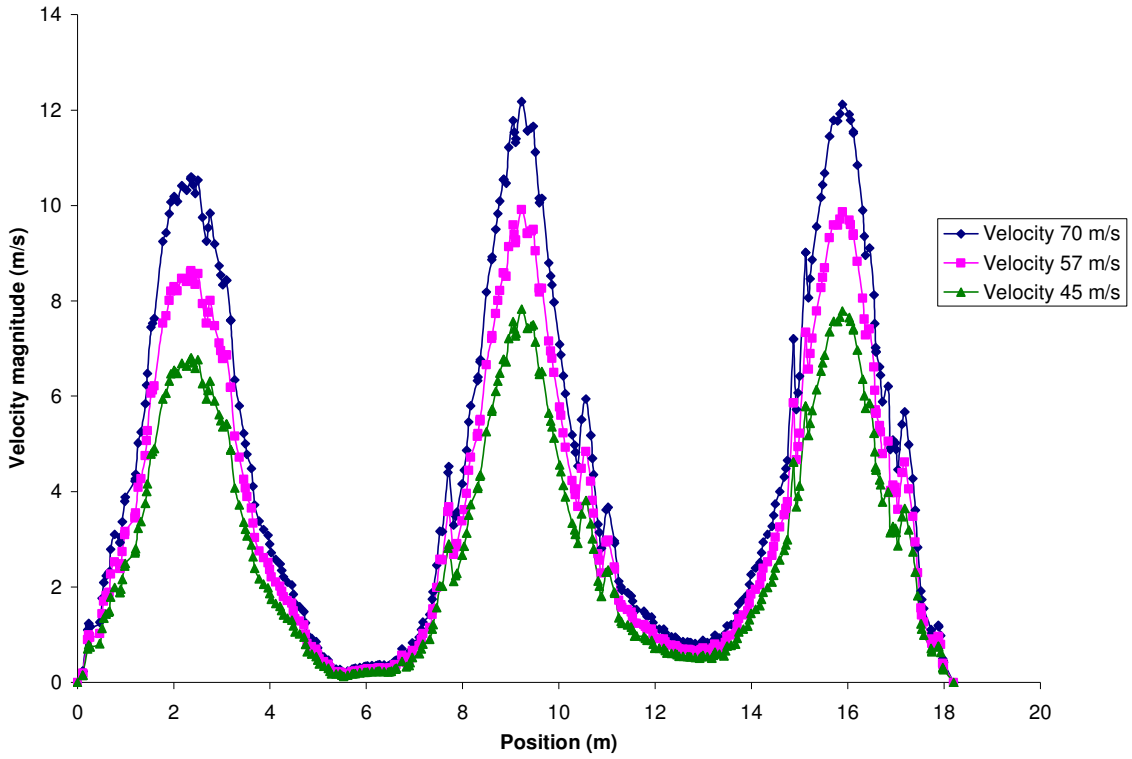

(b)

Figure 8.8: Line plots for three different values of the inlet velocity, these plots present the variation of the velocity magnitude along the z-axis at x = 0 cm and for a catalyst site of 0.3175 cm.

Figure 8.9 shows a plot of velocity values along a line x = -50 cm. This line is just off the center, it lies between (-50, 0, 0) and (-50, 0, 1820). The velocity magnitudes are slightly lower than those velocity along the x = 0 line. The velocity magnitudes, range is between 0.2 and 12 m/s. But the velocity fluctuations are almost the same as for the previous position at x = 0 cm.

Figure 8.10 shows the velocity fluctuations along a line at x = -100 cm. This line lies almost halfway between the center and the wall of the vessel. It is drawn between (-100, 0, 0) and (-100, 0, 1820). The velocity magnitudes are significantly lower than those along the line at x = -50 cm. The velocity ranges between 0.2 and 8 m/s. The first and the last peaks show some interesting behavior. The velocity in the zones of the jet impingement shows limited fluctuations. This fluctuation could be due to the proximity wall and will be further investigated at a later section. The maximum velocity is significantly lower than along the central line (x = 0) and the velocity in between adjacent zones is higher than before.

Figure 8.11 depicts velocities along a line very close to the wall and the position is at x = -200 cm. The line lies in between (-200, 0, 0) and (-200, 0, 1820). In this region the velocity fluctuations become severe and the velocity is much lower than in the previous cases. These fluctuations will be farther investigated. The velocity ranges from 0.1 to 3 m/s. Since this line lies close to the wall so the velocity magnitudes decreases sharply compared to the velocity values along central lines. The difference between the maximum and the minimum velocity values is reduced in the near wall zone.

In summary, a detailed inspection of the flow field was carried out to investigate the flow distribution inside the packed bed for three different values of the inlet velocity. The packed bed, as expected, acted as reasonable flow distributor, however certain fluctuation

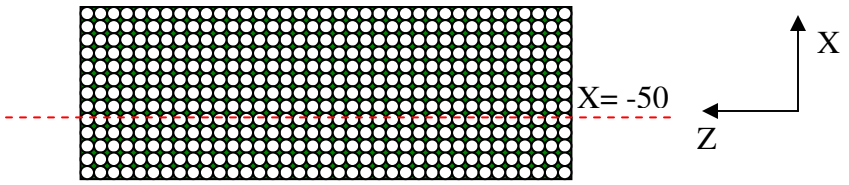

(a)

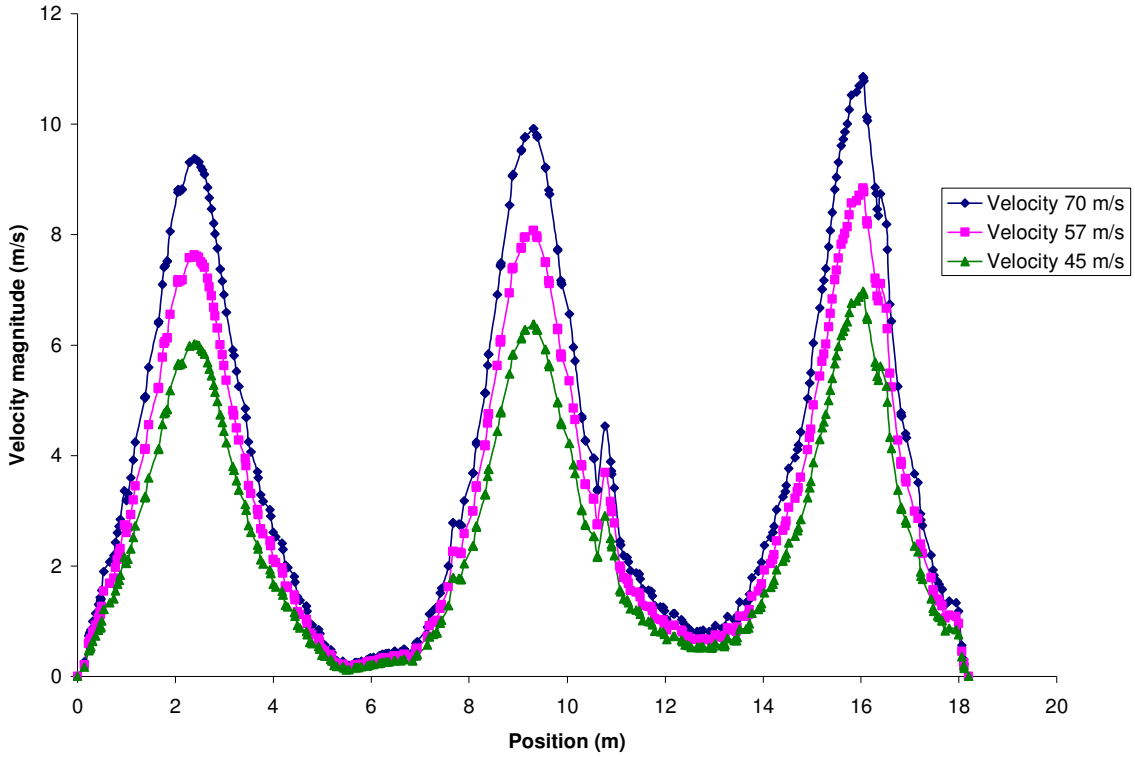

(b)

Figure 8.9: Line plots for three different values of the inlet velocity, these plots present the variation of the velocity magnitude along the z-axis at x = -50 cm and for a catalyst site of 0.3175 cm.

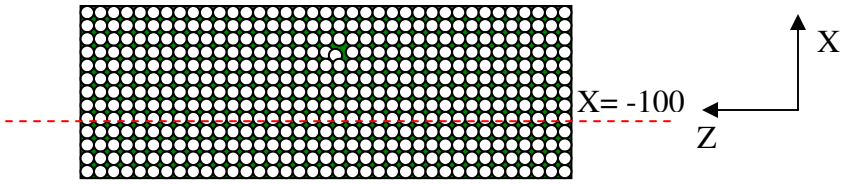

(a)

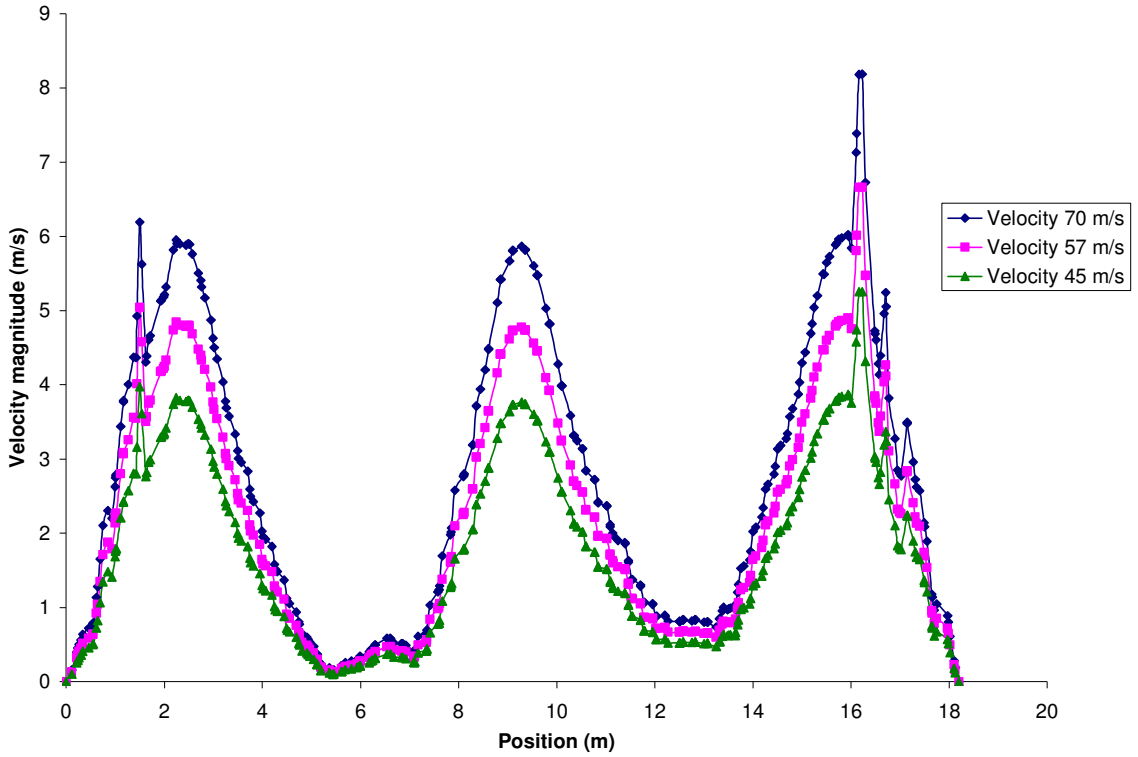

(b)

Figure 8.10: Line plots for three different values of the inlet velocity, these plots present the variation of the velocity magnitude along the z-axis at x = -100 cm and for a catalyst site of 0.3175 cm.

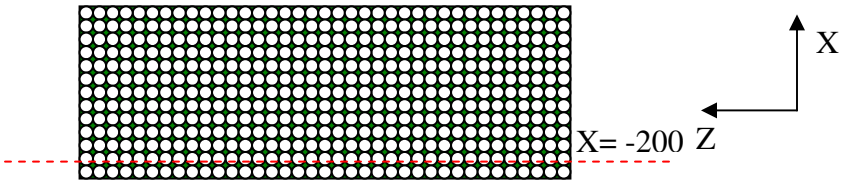

(a)

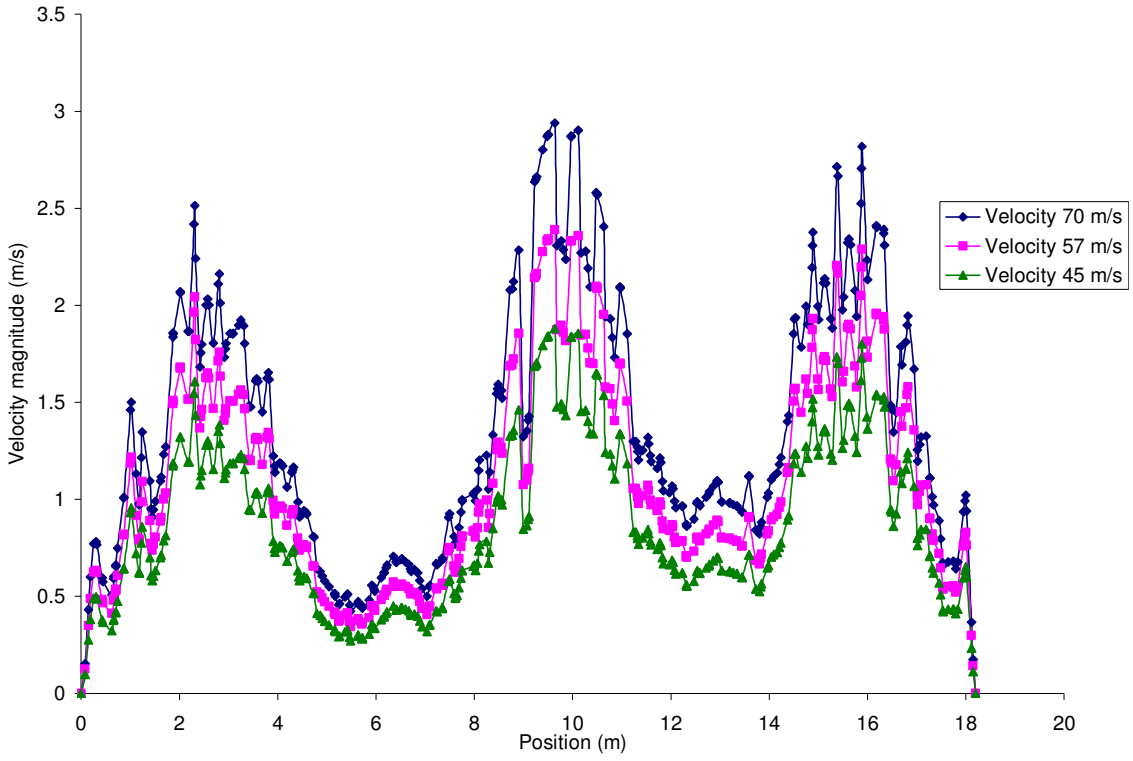

(b)

Figure 8.11: Line plots for three different values of the inlet velocity, these plots present the variation of the velocity magnitude along the z-axis at x = -200 cm and for a catalyst site of 0.3175 cm.

across the depth and the breadth of the bed were still observed. The magnitude of the inlet velocity had little impact on the flow distribution. The flow distribution in the bottom half of the bed is more even compared to that in the top half.

8.3 Simulation Results of the Partially Packed Vessel Using a Catalyst of Diameter 0.254 cm

The previous results dealt with the flow distribution in the bed which consists of particles 0.3175 cm (1/8 inch) in diameter. In this section, the partially packed vessel, provided with a catalyst 0.254 cm (1/10 inch) in diameter, is simulated. The porosity of the bed is taken as 0.5. Figures 8.12 to 8.14 show plots of the velocity contours for three different inlet velocities, namely 45, 57 and 70 m/s. The contours plots are taken in x-z planes at three positions along the depth of the bed that is in y direction.

These x-z planes are located at y = 10 cm, y = -50 cm and y = -100 cm. The total bed depth is 120 cm. The origin of coordinates is located just 10 cm below the top of the bed. Therefore the plane at x= 10 cm is located at the top of the bed where the three jets are impinging. The y = -50 cm line is in the middle of the bed, and the y = -100 cm line is at the bottom of the packed bed.

The relation in the particle size t has some effects on the flow distribution in the bed as discussed in this section. Figure 8.12 shows the velocity contours in central planes near the top of the bed. Due to the high resistance to flow offered by the bed, the velocity suddenly drops when it hits the bed. The velocity magnitudes in these plots range between 0.2 and 18 m/s. The velocity magnitudes are highest in the zones of the jet impingement. Varying the inlet velocity from 45 m/s to 70 m/s did not have a significant impact on the flow distribution in the bed. The distribution was similar for all three inlet velocities; however, the values of

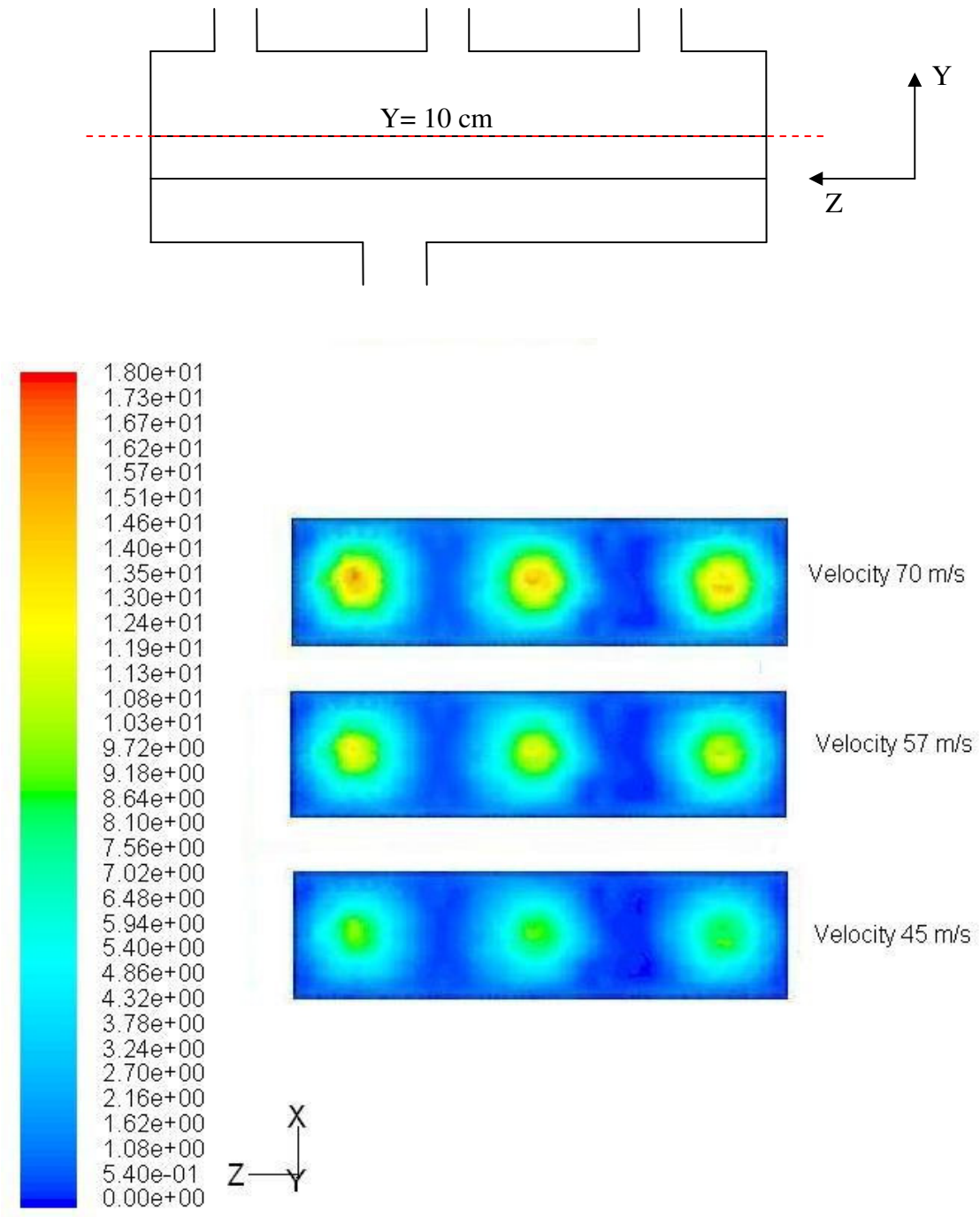

Figure 8.12: Plots of velocity contours for different values of the inlet velocity, the contours are shown in a horizontal plane located at y = 10 cm and for a catalyst size of 0.254 cm.

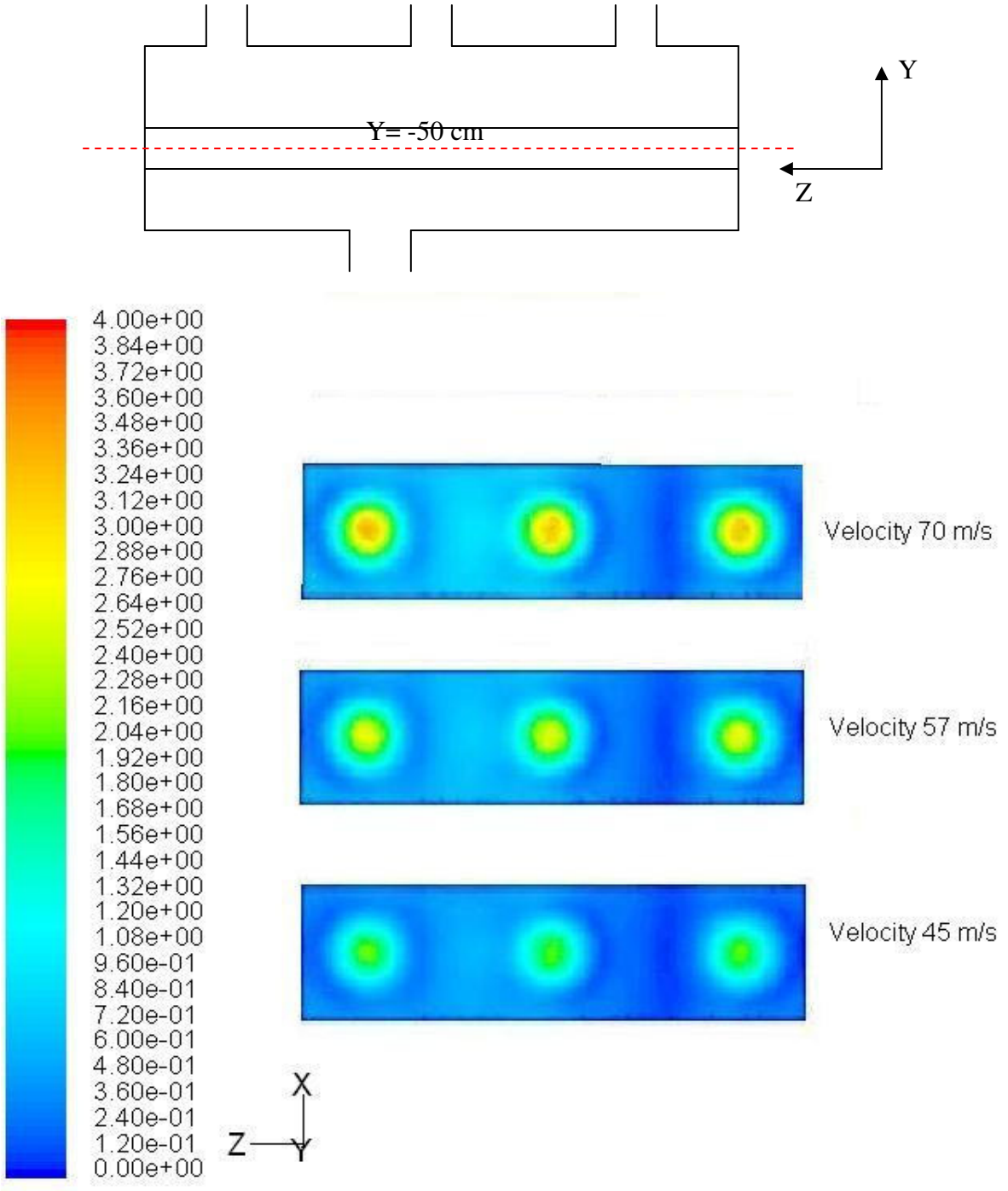

Figure 8.13: Plots of velocity contours for three different values of the inlet velocity, the contours are shown in a horizontal plane located at y = -50 cm and for a catalyst size of 0.254 cm.

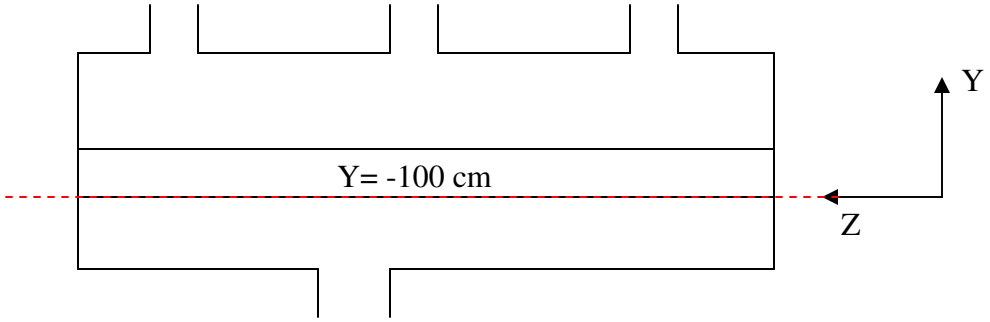

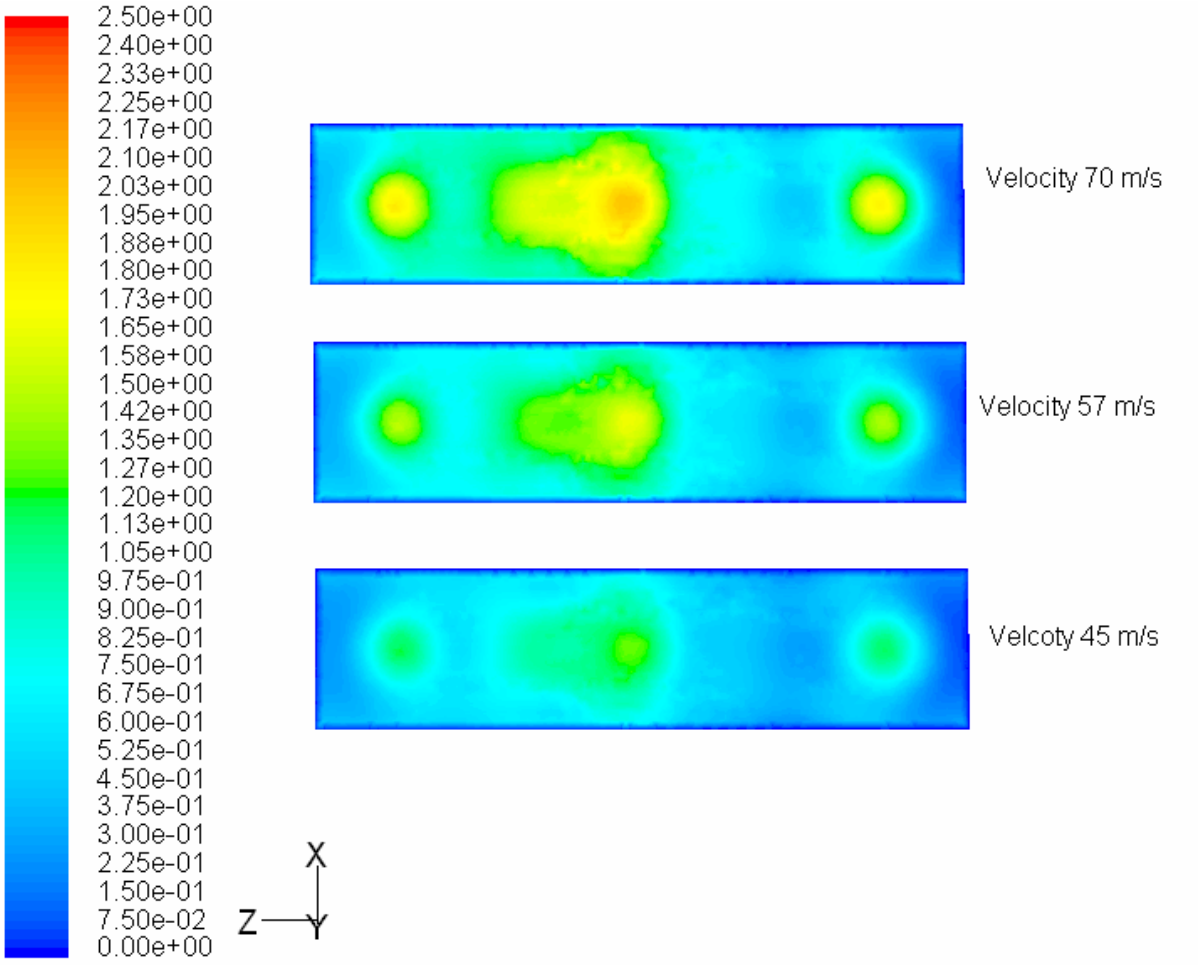

Figure 8.14: Plots of velocity contours for three different values of the inlet velocity, the contours are shown in a horizontal plane located at y = -100 cm and for a catalyst size of 0.254 cm.

the velocity peaks were higher for a higher inlet velocity. Areas in between two adjacent jets have low velocities.

Figure 8.13 shows plots of the velocity contours in a central plane at y = -50 cm for three different inlet velocities. The plane is located halfway through the bed depth. The maximum velocity is sharply reduced from 18 m/s in the previous figure to 3.5 m/s. It is also noted that the velocity has significantly increased from 0.2 m/s to 0.7 m/s in the zone between the middle and the right jets. The maximum value of 3.5 m/s compare with a corresponding value of 5 m/s when catalyst of size 0.3175 cm is used. This could be explained by the fact that beds with smaller size particles are better distributors of the flow however higher pressure drops will be encountered.

Figure 8.14 depicts the velocity contours in a horizontal (x-z) plane at y = -100 cm, that is near the bottom or the outlet of the catalyst bed. The velocity magnitudes decrease slightly compared to those in the plane at y = -50 cm. The velocity magnitudes range from 0.2 to 2.5 m/s. Comparing these results with the corresponding results with catalyst size of 0.3175 cm, it is observed that the smaller particle catalyst offers a little extra resistance to flow and consequently acts as a slightly better flow distributor.

Line plots show clearer and a more quantitative picture of the flow distribution. Three line plots are created at three different depths of the bed. All three lines are taken at the center position of horizontal x-z planes. In all cases, the x position is taken as zero and the variation is along the length of the bed (z-direction) is plotted. The lines arechosen at y = 10 cm, y = -50 cm and y = -100 cm.

Figure 8.15 shows the plots of the velocity distribution along the y = 10 cm line for three values of the inlet velocity. These plots show the variation of the velocity magnitude

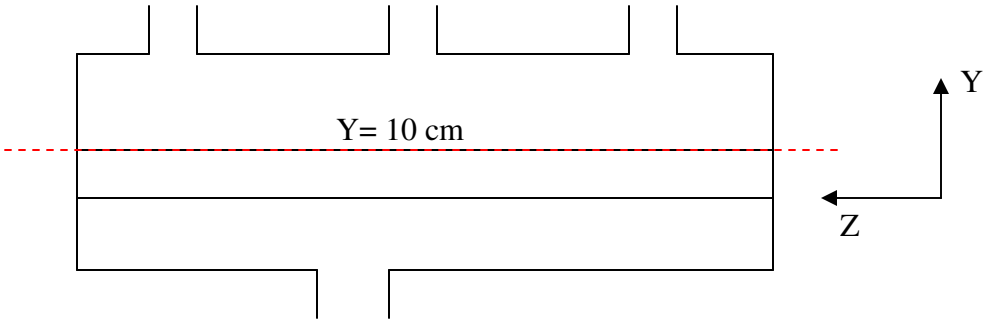

(a)

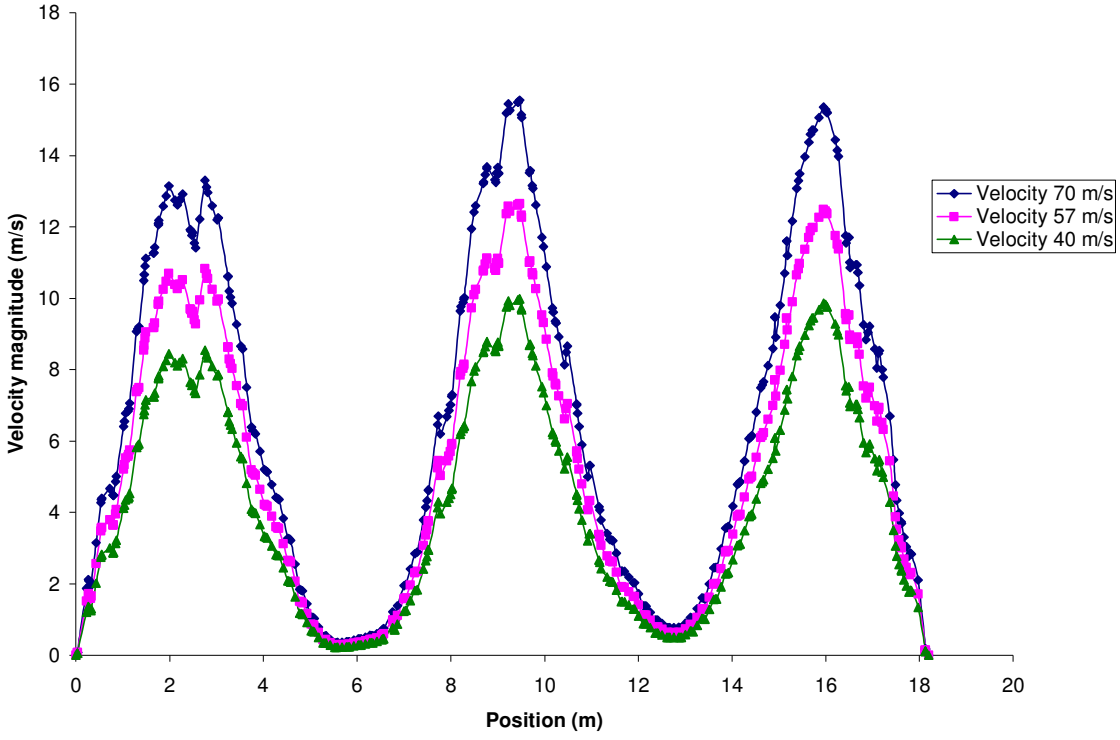

(b)

Figure 8.15: Line plots for three different values of the inlet velocity, these plots present the variation of the velocity magnitude along the z-axis at y = 10 cm and for a catalyst size of 0.254cm.

along the length of the vessel. These plots confirm that the flow distribution at the top of the catalyst bed is not very even and is also very similar for all three inlet velocities. The only difference observed is in the magnitude of the peaks. As expected, the peaks are higher for higher inlet velocities. It is also noticed that the velocity between adjacent jets has very small values. The maximum value of the velocity is 16, 13 and 10 m/s for the inlet velocity 70, 57 and 45 m/s respectively.

Figure 8.16 shows the plots of velocity distribution along the line at y = -50 cm for three different inlet velocities. These lines are located in the middle of the bed. The velocity magnitudes range from 0.1 to 4 m/s which is significantly lower than the maximum in the previous figure. The peaks also show a similar trend to those in the previous figure. However, the bed contribution as a distributor can be seen in two main points: The first is the significant reduction in the magnitude of the peaks and the second is in the noticeable increase in the velocity in the zone located between the middle jet and the jet on its right. The velocities in this zone increased from about 0.1 m/s to about 0.6 m/s.

Figure 8.17 shows the plots of velocity along the line at y = -100 cm. This line is located near the bottom of the bed. The bed action as a distributor is quite clear in this figure. The velocity distribution is significantly more even than in the top or the middle of the bed. For the 57 m/s inlet, the velocity range is between 0.4 and 1.5 m/s compared to 0.1 to 2.7 m/s in the middle of the bed and 0.1 to 13 m/s in the top of the bed. The zones with low velocities are greatly reduced near the bottom of the bed.

The next four figures show the line plots of the velocity distribution along lines in a central horizontal plane at y = 0. These lines are at the center, i.e. x= 0 cm, x = -50 cm,

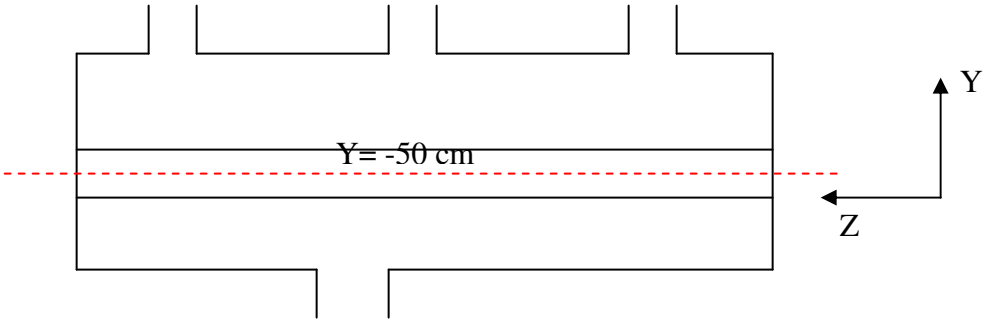

(a)

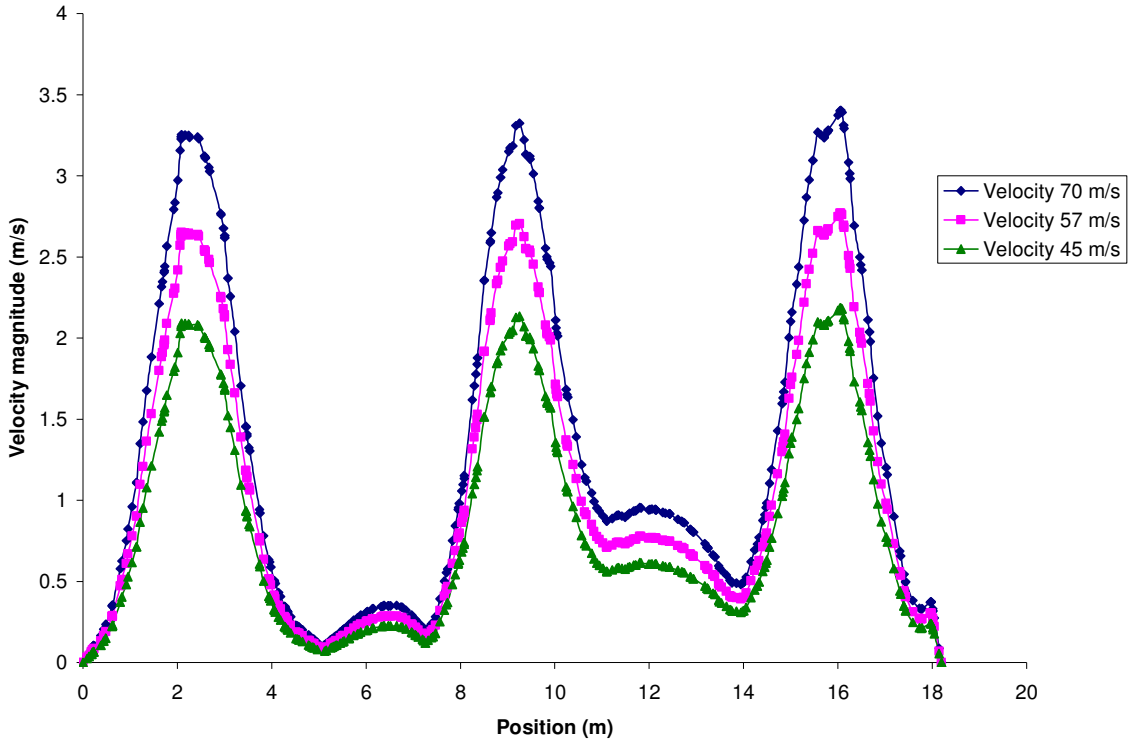

(b)

Figure 8.16: Line plots for three different values of the inlet velocity, these plots present the variation of the velocity magnitude along the z-axis at y = -50 cm and for a catalyst size of 0.254 cm.

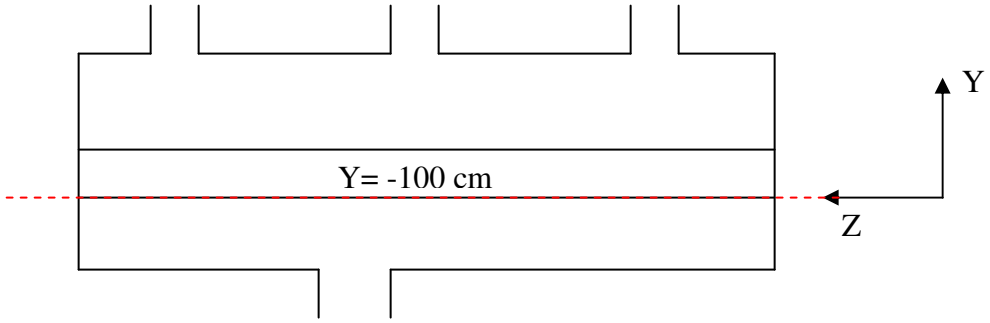

(a)

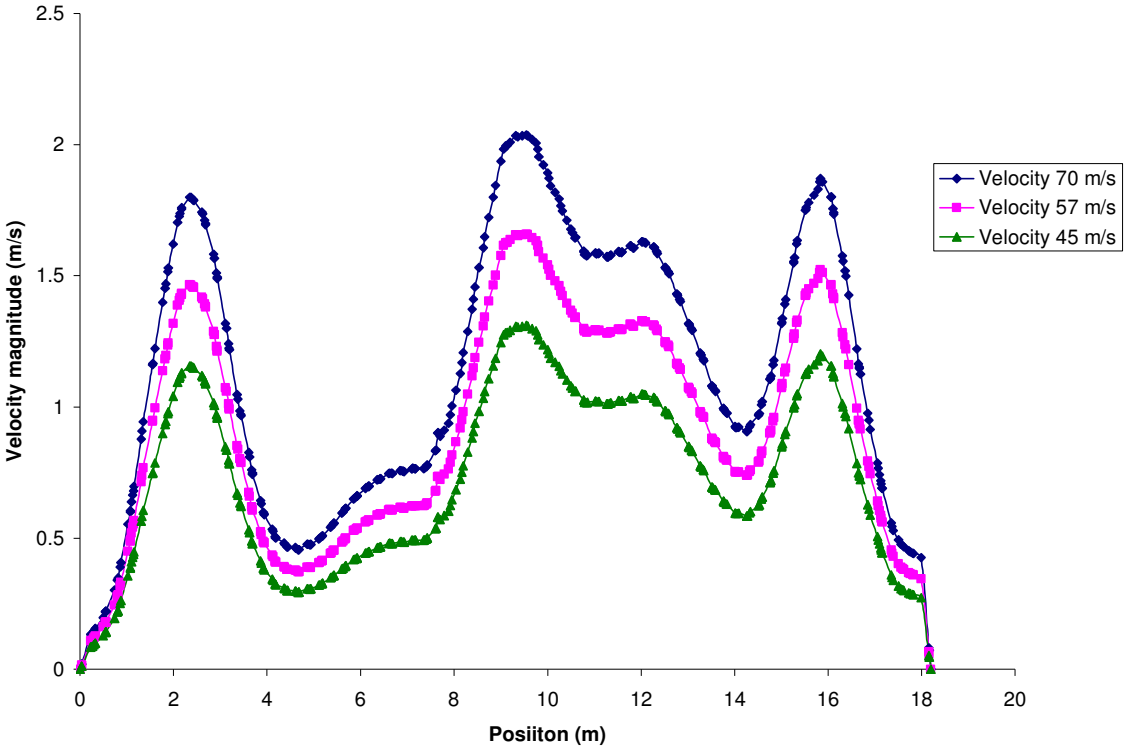

(b)

Figure 8.17: Line plots for three different values of the inlet velocity, these plots present the variation of the velocity magnitude along the z-axis at y = -100 cm and for a catalyst size of 0.254 cm.

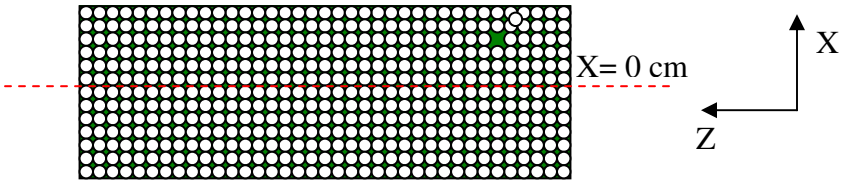

(a)

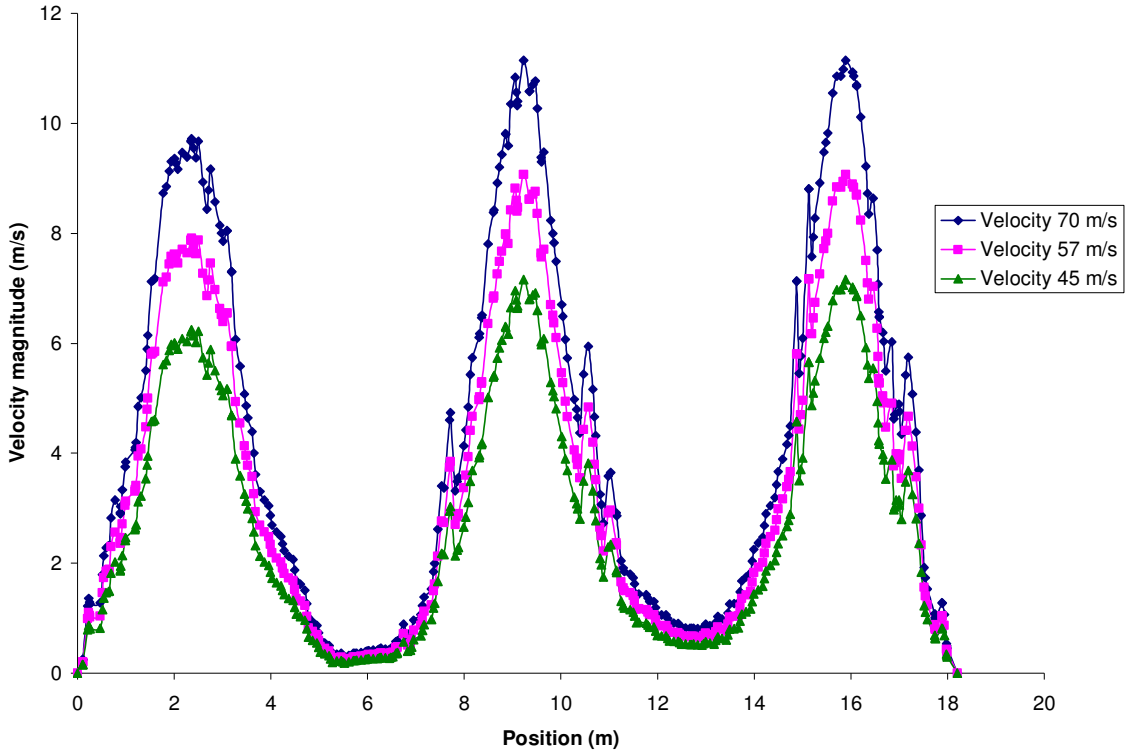

(b)

Figure 8.18: Line plots for three different values of the inlet velocity, these plots present the variation of velocity magnitude along the z-axis at x = 0 cm and for a catalyst size of 0.254 cm.

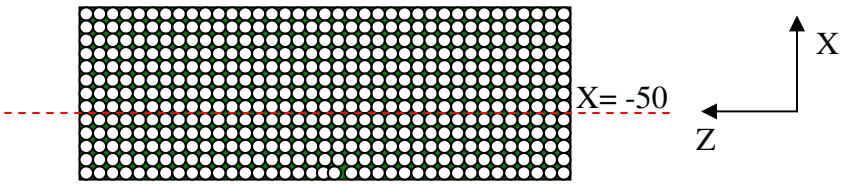

(a)

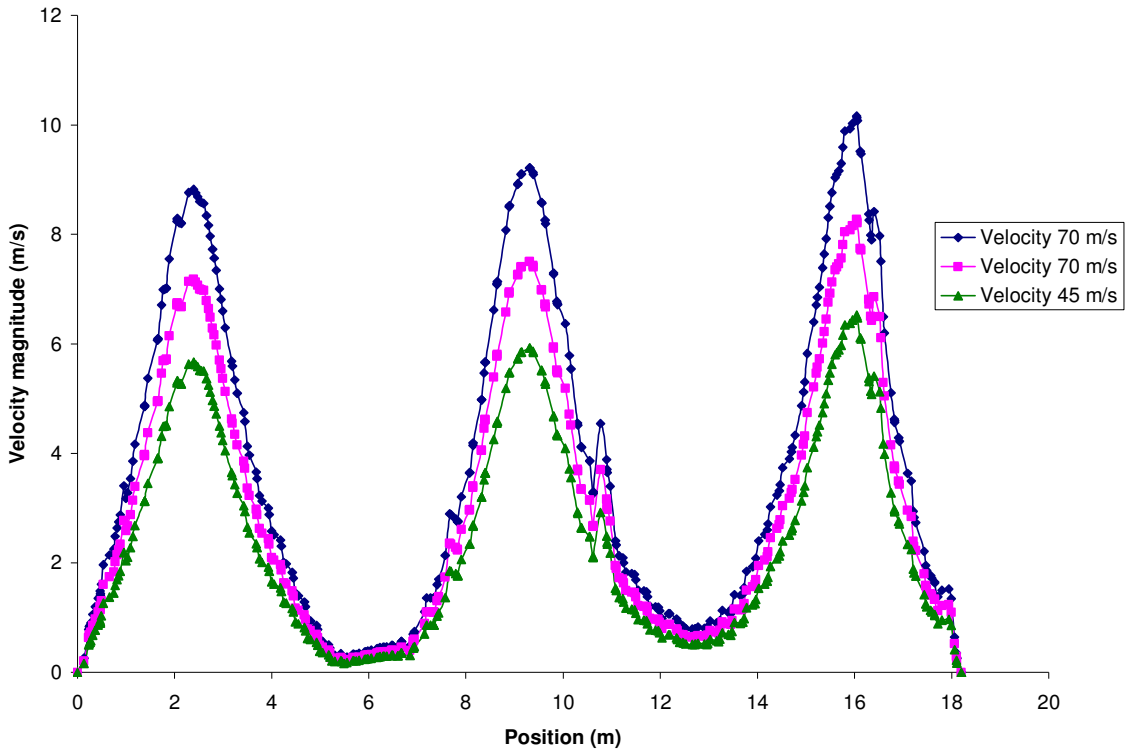

(b)

Figure 8.19: Line plots for three different values of the inlet velocity, these plots present the variation of velocity magnitude along the z-axis at x = -50 cm and for a catalyst size of 0.254 cm.

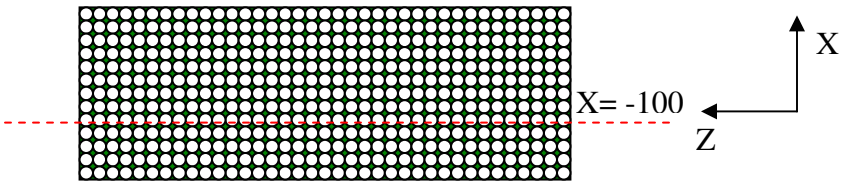

(a)

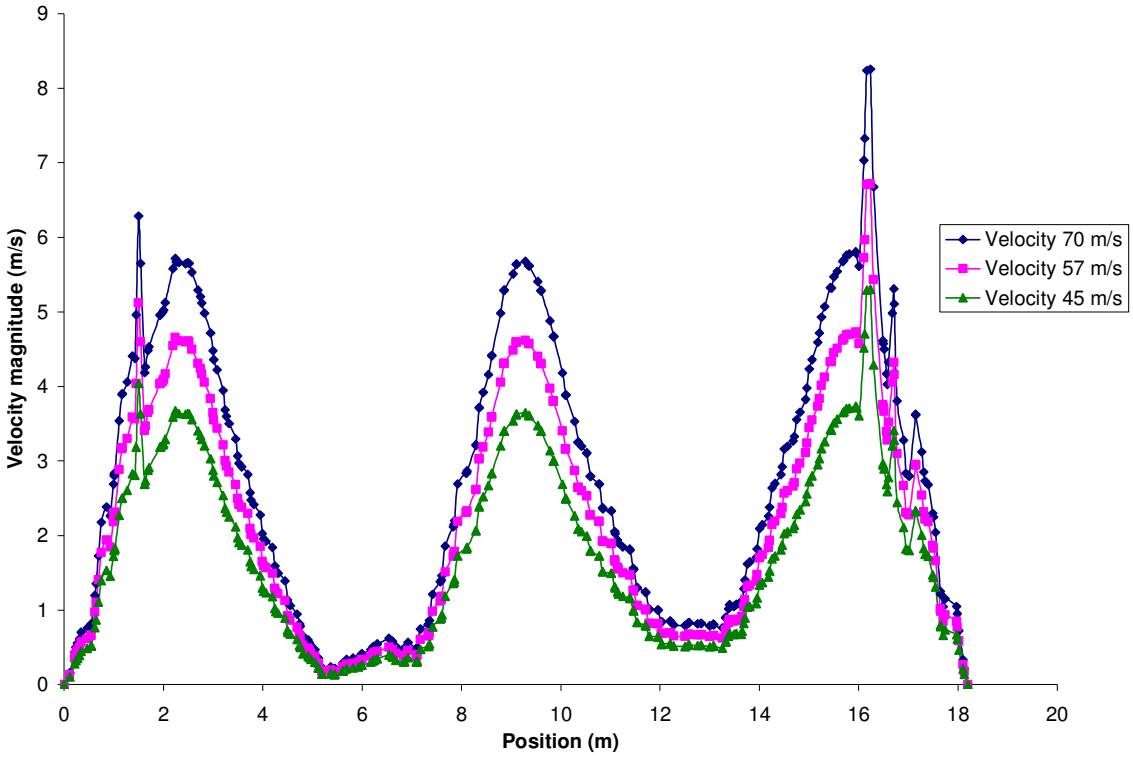

(b)

Figure 8.20: Line plots for three different values of the inlet velocity, these plots present the variation of velocity magnitude along the z-axis at x = -100 cm and for a catalyst size of 0.254 cm.

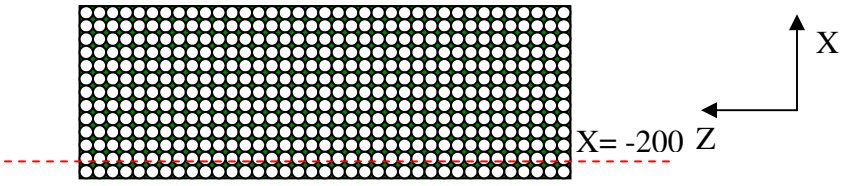

(a)

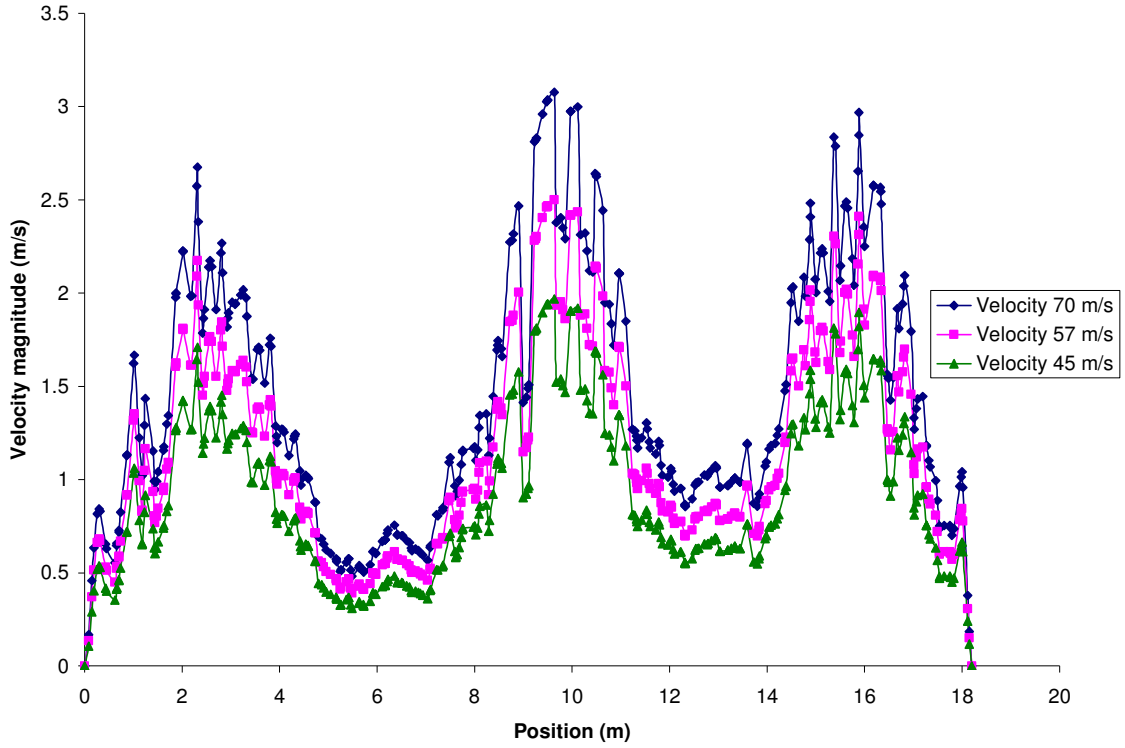

(b)

Figure 8.21: Line plots for three different values of the inlet velocity, these plots present the variation of velocity magnitude along the z-axis at x = -200 cm and for a catalyst size of 0.254 cm.

x = -100 cm and x= -200 cm. This plane is just below the top of the bed.

Figure 8.18 show plots of the velocity distribution along the central line (x = 0) for three different inlet velocities. The trend is similar to that found in the y-z plane at y = 10 cm, but the value of the peaks are slightly lower. Certain sharp velocity fluctuations are observed especially at the edges of the jet impingement areas. At the location which is just below the top of the bed, low velocity is still observed between the adjacent jets.

Figure 8.19 shows similar plots along a line located at x = -50 cm in a z-x plane at y = 0. The trend is similar to the one in the previous figure except that the magnitude of the peaks are reduced by about 2 m/s. Less velocity fluctuations are also observed.

Figure 8.20 depicts velocity plots along line at x = -100 cm in a z-x plane. The plane is located at y = 0 cm. This line placed almost halfway between the center of the converter and its wall. Sharp fluctuations are observed in the zone corresponding to impingement zones of first and the third jets. No such fluctuation is observed in the middle zone. The magnitudes of the peaks are again reduced by about 3 m/s.

Figure 8.21 shows velocity plots along a line at x = -200 cm, i.e. close to the wall. Severe fluctuations in the velocity magnitudes are observed along the length of the converter.

8.4 Simulation Results of the Partially Packed Vessel Using Mesh 20

Large fluctuations were observed in the flow distribution especially in locations clos to the converter wall for the case of mesh 25. This may be due to the mesh size. In order to investigate this point, a new case with a mesh size of 20 mm is simulated. All the previous cases were simulated with a mesh size of 25 mm mesh, the total number of cells was 157922 cells while for a mesh size of 20 mm, the total number of cell is 296260.

Figure 8.22 shows the velocity fluctuations along a line at x = -100 cm. This line lies almost halfway between the center and the wall of the vessel. It is drawn between (-100, 0, 0) and (-100, 0, 1820). The velocity ranges between 0.2 and 8 m/s. The first and the last peaks show some interesting behavior. The velocity in the zones of the jet impingement shows limited fluctuations than the mesh size 25.

Figure 8.23 depicts velocities along a line very close to the wall and the position is at x = -200 cm. The line lies in between (-200, 0, 0) and (-200, 0, 1820). In this region the velocity fluctuations in this region for a mesh of 20 cm are significantly less than in the case of 25 mm.. The velocity ranges from 0.1 to 2.5 m/s. Since this line lie close to the wall so the velocity magnitudes decreases sharply compared to the velocity values along central lines. There is still some fluctuation but it seems be lower than the case of mesh 25.

In summary, mesh sizes have significant influence on the calculation of the velocity distribution in the bed especially as it gets closer to the wall. So to get more smooth distribution of the velocity among the low velocity zone, a finer mesh size is required.

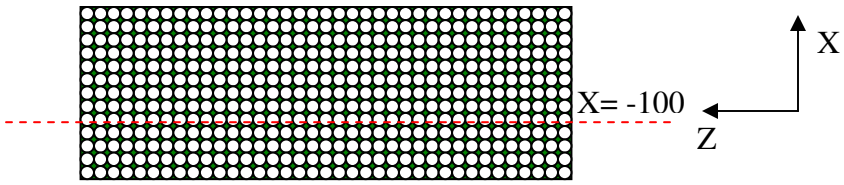

(a)

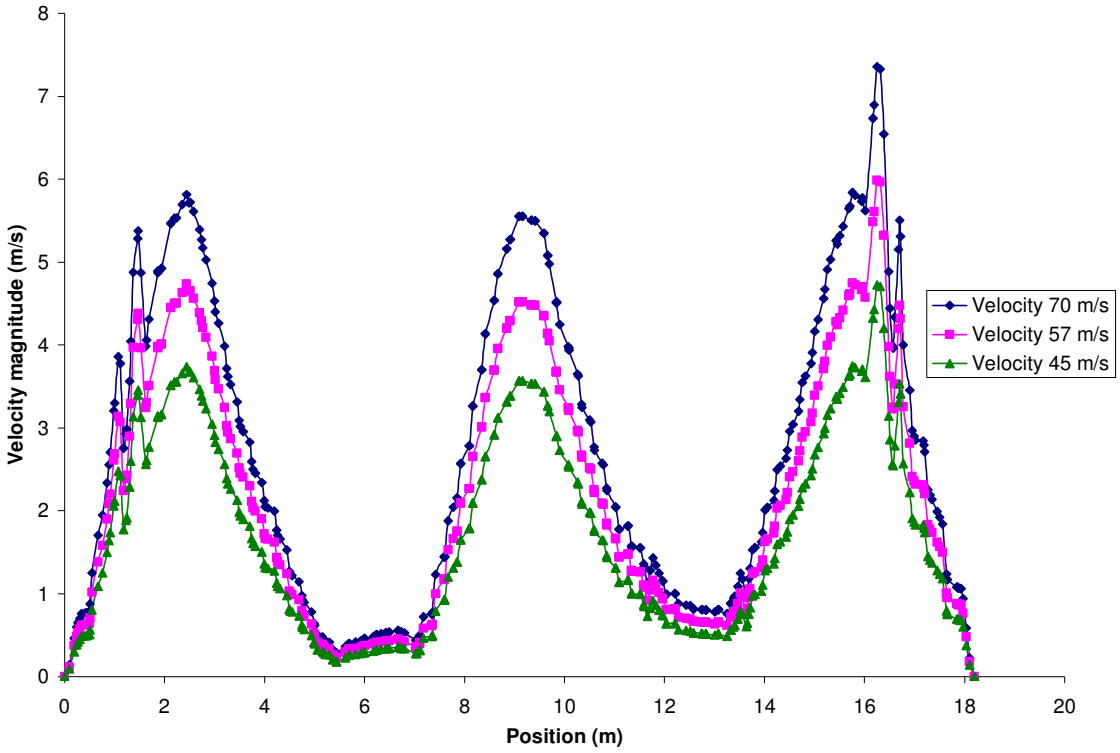

(b)

Figure 8.22: Line plots for three different values of the inlet velocity, these plots present the variation of velocity magnitude along the z-axis at x = -200 cm and for a catalyst size of 0.254 cm.

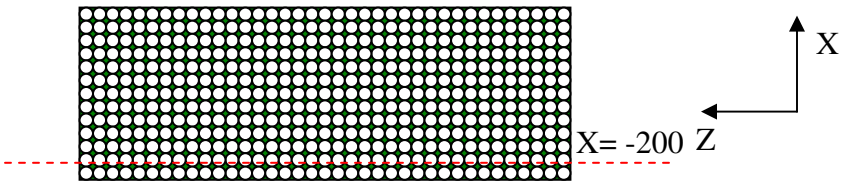

(a)

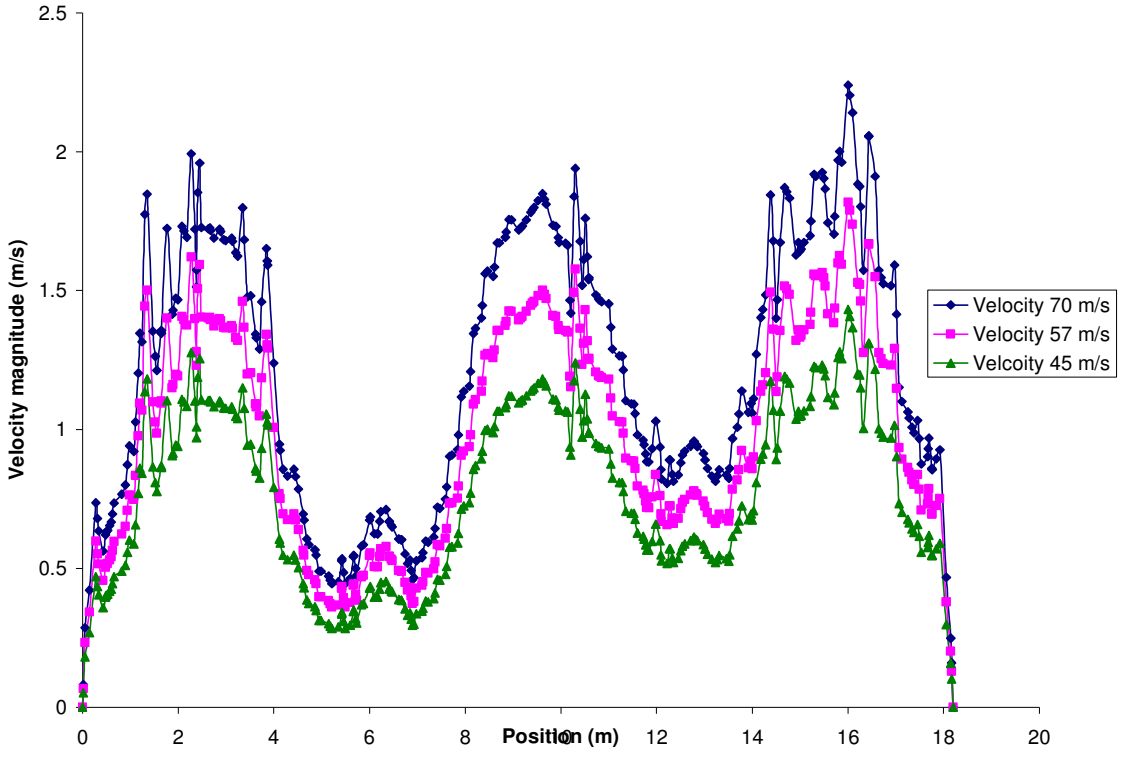

(b)

Figure 8.23: Line plots for three different values of the inlet velocity, these plots present the variation of velocity magnitude along the z-axis at x = -200 cm and for a catalyst size of 0.254 cm.

8.5 Conclusions

Simulations of the flow in a partially packed converter showed that changing the inlet velocity by 60 % from 45 m/s to 70 m/s did not result in significant improvement in the flow distribution.

Results also showed that although the packed bed acts as a good distributor across the converter, significant differences in the velocity across the bed are still observed in the top half of the bed.

The size of the catalyst particles used seems to have limited effect on the results. Using 0.254 cm particles instead of 0.3175 cm particles marginally improved the flow distribution but increased the pressure drop across the bed.

Mesh size 20 gives a good result on the low velocity zone and the zones that closes to the wall. It reduces the fluctuation of the velocities magnitudes.

Chapter 9

Simulation of Flow and Reactions in a Partially Packed Vessel (Claus Converter)

9.1 Introduction

In the process industries, packed beds are frequently used as catalytic reactors, filters or separation processes like absorption, adsorption and distillation. Packed beds are extensively used in many petroleum, petrochemical and biochemical applications. The modified Claus process is used to recover elemental sulfur from hydrogen sulfide present in gases from refineries, and natural gases. A wide range of catalysts dedicated to sulfur recovery and based on the Claus process are available. Catalysts provide the necessary sites to catalyze the conversion of H_2S and SO_2 to elemental sulfur. The Claus reaction is:

$$2H_2S + SO_2 \rightleftharpoons \frac{3}{n}S_n + 2H_2O$$

where n can be 2, 6, 8.

In this chapter, the flow and chemical reactions in a vessel similar to an industrial Claus converter are simulated taking the thermal effects into consideration.

The mixing and transport of chemical species can be modeled by solving conservation equations describing convection, diffusion and reaction sources for each component species. Multiple simultaneous chemical reactions can be modeled with reactions occurring in the bulk phase (volumetric reactions) and/or on a wall or particle surfaces and in

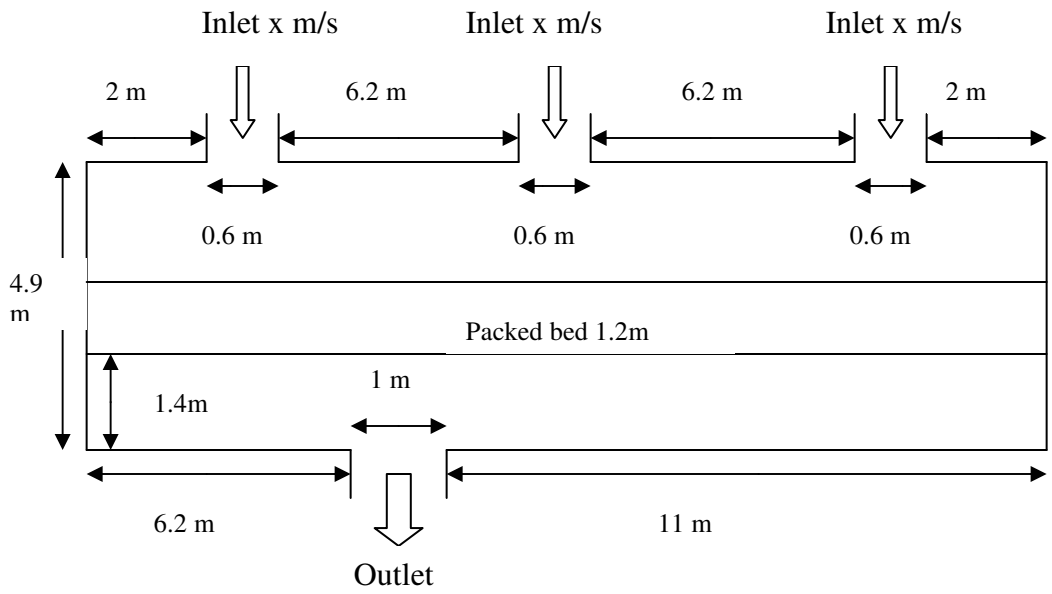

Figure 9.1: A schematic diagram of the partially packed vessel used in the present investigations.

the porous region. The reactions in the Claus converter are surface reactions and they are best modeled using surface reactions in the CFD model.

The use of surface reactions in the model requires detailed information about all the main and side reactions including diffusion and surface reactions. The heat released due to surface reactions can also be modeled. Other effects including those of the surface mass transfer, species diffusion effects in the energy equation and thermal diffusion can also be modeled. Such detailed information about the reactions in a Claus converter is not available in the literature. A thorough search revealed very little about detailed kinetics information. Local[a] and international[b] experts confirmed the findings of the literature survey.

Since the detailed procedure of handling the chemical reactions was not feasible due to a lack of kinetics data, these reactions were simulated using a volumetric reaction model. A volumetric reaction with species transport can be handled in FLUENT using three different models. These are:

i) **The laminar finite rate model**: The effects of turbulent fluctuations are ignored, and reaction rate is determined by Arrhenius expressions.

ii) **The eddy-dissipation model**: The reaction rates are assumed to be controlled by the turbulence. So Arrhenius chemical kinetic calculations can be avoided.

iii) **The eddy-dissipation concept model**: A detailed Arrhenius chemical kinetics expression can be incorporated in the turbulence flames. It should be noted that detailed chemical kinetic calculations are computationally expensive.

---

a. Mr. Pierre Crevier, Sulfur Recovery Specialist, Saudi ARAMCO, Private communication 2003.

b. Professor Peter Clark, Director, Alberta Sulfur Research Lab (ASRL), Canada, Private communication 2003.

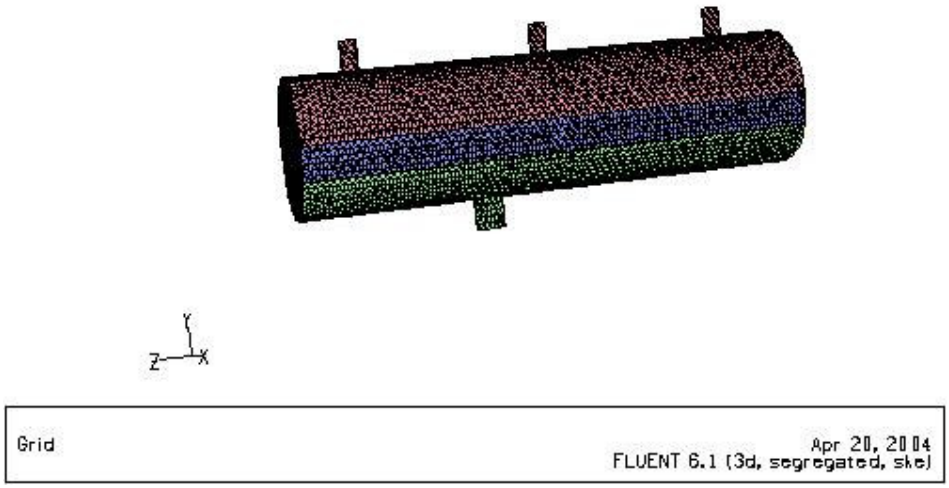

Figure 9.2: A 3D diagram of the partially packed vessel used in this chapter.

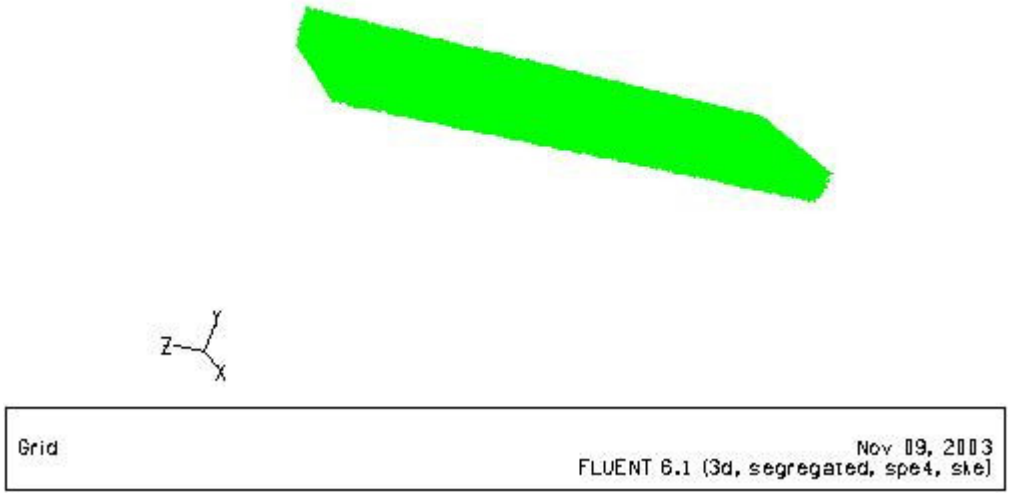

Figure 9.3: A 3D diagram of the packed bed used in this chapter.

Each of these three models is discussed in more details in the following sections. The current investigations were carried out for the same geometry as that used in the previous chapter. Figure 9.1 shows a schematic diagram of the actual industrial Claus converter dimension. Figure 9.2 shows a 3D diagram of the converter and Figure 9.3 shows the bed that is used in the present study.

9.2 The Finite Rate Model

The laminar finite-rate model computes the chemical source terms using Arrhenius expressions, and ignores the effects of turbulent fluctuations. The model is exact for laminar flames, but is generally inaccurate for turbulent flames due to highly non-linear Arrhenius chemical kinetics. The laminar model may, however, be acceptable for combustion with relatively slow chemistry and small turbulent fluctuations, such as supersonic flames. But the finite rate model is suitable for the catalytic reaction where the reaction depends on some extra kinetic energy that is provided by the catalyst. The finite rate model is more suitable to handle the reaction in the present study than the other models available in FLUENT. The choice of the model that is the best for the Claus reaction will be further explained in the next few paragraphs.

The net source of chemical species i due to reaction R_i is computed as the sum of the Arrhenius reaction sources over the N_R reactions that the species participate in:

$$R_i = M_{w,i} \sum_{r=1}^{N_R} \hat{R}_{i,r} \tag{9-1}$$

where $M_{w,i}$ is the molecular weight of species i and $\hat{R}_{i,r}$ is the Arrhenius molar rate of creation/destruction of species i in reaction r. A Reaction may occur in the continuous phase

between continuous-phase species only, or at wall surfaces resulting in the surface deposition or evolution of a continuous-phase species. Consider the r^{th} reaction written in general form as follows:

$$\sum_{i=1}^{N} \nu'_{i,r} M_i \underset{k_r}{\overset{k_{f,r}}{\rightleftharpoons}} \sum_{i=1}^{N} \nu''_{i,r} M_i \tag{9-2}$$

where

$N =$ number of chemical species in the system

$\nu'_{i,r}$ = stoichiometric coefficient for reactant i in reaction r

$\nu''_{i,r}$ = stoichiometric coefficient for product i in reaction r

$M_i =$ symbol denoting species i

$k_{f,r} =$ forward rate constant for reaction r

$k_{b,r} =$ backward rate constant for reaction r

Equation 9.2 is valid for both reversible and non-reversible reactions, (reactions in **FLUENT** are non-reversible by default). For non-reversible reactions, the backward rate constant, $k_{b,r}$, is simply omitted.

The summations in Equation 9.2 are for all chemical species in the system, but only the species that appears as reactants or products will have non-zero stoichiometric coefficients. Hence, species that are not involved in the reaction will drop out of the equation. The molar rate of creation/destruction of species i in reaction r ($R_{i,r}$) is:

$$\hat{R}_{i,r} = \left(\nu''_{i,r} - \nu'_{i,r}\right)\left(\kappa_{f,r}\prod_{j=1}^{N_r}\left[C_{j,r}\right]^{\eta'_{j,r}}\right) - k_{b,r}\prod_{j=1}^{N_r}\left[C_{j,r}\right]^{\eta''_{j,r}} \tag{9-3}$$

where

$N_r =$ number of chemical species in reaction r

$C_{j,r} =$ molar concentration of each reactant and product species j in reaction r (kgmol/m^3).

$\eta'_{j,r} =$ forward rate exponent for each reactant and product species j in reaction r (kgmol/m^3).

$\eta''_{j,r} =$ backward rate exponent for each reactant and product species j in reaction r (kgmol/m^3).

The forward rate constant for reaction r, $k_{f,r}$, is computed using the Arrhenius expression

$$k_{f,r} = A_r T^{\beta_r} e^{-E_r/RT} \tag{9-4}$$

where

$A_r =$ pre-exponential factor (consistent units)

$\beta_r =$ temperature exponent (dimensionless)

$E_r =$ activation energy for the reaction (J/kgmol)

$R =$ universal gas constant (J/kgmol-K)

If the reaction is reversible, the backward rate constant for reaction r, $k_{f,r}$, is computed from the forward rate constant using the following relation:

$$k_{b,r} = \frac{k_{f,r}}{K_r} \tag{9-5}$$

where K_r is the equilibrium constant for the r th reaction, computed from

$$K_r = \exp\left(\frac{\Delta S_r^0}{R} - \frac{\Delta H_r^0}{RT}\right)\left(\frac{p_{atm}}{RT}\right)^{\sum_{r=1}^{N_R}\left(\nu_{j,r}^{"}-\nu_{j,r}^{'}\right)} \tag{9-6}$$

where p_{atm} denotes atmospheric pressure (101325 Pa). The term within the exponential function represents the change in Gibbs free energy, and its components are computed as follows:

$$\frac{\Delta S_r^0}{R} = \sum_{i=1}^{N}\left(\nu_{i,r}^{"} - \nu_{i,r}^{'}\right)\frac{S_i^0}{R} \tag{9-7}$$

$$\frac{\Delta H_r^0}{RT} = \sum_{i=1}^{N}\left(\nu_{i,r}^{"} - \nu_{i,r}^{'}\right)\frac{h_i^0}{RT} \tag{9-8}$$

where S_i^0 and h_i^0 are the standard-state entropy and standard-state enthalpy (heat of formation). These values are specified in **FLUENT** as properties of the mixture material.

The main objective of the present work is to consider the Claus reaction of the converter, by which sulfur is removed from sour gas. The Claus reaction is

$$2H_2S + SO_2 \rightleftharpoons \frac{3}{n}S_n + 2H_2O$$

Where n could be 2, 6 or 8.

The kinetics of the Claus-process manufacturing of elemental sulfur that used in the model is developed by, Abaskuliev et al [1990] is:

$$R(C,T) = 7.3919 * 10^4 \exp\left(\frac{-30594}{8.314T}\right) \frac{T^{1.5} C_{H_2S} C_{SO_2}^{0.5}}{\left(1 + 46.56 T C_{H_2O}\right)^2} \tag{9-9}$$

To apply this kinetic model for the laminar finite rate chemistry in FLUENT it needs further simplification. In this simplification, the smallest term of the denominator that is the one (1), was removed. Following the simplification the model becomes:

$$R(C,T) = 34.0981 \exp\left(\frac{-30594}{8.3145T}\right) T^{-0.5} C_{H_2S} C_{SO_2}^{0.5} C_{H_2O}^{-2} \tag{9-10}$$

The error resulting from the above simplification is calculated using values of temperature and concentrations that are similar to those found in an industrial Claus converter. Suppose that is an the industrial converter temperature T = 500^0K, $C_{H_2S} = 0.06377$, $C_{SO_2} = 0.06075$ and $C_{H_2O} = 0.04443$. Submitting these data in equation (9.9) and (9.10) it is found, $R(C,T)_1 = -0.1783$ (eq. 9.9) and $R(C,T)_2 = -0.1787$ (eq. 9.10). These values are very close and the error resulting from the previous simplification is about 0.2%. One can conclude that equation 9.10 can be used in the present simulations.

9.3 The Eddy Dissipation Model

Most fuels are fast burning, and the overall rate of reaction is controlled by turbulent mixing. In non-premixed flames, turbulence slowly convects/mixes the fuel and the oxidizer into the reaction zones where they burn quickly. In premixed flames, the turbulence slowly convects/mixes cold reactants and hot products into the reaction zones, where the reaction occurs rapidly. In such cases, the combustion is said to be mixing-limited, and the complex and often unknown, chemical kinetic rates can be safely neglected.

FLUENT provides a turbulence-chemistry interaction model, based on the work of Magnussen and Hjertager [1976], called the eddy-dissipation model. The net rate of production of species i due to reaction r, $R_{i,r}$, is given by the smaller (i.e., limiting value) of the two expressions below:

$$R_{i,r} = \nu'_{i,r} M_{w,i} A \rho \frac{\varepsilon}{\kappa} \min_R \left(\frac{Y_R}{\nu'_{R,r} M_{w,R}} \right) \tag{9-11}$$

$$R_{i,r} = \nu'_{i,r} M_{w,i} A B \rho \frac{\varepsilon}{\kappa} \frac{\sum_P Y_P}{\sum_j^N \nu''_{j,r} M_{w,j}} \tag{9-12}$$

where

Y_P is the mass fraction of any product species, P

Y_R is the mass fraction of a particular reactant, R

A is an empirical constant equal to 4.0

B is an empirical constant equal to 0.5

In Equations 9.1 and 9.2, the chemical reaction rate is governed by the large-eddy mixing time scale, $\frac{\kappa}{\varepsilon}$, as in the eddy-breakup model of Launder and Spalding [1972]. Combustion proceeds whenever turbulence is present ($\frac{\kappa}{\varepsilon} > 0$), and an ignition source is not required to initiate combustion. This is usually acceptable for non-premixed flames, but in premixed flames, the reactants will burn as soon as they enter the computational domain, upstream of the flame stabilizer. To remedy this, **FLUENT** provides the finite-rate/eddy-dissipation model, where both the Arrhenius (Equation 9-3) and eddy-dissipation (Equations 9-11 and 9-

12) reaction rates are calculated. The net reaction rate is taken as the minimum of these two rates. In practice, the Arrhenius rate acts as a kinetic ``switch'', preventing reaction before the flame. Once the flame is ignited, the eddy-dissipation rate is generally smaller than the Arrhenius rate, and reactions are mixing-limited.

9.3.1 Simulation using the EDM

Some preliminary attempts were made to simulate the flow and reactions in the Claus converter using the Eddy Dissipation Model (EDM). A mixed feed of H_2S and SO_2 was defined in the zone where the reaction takes place. The feed temperature is the same as that in a typical industrial case, namely 505°K. The results showed that the overall reaction was endothermic while in reality it is exothermic.

These unlikely results can be explained by the fact that the EDM depends on the turbulence mechanism and it requires very fast reaction kinetics. The Claus reaction in the converter is catalytically controlled and it does not exactly fit in the very fast category. Consequently the EDM proved not to be appropriate for the current study. Figure 9.4 shows the temperature contours in a vertical plane passing through the inlets and the outlet. It can be seen that the outlet temperature is 283°K, which is lower than the inlet temperature which does not agree with the actual exothermocity of the reaction.

To test the EDM furthers a two-dimensional model of combusting un-mixed SO_2 and H_2S is used. Figure 9.5 shows that H_2S is fed through the main pipe while SO_2 is supplied through the nozzle. Simulation of the flow and reactions was done using the EDM. Results shown in Figure 9.5 indicate an exothermic reaction. Simulation results could not be obtained when pre-mixed feeds are used. When an un-mixed feed is used, a fast reaction is implied

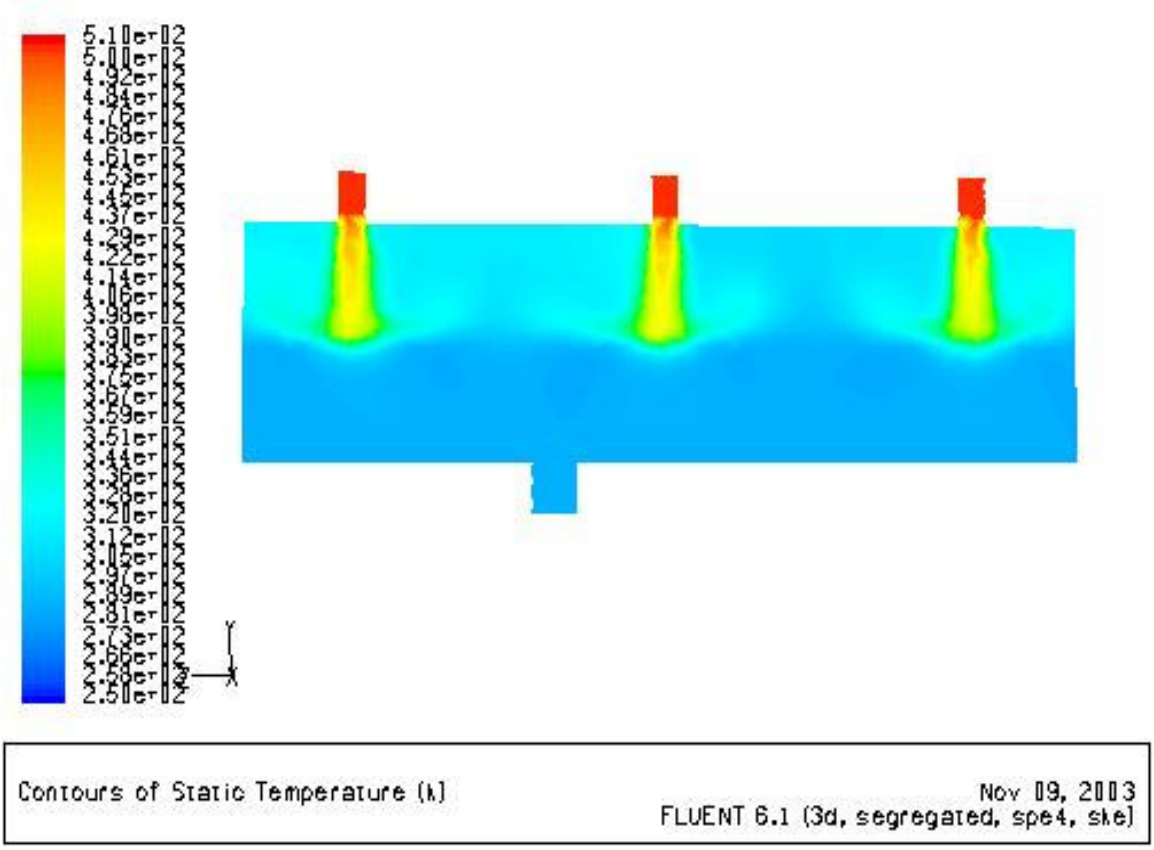

Figure 9.4: Temperature profile when using EDM to simulate the reaction in the Claus vessel.

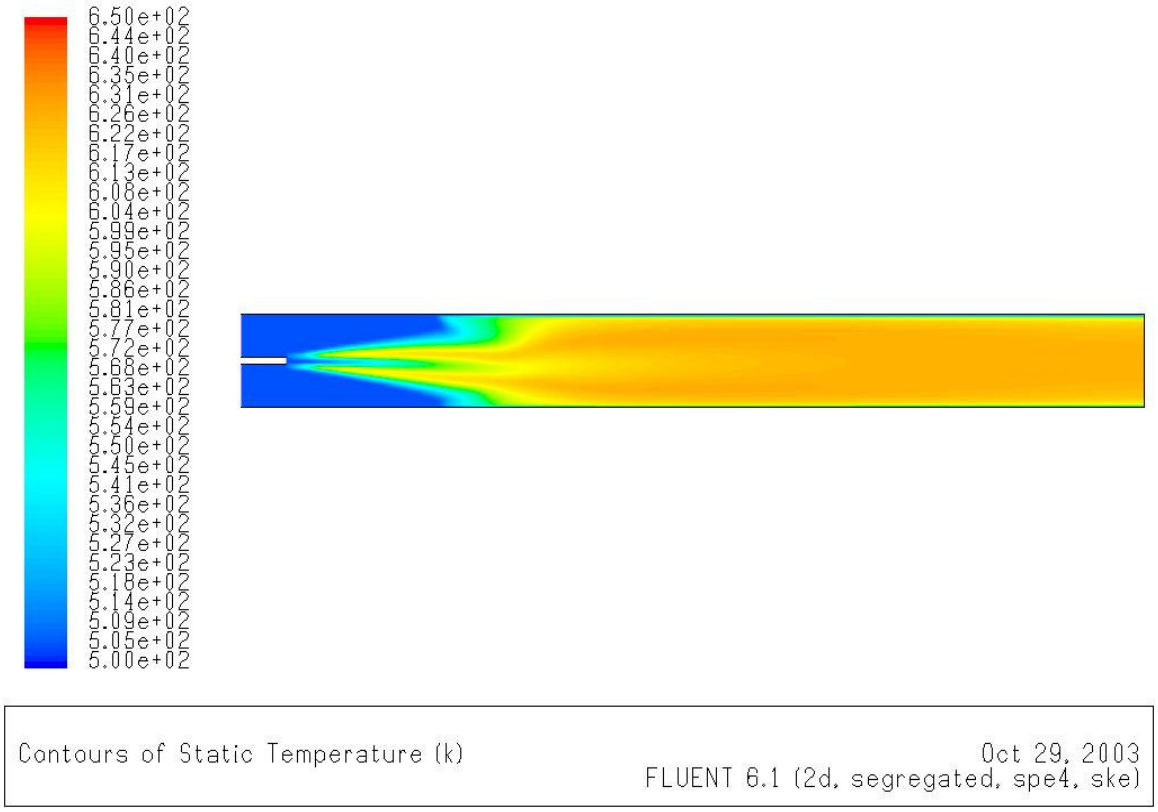

Figure 9.5: Temperature Contours for an un-mixed feed of SO_2 and H_2S, the velocity of H_2S is 5 m/s and that of SO_2 is 30 m/s.

and turbulence properties could be used to predict reaction characteristics. The same assumption could not be made for pre-mixed feeds. It can be concluded that the EDM is not suitable to simulate relatively low temperature catalytic reactions.

9.4 Eddy Dissipation / Finite Rate Model

9.4.1 Introduction

This is a mixed model of the Eddy dissipation model (EDM) and the finite rate model. For the finite rate chemistry, the reaction model proposed by Abaskuliev et al. [1990] for the production of elemental S is used. This was explained in section 9.2.

9.4.2 Simulation Using H_2S and SO_2 as a Premixed Feed

In the premixed case, the two main reactant H_2S and SO_2, are combined and fed through the three inlets. The converged solution showed that the reaction is exothermic. Figure 9.6 shows the exothermic nature of the reaction. The outlet temperature is found to be about 580 K whereas the inlet temperature is the same as industrial case 505 K for the first converter. The conversion is somewhat significant in this method. However, it seems that the finite rate model may give better results than the EDM, since the EDM model showed that the reaction is endothermic.

9.4.3 Simulation of Industrial Feed Compositions

To ensure the suitability of the EDM/Finite rate model for the simulation of the flow and reactions in a Claus converter, a case was run with an industrial feed composition and operating temperature and pressure. As mentioned earlier, a typical industrial arrangement of a Claus process consists of a furnace followed by three catalytic converters. The term “The first converter” in

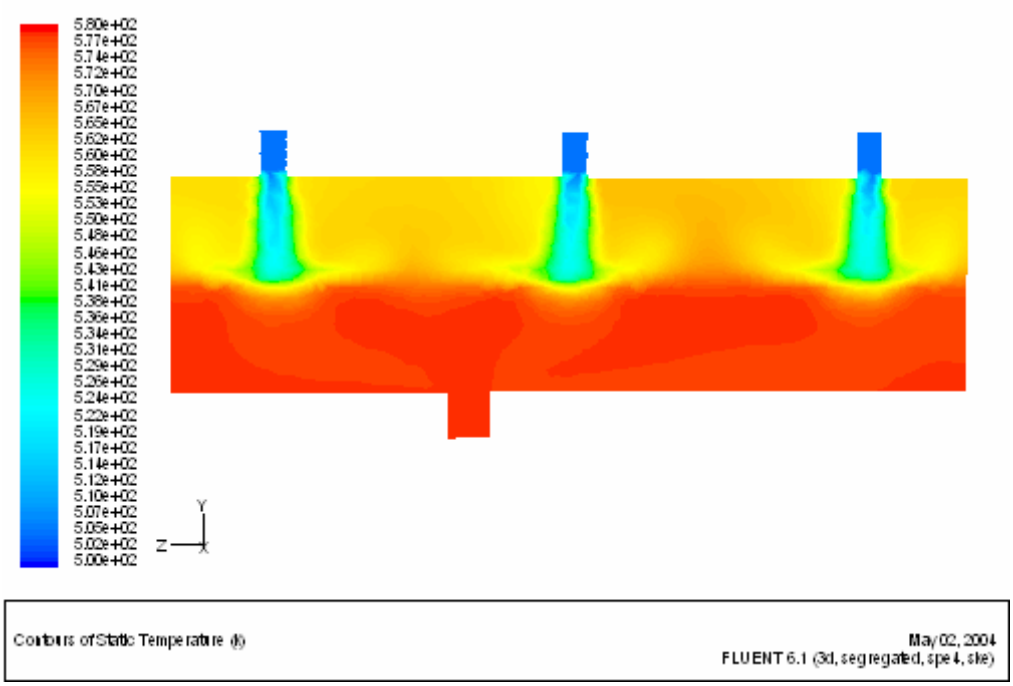

Figure 9.6: Contours of temperature when an of EDM/Finite model is used with a for H_2S-SO_2 premixed feed to model the chemical reaction in the Claus converter.

this study refers to the first converter following the furnace. A typical composition of the feed to the first converter is summarized in Table 9.1.

Table 9.1: Composition of the feed to the first converter

Name of Component	**Feed composition (mass fraction)**	**Feed composition (mole fraction)**
Hydrogen	0.00018	0.003357
Argon	0.003043	0.002863
Nitrogen	0.1784	0.2394
Methane	0.0005165	0.00121
Carbon Monoxide	0.001193	0.001263
Carbon Dioxide	0.6453	0.5497
Ethane	0.000062	0.0001476
Hydrogen Sulfide	**0.06377**	**0.07063**
Water	0.04443	0.0927
Sulfur Dioxide	**0.06075**	**0.03564**
Carbon Disulfide	0.001141	0.0005636
Others	0.001245	0.0025253
Total	1.0000	1.0000

The simulation results show a slight degree of exothermocity. The exit temperature as can be seen from Figure 9.7 is 488°K compared to an actual value of 572°K. It was concluded that the EDM/Finite Rate model is not suitable to the simulate the reaction in the Claus converter.

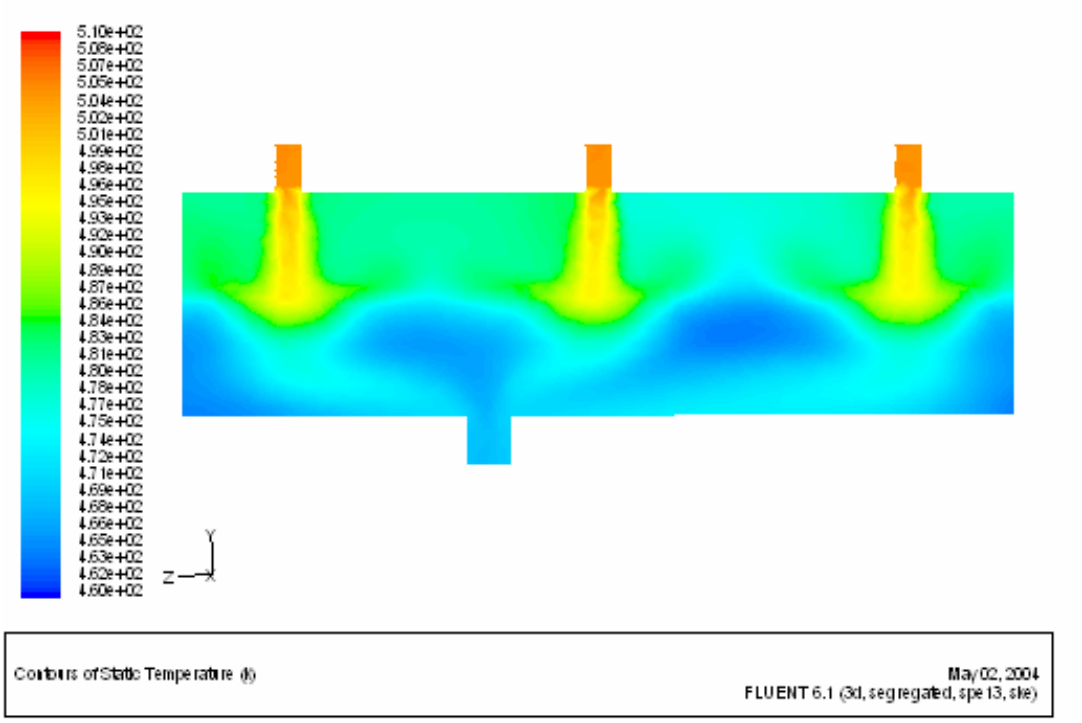

Figure 9.7: Temperature contours of profile when the EDM/Finite model for all species premixed feed is used to simulate the chemical reactions.

9.5 Finite Rate Model with Multiple Sulfur Components

9.5.1 Introduction

The Claus reaction is exothermic at converter temperatures, and the reaction is favored by lower temperatures. Process calculations for a Claus sulfur recovery unit are complicated by the existence of various species of gaseous sulfur (S_2, S_6 and S_8) whose equilibrium concentrations in reaction with each other are often not precisely known, and by a number of side reactions involving other feed gas components such as carbon-dioxide (CO_2), hydrocarbons, ammonia (NH_3), carbonyl sulfide (COS), carbon disulfide (CS_2) etc., which take place simultaneously. Figure 9.8 shows variation of sulfur vapor composition with the temperature at atmospheric pressure. This Figure is taken from "Gas and Liquid Sweetening" by Maddox, [1974]. The temperature inside the converter lies between 477°K and 589°K. From this figure, it is clear that most of the products is S_8, and then S_6, with very little amount of S_2 produced as a sulfur vapor. The present investigation focuses on these three different products. In this simulation the side reactions are ignored. Since the compositions of the reactants involved in the side reactions are very small, the effect of these side reactions on the overall Claus reaction is expected not to be significant. The actual model that is used for this present study is that of Abaskuliev et al. [1990] which was discussed earlier in section 9.2.

The general form of the kinetics model is :

$$R(C,T) = 7.3919 * 10^4 \exp\left(\frac{-30594}{8.314T}\right) \frac{T^{1.5} C_{H_2S} C_{SO_2}^{0.5}}{\left(1 + 46.56 T C_{H_2O}\right)^2} \tag{9-16}$$

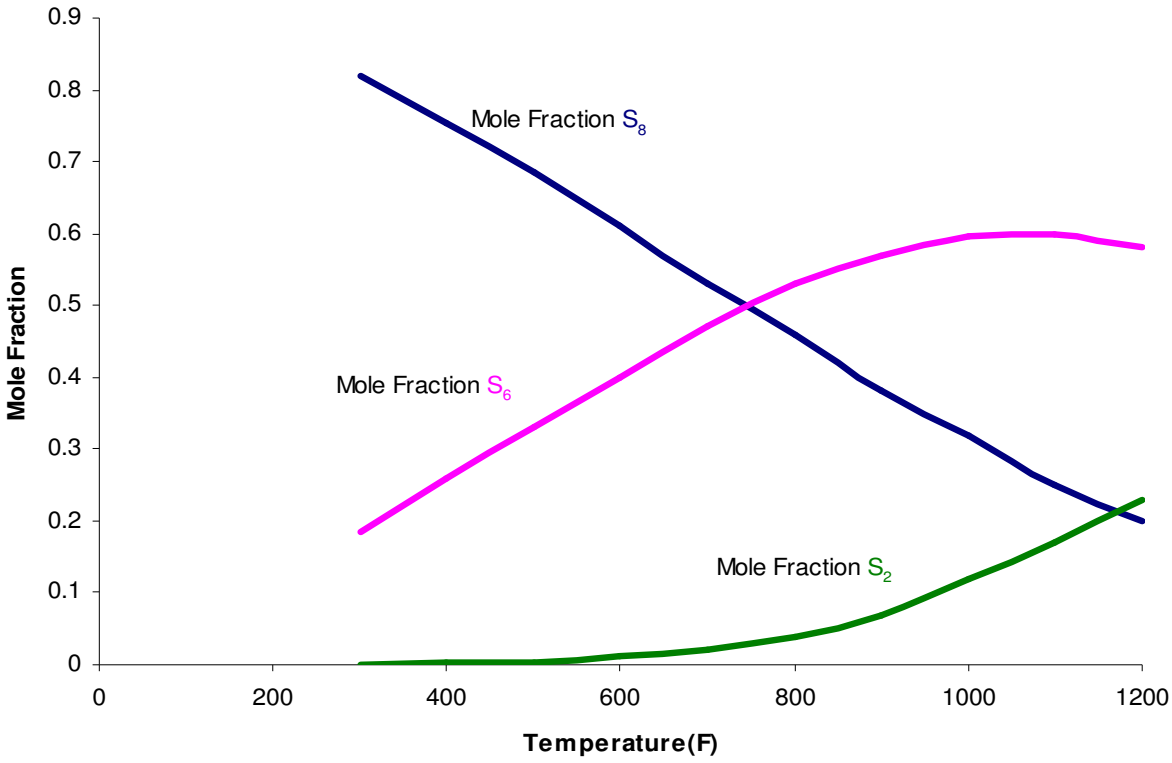

Figure 9.8: Variation of sulfur vapor composition with temperature at one atmospheric pressure (Reference "Gas and Liquid Sweetening" by Maddox R.N., 1974).

To apply this kinetic model for the laminar finite rate chemistry in FLUENT it needs further simplified. Following the simplification, the model becomes,

$$R(C,T) = 34.0981 \exp\left(\frac{-30594}{8.3145T}\right) T^{-0.5} C_{H_2S} C_{SO_2}^{0.5} C_{H_2O}^{-2} \tag{9-17}$$

Since the reaction produces S_2, S_6 and S_8, there is a need for a kinetic model for a kinetic model for each of these reactions:

$$2H_2S + SO_2 \rightarrow \frac{3}{2} S_2 + 2H_2O \tag{9-18}$$

$$2H_2S + SO_2 \rightarrow \frac{3}{6} S_6 + 2H_2O \tag{9-19}$$

$$2H_2S + SO_2 \rightarrow \frac{3}{8} S_8 + 2H_2O \tag{9-20}$$

Such kinetics models for the reactions producing S_6 and S_8 are not available. The general kinetic model proposed by Abaskuliev *et al*. [1990] was slightly modified to account for the S_2, S_6 and S_8 reaction as shown in equations (9-18), (9-19) and (9-20)

$$R(C,T) = 34.0981 \exp\left(\frac{-30594}{8.3145T}\right) T^{-0.7} C_{H_2S} C_{SO_2}^{0.7} C_{H_2O}^{-2} C_{S_2}^{0} \tag{9-21}$$

$$R(C,T) = 34.0981 \exp\left(\frac{-30594}{8.3145T}\right) T^{-0.5} C_{H_2S} C_{SO_2}^{0.7} C_{H_2O}^{-2} C_{S_6}^{0} \tag{9-22}$$

$$R(C,T) = 34.0981 \exp\left(\frac{-30594}{8.3145T}\right) T^{-0.4} C_{H_2S} C_{SO_2}^{0.7} C_{H_2O}^{-2} C_{S_8}^{0} \tag{9-23}$$

These modifications were done empirically. The results obtained from simulation cases where the above expressions were used showed reasonable industrial agreement with the results.

9.5.2 Simulation of the First Converter

A stream with an industrial feed composition is introduced through the three inlets of the converter. The inlet temperature is 512°K. The outlet and other temperatures are examined following the convergence of the simulation runs. Figure 9.9 depicts the temperature profile in the first converter. This profile is found to be in close agreement with the industrial one. The practical outlet temperature for this case is found to be 575°K, compared with an industrial value of 572°K.

Figure 9.10 shows the contours of are main reactant, H_2S. The feed composition of this reactant is 0.06377. The outlet composition is found to be 0.01526 which is little lower than the actual industrial value of 0.01585.

Figure 9.11 shows the contours of the other main reactant, SO_2. The contours show the location of the reaction zone of the SO_2 by analyzing the composition distribution across the bed. Most of the SO_2 is consumed at the bed. The inlet composition of SO_2 is 0.06075. When the converged solution reached the outlet composition is found to be 0.01515. This is close to the industrial value of 0.01485. The fluid distribution in the bed may be more even than in the industrial case, and this may enhance the production of gaseous sulfur. Another possible reason for the discrepancy between the simulation and the actual results may be related to the life of the catalyst. The simulation assumes fast catalyst while it is not known at which point of the catalyst life, the industrial results were reported.

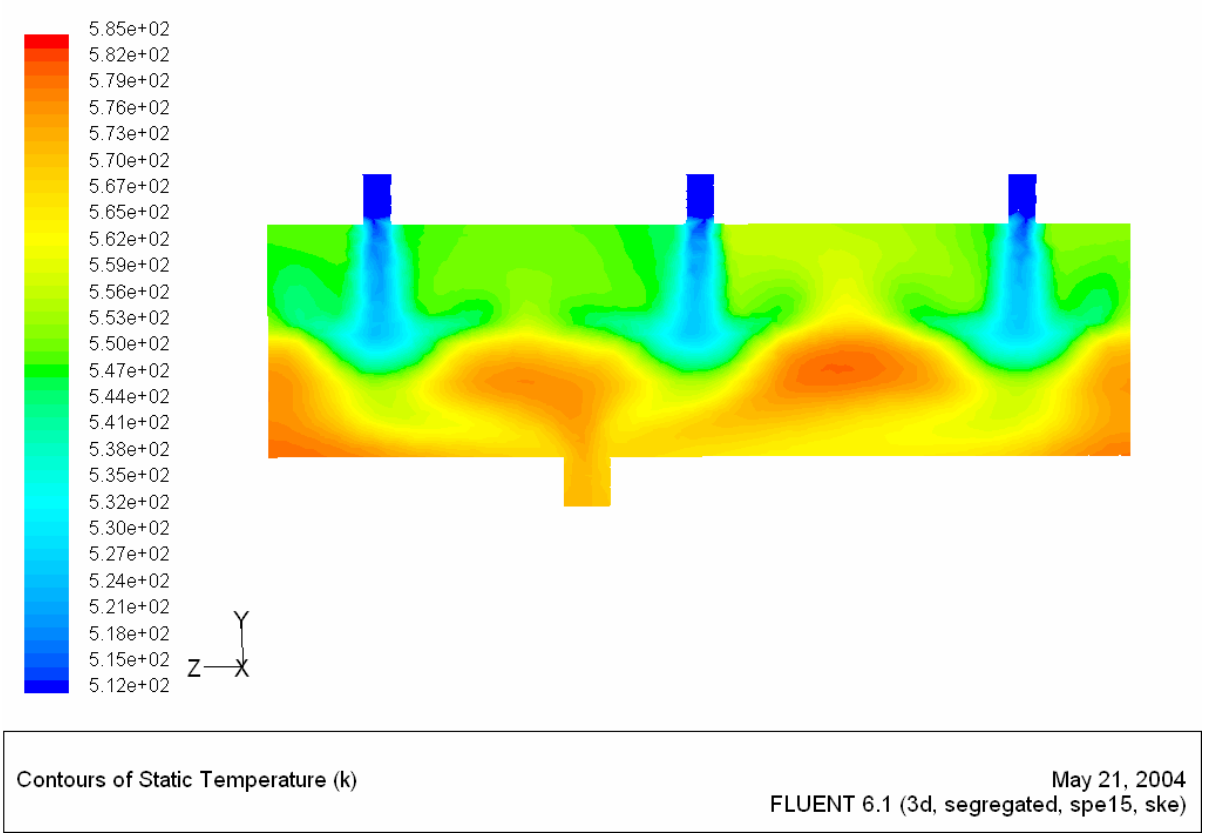

Figure 9.9: Temperature contours in a vertical plane passing through the inlets and the outlet of the first converter using the finite rate model.

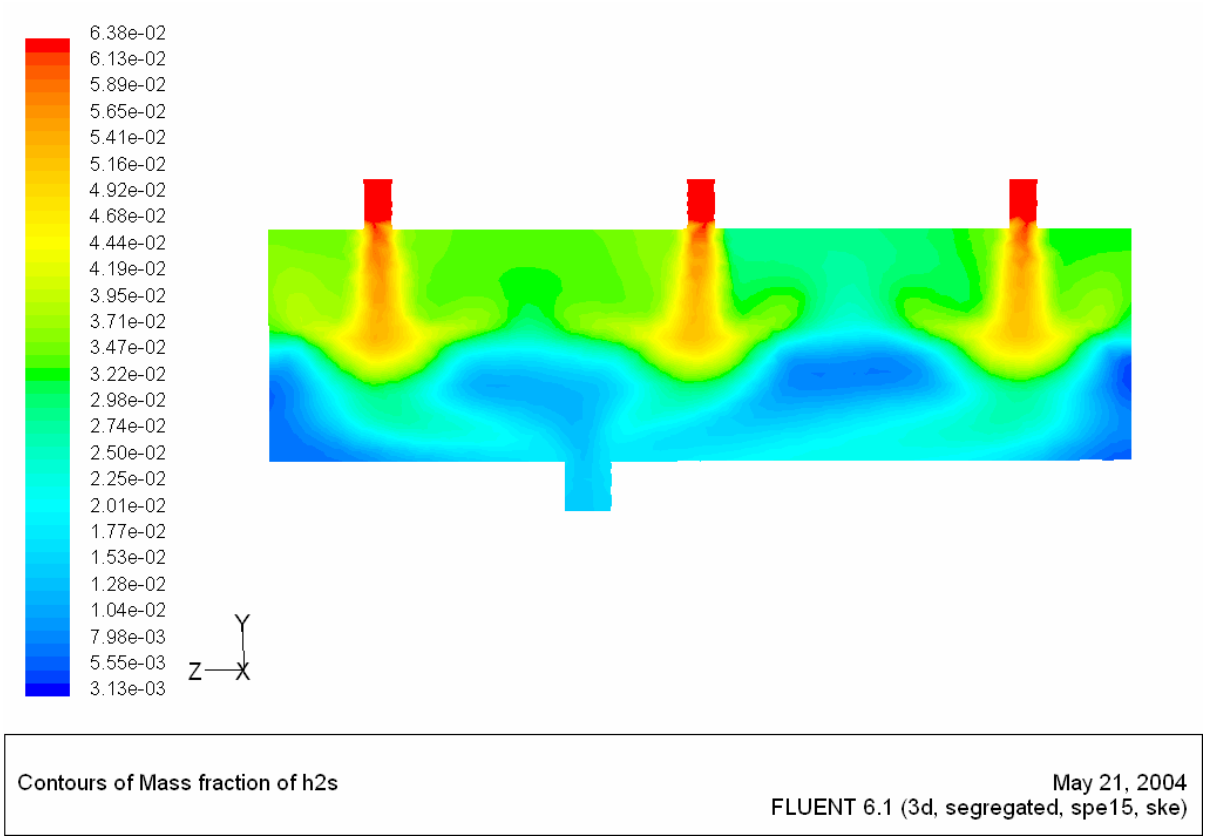

Figure 9.10: Contours of H_2S mass fraction in a plane passing through the inlets and the outlet of the first converter for a case using the finite rate model.

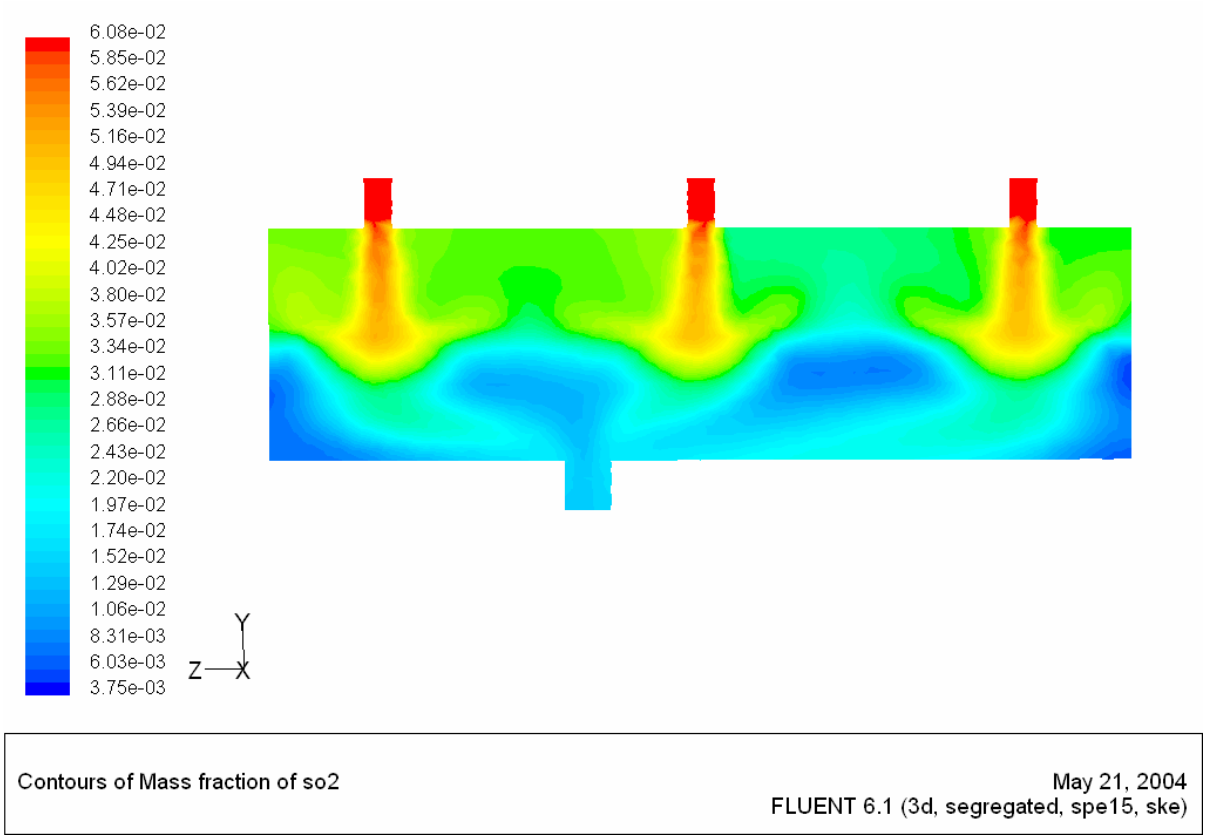

Figure 9.11: Contours of SO_2 mass fraction in a plane passing through the inlets and the outlet of the first converter for a case using the finite rate model.

The experimental degree of conversion of SO_2 is found to be 75.5%. This is compared with a predicted conversion of 76.06%.

More experimental data is available in the form of temperature readings at nine locations. These locations are inside the bed, three across the bed below each inlet. The exact locations are specified in the first column of Table 9.2 and Figure 9.12. The simulation values of temperature are obtained from Figure 9.12. Temperatures at identical locations were obtained from the simulation results and both sets are compared in table 9.2.

Table 9.2 Comparison of predicted and experimental temperatures at identical locations in the bed

Position No.	Positions (y, z)	Experimental(K)	Simulation(k)
1	(-15,260)	540	536
2	(-15,1060)	560	548
3	(-15,1600)	511	533
4	(-60,260)	602	554
5	(-60, 1060)	610	572
6	(-60, 1600)	562	551
7	(-105,260)	607	573
8	(-105, 1060)	610	578
9	(-105, 1600)	596	568

It can be seen from Table 9.2 that the simulation results are under predicting the temperature in the bed except for one location where the simulation value is

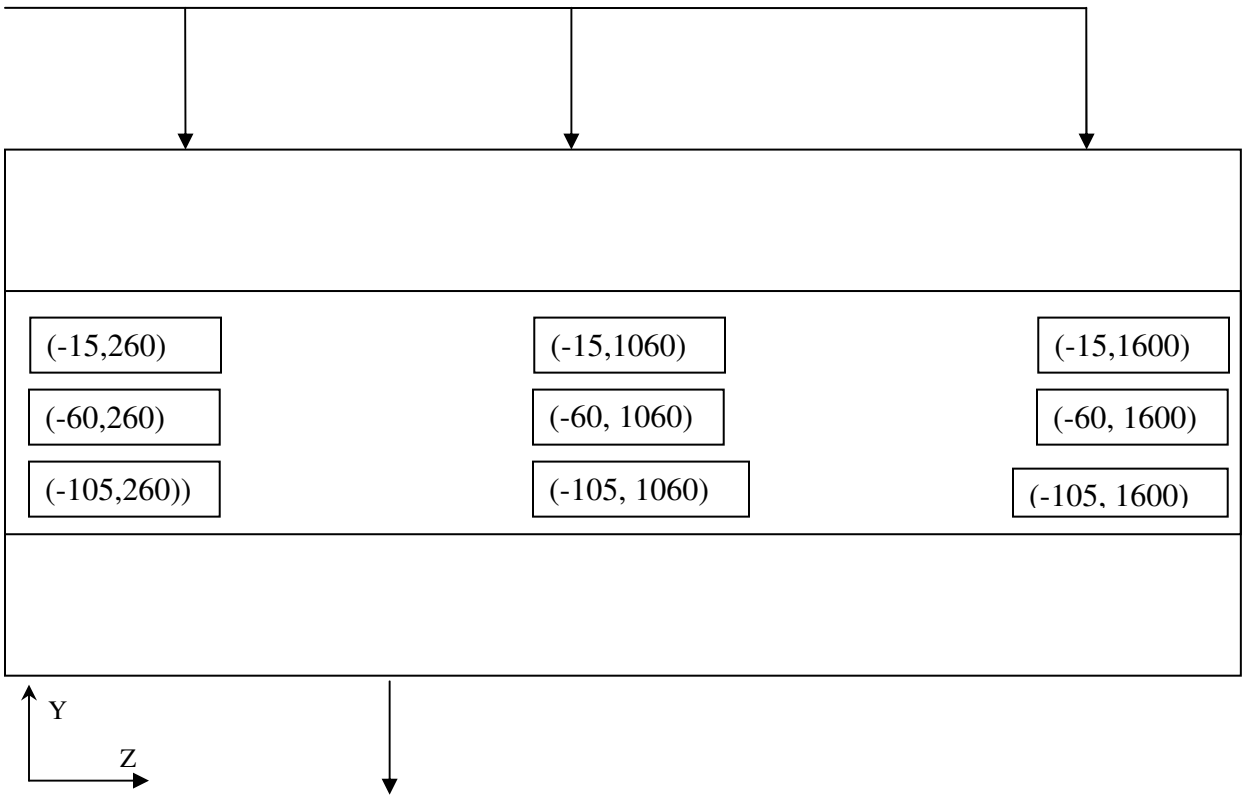

Figure 9.12: Nine different locations of the bed which consider to compare the different experimental and predicted temperatures.

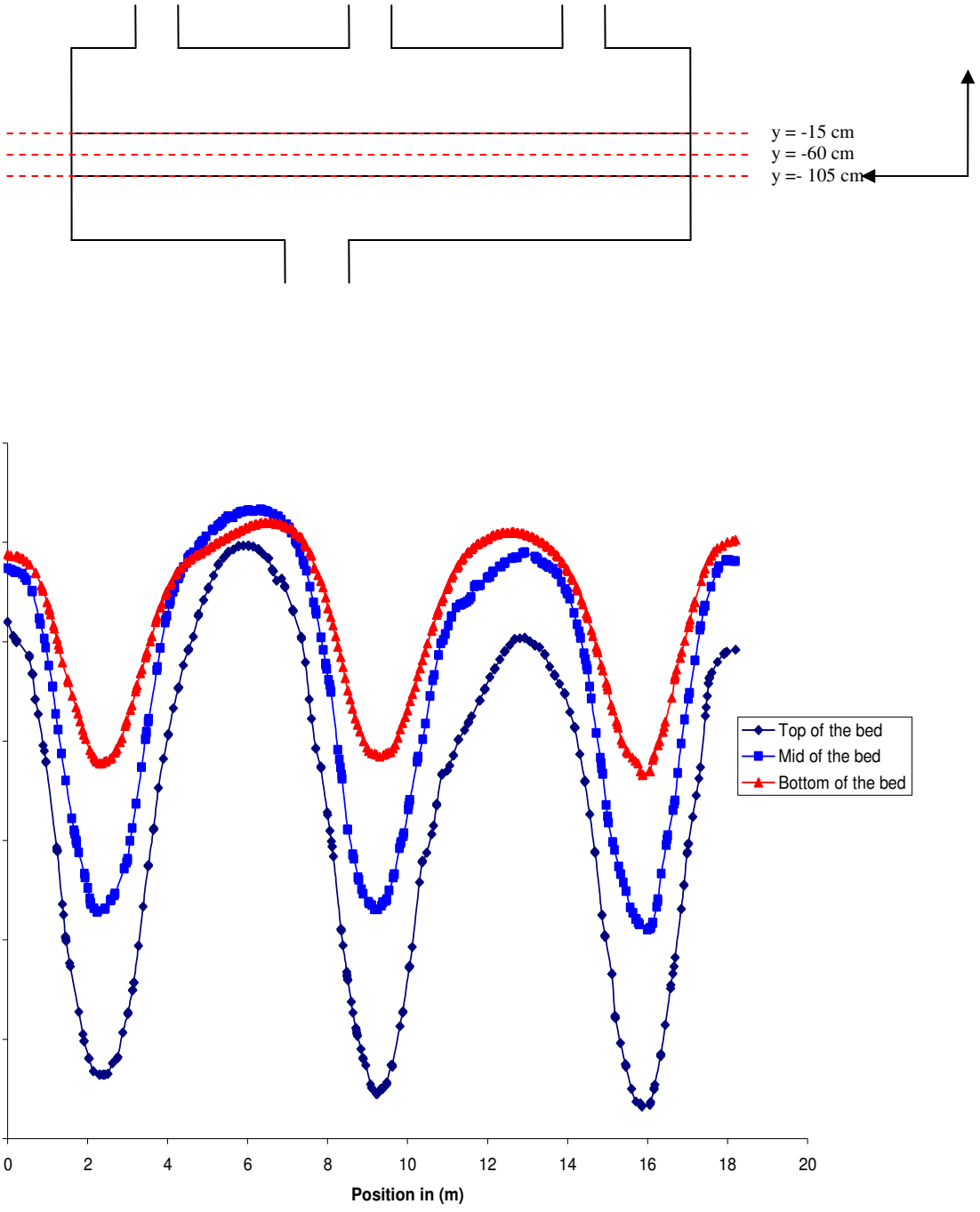

Figure 9.13: line plots of temperature profile for different position of the bed.

higher than the experimental one. However the same trend is shown. A better agreement may be obtained by adjusting the kinetics models used the simulations.

The industrial and numerical full compositions of the outlet gas are compared in Table 9.3. The predicted compositions of S_8, S_6 and S_2 are in close agreement with the actual values and these also agreed with values obtained from the equilibrium curves in Figure 9.8. At the relatively low temperature of the converter (compared to the furnace), most of the sulfur vapor produced by the Claus reaction is S_8, followed by S_6 and a trace of S_2. At higher temperatures such as those in the furnace, S_2 is the dominant species.

Figures 9-14 to 9-16 show that the mass fractions of S_2, S_6 and S_8 are 0.0113, 0.0213 and 0.0401 respectively. Figure 9-17 shows the contours of the mass fraction of steam. Steam is a main product of the Claus reaction. The steam mass fraction in the inlet stream is 0.044 compared to a mass fraction of 0.0716 in the outlet stream. The value reported in the industrial operation is 0.07479.

Figure 9-18 shows the contours of the mass fraction of H_2S in three horizontal planes; one near the bottom of the packed bed, one passing through the middle and one near the top of the bed. This figure shows clearly that the conversion is influenced by the velocity and therefore mass transfer. The contours in this figure are similar to the velocity contours in the same plane show in Figure 9.19.

Table 9.3: A comparison of the industrial and predicted temperature and compositions of the product gas for the first converter

Name	Inlet Industrial	Outlet	
		Predicted	Industrial
Temperature	511^0K	575^0K	572^0K
H_2S	0.06377	0.01527	0.01585
SO_2	0.06075	0.01515	0.01485
H_2O	0.044	0.0716	0.07479
S_2	0	0.0113	----
S_6	0	0.0213	----
S_8	0	0.0401	----

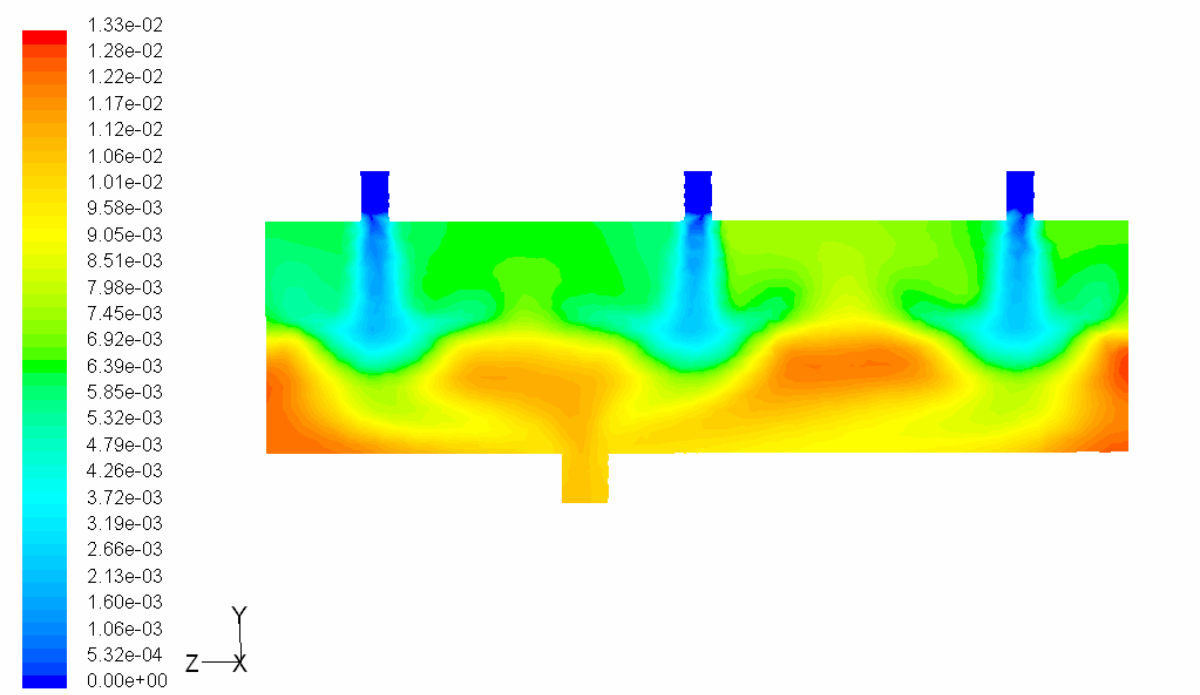

Figure 9.14: Contours of the S_2 mass fraction in a vertical plate passing through the inlets and the outlet of the first converter.

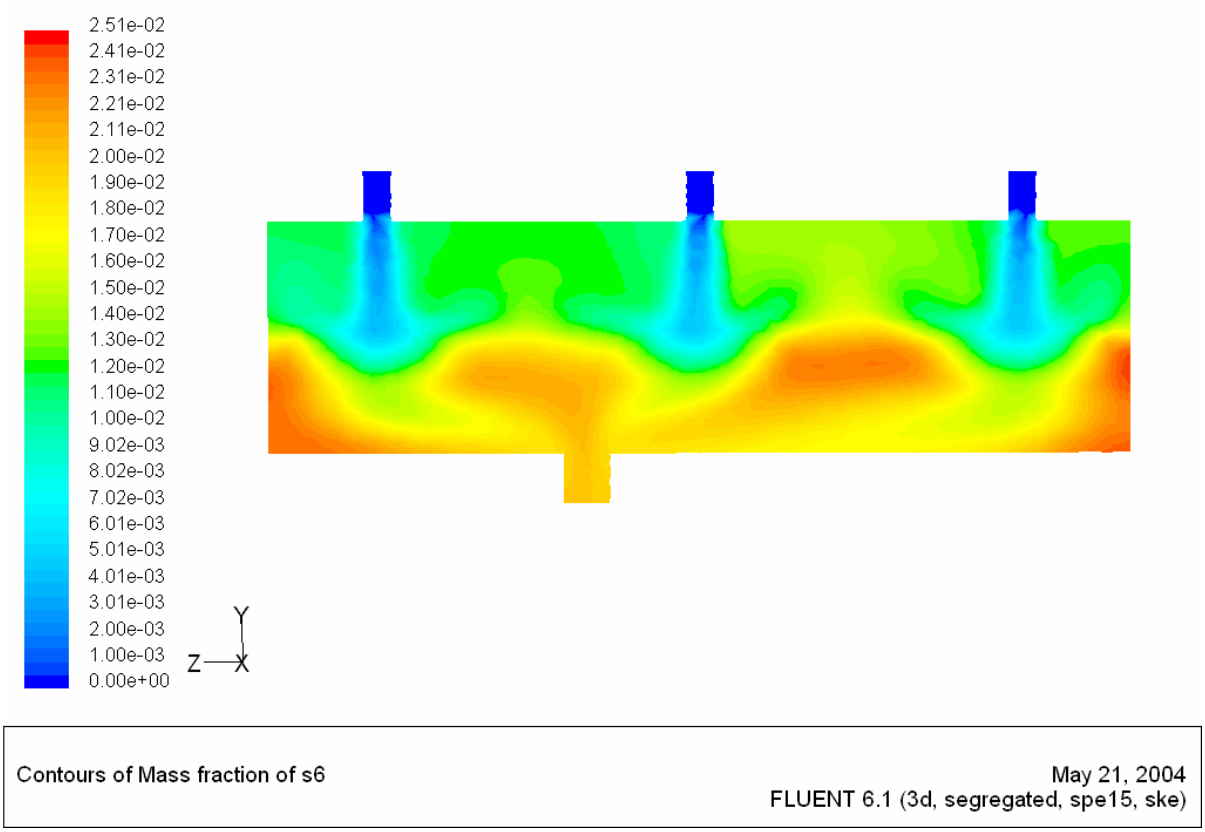

Figure 9.15: Contours of the S_6 mass fraction in a vertical plate passing through the inlets and the outlet of the first converter.

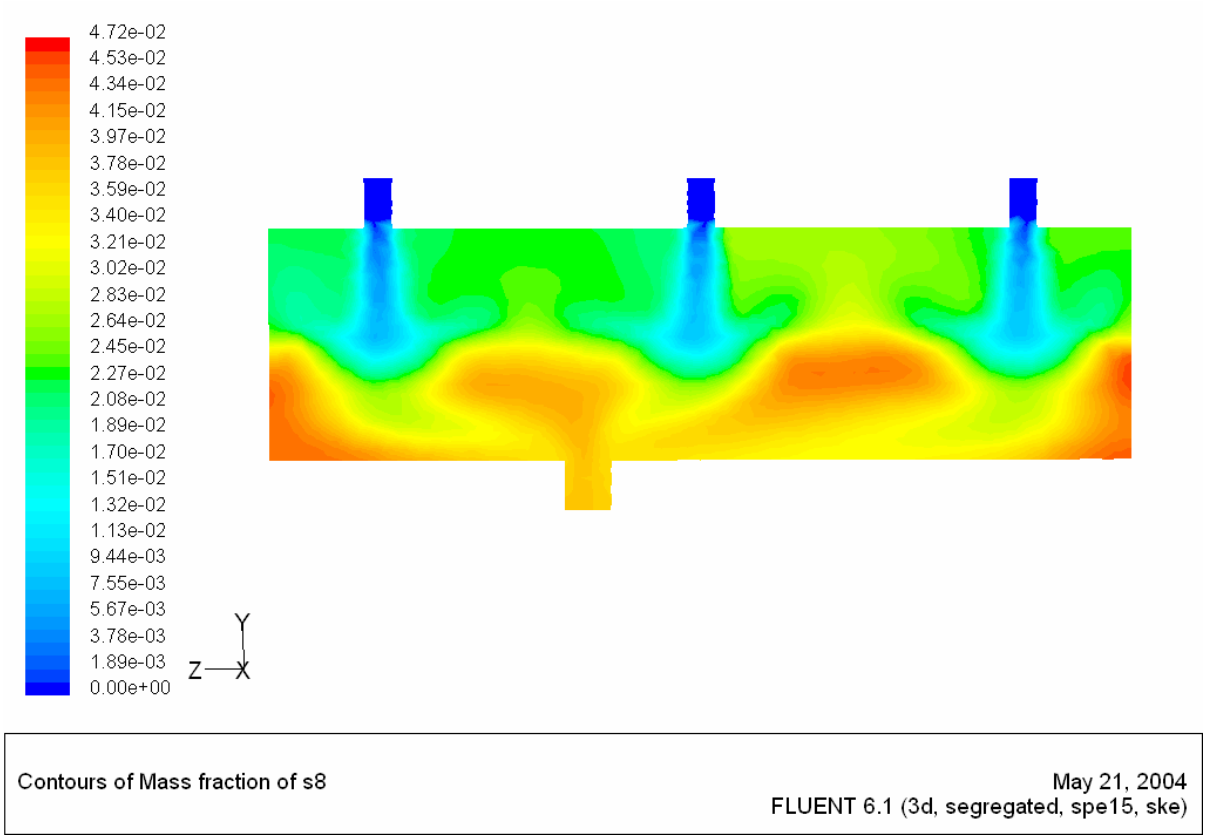

Figure 9.16: Contours of the S_8 mass fraction in a vertical plate passing through the inlets and the outlet of the first converter.

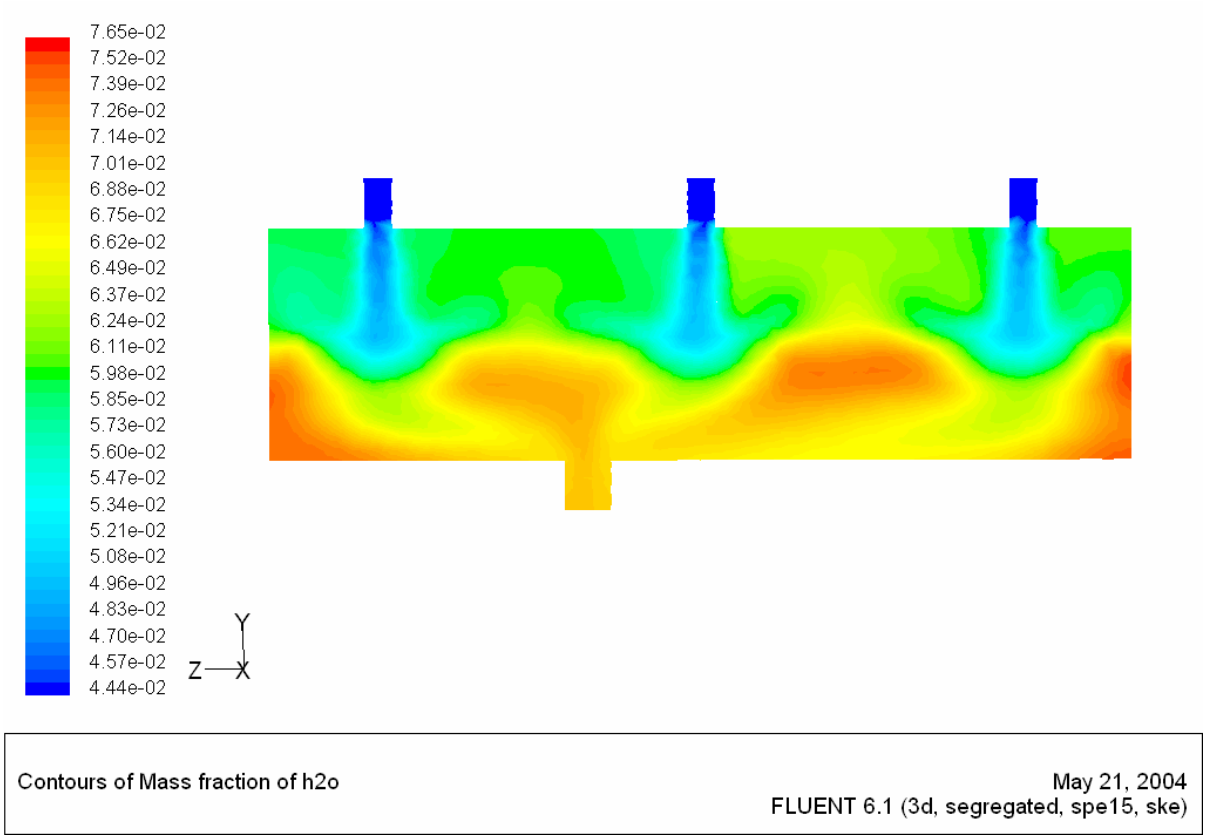

Figure 9.17: Contours of the H_2O mass fraction in a vertical plate passing through the inlets and the outlet of the first converter.

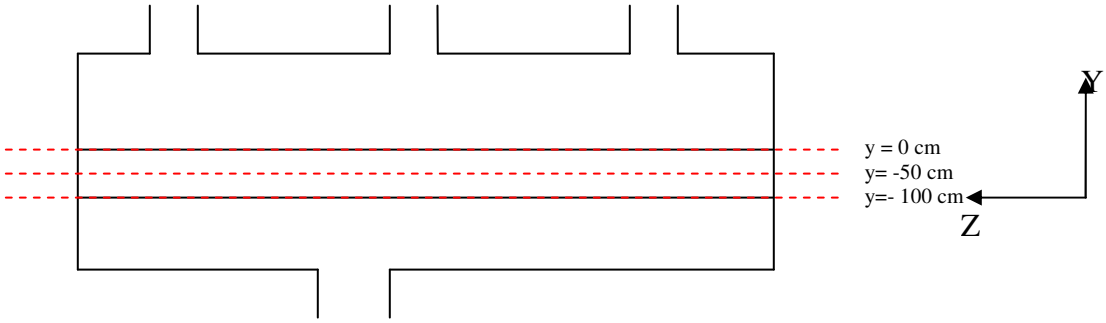

(a)

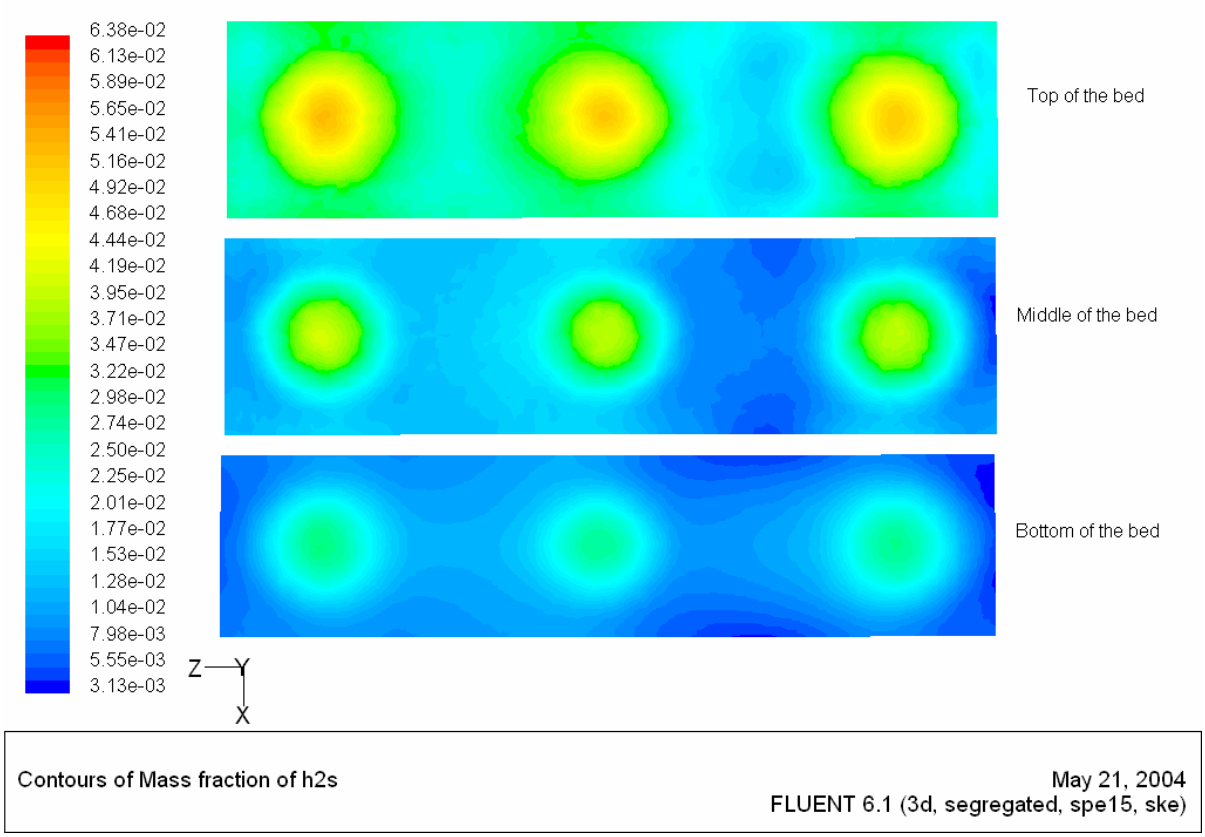

(b)

Figure 9.18: Contours of the H_2S mass fraction in horizontal planes in different positions of the packed bed of the first converter.

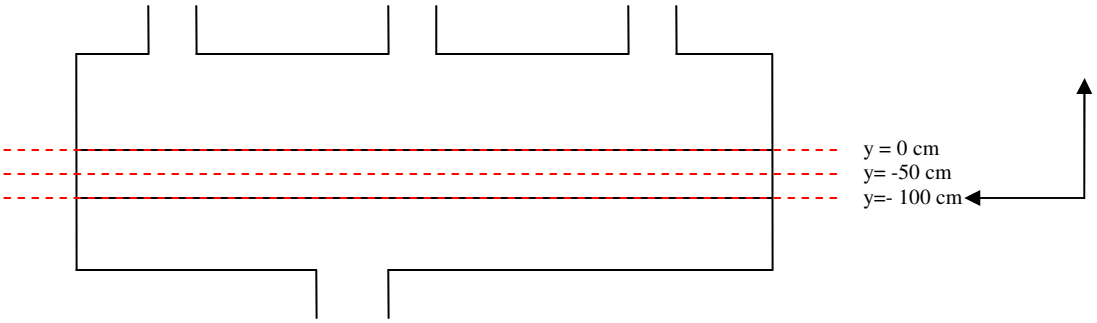

(a)

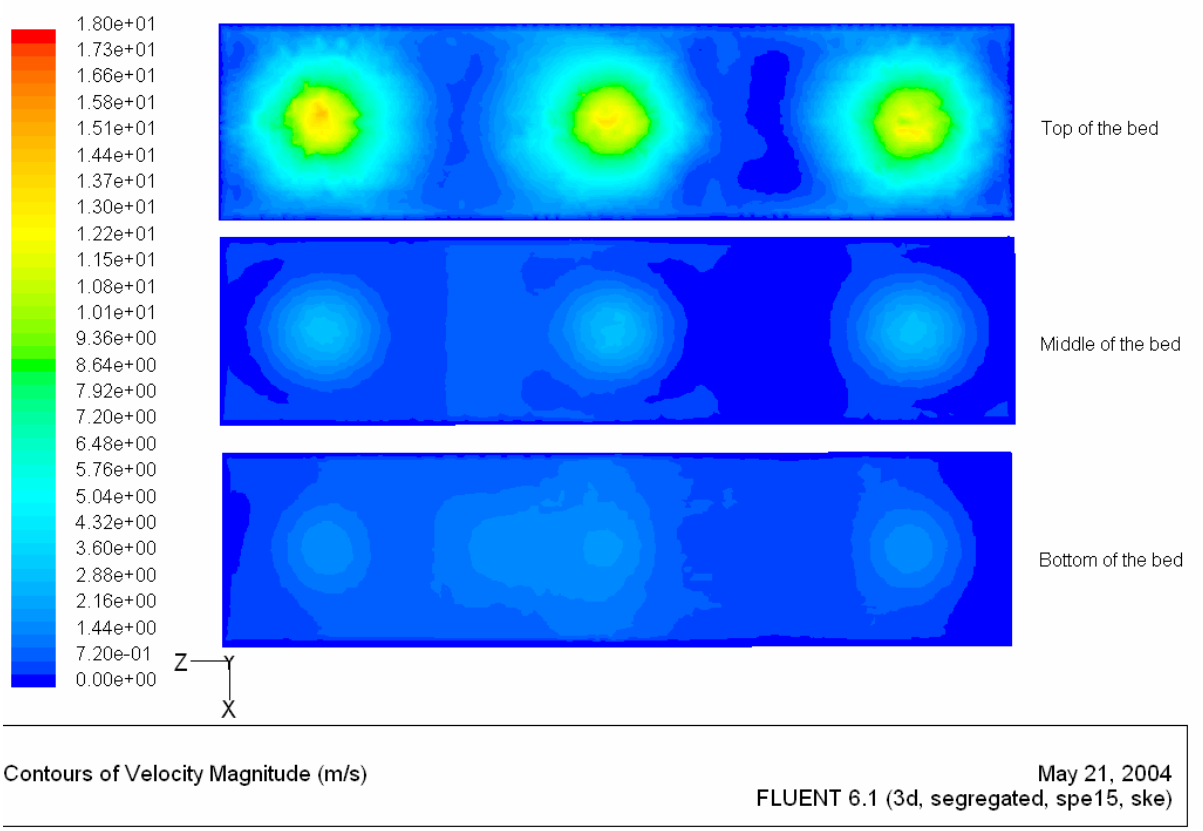

(b)

Figure 9.19: Velocity contours in horizontal planes located at different positions of the bed of the first converter.

9.5.3 Simulation of the Second Converter

Following the successful simulation of the flow and chemical reactions in the first converter, the same model and reaction kinetics are now applied to the second converter. It is assumed that all three converters used in the Claus process have identical geometries. The composition of the feed to the second converter and that of the product gas gives in Table 9.4.

Table 9.4: Composition of the feed to the second converter

Name of Component	**Feed composition (mass fraction)**	**Feed composition (mole fraction)**
Hydrogen	0.0001916	0.003412
Argon	0.003238	0.002909
Nitrogen	0.1898	0.2432
Methane	0.0005494	**0.001230**
Carbon Monoxide	0.001270	0.001627
Carbon Dioxide	0.6858	0.5593
Ethane	0.00006599	0.00007877
Hydrogen Sulfide	**0.01585**	**0.01669**
Water	0.07479	0.149
Sulfur Dioxide	**0.01485**	**0.008321**
Carbon Disulfide	0.0007292	0.0003438
Others	0.01286581	0.01388843
Total	1.0000	1.0000

A feed with a typical industrial composition (see Table 9.4) is introduced through the three inlets of the converter. The inlet temperature is 490°K. The flow and chemical reactions are simulated as was done for the first converter.

Figure 9.20 depicts the temperature profile in a vertical plane passing through the inlets and the outlet for this converter. The predicted results are in close agreement with the industrial data. The predicted outlet temperature for this case is found to be 498°K compared with the industrial value of 502°K.

Figure 9.21 shows the mass fraction contours of one of two reactants SO_2. The contours show the distribution of the mass fraction of SO_2 across the bed. This figure gives also an indication of the distribution of SO_2 showing that the SO_2 is consumed in the bed. The inlet composition of SO_2 is 0.01485, while the outlet composition is found 0.0092. The predicted value of the degree of conversion of SO_2 is 38.07% compared to an industrial value of 43.96 %.

Figure 9.22 shows the contours of the other main reactant H_2S. The feed composition of this reactant is 0.01585. The outlet composition is found 0.0098 which is also a little lower than the actual industrial value.

More experimental data is available in the form of temperature readings at various locations inside the bed. These locations are the same as for the first converter. Temperatures at identical locations were obtained from the simulation results shown in Figure 9.22, and both sets are compared in Table 9.5 and the position defined in Figure 9.12.

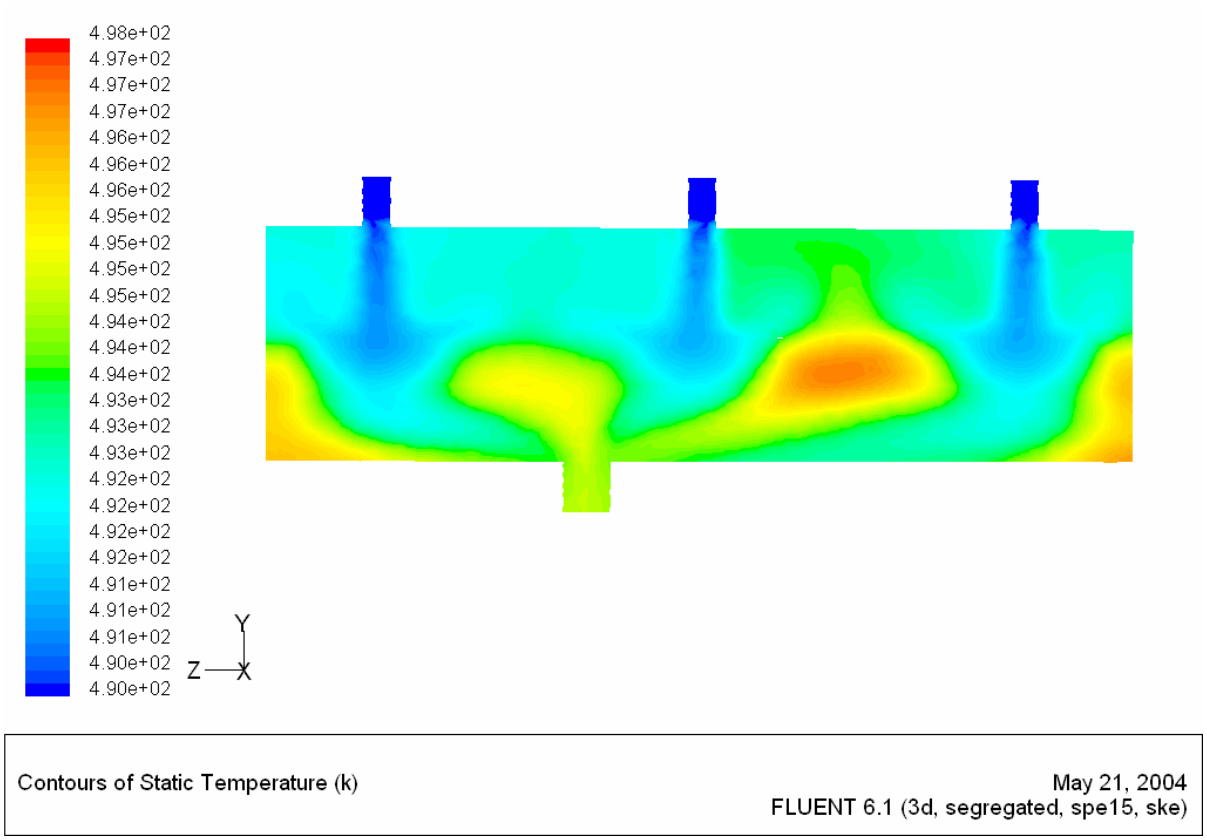

Figure 9.20: Temperature Contours in a central plane passing through the inlets and the outlet of the second converter.

Table 9.5 Temperatures at the identical locations in the bed

Position No.	Positions (y, z)	Experimental(K)	Simulation(k)
1	(-15,260)	489.82	491.7
2	(-15,1060)	489.07	492.82
3	(-15,1600)	490.21	494.16
4	(-60,260)	497.71	493.53
5	(-60, 1060)	498.11	495.25
6	(-60, 1600)	497.71	496.06
7	(-105,260)	503.76	491.44
8	(-105, 1060)	503.82	492.40
9	(-105, 1600)	503.37	493.18

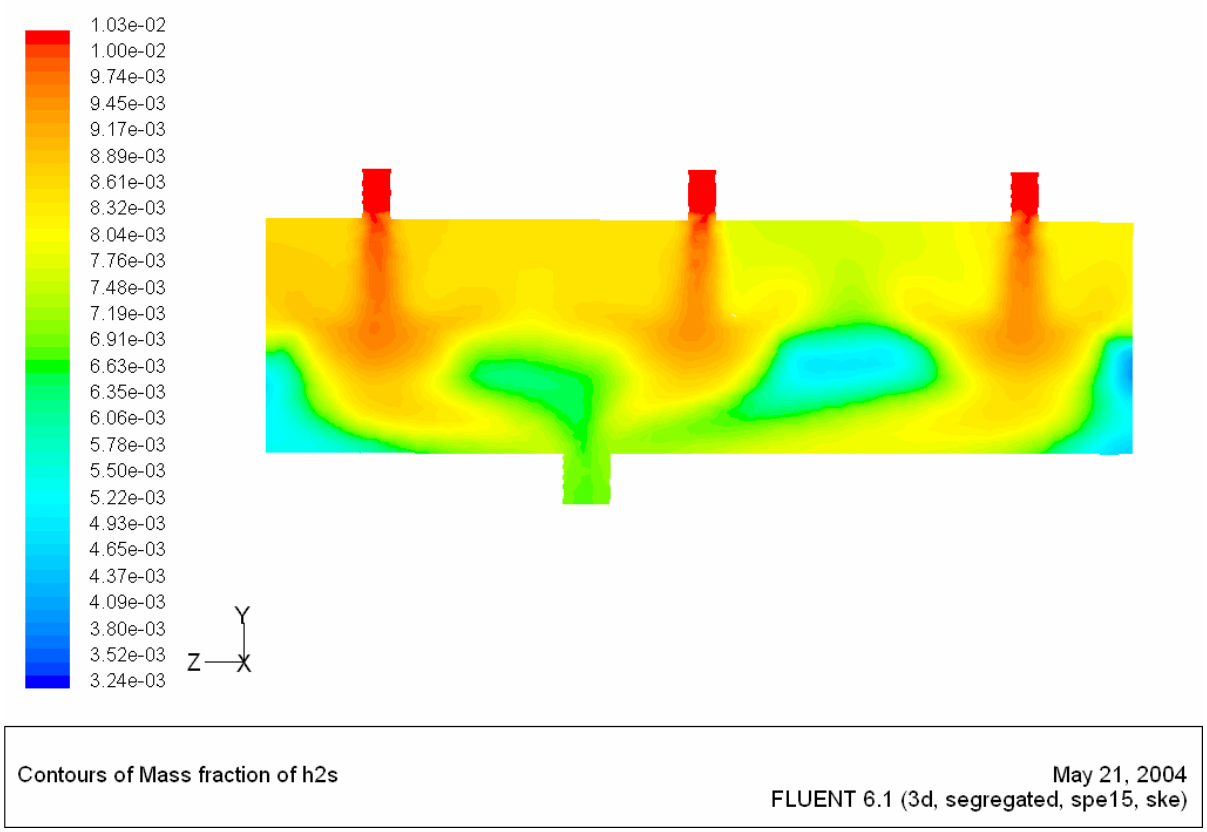

Figure 9.21: Contours of H_2S mass fraction in a vertical plane passing through the inlets and the outlet of the second converter.

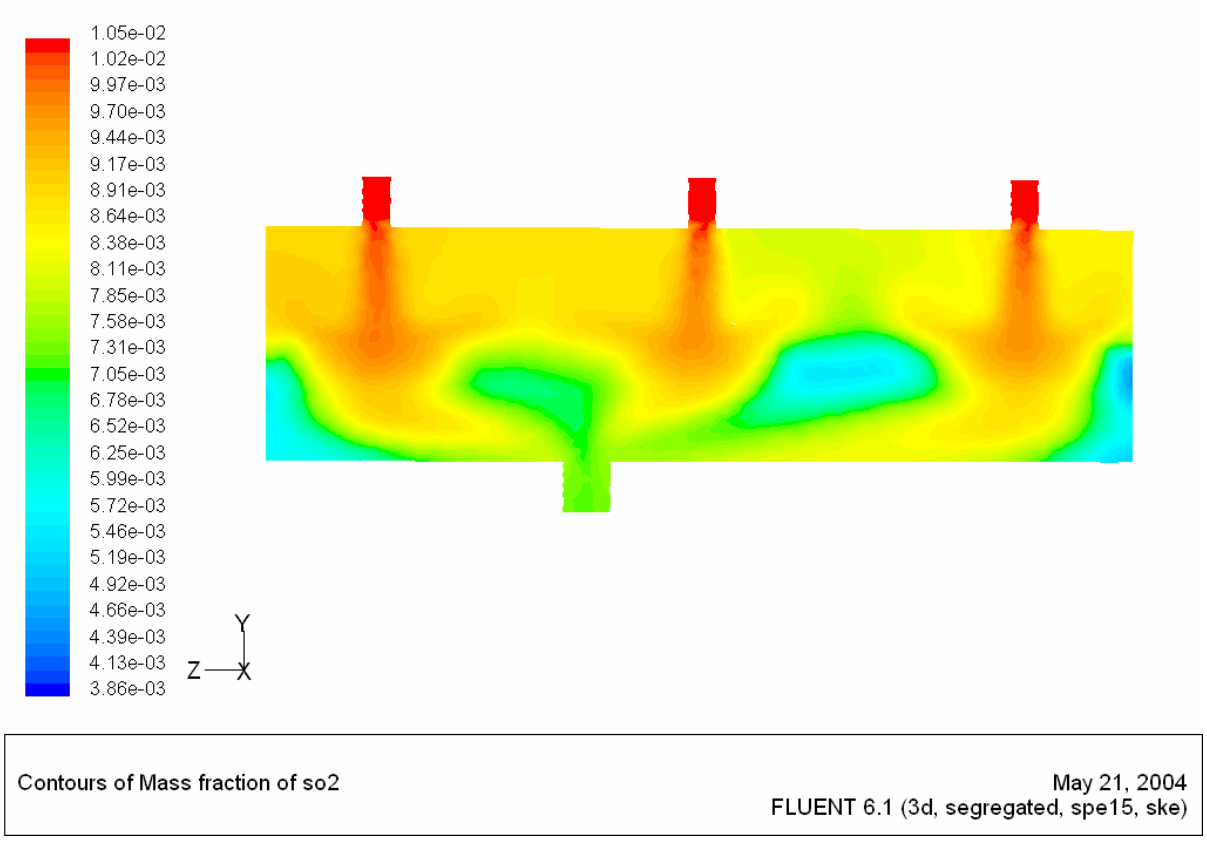

Figure 9.22: Contours of SO_2 mass fraction in a vertical plane passing through the inlets and the outlet of the second converter.

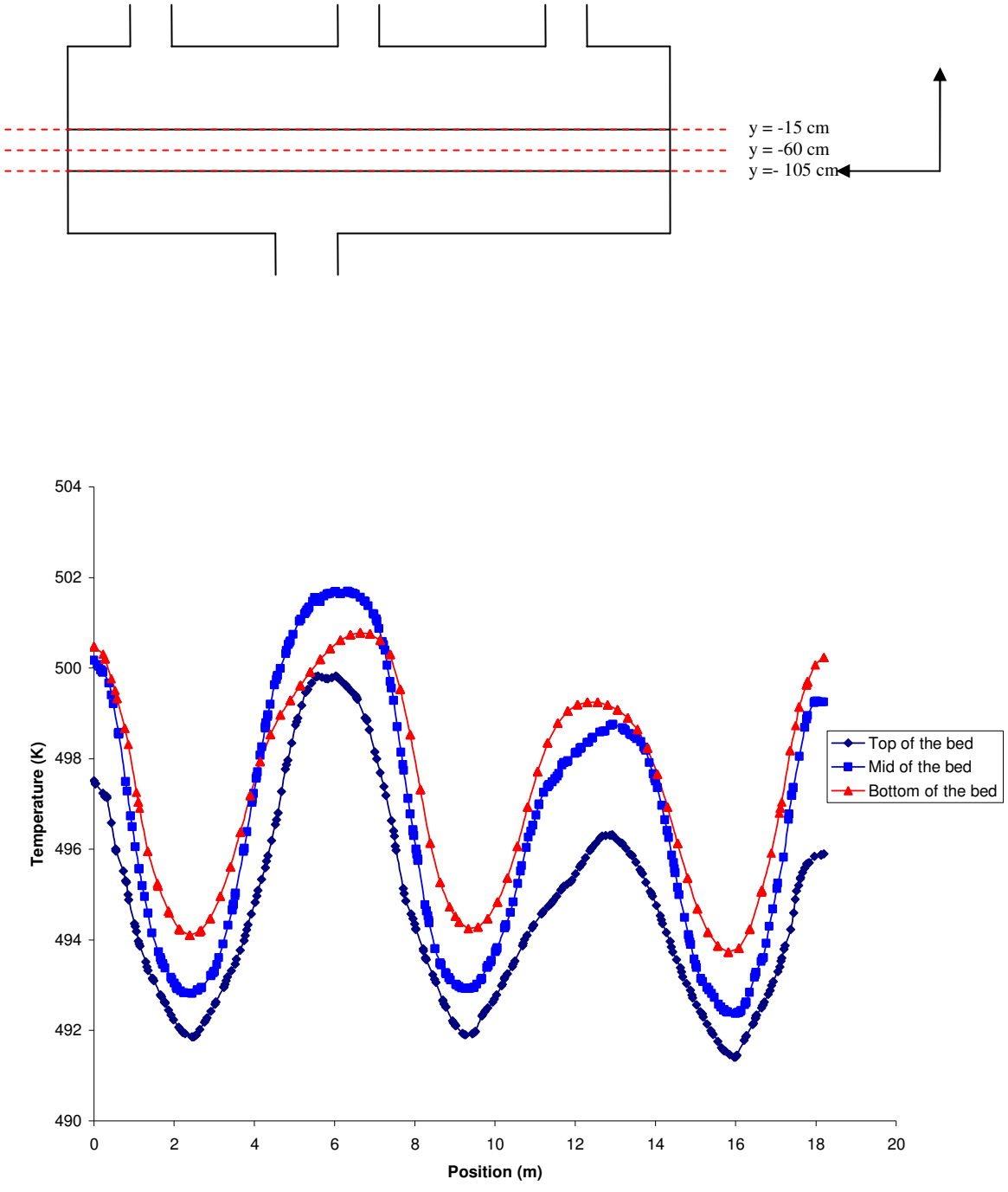

Figure 9.23: Line plots of the temperatures in different positions of the bed of the second converter.

According to the equilibrium curve shown in Figure 9.8 most of the elemental species in the second converter is in fact S_8. At an approximate average temperature of 494^0K, the equilibrium composition indicates the S_8, S_6 and S_2 constitute 72%, 26% and 2% respectively of the gaseous sulfur.

Figure 9.24 shows contours of the mass fraction of the S_2 produced. Most of this S_2 is produced in the bed as usual. The outlet composition of S_2 is found to be 0.00078. Figures 9.25 and 9.26 depict the S_6 and S_8 compositions. The outlet mass fraction of these compounds is 0.0027 and 0.00498 respectively. This means that 59 % of the elemental sulfur leaving the second converter is S_8, 32% is S_6 and remaining 9% is S_2.

Figure 9.27 shows the contours of the mass fraction of water vapor. The inlet mass fraction of the vapor is 0.07479, while the outlet the composition is 0.078. Table 9.6 lists the inlet composition and the experimental and predicted outlet results. This matches the values obtained from the equilibrium curve at the average temperature of 494°K.

Figure 9-28 shows the contours of the mass fraction of H_2S in three horizontal planes; one near the bottom of the packed bed, one passing through the middle and one near the top of the bed. This figure shows clearly that conversion is influenced by the velocity and therefore mass transfer. The contours in this figure are similar to the velocity contours in the same plane shown in Figure 9.29. Table 9.6 shows a comparison between the simulation and industrial results for the second converter.

Table 9.6: A comparison of the industrial and predicted temperature and compositions of the product gas

Name	Inlet Industrial	Outlet	
		Predicted	Industrial
Temperature	490^0K	498^0K	501^0K
H_2S	0.01585	0.0098	N/A
SO_2	0.01485	0.0092	N/A
H_2O	0.07479	0.078	N/A
S_2	0	0.00078	N/A
S_6	0	0.0027	N/A
S_8	0	0.00498	N/A

* N/A not available.

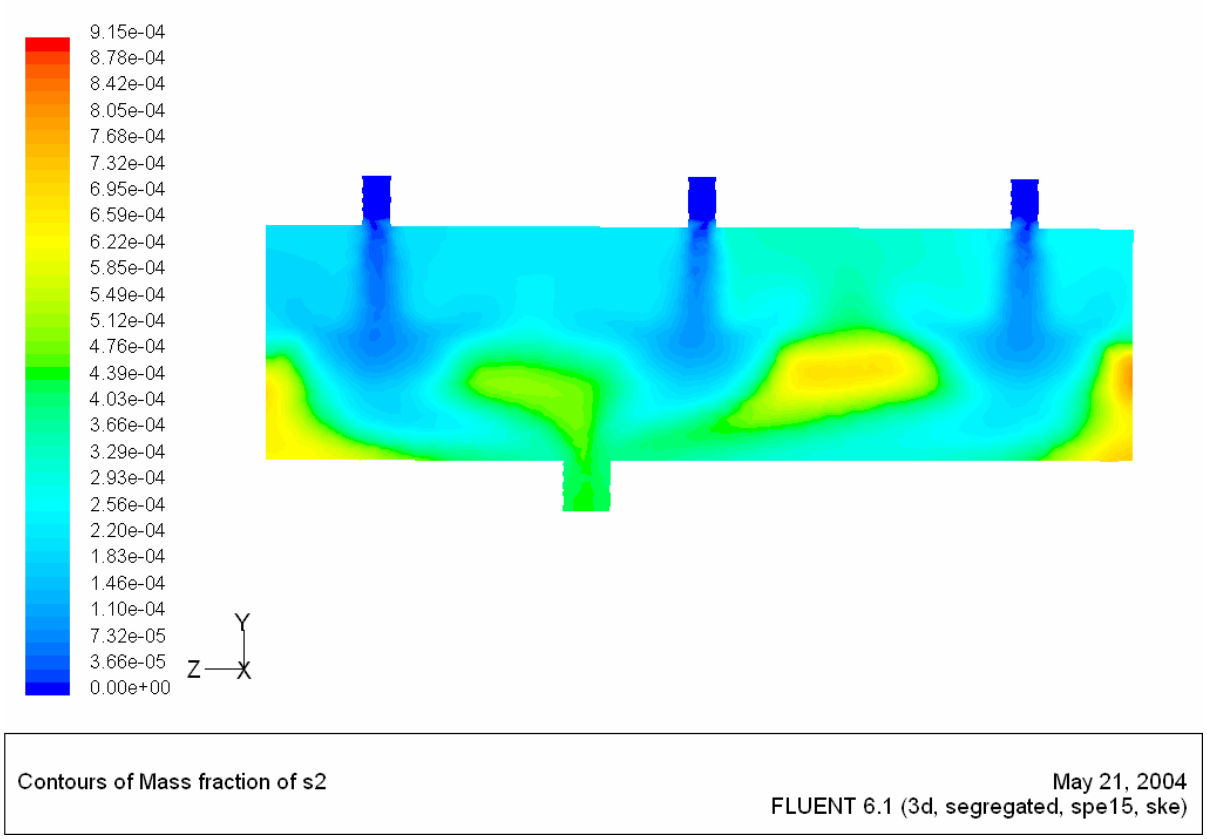

Figure 9.24: Contours of the S_2 mass fraction in a vertical plane passing through the inlets and the outlet of the second converter.

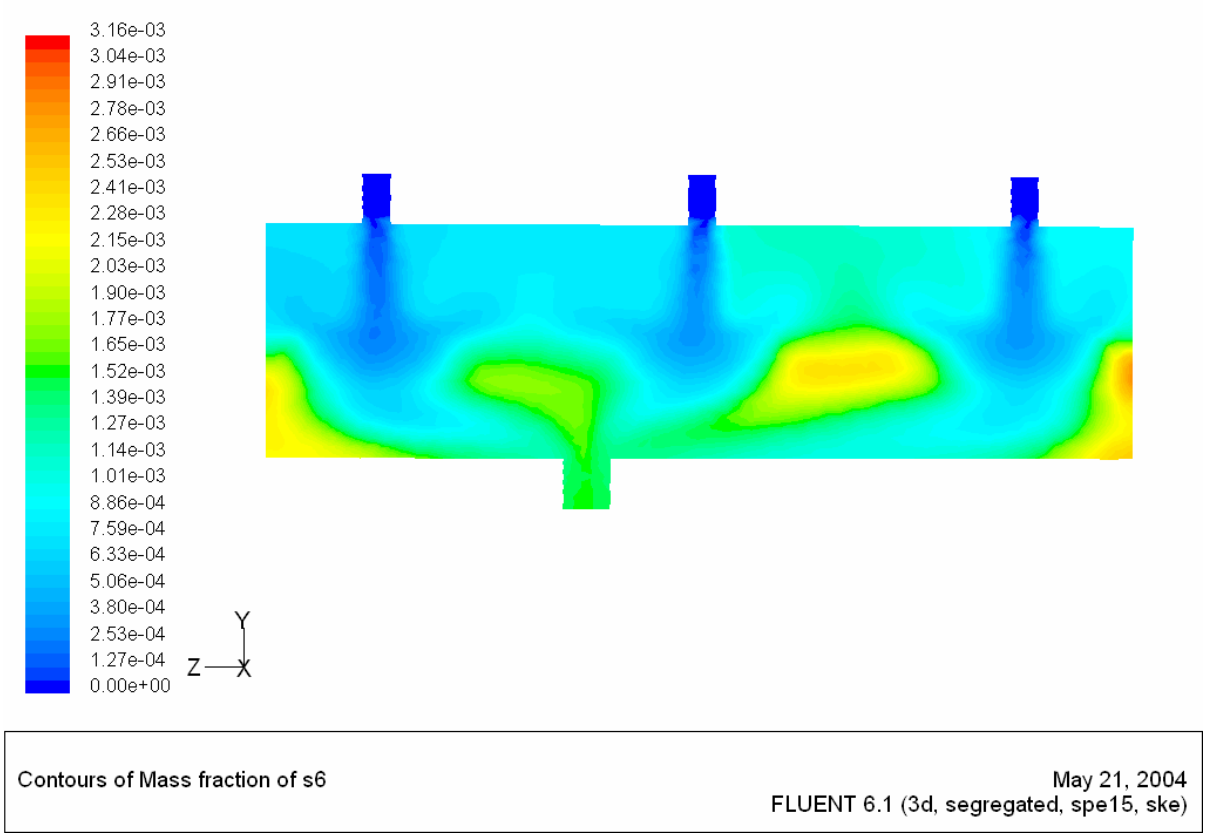

Figure 9.25: Contours of the S_6 mass fraction in a vertical plane passing through the inlets and the outlet of the second converter.

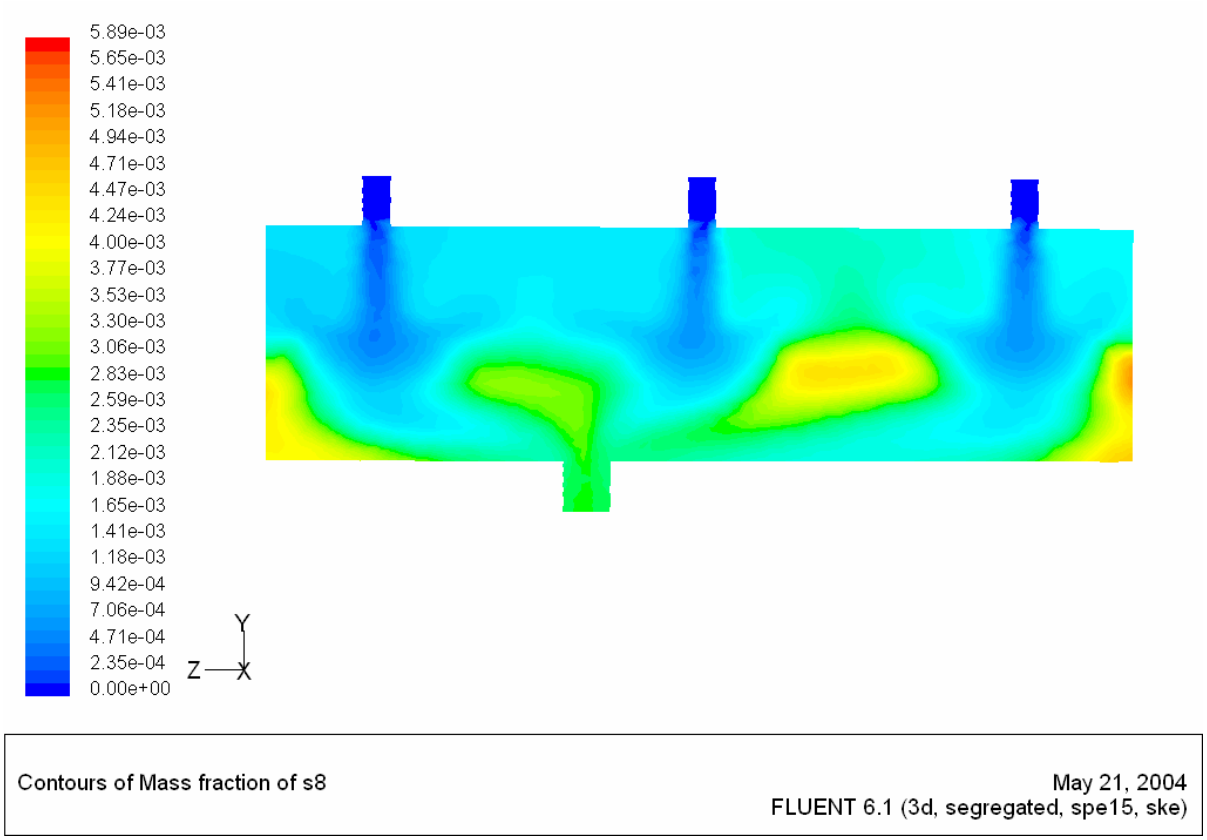

Figure 9.26: Contours of the S_8 mass fraction in a vertical plane passing through the inlets and the outlet of the second converter.

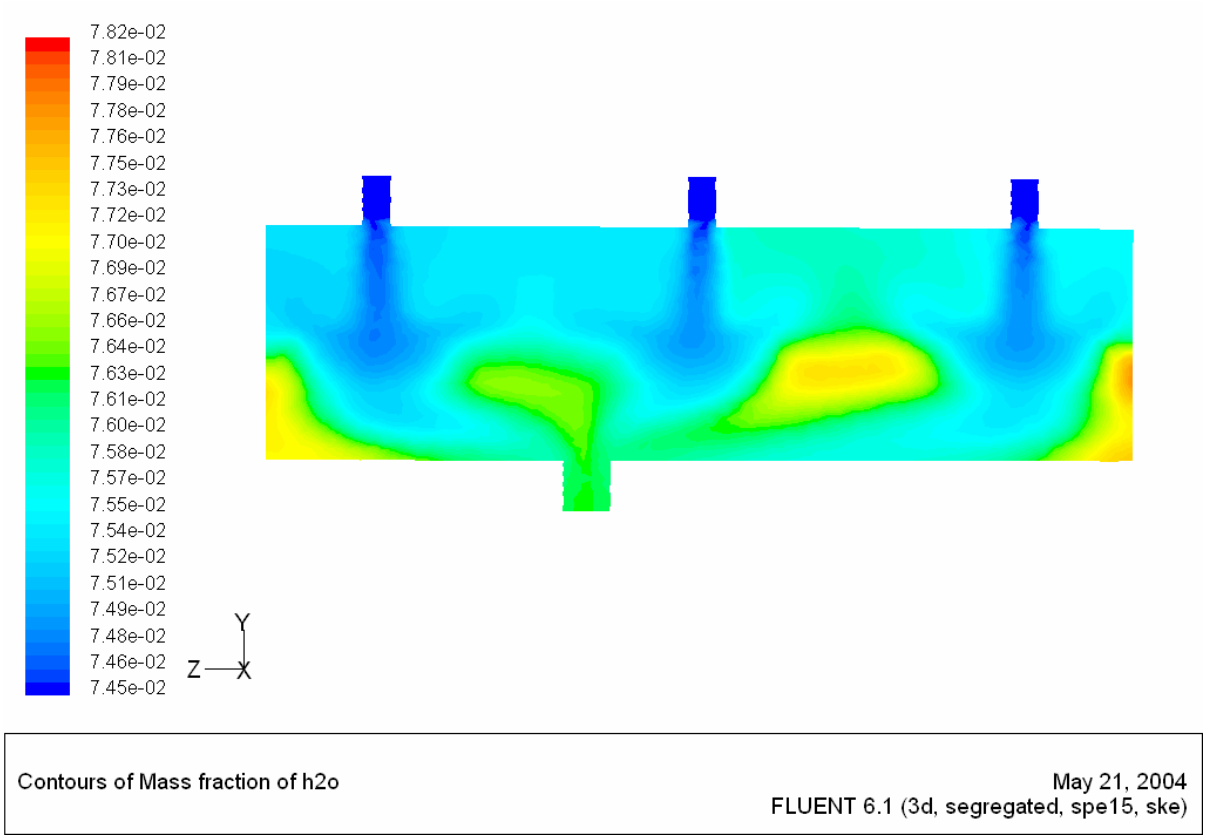

Figure 9.27: Contours of the H_2O mass fraction in horizontal plates in the different positions of the packed bed of the second converter.

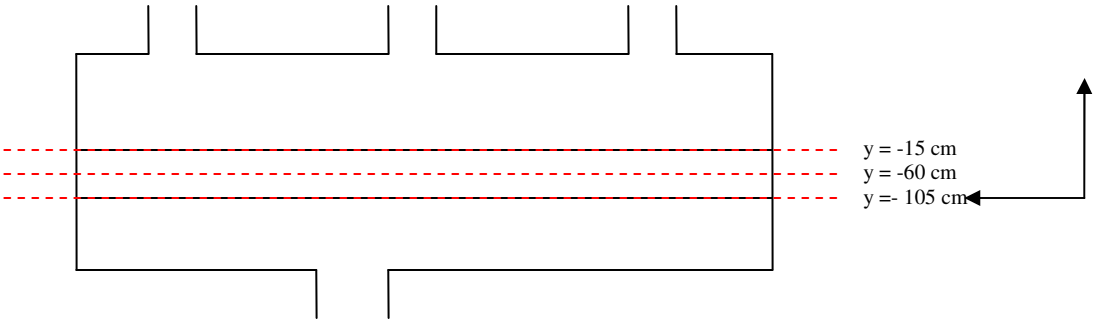

(a)

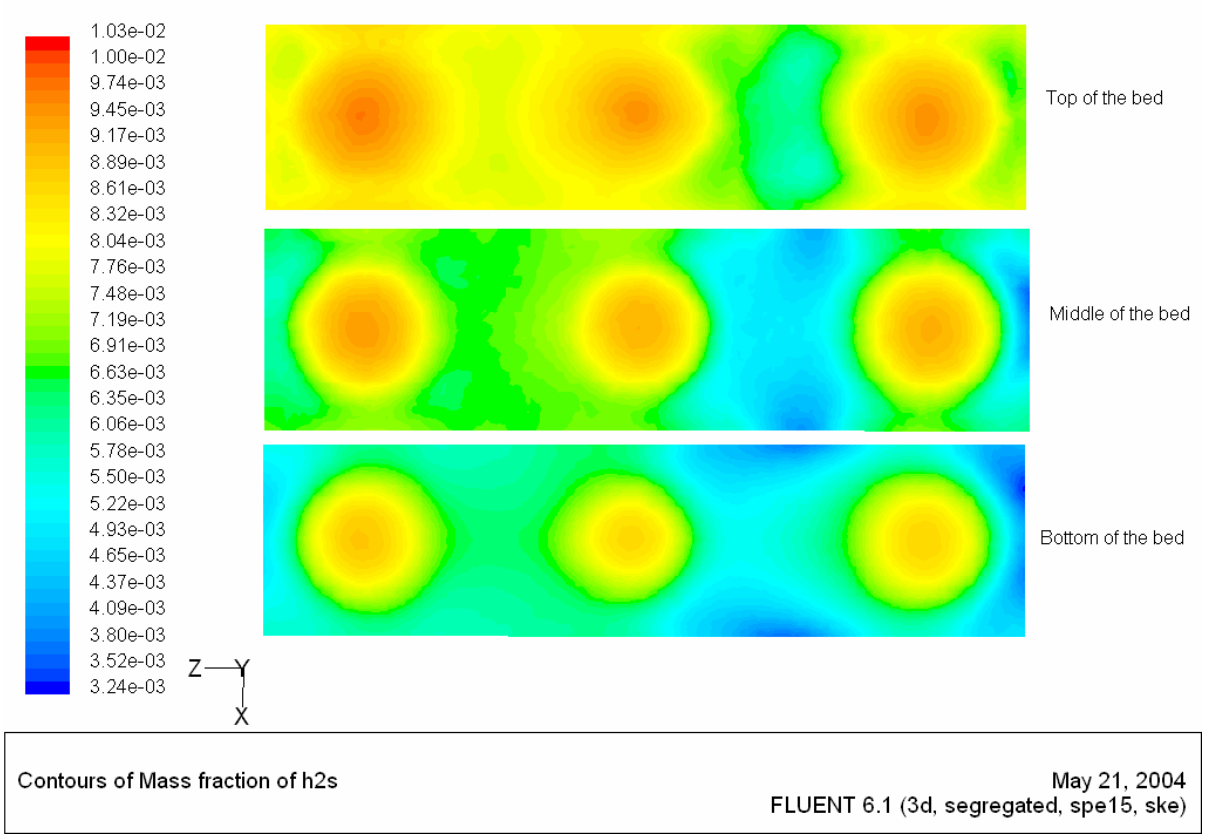

(b)

Figure 9.28: Contours of the H_2S mass fraction in horizontal plates in three different positions of the packed bed of the second converter.

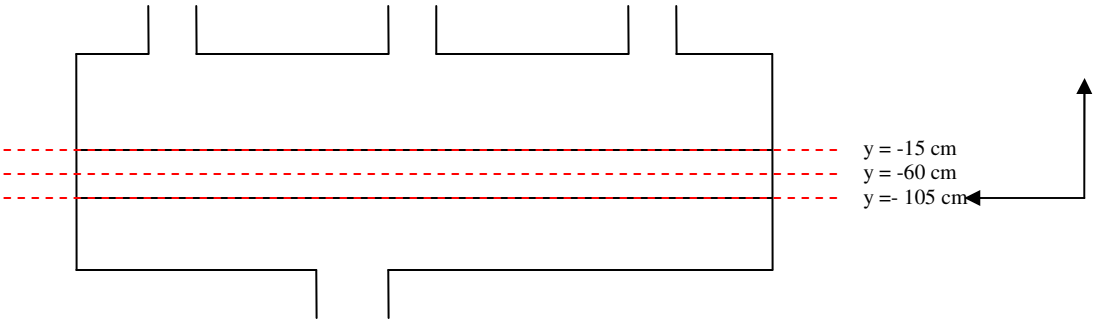

(a)

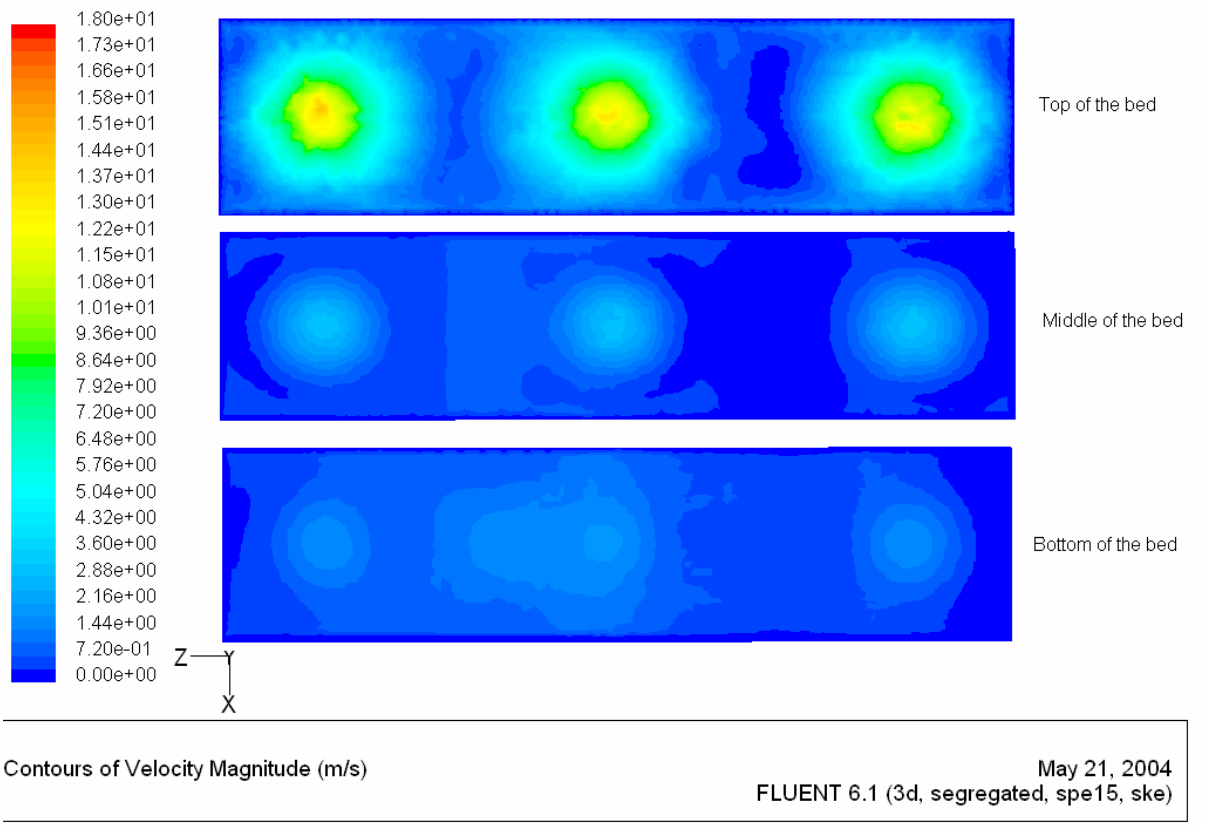

(b)

Figure 9.29: Velocity contours in horizontal plates in three different positions of the packed bed of the second converter.

9.5.4 Simulation Results for the Third Converter

Following the simulation of the first two converters, the third converter is now simulated. This converter has a geometry identical to the first two. The same feed flow rate is used; this means that the reduction in volume of the gas stream due to the Claus reaction is assumed negligible.

The feed to the third converter has the same composition as the stream leaving the second one. The industrial temperature is used so that the results of the simulations can be validating against industrial data. The temperature of the feed is 473°K and the composition is given in Table 9.7.

Table 9.7: Composition of the feed to the third converter

Name of Component	**Feed composition (mass fraction)**
Hydrogen	0.0001916
Argon	0.003238
Nitrogen	0.1898
Methane	0.0005494
Carbon Monoxide	0.001270
Carbon Dioxide	0.6858
Ethane	0.00006599
Hydrogen Sulfide	**0.0098**
Water	0.078
Sulfur Dioxide	**0.0092**

Carbon Disulfide	0.0007292
Others	0.0213505
Total	1.0000

Figure 9.30 shows the temperature profile in a central plane passing through the inlets and outlet. The side reactions were neglected. The outlet temperature is found to be 476°K compared to an outlet temperature of 474.7°K recorded industrially.

More experimental data is available in the form of temperature readings at various locations inside the bed. Temperatures at identical locations were obtained from the simulation results and both sets are compared in Table 9.8. The simulation values deduced from Figure 9.31.

Table 9.8 Temperatures at the identical locations in the bed

Position No.	**Positions (y, z)**	**Experimental(K)**	**Simulation(k)**
1	(-15,260)	471.2	473.76
2	(-15,1060)	472.31	474.44
3	(-15,1600)	472.15	473.55
4	(-60,260)	473.59	474.04
5	(-60, 1060)	473.2	474.99
6	(-60, 1600)	475.09	473.81
7	(-105,260)	475.2	474.48
8	(-105, 1060)	476.53	475.19
9	(-105, 1600)	476.77	474.29

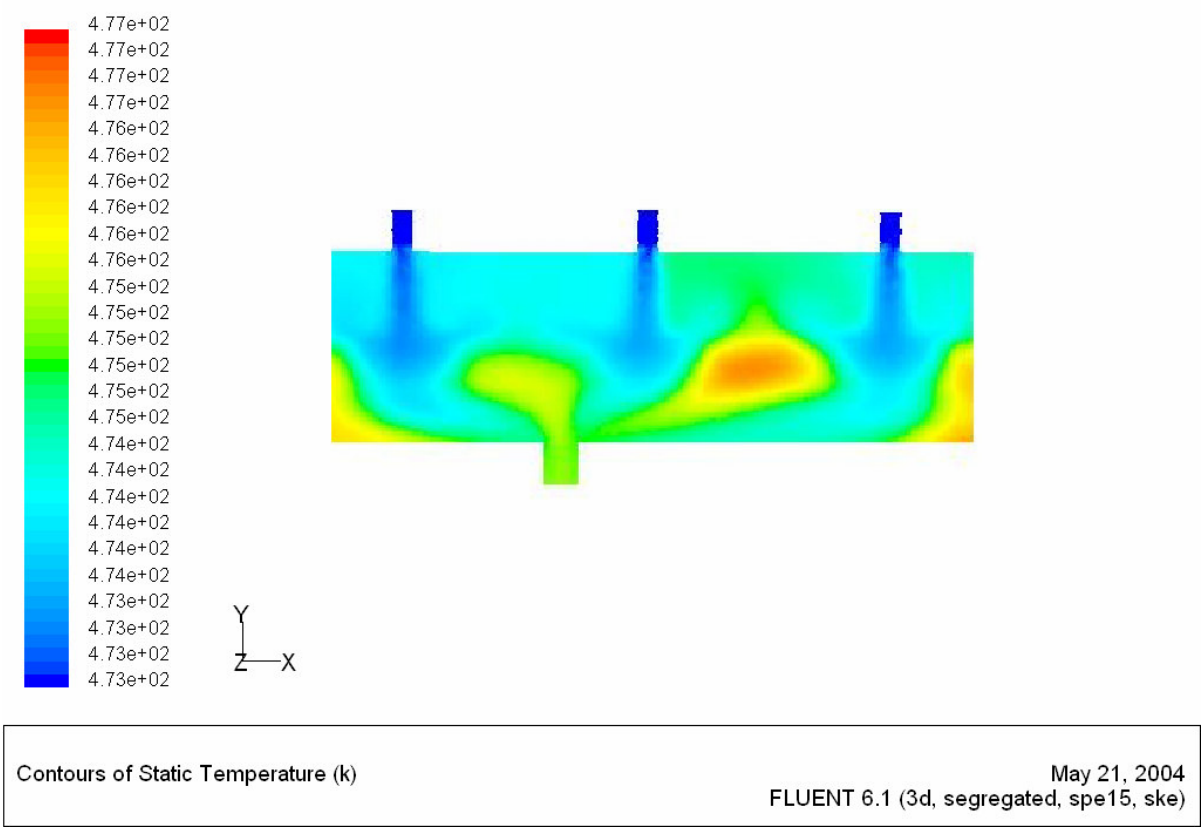

Figure 9.30: Temperature Contours in a central plane passing through the inlets and the outlet of the third converter.

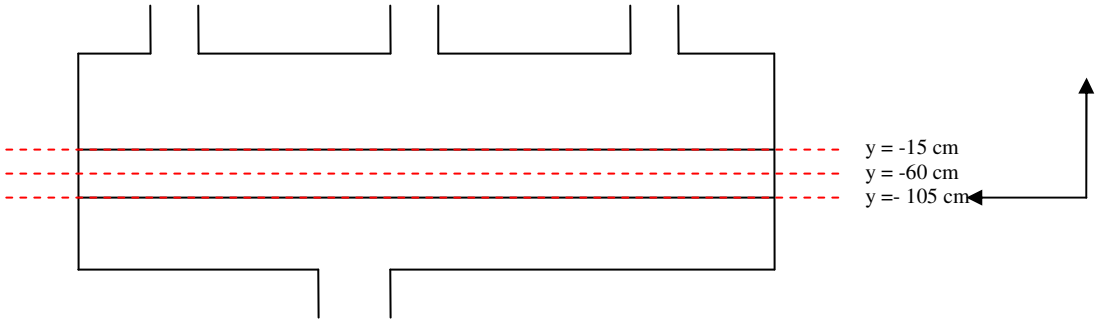

(a)

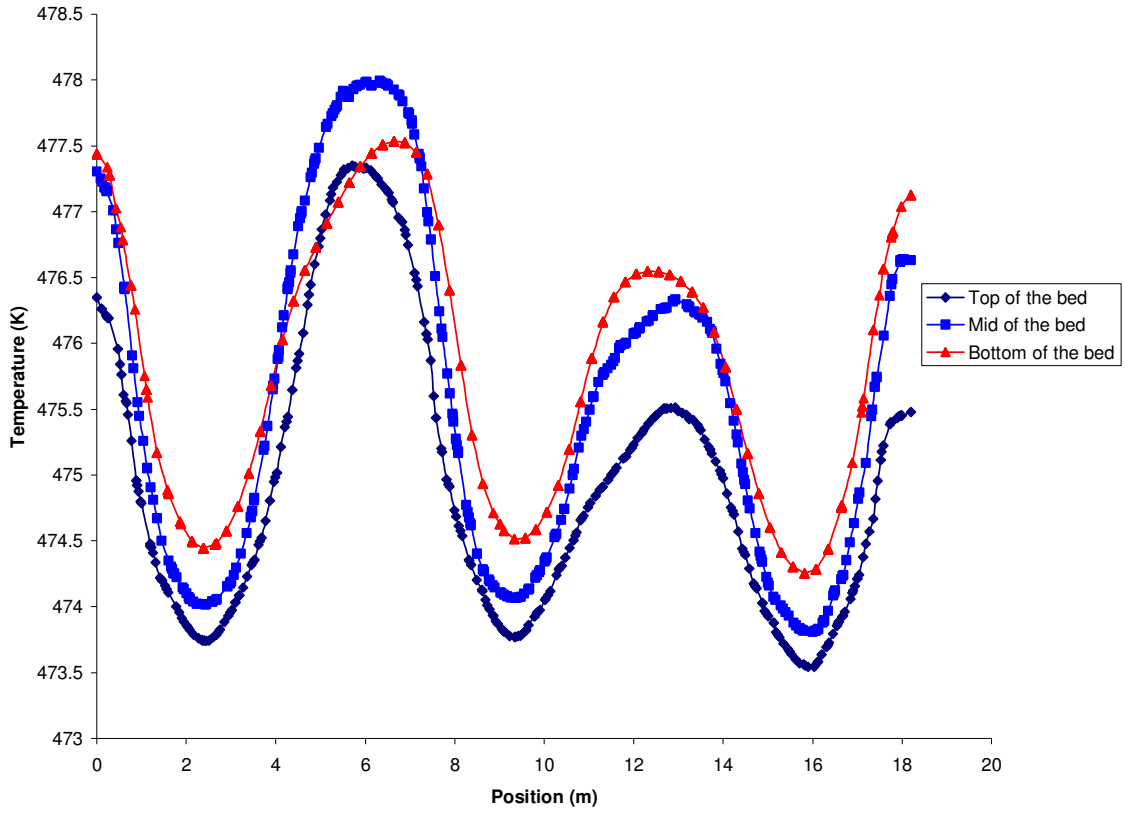

(b)

Figure 9.31: Line plot of the temperature profile in different position of the bed.

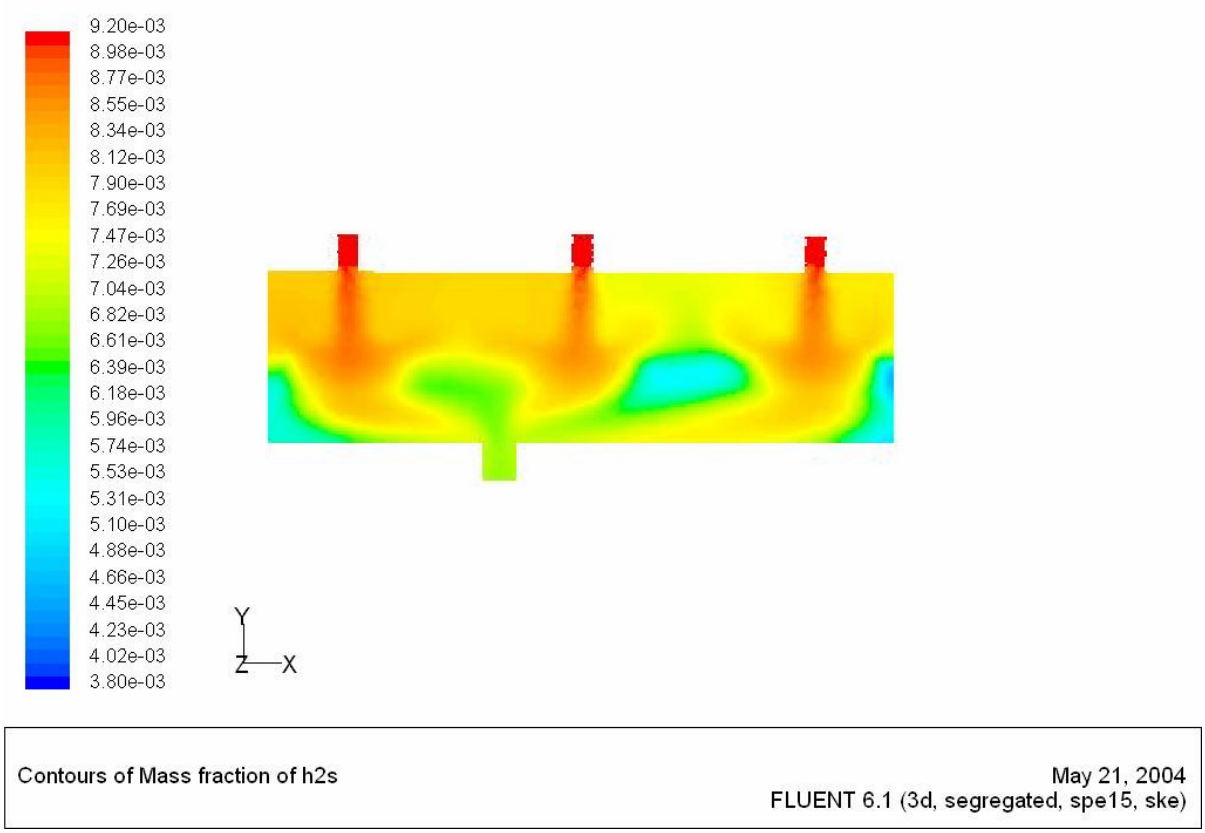

Figure 9.32: Contours of H_2S mass fraction in a vertical plane passing through the inlets and the outlet.

Figure 9.32 shows the mass fraction contours of H_2S in the same vertical plane. The H_2S mass fraction in the feed stream is 0.0098 and 0.00693 in the outlet stream.

Figure 9.33 shows the mass fraction contours of SO_2. The contours give indications of the consumption distribution of SO_2 with the bed. SO_2 is consumed in the bed and the SO_2 concentration is largely reduced at the outlet. This figures show similar contours to those of H_2S consumption. The inlet composition of the SO_2 is 0.0092. The outlet composition is found 0.0076.The predicted value of the degree of conversion of SO_2 is found to be 17.4%

The mass fraction of S_2, S_6 and S_8 in the product stream obtained in the current simulation agrees well with those values obtained from the equilibrium curve at the average temperature of the converter.

Figure 9.34 shows the mass fraction contours of S_2 production. Most of this S_2 is produced in the bed. The outlet composition of S_2 is found to be 0.00078. Figure 9.35 and Figure 9.36 depicts the S_6 and S_8 compositions. The mass fractions of these compounds are 0.0027 and 0.00498 respectively.

Figure 9.37 shows the mass fraction contours of water vapor. The inlet mass fraction of the vapor is 0.07479 and it increased, following the reaction, at the outlet to a value of 0.078. These results are summarized in Table 9.8,

Figure 9-38 shows the contours of the mass fraction of H_2S in three horizontal planes; one near the bottom of the packed bed, one passing through the middle and one near the top of the bed. This Figure shows clearly that the conversion is influenced by the velocity and therefore mass transfer. The contours in this figure are similar to the velocity contours in the same plane shown in Figure 9.39.

0.Table 9.9: A comparison of the industrial and predicted temperature and compositions of the product gas

Name	Inlet Industrial	Outlet	
		Predicted	Industrial
Temperature	473^0K	474.7^0K	476^0K
H_2S	0.0098	0.00693	N/A
SO_2	0.0092	0.0076	N/A
H_2O	0.078	0.0792	N/A
S_2	0	0.0003	N/A
S_6	0	0.001	N/A
S_8	0	0.0019	N/A

* N/A not available.

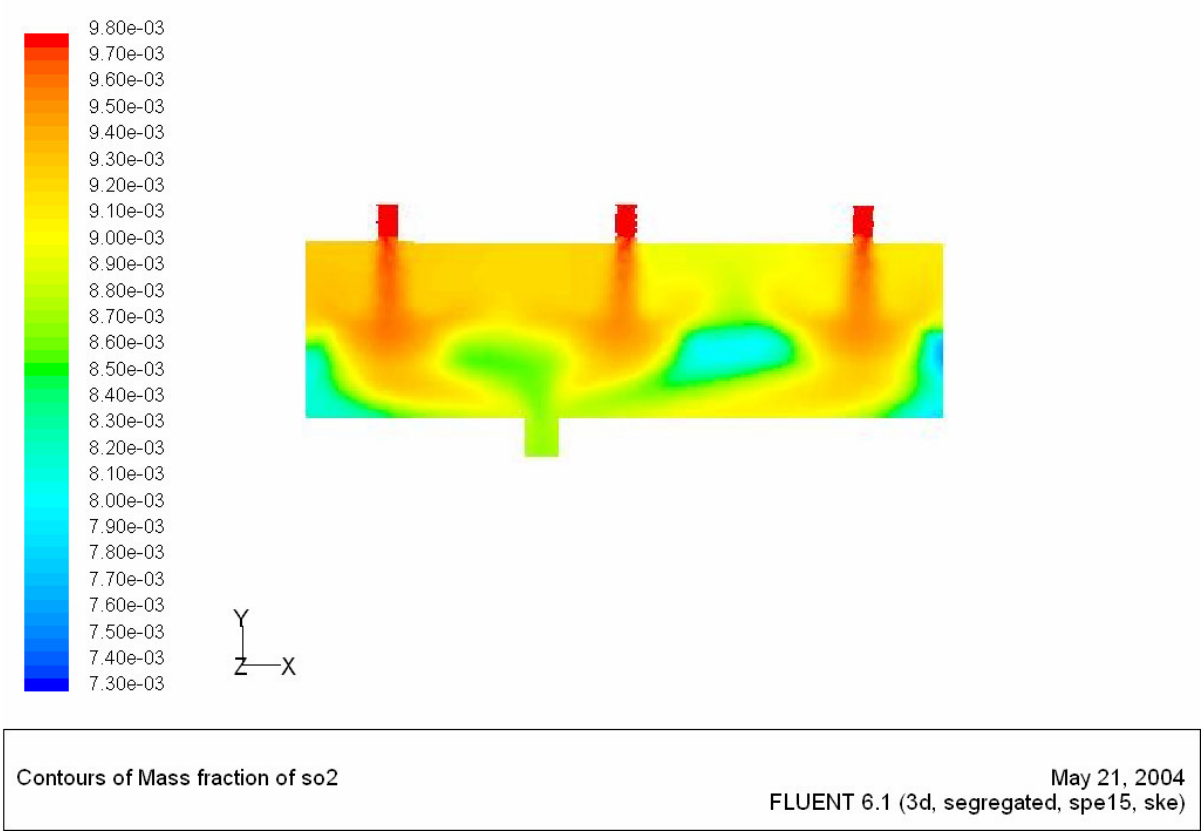

Figure 9.33: Contours of SO_2 mass fraction in a vertical plane passing through the inlets and the outlet of the third converter.

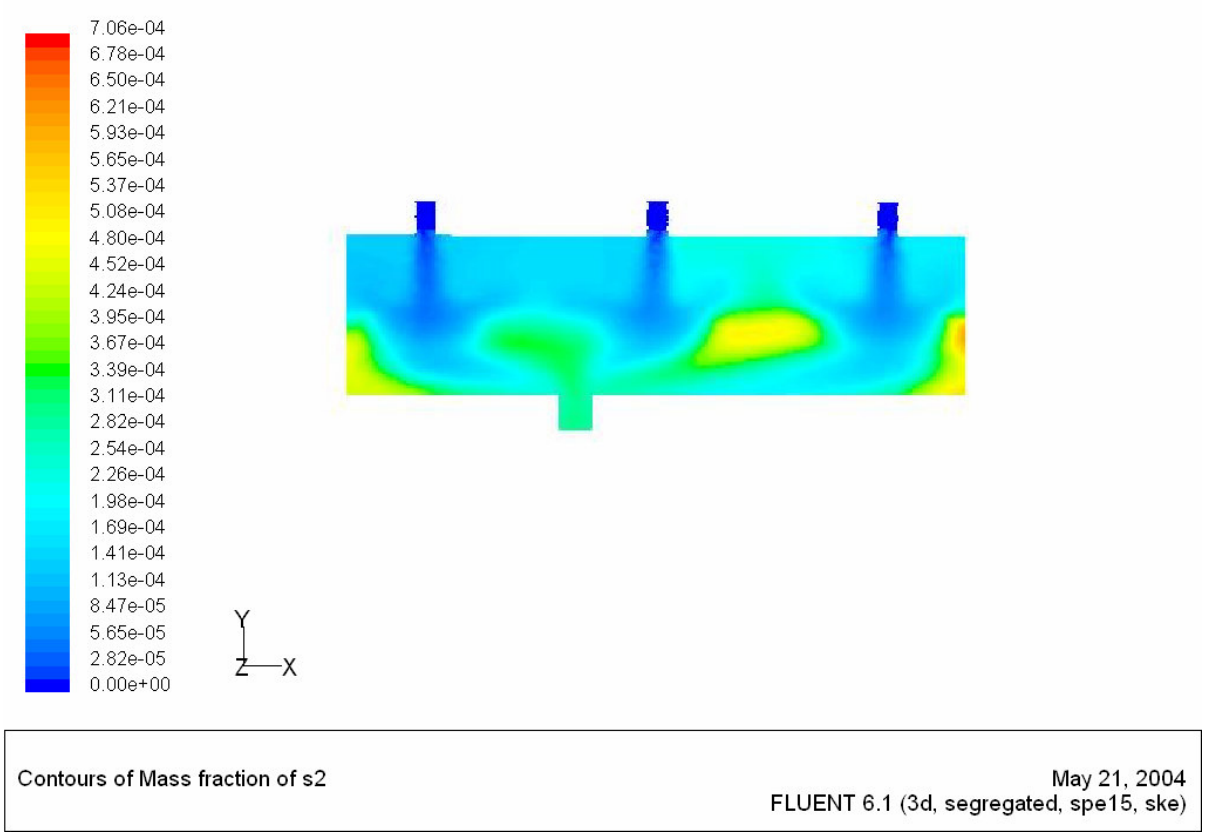

Figure 9.34: Contours of S_2 mass fraction in a vertical plane passing through the inlets and outlet of the third converter.

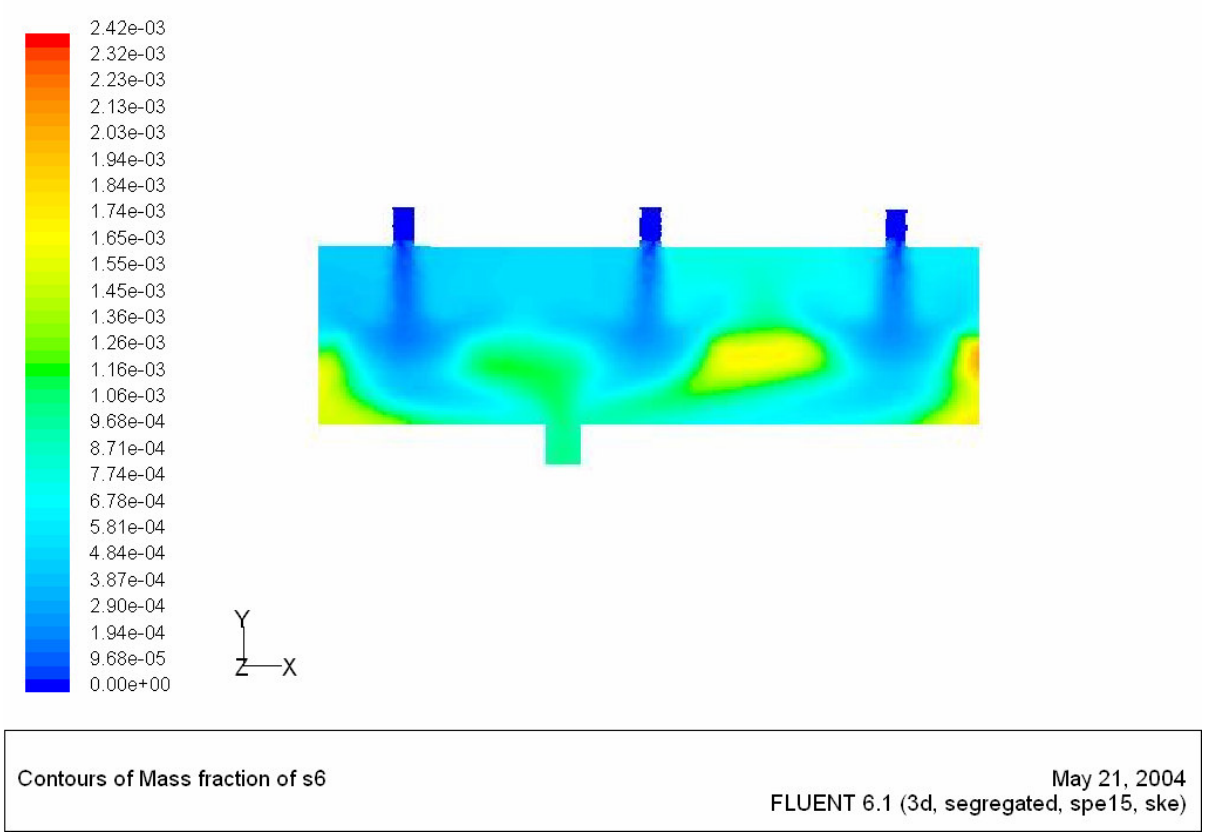

Figure 9.35: Contours of S_6 mass fraction in a vertical plane passing through the inlets and outlet of the third converter.

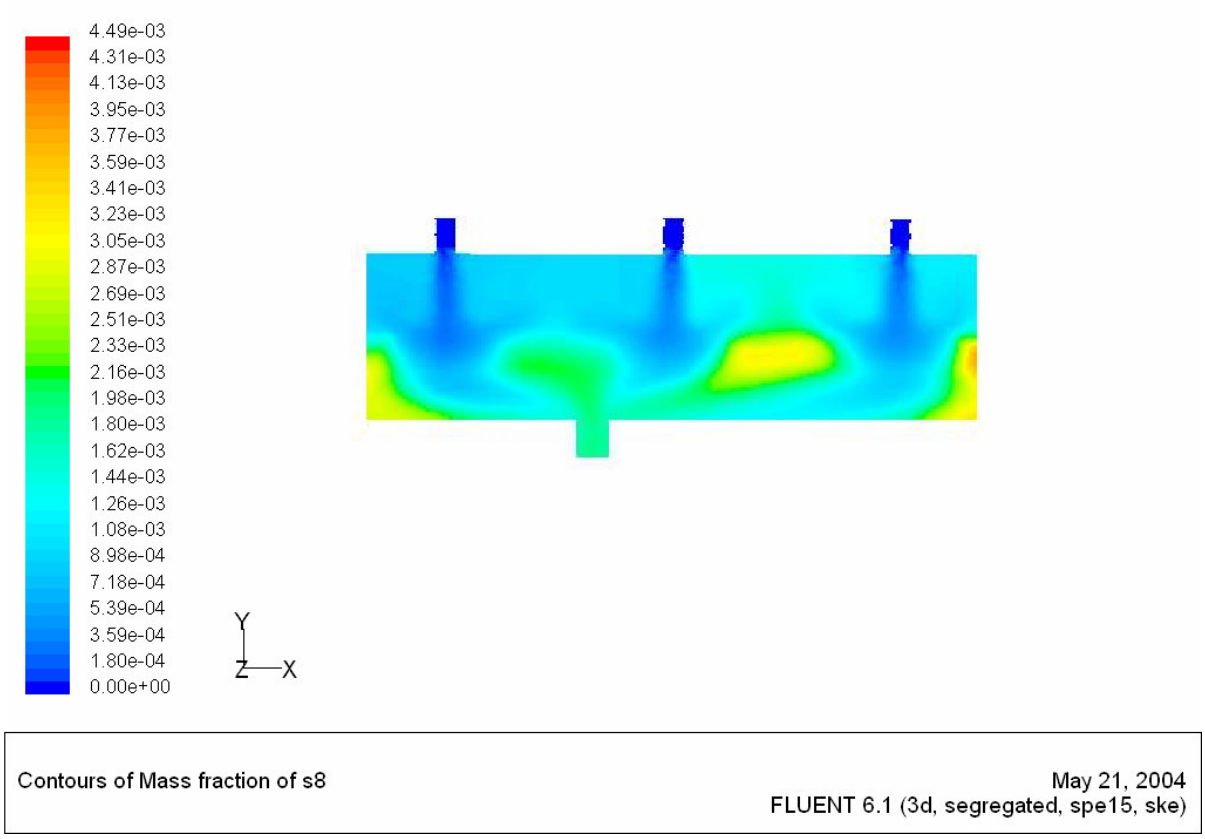

Figure 9.36: Contours of S_8 mass fraction in a vertical plane passing through the inlets and outlet of the third converter.

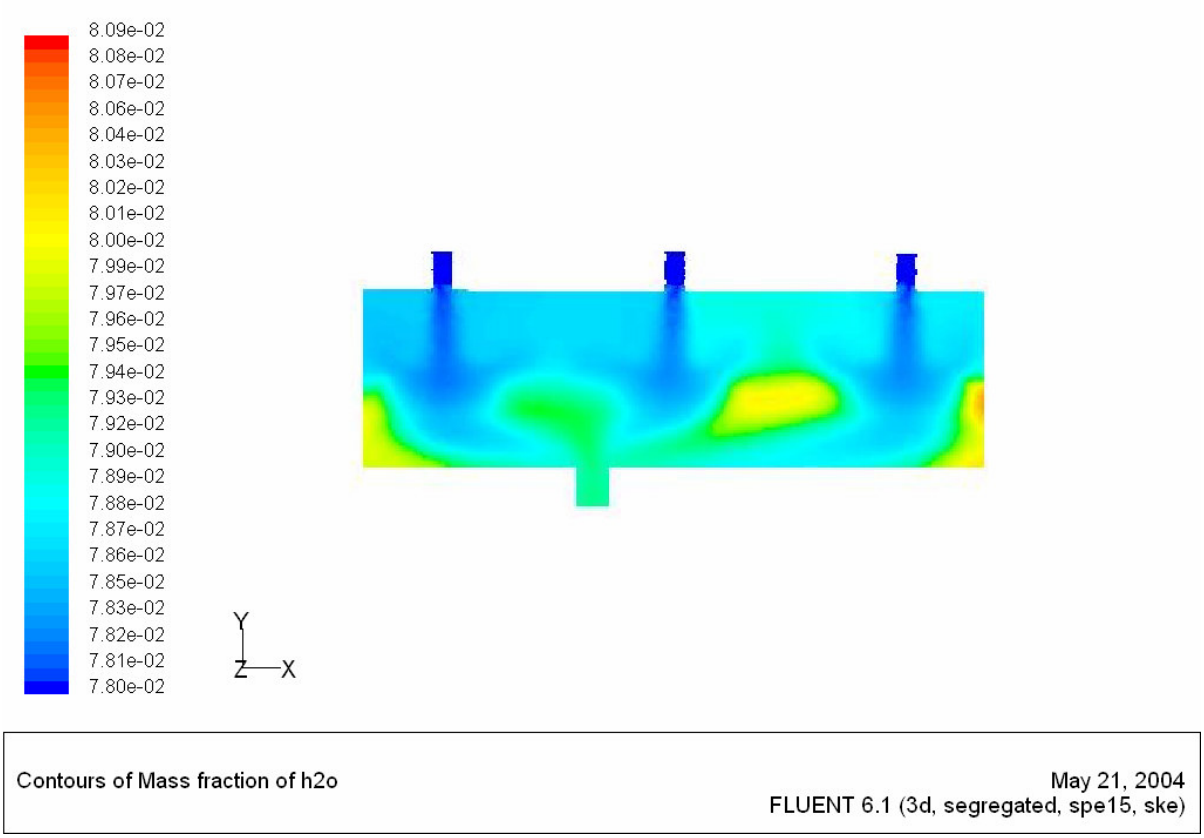

Figure 9.37: Contours of H_2O mass fraction in a vertical plane passing through the inlets and outlet of the third converter.

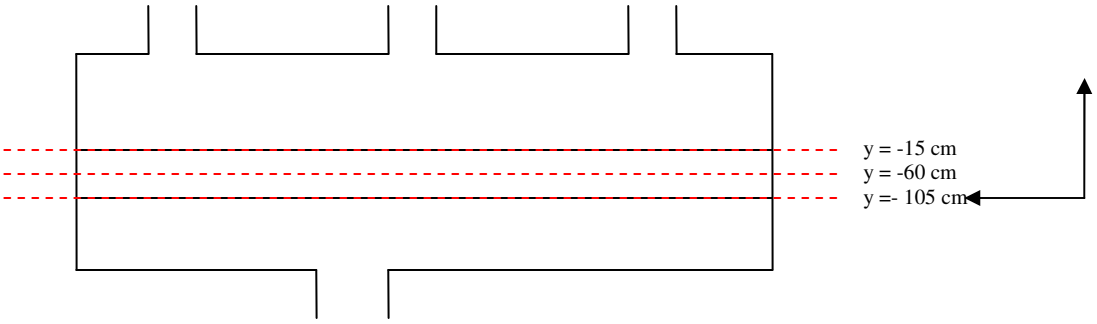

(a)

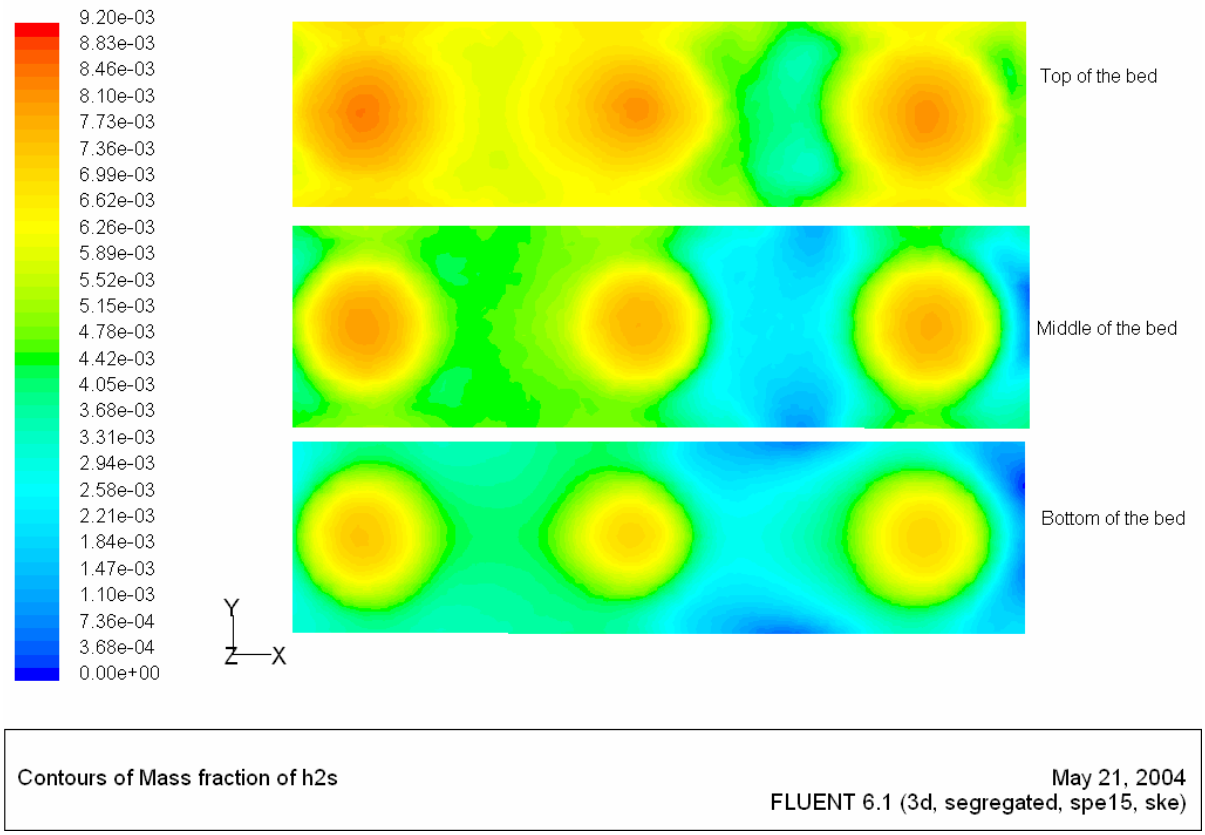

Figure 9.38: Contours of H_2S mass fraction in horizontal plates in different positions of the packed bed of the third converter.

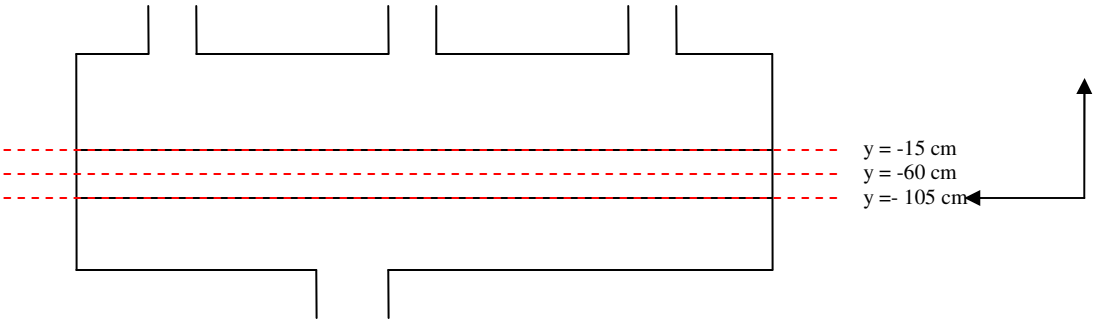

(a)

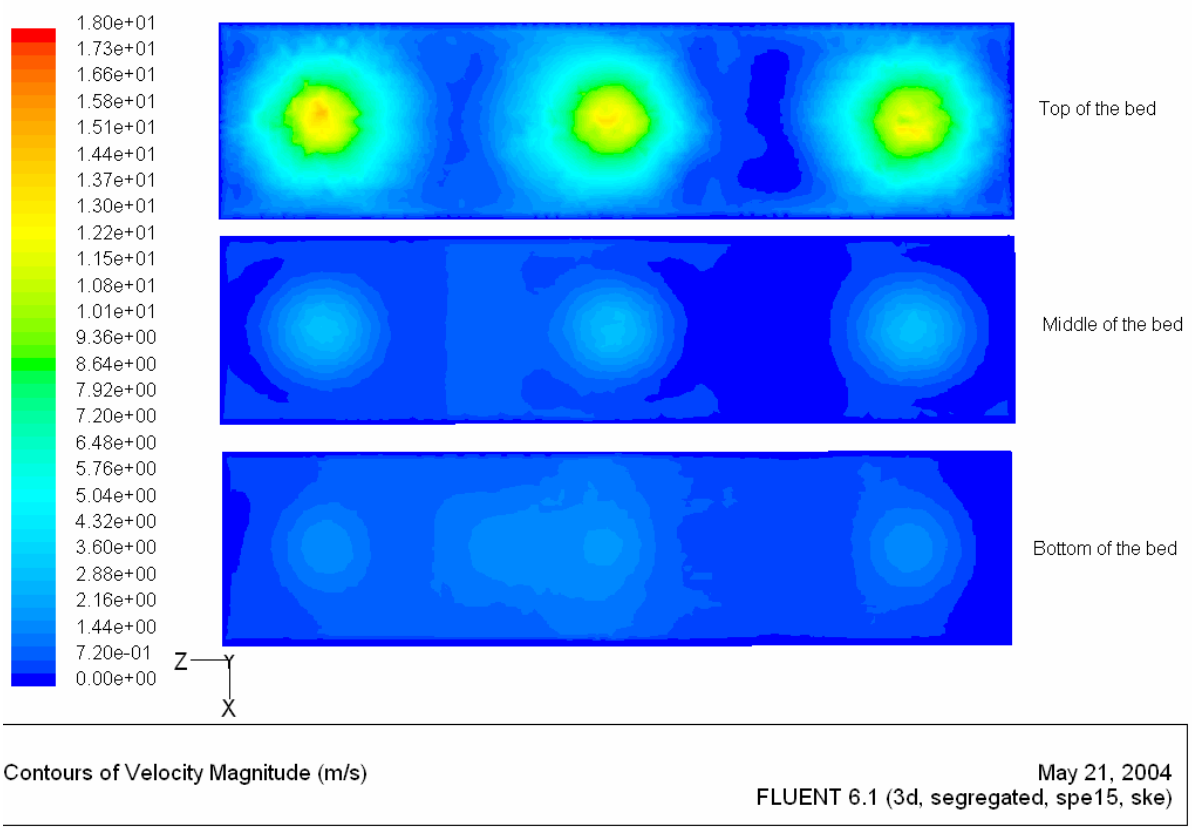

Figure 9.39: Temperature contours in horizontal plates in different positions of the packed bed of the third converter.

9.5.5 Conclusions

The flow, chemical reactions and thermal effects in catalytic converters were simulated. A reaction kinetics model suggested by Abaskuliev et al. [1990] was used. This model was accepted to account for the production of S_2, S_6 and S_8.

Numerical results showed reasonable agreement with industrially obtained results. The catalytic beds act as a good distributor of the flow, however a certain degree of velocity variation still exist especially in top half of the bed. The predicted conversion and the temperatures were within a few percent of the industrially obtained values.

Chapter 10
Conclusions

10.1 Conclusions

Three-dimensional numerical models of flow in an unpacked and partially packed vessel have been developed. The vessel has the same dimensions as those of an industrial sulfur converter. This vessel has three inlets and one outlet. Simulations of flow, chemical reactions and thermal effects in vessel similar to an industrial CLAUS converter were also carried out. Based on results the following conclusions can be drawn:

1. Simulations of flow in an unpacked vessel with three inlets and one outlet show large regions of low velocity. These regions are mainly concentrated between adjacent jets.
2. An increase of 56% in the inlet velocity did not result in a significant improvement of the flow distribution. In let velocities of 45, 57 and 70 m/s were tested. The size of the low velocity zones was hardly reduced. However, the value of the jet velocity increased with an increase in the inlet velocity.
3. An increase in the number of outlets from one to two and then to six resulted in limited improvement in the flow distribution in the unpacked vessel. The sizes of the low velocity zones are definitely lower, however such zones are still observed between adjacent jets.
4. A model of flow in a packed bed was constructed and results were qualitatively compared with those published by Szekely and Poveromo [1975]. Reasonable qualitative agreement was observed between simulated and published results.

5. The flow distribution in the partially packed vessel was significantly improved by the bed which acted as a reasonable distributor of the flow. However, significant variations in the velocity values were still observed across the bed. These variations were more observed in the top half (entry side) of the bed. The distribution becomes reasonable near the exit of the bed.
6. Results obtained from the simulation of the flow, chemical reactions and thermal effects in three Claus converters showed good agreement with industrial results. A finite rate model was used to simulate the chemical reactions. This model was found to simulate the Claus reaction better than two other models which are also available in FLUENT. These other models are the Eddy Dissipation model and Eddy dissipation/finite rate model, (also known as the Eddy concept model).

   The predicted values of the composition of the outlet gas and its temperature agree well with the industrial data.
7. Temperatures across the bed, the outlet temperature, and the composition of the outlet stream all showed good agreement with industrial results.
8. The elemental sulfur produced in the Claus converter, consists of S_8, S_6 and S_2. At temperatures similar to those dominant in a Claus converter, S_8 is dominant followed by S_6 and a trace of S_2. The amounts of these three species produced according to the model agree well with the values based on published equilibrium information.
9. Very limited information about the detailed kinetics of the Claus reactions in a catalytic converter is available in the literature. Better kinetics information will help to improve the control model.

References

Abaskuliev, D. A.; Guseinov, N. M. and Mekhraliev, A. Ch., "Mathematical model of the catalytic convertor of a Claus unit" Gazovaya Promyshlennost, **9**, 60-1, 1990.

Abbott, M. B. and Basco, D. R. "Computational Fluid Dynamics", Longman Scientific & Technical, Essex, England, 1989.

Abid, M., Xuereb, C. and Bertrand, J., "Hydrodynamics in Vessels Stirred with Anchors and Gate Agitators", *Trans. I. Chem. Eng.*, **70**, 377-384, 1992.

Alaverz, E., Mendoroz, S., Munoz, V. and Palacios, J. M., "Sulfur recovery from sour gas by using a modified low-temperature Claus process on sepiolite", Applied Catalysis B: Environmental, **9,** 179-199, 1996.

Berninger, R. and Vortemeyer, D. "Die Umstromung von Hindernissen in Schuttungen", *Chem. Ing. Tech.*, **59**, 224, 1987.

Berninger, R., and Vortemeyer, D., "Der Einflub von Versperrung auf das reaktionstechnische Verhalten eines adiabaten Festbettreaktors", *Chem. Ing. Tech.*, **60**, 1052, 1987.

Bey, O. and Eigenberger, G. "Fluid Flow Through Catalyst Filled Tubes", *Chem. Eng. Sci.*, **52**, 1365-1376, 1997.

Bird, R., Stewart, W. E. and Lightfoot, E. N., "Transport Phenomena", John Wiley & Sons, New York, 2002.

Chen, J.K., Chow, T. K. and Wong, V. W., "Desulfurizing Fuels: Know The Basics", *Chem. Eng.,* 66-71, September 2002.

Coleman, D.A., "Computational Fluid Dynamics", Understanding Unit Operations, PTQ, 1999.

Daszkowski, T. and Eigenberger, G., "A Revaluation of Fluid Flow, Heat Transfer and Chemical Reaction in Catalyst Filled Tubes". *Chem. Eng. Sci.*, **47**, 2245-2250, 1992.

Delmas, H. and Froment, G. F. "A Simulation Model Accounting for Structural Radial Nonuniformites in Fixed Bed Reactors", *Chem. Eng. Sci.*, **43**, 2281-2287, Jun 1988.

Ergun, S. "Fluid Flow Through Packed Columns", *Chem. Eng. Prog.*, **48**, 89-94. Feb 1952.

Fluent User Guide, Fluent Incorporation. Lebanon, NJ, 1998.

Harris, C. K., Roekaerts, D., Rosendal, F. J. J., Buitendijk, F. G. J., Daskopoulous, Ph., Vreenegoor, A. J. N. and Wang, H., "Computational Fluid Dynamics for Chemical Reactor Engineering", *Chem. Eng. Sci.*, **51**, 1569-1594, 1996.

Harvey, P. S. and Greaves, M., "Turbulent Flow in an Agitated Vessel, Parts I & II", *Trans. I. Chem. Eng.*, **60**, 195-210, 1982.

Howboldt, K. A., Monnery, W.D., Svreck, W. Y. " A study on the effect of quench design on the quality of experimental kinetic data", *Indsutrial Engineering and Chemical research,* **38**, 2260-2263, 2002.

Jaree, A., Silveston,, P .L., Hudgins, R. R., Budman, H. and Menazinger, M., "Temperature Response to reactant concentration Perturbations in a Packed-Bed Reactor", *The Canadian Journal Of Chemical Engg.,* **79**, Oct 2001.

Jiang, Y., Khadilkar, M. R., Al-Dahhan, M. H., and Dudukovic, M. P., "Single Phase Flow Distribution in Packed Beds: Discrete Cell Approach Revisited", *Chem. Eng. Sci.*, **55**, 1829-1844, 2000.

Jiang, Y., Khandilkar, M. R., Al-Dahnan, M.H. and Dudukovic, M.P., "CFD of Multiphase flow in Packed-Bed Reactors:I. *K*- Fluid Modeling Issues", *AIChE. Journal*, **48**, 701, April 2002.

Johnson, G. W. and Kapner, R. S., "The Dependence of Axial Dispersion on Non-uniform Flows in Beds of Uniform Packing", *Chem. Eng. Sci.*, **45**, 3329-3341, 1990.

Joseph, D.D., "Flow Induced Microstructure and Direct Simulation of Liquid-Solid Flow", *AIChE Annual Meeting*, PTF Topical Conference, Miami Beach, FL, USA, 1998.

Kuipers, J. A. M. and Swaaij, W. P. M. ,"Applications of Computational Fluid Dynamics to Chemical Reaction Engineering", *Reviews in Chemical Engineering*, **13**(3), 2-75, 1997.

Kuipers, J. A. M.., and Swaaik, W.P.M., "Computational Fluid Dynamics to Chemical Reaction Engineering", *Advances in Chemical Engineering*, **24**, J. Wei et al., eds., Academic Press, New York, 227, 1998.

Lane, A. G. C., Ph.D. Thesis, "Liquid Jet Mixing", Loughborough University of Technology, Loughborough, UK., 1981.

Larraz, B., "Claus catalyst pore structure optimization", *Hydrocarbon Processing*, July 1999.

Launder, B. E. and Spalding, D. B., "Lectures in Mathematical Models of Turbulence", Academic Press, London, England, 1972.

Lerou, J. J. and Froment, G. F. , "Velocity, Temperature and Conversion Profiles in Fixed Bed Catalytic Reactors", *Chem. Eng. Sci.*, **32**, 853-861, 1977.

Levenspiel, O., Chemical Reaction Engineering, Wiley, New York, 1972.

Maddox, R. N. "Gas and Liquid Sweetening", John M Campbell; 1974

McGreavy, C., Foumeny, E. A. and Javed, K. H. "Characterization of Transport Properties for Fixed Bed in terms of Local Bed Structure and Flow Distribution", *Chem. Eng. Sci.*, **41**, 787-797, 1986.

Magnussen. B. F, Hjertager, B. H. "On mathematical models of turbulent combustion with special emphasis on soot formation and combustion", In *16th Symp. (Int'l.) on Combustion*. The Combustion Institute, 1976.

Mier, H. F., Alves, J. J. N. and Mori, M. "Comparison Between Staggered and Collocated Grids in the Finite-Volume Method Performance for Single and Multi-phase Flows", *Comp. and Chem. Eng.*, **23**, 247-262 , 1999.

Monnery, W.D., Hawboldt, K.A., Pollock, A., Svreck, W. Y., "New experimental data and kinetic rate expression for the Claus reaction", *Chem. Eng. Sci.,* **55,** 5141-5148, 2000.

Oleimans, R. V. A., "Computational Fluid Dynamics for the Petrochemical Process Industry", Kluwer Academic Press, Netherlands, 1991.

Pipino, M. and Fox, R. O. "Reactive Mixing in a Tubular Jet Reactor: A Comparison of PDF Simulation with Experimental Data", *Chem. Eng. Sci.*, **24** 5229-5241, 1994.

Rase, H. F. "Fixed Bed Reactor", Butterworths Publishers, Ma, USA., 1990.

Razzaghi, M. and Dalla Lana, I. G. , Kaliaguine, S. A. and Mahay, A., "Catalysis on the Energy scene", *Stud. Surf. Sc. Catal.,* **56,** 711, 1978.

Sheikh, S., M.Sc.. Thesis, " Numerical Simulation of One- and Two-Phase Flows in Unpacked and Partially Packed Vessel, KFUPM, May 2002.

Stanek, V. "Fixed Bed Operations: Flow Distribution and Efficiency", Ellis Horwood, Chichester, 1994.

Stanek, V. and Szekely, J. "Three-dimensional Flow of Fluids through Nonuniforn Packed Beds". *AIChE Journal.*, **20**, 974-980, 1974.

Szkely, J.L. and Poveromo, J. J., "Flow maldistrinution in packedbeds: A comparison of mesurments with predictions", *AIChE. Journal*, 21, 769, 1975.

Teng, H. and Zhao, T. S. "An extention of Darcy's law to non Stokes flow in porous media", *Chem. Eng. Sc.*, **55**, 2727-2735, 2000.

Trambouze, P., "Computational Fluid Dynamics Applied Chemical Reaction Engineering". *Rev. Inst. Fr. Pet,* 48, 595, 1993.

Vortemeyer, D. and Schuster, J. "Evaluation of Steady Flow Profiles in Rectangular and Circular Packed Beds by a Variational Method", *Chem. Eng. Sci.*, **38**, 1691-1699, 1983.

Wang J. W. and Andrews, J. R. G. , "Numerical Simulation of Flow in Helical Ducts", *AIChE Journal.*, **41**, 1071-1080, 1995.

Ziolkowska, I. and Ziolkowski, D., "Modeling of Gas Interstitial Velocity Radial Distribution over a Cross-Section of a Tube Packed with a Granular Catalyst Bed", *Chem. Eng. Sc*, **48**, 3283-3292, 1993.

Zughbi, H. D. and Sheikh, S., "Numerical Simulation of one- and two- phase flows in unpacked and packed vessel", Mathematical and computational Applications, **9**, 25-39, 2004.